

OPTICAL INVESTIGATION OF COMETARY NUCLEI

by

KAREN JEAN MEECH

B.A., Rice University
(1981)

SUBMITTED TO THE DEPARTMENT OF
EARTH, ATMOSPHERIC & PLANETARY SCIENCES
IN PARTIAL FULFILLMENT OF
THE REQUIREMENTS FOR THE
DEGREE OF
DOCTOR OF PHILOSOPHY

at the

MASSACHUSETTS INSTITUTE OF TECHNOLOGY

July 1987

©Karen Jean Meech 1987

The author hereby grants to M.I.T. permission to reproduce and to distribute copies of this thesis document in whole or in part.

Signature of Author _____
Department of Earth, Atmospheric & Planetary Sciences
July 17, 1987

Certified by _____
David C. Jewitt
Thesis Supervisor

Accepted by _____
William F. Brace
Chairman, Committee on Graduate Students

WITHDRAWN
FROM
MIT LIBRARIES

OPTICAL INVESTIGATION OF COMETARY NUCLEI

by

KAREN JEAN MEECH

Submitted to the Department of Earth, Atmospheric & Planetary Sciences
on July 17, 1987 in partial fulfillment of the
requirements for the Degree of
Doctor of Philosophy in Planetary Science

ABSTRACT

A simple H₂O ice sublimation model is developed for comet P/Halley from observations at large heliocentric distances $5.1 < R \text{ [AU]} < 11.0$. The rapid brightening of the comet which began at a distance of $R = 5.9$ AU is explained by the onset of sustained sublimation from an H₂O ice nucleus. From the observations at large R the Bond albedo of the nucleus is found to lie in the range $0.02 < A_B < 0.15$. The nucleus is found to have a mean radius $2.8 < \beta_n < 8$ km, with an axis ratio 2.5:1.

The H₂O sublimation model incorporates many parameters pertaining to physical characteristics of the nucleus and the dust in the coma. Typically, these parameters are poorly constrained. In order to develop an understanding of cometary physical characteristics in general, and to better constrain the H₂O sublimation model for P/Halley in particular, observations at near infrared and visible wavelengths are presented for ≈ 30 additional comets. The albedo of the dust grains of P/Halley is found to be $p_\lambda = 0.06 \pm 0.01$ at $\lambda = 1.25$ μm . The phase dependence of the scattering from the dust from this comet is consistent with a small linear phase coefficient of $\beta = 0.02 \pm 0.01$ mag deg⁻¹ (for $1.3 < \alpha \text{ (deg)} < 8.6$), with no apparent opposition surge. The phase function of the dust is similar to that found for 3 other comets; all of the comet phase functions lack the opposition surge seen for asteroids. The cometary dust phase function is shown to be steeper than that of the Zodiacal dust. The scattered light from the dust grains in the comae of $n > 10$ comets (including P/Halley) indicates that the color of the dust changes from reddened with respect to the solar continuum to neutral to blue as the wavelength changes from $\lambda = 0.5$ μm to $\lambda > 2$ μm . The trend is indicative of scattering from micron-sized and larger grains. The surface brightness profiles of $n = 10$ comets show the effects of radiation pressure on the dust comae. The grain velocities in the comae are found to be lower than the typically assumed empirical relationship of Bobrovnikoff. The rotation periods for 5 comet nuclei are investigated. Observations of P/Halley at $R > 5$ AU only provide a lower limit to the period, $T > 18$ hr. The rotation periods of P/Arend-Rigaux, P/Neujmin 1 and P/Encke are found to be 13.54 ± 0.05 , 12.67 ± 0.06 and 22.47 ± 0.07 hr respectively. The period of comet P/Tempel 2 may be either $T = 8.93$ or $T = 7.48$ hr.

The H₂O ice sublimation model is re-examined given these measurements of specific coma and nucleus properties. The model is able to match the general photometric behavior of P/Halley from recovery ($R = 11.0$ AU) through perihelion ($R = 0.59$ AU). The model is found to be a powerful tool for learning about basic physical properties of the nucleus, but is inadequate for studying detailed properties of the lightcurve.

Observations are presented for the dynamically new comet Bowell at the record distance $R =$

ABSTRACT, CONTD.

13.56 AU. Remarkably, the comet is found to possess a substantial coma at this distance. The coma cannot be produced by H₂O sublimation. A simple sublimation model similar to that applied to P/Halley suggests that the activity in comet Bowell is due to sublimation of CO₂ (or an ice with a similar latent heat of sublimation). Comparison of the sublimation models for comets P/Halley and Bowell show that the Bowell lightcurve is less steep; it does not show the sharp increase in activity caused by the onset of H₂O sublimation at $R \approx 6$ AU. Observations of another dynamically new comet, Cernis, at $R = 11.25$ AU are presented. The behavior of the comet as a function of R is very similar to that of comet Bowell. The work presented in this thesis shows that comet observations at very large distances, $R > 10$ AU, are possible, and that they provide very interesting information concerning compositional differences between the thermally evolved periodic comets and the little altered dynamically new comets.

Thesis Supervisor: Dr. David C. Jewitt

Title: Assistant Professor of Planetary Science

ACKNOWLEDGEMENTS

The observations described in this thesis were obtained in large part at various National Observing facilities. I am grateful for the time that was granted for thesis research at: the Kitt Peak National Observatory (KPNO), the Cerro Tololo Interamerican Observatory (CTIO) and the NASA Infra-Red Telescope Facility (IRTF). In particular, at Kitt Peak I wish to thank Pat Patterson, Monique Chapman and Peggy Wiggins for making all of the logistical arrangements on the mountain and downtown; Jeannette Barnes, Ed Anderson, Lindsey Davis and Suzanne Hammond for their extraordinary downtown data reduction assistance; Bill Schoening, Jim DeVeney and Ed Carder (*who always* seemed to know instinctively where I was) for their patient assistance with equipment both on and off the mountain; Hal Halbedel and Lee Craven for technical assistance on the mountain; Dean Hudek for efficient and most enthusiastic control of the telescopes; and finally Frank Bull, Glen Pickens and the Director of KPNO, Sydney Wolff for their patience during the "heavy use" of the photographic facilities downtown. At CTIO I wish to thank the Director, Bob Williams, for his efforts to obtain special observations of comet Cernis. In addition, I am especially grateful for all of the assistance I received while observing from Arturo Gómez, Daniel Maturana, Manuel Hernández, Mauricio Hernández and Edgardo Cosgrove. Special thanks goes to Oscar Saá, Hugo Vargas and the electronics staff for arranging it so I could use the 4m Prime Focus CCD System remotely from the 60 inch telescope; something crucial to the success of the observations. Finally, I wish to thank Charlie Kaminski at the IRTF for efficient control of the telescope and assistance with the observations.

In addition to the National Facilities, extensive use was made of M.I.T.'s McGraw-Hill Observatory located on Kitt Peak in Arizona. Matt Johns, Mike Dreslin, Larry Breuer and Paul Delhaney provided much appreciated assistance with the telescope and equipment at the observatory. I would like to thank several people at M.I.T. who provided assistance and support for the McGraw-Hill Observations. These include Gerry Luppino, Ron Remillard, Roland Vanderspeck and especially George Ricker. Ron Remillard was particularly helpful in showing Dave Jewitt and me how to use the MkII spectrograph at McGraw-Hill and its associated data reduction packages at MIT.

Special thanks go to Jim Elliot for his encouragement and for the opportunity he gave me to obtain observing experience prior to the start of my thesis at CTIO, the IRTF, McDonald Observatory in Texas, and on various occultations with portable equipment in Kansas,

Virginia and Great Exuma, Bahamas. Special thanks are also in order for Dick French for his helpful discussions, his help with an unruly Planetary Astronomy VAX at M.I.T., and his careful reading of an early version of this thesis. I am also grateful to Shelly Pope for her willingness to obtain observations for me at a moment's notice when illness prevented me from going on an observing run. In addition, I would like to thank Brian Marsden and Dan Green who provided me with updated orbital elements and ephemerides for some of the comets on hyperbolic orbits. I also thank Jeff McClintock from the Center for Astrophysics for obtaining a spectrum of comet Wilson just after perihelion using the CTIO 4m telescope.

The photographic work in this thesis was reproduced by the photographic lab at KPNO headquarters in Tucson and by Don Pickett at Colorguild in Needham, MA. I thank Don for his careful and quick work, and willingness to make sure the cometary "ether" showed up clearly in all the photographs.

Finally, extra special thanks go to my advisor, David Jewitt, for all of his patient encouragement, discussions and the support he offered during the research and writing of this thesis. I would also like to thank Sid Grollix and Alf Guthridge for their careful reading of several manuscripts prior to publication.

This research has been supported, in part, by a fellowship from the NASA Graduate Student Researchers Award Program.

TABLE OF CONTENTS

Abstract	2
Acknowledgements	4
Table of Contents	6
List of Figures	9
List of Tables	12
1. Introduction	14
1.1 Development of The Study of Comets	14
1.1.1 Evidence for a Solid Nucleus	15
1.1.2 Evidence for H ₂ O - Dominated Nuclei	17
1.2 Goals of the Present investigation	18
2. Modelling P/Halley Preperihelion	24
2.1 Introduction	24
2.2 Observations	25
2.3 Data Reduction	29
2.4 Discussion	33
2.4.1 Sublimating Nucleus Model	33
2.4.2 Comparison of Model with Other Observations	39
2.4.3 Other Coma Producing Mechanisms	44
2.5 Conclusions	46
3. Albedo Determination	50
3.1 Introduction	50
3.2 IR Techniques for Measuring Albedos	51
3.2.1 The Radiometric Method	51
3.2.2 Albedo of Coma Grains - Method of O'Dell	55
3.2.3 Albedo of Coma Grains - Alternate Method	56
3.3 Measurements of P/Halley	57
3.3.1 Present Work	57
3.3.2 Other Sources of P/Halley Albedos	61
3.4 Other Comets	62
3.5 Conclusions	64
4. Cometary Phase Functions	68
4.1 Introduction	68
4.2 Observations	70

TABLE OF CONTENTS CONTD.

4.3	Analysis and Discussion	72
4.4	Phase Function	80
4.4.1	Comet P/Halley	80
4.4.2	Comet P/Ashbrook Jackson	83
4.4.3	Comet Bowell	85
4.4.4	Comet P/Stephan-Oterma	87
4.4.5	Comet P/Encke	87
4.4.6	Comparison with Other Solar System Bodies	90
4.5	Conclusions	97
5.	Cometary Rotation Periods	100
5.1	Introduction	100
5.1.1	Period Determination	100
5.2	Observations	102
5.2.1	Comet P/Arend-Rigaux	102
5.2.2	Comets P/Neujmin 1 and P/Encke	109
5.2.3	Comet P/Tempel 2	118
5.2.4	Comet P/Halley	121
5.3	Analysis	125
5.4	Discussion	127
5.4.1	Comet P/Arend-Rigaux	127
5.4.2	Comet P/Neujmin 1	131
5.4.3	Comet P/Encke	131
5.4.4	Comet P/Tempel 2	136
5.4.5	Comet P/Halley	137
5.5	Comets as Slow Rotators	141
5.6	Conclusions	142
6.	Grain Sizes in Cometary Comae	146
6.1	Introduction	146
6.2	Observations	146
6.3	Analysis	149
6.4	Scattering as a Function of Wavelength	153
6.5	Conclusions	158

TABLE OF CONTENTS CONTD.

7. Effects of Radiation Pressure on the Coma	160
7.1 Introduction	160
7.2 Observations	161
7.3 Interpretation and Discussion	171
7.4 Conclusions	177
8. Modelling P/Halley - All Observations	179
8.1 Introduction	179
8.2 Observations	179
8.3 Discussion	190
8.3.1 Comparison of Pre- and Post-Encounter Information	190
8.3.2 The Visual Lightcurve	193
8.4 Conclusions	201
9. Dynamically New Comets	206
9.1 Introduction	206
9.1.1 Differences Between New and Old Comets	207
9.1.2 Characteristics of Comets Active at Large Heliocentric Distances	215
9.2 Comet Bowell - Observations at 13.6 AU	228
9.2.1 Observations	230
9.2.2 Nature of the Activity	238
9.2.2.1 Possible Mechanisms	238
9.2.2.2 CO ₂ Sublimation Model	239
9.3 Comet Cernis	245
9.4 Other Dynamically New Comets	251
9.5 Comet Stearns (1927IV)	259
9.6 Conclusions	264
10. Summary/Future Work	272
Biographical Note	274
Appendix 1 - Computation of Ephemerides	279
Appendix 2 - Relationship Between Albedo, Size and Brightness of the Nucleus	291
Appendix 3 - Latent Heats of Sublimation	298
Appendix 4 - Cometary Comae	300
Appendix 5 - Radiation Pressure	306
Appendix 6 - Grain Terminal Velocity in a Gas Flow	311

LIST OF FIGURES

2-1	P [†] CCD Image of P/Halley at R = 5.9 AU	28
2-2	P/Halley V Magnitude vs. Julian Day / H ₂ O Sublimation Model	32
2-3	P/Halley V(1,1,α) Magnitude vs. Julian Day (All sources)	41
2-4	P/Halley Surface Brightness Profile	43
3-1	Spherical Coordinate System - Radiometric Model	53
3-2	P/Halley Infra-Red Fluxes - Blackbody Fit	60
4-1	Average of P/Halley Spectra	73
4-2	Changes in P/Halley Spectra over 7 Days	74
4-3	P/Halley Continuum Flux Density vs. Julian Day	81
4-4a	Continuum Magnitude vs. Phase Angle for Comet P/Halley	82
4-4b	Continuum Magnitude vs. Phase Angle for Comet P/Ashbrook-Jackson	84
4-4c	Continuum Magnitude vs. Phase Angle for Comet P/Bowell	86
4-4d	Continuum Magnitude vs. Phase Angle for Comet P/Stephan-Oterma	88
4-4e	Continuum Magnitude vs. Phase Angle for Comet P/Encke	89
4-5a	Comparison of Asteroid and Comet Phase Functions	91
4-5b	Comparison of the Phase Functions of the Uranian Satellites and Comets	93
4-5c	Comparison of the Phase Functions of the Zodiacal Light and Comets	96
5-1	P Five Comet Nuclei	104
5-2	Comet P/Arend-Rigaux Photometry	108
5-3	Comet P/Neujmin 1 Photometry	115
5-4	Comet P/Encke Photometry	117
5-5	Comet P/Tempel 2 Photometry	119
5-6	Comet P/Halley Photometry	124
5-7	χ^2 vs. Rotation Frequency for P/Arend-Rigaux and P/Tempel 2	129
5-8	Surface Brightness Profile of P/Arend-Rigaux at Max and Min Brightness	130
5-9a	χ^2 vs. Rotation Frequency for Comet P/Neujmin 1 - 2 Data Sets	132
5-9b	χ^2 Period Search for Comet P/Neujmin 1, Combined Data Set	133
5-10a	χ^2 vs. Rotation Frequency for Comet P/Encke - 2 Data Sets	134
5-10b	χ^2 Period Search for Comet P/Encke, Combined Data Set	135
5-11	χ^2 vs. Rotation Frequency for Comet P/Halley - 2 Data Sets	138
5-12	Variation of the CN($\Delta v=0$) Band Flux vs. Julian Day for P/Halley	140
6-1	Optical Spectra of 3 Comets Observed with the IIDS	148

LIST OF FIGURES, CONTD.

6-2	Optical Reflectivities of 3 Comets	151
6-3	Normalized Reflectivity Gradient as a Function of Wavelength	154
7-1	P CCD Images of 10 Comets	164
7-2	Continuum Surface Brightness Profiles for 4 Comets	167
7-3	Effect of Radiation Pressure on Surface Brightness Profile	173
7-4	Effect of Phase Angle on Surface Brightness Profile	174
8-1	P/Halley Lightcurve From Recovery	181
8-2a	P Pre-Perihelion Development of the Coma of P/Halley - $11.0 < R < 1.9$ AU	184
8-2b	P Plasma Tail of P/Halley - 1.0 and 1.6 AU	186
8-2c	P Post-Perihelion Images of P/Halley - $0.82 < R < 5.65$ AU	188
8-3	P/Halley Lightcurve and H ₂ O Sublimation Model	194
8-4a	P Inner Coma of P/Halley - Nightly Variations ($R \approx 0.8$ AU)	196
8-4b	Contour Plots of Images in 8-4a	197
8-5	P Coma of P/Halley at $R = 5.6$ AU	199
9-1	Farthest Observed Distance of Nearly Parabolic Comets vs. Date	213
9-2a	P Characteristic Tails Seen at Large Heliocentric Distances	222
9-2b	P Characteristic Appearance of Recently Observed Oort Cloud Comets	224
9-3a	P CCD Image of Comet Bowell at $R = 13.6$ AU	233
9-3b	Line Drawing of Comet Bowell	234
9-4	Surface Brightness Profile of Comet Bowell	235
9-5	Comet Bowell Coma Radius vs. Julian Day	236
9-6	Critical Grain Radius vs. Heliocentric Distance	240
9-7	CO ₂ Sublimation Model For Comet Bowell	242
9-8	Grain Terminal Velocity vs. Heliocentric Distance	244
9-9	P Comet Cernis at $R = 11.25$ AU	249
9-10	Lightcurve Comparison: P/Halley, Bowell and Cernis	250
9-11	P Tails of Comets Shoemaker (1985 XII) and Wilson	254
9-12	P Comparison of Comets Active at Large R	256
9-13	H ₂ O Sublimation Model for Comet Stearns (1927VI)	262
A1-1	Celestial Sphere - Definition of Variables - Ephemeris Calculations	281
A1-2	Spherical Angles	282
A1-3	Geocentric Coordinates	284
A1-4	Celestial Sphere - Geocentric Coordinates	285

LIST OF FIGURES, CONTD.

A2-1	Scattering Coordinate System	292
A4-1	Coma Surface Brightness Coordinate System	300
A5-1	Grain Sorting in the Coma of P/Halley	309
A6-1	Gas Drag	311
A6-2	Dust Grain Collisions with Gas Molecules in a Cometary Coma	312
A6-3	Grain Velocities in a Gas Flow	316
A6-4	Grain Terminal Velocity vs. Distance From Nucleus	317

†Indicates the Figure is a photograph.

LIST OF TABLES

2-1	P/Halley Photometry	30
2-2	Other Sources of P/Halley Magnitudes	34
2-3	H ₂ O Model Parameters	40
3-1	IRTF Observations of Comet P/Halley	59
3-2	Derived Comet Halley Albedo	59
3-3	Cometary Albedos - Nucleus and Coma	63
4-1	Observing Geometry	71
4-2a	Gas Band and Local Continuum Windows	79
4-2b	Continuum Windows	79
5-1	Geometry of Comet P/Arend-Rigaux	105
5-2	Photometry of Comet P/Arend-Rigaux	106
5-3	Geometry of Comet P/Neujmin 1	109
5-4	Geometry of Comet P/Encke	110
5-5	Photometry of Comet P/Neujmin 1	112
5-6	Photometry of Comet P/Encke	113
5-7	Geometry of Comet P/Tempel 2	118
5-8	Photometry of Comet P/Tempel 2	120
5-9	Geometry of Comet P/Halley	122
5-10	Photometry of Comet P/Halley	123
5-11	Rotation Frequencies	126
5-12	Measured Nucleus Rotation Periods	127
6-1	Journal of IIDS Observations	149
6-2	Optical Reflectivities	152
6-3	Normalized Reflectivity Gradients	155
7-1	Journal of Profile Observations	165
7-2	Parameters of Fitted Models	175
8-1	Geometry of P/Halley Observations	180
8-2	Halley Model Parameters	191
8-3	Photographic Figure Information	202
9-1	Characteristics of Comets Active at Large Distances	217
9-2	Comet Tail Types	226
9-3	Comet Bowell Observations - Discovery Through Perihelion	229
9-4	Observational Parameters - Comet Bowell	230

LIST OF TABLES, CONTD.

9-5	Comet Cernis Photometry	246
9-6	Other Active Comets Currently Observed	251
9-7	Summary of Comet Stearns (1927IV) Observations	260
9-8	Photographic Figure Information	266

Chapter 1 - Introduction

1.1 Development of the Study of Comets

Fundamental scientific interest in comets stems from the belief that comets probably formed at the same time as the Solar System from the accretion of grains composed of interstellar dust and ices. Comets reside in a vast cloud orbiting the Sun at distances of about 50,000 AU, and are occasionally perturbed by passing stars into the inner Solar System where they may be gravitationally captured into lower energy orbits. The existence of this cloud was deduced in 1950 by J. Oort from the frequency distribution of the reciprocal semimajor axes of 19 comets with well known orbits (Oort, 1950; Oort and Schmidt, 1951). Because of their large aphelion distances, comets first coming in from the Oort cloud have probably never been heated much above their condensation temperatures. These objects may represent the most primitive relics of Solar System formation - and as such, may provide the most valuable means of learning about conditions in the early proto-solar nebula. Therefore, by investigating the nature of comets one hopes to understand some of the processes involved in the formation of the Solar System.

The current understanding of comets is quite limited. Until recently, most physical observations were only of a qualitative nature. In fact, it was not until the 19th century that significant progress was made in trying to explain the physical nature of comets. Observations were restricted to positional determinations and descriptions of appearance and brightness. Our present understanding of the cometary nucleus, the solid body which gives rise to all of the observed "cometary" phenomena, was formulated in 1950 by Whipple who argued that the nucleus, of dimensions of the order a few km, is a conglomerate of ices such as H₂O, NH₃, CH₄ and CO₂ and meteoritic materials (dust) (Whipple 1950, 1951). According to Whipple, a fraction of the solar radiation incident on the nucleus provides the

energy for the sublimation of the ices which drag dust grains into the coma. Whipple developed this model in order to explain the non-gravitational behavior exhibited by several comets (deceleration/acceleration in the mean motions resulting in a change in the expected perihelion passage date), in particular, for comet P/Encke. For a rotating nucleus with low thermal conductivity there will be a time lag between the passage under the sub-solar point and the penetration of the thermal wave into the surface of the nucleus. If this time lag is an appreciable fraction of the nucleus rotation period, the resultant sublimating gases will exert a non-radial force on the nucleus. This force will decelerate or accelerate the comet in its orbit depending on whether the rotation is prograde or retrograde with respect to the orbital motion.

An alternate theory (the sandbank model) was proposed by Lyttleton (1953), which maintained that comets consist of large swarms of dust-sized particles separated by $\approx 10^3$ times the particle dimensions. Lyttleton (1972, 1975) maintained that because a discrete nucleus had never been observed the icy conglomerate theory was an unnecessary hypothesis. Since the development of this theory in the early 1950's, much of the scientific investigation has focussed its attention on ascertaining the validity of the Whipple theory. Prior to the spacecraft encounters with comets P/Halley and P/Giacobini-Zinner, there existed several lines of evidence which suggested that Whipple's model is a good description of cometary nuclei.

1.1.1 Evidence for a Solid Nucleus

Whipple (1961) gave several strong arguments which suggest that Lyttleton's sandbank model for the cometary nucleus is incorrect, and that solid cometary nuclei do exist. Lyttleton maintained that the secular decrease in the motion of P/Encke could be due to Poynting-Robertson drag on the particles. Whipple pointed out, however, that no mechanism such as Poynting-Robertson drag or a resisting medium could account for *both* the observed

accelerations and decelerations of comets. Additionally, there have been many observations of jets of material from cometary nuclei (see Bobrovnikoff 1931; Larson & Sekanina, 1985; Sekanina & Larson, 1986); it is difficult to imagine how such jets might be produced from small dust grains in a cometary swarm.

There have been many observations of sun-grazing comets, some of which have survived with perihelion distances of $q \approx 0.005$ AU (Wyckoff, 1982). A perihelion distance of 0.005 AU ($\approx 7.5 \times 10^8$ m) is well inside the Roche limit of the sun ($\approx 4 \times 10^9$ m $\approx 6R_{\odot}$) for a zero tensile-strength body (assuming a comet density of $\rho \approx 100$ kg m⁻³); survival of sungrazing comets therefore implies a solid nucleus with a finite tensile strength. Whipple (1963) estimated the tensile strength against tidal disruption for comets with radii $1 < r_n < 10$ km at $\Delta = 0.005$ AU to be $GM\rho r_n^2 R^{-3}$ giving 10^3 - 10^5 N m⁻² as a lower limit. This is roughly 100 times weaker than solid ice. Lyttleton (1953) admitted that a swarm of particles would be completely vaporized by such a close passage to the sun, but maintained that recondensation would occur after the perihelion passage. Whipple (1961) pointed out that in this scenario fewer than 1% of the original cometary material would be available for condensation because of the spreading of the gas along the orbit during the disruption and the effects of radiation pressure on small particles while they are recondensing. A particularly spectacular example of a comet breaking up near perihelion was comet West (1976 VI). The breakup of the nucleus into 4 components was accompanied by a dramatic brightening of approximately 7 magnitudes coincident with a substantial increase in dust production (Sekanina & Farrell, 1978). These observations can best be interpreted using the icy nucleus model.

More recently, there has been a direct radar detection of the nucleus of comet P/Encke (Kamoun *et al.*, 1982a), from which the radius of the solid body was estimated to be within the range ≈ 0.4 - 4.0 km. Kamoun *et al.* (1982b) have also observed comet P/Grigg-Skjellerup with radar and placed a lower limit on the radius of the nucleus at ≈ 0.4 km. The nucleus of

comet IRAS-Araki-Alcock has also been detected by radar with an average radius of 3-4 km (Goldstein *et al.*, 1984). Finally, direct images of cometary nuclei have been obtained from the spacecraft flyby's of comets P/Giacobini-Zinner and P/Halley. Spectacular images of the nucleus of comet P/Halley show an irregularly shaped nucleus (Reitsema *et al.*, 1986) of approximate dimensions 16 x 10 x 9 km (Wilhelm *et al.*, 1986).

1.1.2 Evidence for an H₂O - Dominated Nucleus

Marsden *et al.* (1973) have modelled the variation of the non-gravitational forces with heliocentric distance and found that the observations are best represented by the vaporization of H₂O ice. There is a sharp drop in the magnitude of the non-gravitational acceleration beyond 3-4 AU; as is expected for vaporization from H₂O ice. More volatile substances were also considered in the analysis, but they were found incompatible with the data unless comet albedos were extremely high.

A more direct piece of evidence suggesting H₂O ice was reported by Herbig (1973) who detected 3 unidentified features in the spectrum of comet Kohoutek (1973f). These same lines were observed by Benvenuti and Wurm (1974), also in comet Kohoutek. The lines were only visible on the tailward side, extending some 4×10^5 km along the tail. There had been previous observations of these lines in comet Ikeya (1963a) by Miller (1964), but these remained unidentified until Herzberg and Lew (1974) suggested that the lines were due to rotational bands of H₂O⁺. Subsequent observations by Wehinger *et al.* (1974) of comet Kohoutek revealed approximately 50 new lines in the spectra between 4500 - 7900Å, almost all attributable to H₂O⁺. Water ions were also detected in comet Bradfield (1974b) by Wehinger and Wyckoff (1974). The strength of the emission suggested that the parent molecule (most likely neutral H₂O) was very abundant. There was also a possible detection of the 1.35cm line of H₂O in comet Bradfield by Jackson *et al.* (1976).

There is also other evidence that water-ice is the major constituent of the nucleus. Ultraviolet observations of comet Bennett (1970 II) (Code *et al.* 1972; Code and Savage, 1972) from the Orbiting Astronomical Observatory showed very high abundances of OI, OH and Lyman- α , suggesting that water, the probable parent molecule, was very abundant. This finding has been amply confirmed by repeated observations of the UV lines of O, H and OH by the IUE satellite. Although plasma experiments carried aboard the International Cometary Explorer made measurements of H_2O^+ (Ogilvie *et al.*, 1986), the existence of neutral H_2O could not be inferred because the specific ionization processes within cometary comae are not well understood. The first direct measurements of neutral gaseous H_2O in a comet were made by Mumma *et al.* (1986) who used the Kuiper Airborne Observatory to observe comet P/Halley in the near infra-red. Subsequent spacecraft measurements with the neutral mass spectrometer carried by Giotto (Krankowsky *et al.*, 1986) indicated that the composition of the gas in the coma of P/Halley was 80% water vapor by volume.

1.2 Goals of the Present Investigation

It seems from the previous section that Whipple's icy conglomerate model of the nature of the cometary nucleus has been well established, both from ground-based and spacecraft observations. Although the spacecraft observations provide direct and instantaneous measurements of some aspects of the comet (nucleus morphology, size, mass and composition of the gas and dust etc.), spacecraft missions do not in general provide information on the long term behavior of a given comet. Furthermore, these missions will be able to sample only a very small number of periodic comets with well-known orbits, so that a clear picture of the properties of comets as a group cannot be obtained. There is, therefore, a continuing (not to say enhanced) need for ground-based comet observations.

The aim of this thesis is to show how ground-based observations (CCD photometry,

low resolution spectroscopy and near and thermal infra-red photometry) can contribute significant advances to the understanding of the physical nature of cometary nuclei. For instance, many of the important physical characteristics of P/Halley, including shape, size, albedo and crude composition, were determined by the writer prior to the encounter with the comet by five spacecraft. (For a summary of the spacecraft results, see the *Proceedings of the 20th ESLAB Symposium on the Exploration of Halley's Comet*, eds. B. Battrock, E. J. Rolfe and R. Reinhard, ESA Pub. Div., ESA SP-250, The Netherlands). The techniques used on Halley can be applied with some confidence to the study of comets which are unlikely to be visited by spacecraft. The ability to use telescopes to investigate comets is especially important in order to study the more primitive comets which are entering the region of the inner Solar System for the first time.

In Chapter 2 of this thesis a very simple sublimation model will be presented for and applied to comet P/Halley. This chapter is an expanded version of Meech *et al.* (1986). Observations at large heliocentric distances will be discussed and it will be shown that these observations are consistent with sublimation being controlled by H₂O ice. A few physical parameters are constrained by the model. The model, however, contains many free parameters for which only reasonable estimates may be made. The subsequent chapters (3-7) discuss methods of determining values for many of the input parameters in the sublimation model. Measurements of cometary albedos, phase functions, rotation periods, grain sizes and the effects of radiation pressure on the coma are discussed.

In Chapter 8 the sublimation model is re-evaluated based on the results of the previous chapters and a comparison is made with the knowledge obtained from the spacecraft missions. Ground-based remote observations prove to be an excellent technique for understanding cometary physics. Finally, in Chapter 9, the simple sublimation model will be applied to comets which can *only* be observed remotely: dynamically new comets active at large R . Evidence will be presented which suggests that these comets are compositionally different

from the periodic comets in that the sublimation may be controlled by substances more volatile than water.

The central, most important work in this thesis is the measurement and interpretation of the lightcurve of comet P/Halley spanning 20 magnitudes (a factor of 10^8 in brightness) in Chapters 2 and 8, and the extension of the same type of measurement and analysis to dynamically new comets (Chapter 9).

Most of the observations presented in this thesis were obtained in collaboration with my advisor, D. C. Jewitt. Some of the work presented in this thesis has not yet been published, the rest of the work is a synthesis of the following papers:

Jewitt, D. and K. Meech (1985), "Rotation of the Nucleus of Comet P/Arend-Rigaux", *Icarus* **64**, 329-335.

Jewitt, D. and K. J. Meech (1986), "Cometary Grain Scattering Versus Wavelength, or, 'What Color is Comet Dust' ", *Astrophys. J.* **310**, 937-952.

Jewitt, D. and K. Meech (1987), "CCD Photometry of Comet P/Encke", *Astron. J.* **93**, 1542-1548.

Jewitt, D. C. and K. J. Meech (1987), "Surface-Brightness Profiles of 10 Comets", *Astrophys. J.* **317**, 992-1001.

Meech, K. J., D. Jewitt and G. R. Ricker (1986), "Early Photometry of Comet P/Halley: Development of the Coma", *Icarus* **66**, 561-574.

Meech, K. J. and D. Jewitt (1987), "Comet Bowell at Record Heliocentric Distance", *Nature* (in press).

Meech, K. J. and D. C. Jewitt (1987), "Observations of Comet P/Halley at Minimum Phase Angle", *Astron. Astrophys.* (in press).

References

- Benvenuti, P. & Wurm, K. (1974), "Unidentified Bands in Comet Kohoutek", *Astron. & Astrophys.* **31**, 121-122.
- Bobrovnikoff, N. T. (1931), "Halley's Comet in its Apparition of 1909-1911", *Pub. Lick Obs.* **17**, 309-482.
- Code, A. D. and B. D. Savage (1972), "Orbiting Astronomical Observatory: Review of Scientific Results", *Science* **177**, 213-221.
- Code, A. D., T. E. Houck and C. F. Lillie (1972), "Ultraviolet Observations of Comets", in *The Scientific Results From Orbiting Astronomical Observatory (OAO-2)*, ed. A. D. Code, NASA SP-310, Washington, p. 109-114.
- Goldstein, R. M., R. F. Jurgens and Z. Sekanina (1984), "A Radar Study of Comet IRAS-Araki-Alcock 1983d", *Astron. J.* **89**, 1745-1754.
- Herbig, G. H. (1973), "Comet Kohoutek (1973f)", *IAU Circ.* **2596**
- Herzberg, G. & Lew, H. (1974), "Tentative Identification of the H₂O⁺ Ion in Comet Kohoutek", *Astron. Astrophys.* **31**, 123-124.
- Jackson, W. M., Clark, T., & Donn, B. (1976), "Radio Observations of H₂O in Comet Bradfield", in *The Study of Comets, Part 1*, eds. B. Donn, M. Mumma, W. Jackson, M. A'Hearn, R. Harrington, NASA SP-393, NASA, Washington D. C., p. 272-280.
- Kamoun, P. G., G. H. Pettengill and I. I. Shapiro (1982a), "Radar Detectability of Comets", in *Comets*, ed. L. L. Wilkening, Univ. of AZ Press, Tucson, AZ, p. 288-296.
- Kamoun, P., G. Pettengill and I. Shapiro (1982b), "Comet Grigg-Skjellerup: Radar Detection of Nucleus", *Bull. Amer. Astron. Soc.* **14**, 753.
- Krankowsky, D., P. Lämmerzahl, I. Herrwerth, J. Woweries, P. Eberhardt, U. Dolder, U. Herrmann, W. Schulte, J. J. Berhtelie, J. M. Illiano, R. R. Hodges and J. H. Hoffman (1986), "In Situ Gas and Ion Measurements at Comet Halley", *Nature* **321**, 326-329.
- Larson, S. M. and Z. Sekanina (1985), "Coma Morphology and Dust-Emission Pattern of Periodic Comet Halley. III. Additional High-Resolution Images Taken in 1910", *Astron. J.* **90**, 823-826.
- Lyttleton, R. A. (1953), *The Comets and Their Origin*, University Press, Cambridge.
- Lyttleton, R. A. (1972), "Does a Continuous Solid Nucleus Exist in Comets?", *Astrophys. Space Sci.* **15**, 175-184.
- Lyttleton, R. A. (1975), "Development of a Comet as it Pursues its Orbit", *Astrophys. Space Sci.* **34**, 491-510.

References, contd.

- Marsden, B. G, Z. Sekanina and D. K. Yeomans (1973), "Comets and Non-Gravitational Forces. V.", *Astron. J.* **78**, 211-225.
- Miller, F. D. (1964), "Note on the Spectrum of Comet Ikeya (1963a)", *Astrophys. J.* **139**, 766-767.
- Mumma, M. J., H. A. Weaver, H. P. Larson, D. S. Davis and M. Williams (1986), "Detection of Water Vapor in Halley's Comet", *Science* **232**, 1523-1528.
- Ogilvie, K. W., M. A. Coplan, P. Buchsler and J. Geiss (1986), "Ion Composition Results During the International Cometary Explorer Encounter with Giacobini-Zinner", *Science* **232**, 374-377.
- Oort, J. H. (1950), "The Structure of the Cloud of Comets Surrounding the Solar System, and a Hypothesis Concerning its Origin", *Bull. Astron. Institute Neth.* **408**, Vol. 11, 91-110.
- Oort, J. H. and M. Schmidt (1951), "Differences Between New and Old Comets", *Bull. Astron. Insitute Neth.* **419**, Vol. 11, 259-270.
- Reitsema, H. J., W. A. Delemere, W. F. Huebner, H. U. Keller, W. K. H. Schmidt, K. Wilhelm, H. U. Schmidt and F. L. Whipple (1986), "Nucleus Morphology of Comet Halley", in *Proceedings of the 20th ESLAB Symposium on the Exploration of Halley's Comet*", eds. B. Battrick, E. J. Rolfe and R. Reinhard, ESA Pub. Div., The Netherlands, Vol. II. p. 351-354.
- Sekanina, Z. and J. A. Farrell (1978), "Comet West 1976 VI: Discrete Bursts of Dust, Split Nucleus, Flare-Ups, and Particle Evaporation", *Astron. J.* **83**, 1675-1680.
- Sekanina, Z. and S. M. Larson (1986), "Coma Morphology and Dust-Emission Pattern of Periodic Comet Halley. IV. Spin Vector Refinement and Map of Discrete Dust Sources for 1910", *Astron. J.* **92**, 462-482.
- Wehinger, P. and S. Wyckoff (1974), " H_2O^+ in Spectra of Comet Bradfield (1974b)", *Astrophys. J.* **192**, L41-L42.
- Wehinger, P. A., S. Wyckoff, G. H. Herbig, G. Herzberg, and H. Lew (1974), "Identification of H_2O^+ in the Tail of Comet Kohoutek (1973f)", *Astrophys. J.* **190**, L43-L46.
- Whipple, F. L. (1950), "A Comet Model. I. The Acceleration of Comet Encke." *Astrophys. J.* **111**, 375-394.
- Whipple, F. L. (1951), "A Comet Model. II. Physical Relations for Comets and Meteors." *Astrophys. J.* **113**, 464-474.
- Whipple, F. L. (1961), "Problems of the Cometary Nucleus", *Astron. J.* **66**, 375-380.

References, contd.

- Whipple, F. L. (1963), "On the Structure of the Cometary Nucleus", in *The Solar System IV. The Moon, Meteorites and Comets*, eds. B. A. Middlehurst and G. P. Kuiper, Univ. of Chicago Press, Chicago, p. 639-664.
- Wilhelm, K., C. B. Cosmovici, W. A. Delamere, W. F. Huebner, H. U. Keller, H. Reitsema, H. U. Schmidt and F. L. Whipple (1986), "A Three-Dimensional Model of the Nucleus of Comet Halley", in *Proceedings of the 20th ESLAB Symposium on the Exploration of Halley's Comet*, eds. B. Battrock, E. J. Rolfe and R. Reinhard, ESA Pub. Div., The Netherlands, Vol. II. p. 367-369.
- Wyckoff, S. (1982), "Overview of Comet Observations", in *Comets*, ed. L. L. Wilkening, Univ. of AZ Press, Tucson, AZ, p. 3-55.

Chapter 2 - Modelling P/Halley Preperihelion

***"I can hardly doubt that the comet was fairly evaporated . . .
by the heat, and resolved into transparent vapour . . . "***

John Herschel (1847) of comet Halley on Jan 28, 1836.

2.1 Introduction

There is much to be learned from observations of comets over a large range of heliocentric distances. Such observations might reveal, for instance, the heliocentric distance at which true cometary characteristics first appear and so might provide a critical test of water ice sublimation models. It is generally believed that the sublimation of water ice does not contribute significantly to coma production at distances much beyond 2 - 3 AU. A few comets have been discovered at large heliocentric distances with very extended comae (e.g.: Kohoutek at $R = 4.6$ AU and Bowell (1980b) at $R = 7.3$ AU); however, processes other than H_2O sublimation are thought to control the coma formation in these cases. Comet P/Halley is especially interesting in this regard since it was recovered at an unusually large heliocentric distance, more than three years before perihelion. In this chapter a simple model for the cometary activity will be presented which will show evidence of coma formation at $R \approx 5.9$ AU which can be attributed to water ice sublimation.

The first observations at $R = 11.04$ AU (Jewitt *et al.*, 1982) marked the beginning of a concerted effort to monitor the brightness as a function of heliocentric distance; the following is a brief review of the main results of this effort. The earliest post-recovery observations (Belton and Butcher, 1982; Baudrand *et al.*, 1982; Belton *et al.*, 1983; Belton and Butcher, 1983 and Sicardy *et al.*, 1983) showed that the comet had a stellar profile, without a hint of coma or tail. Fluctuations in the brightness on timescales of hours and days were reported by several observers while the comet was between $R = 8$ and 11 AU. For example, West and Pedersen (1983) observed a brightness increase of 1.0 ± 0.4 mag at $R \approx 10.6$ AU (between

1982 December 10 and 1983 January 14). They found the image of P/Halley in 1983 January to be somewhat larger than the measured seeing but they could not uniquely attribute the larger profile to coma as opposed to guiding errors. Photometry at $R = 8.2$ AU (1984 January) by Jewitt and Danielson (1984) showed a stellar comet image but again with brightness variations of about 1 mag. The variations occurred on timescales less than the diaphragm-crossing time, suggesting that they could not be due to a freely expanding coma of refractory grains. A limit to the surface brightness of any coma was placed at $V_s > 28.0$ mag arcsec⁻² at 4 arcsec from the nucleus. A comparable limit was obtained from observations later in the month by West and Pedersen (1984). Le Fevre *et al.* (1984) reported recurrent brightness increases of about 2 magnitudes when the comet was at $R = 8$ AU (1984 February). They suggested that the variations were caused by rotation of the nucleus, although they did not completely rule-out periodic bursts of dust from the nucleus as being responsible. They were unable to specify the rotation period. The first evidence of coma was announced by Spinrad *et al.* (1984). Their observation of a faint extension 6 arcsec to the north of the nucleus was taken when P/Halley was at $R = 6.1$ AU (1984 September 25 - 27).

In the following sections new photometry of P/Halley will be presented which was obtained when the comet was at $R = 5.9$ and $R = 5.1$ AU, during 1984 October and 1985 January, respectively. These observations will be compared and contrasted with data obtained at larger heliocentric distances. It will be argued that sustained mass loss from the nucleus began at about $R = 5.9$ AU, at a rate which is consistent with production by sublimation from a predominately water-ice nucleus.

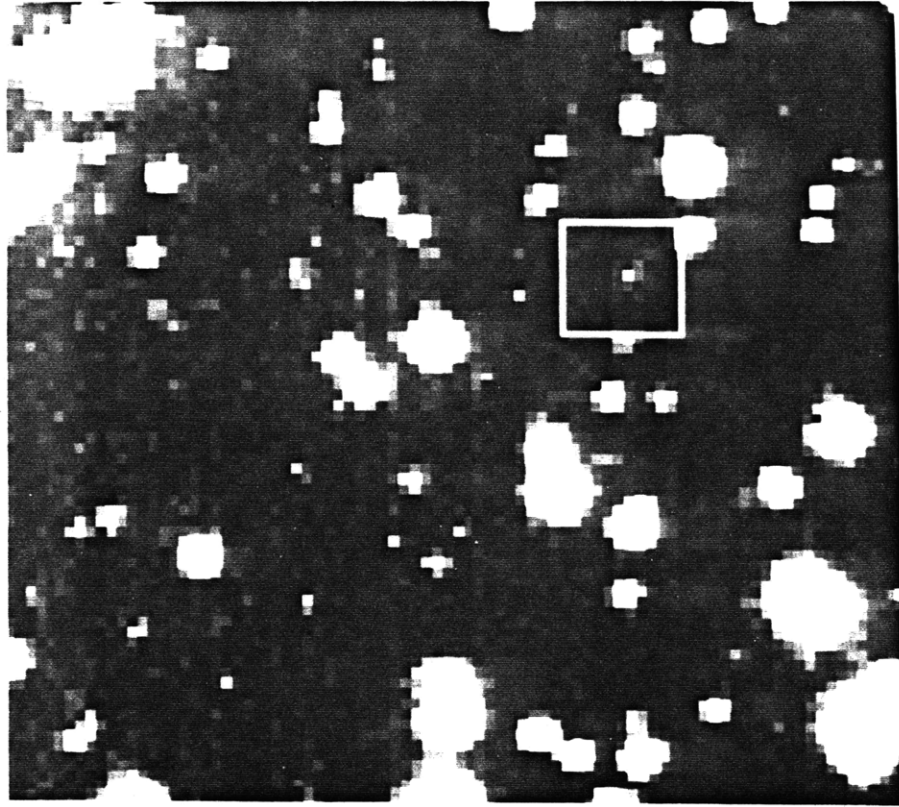
2.2 Observations

The present observations were obtained using the MASCOT charge coupled device (CCD) camera (Meyer *et al.*, 1980). This two-channel instrument was used in its direct

imaging mode with a Johnson filter, R_J (central wavelength $0.7 \mu\text{m}$ and $0.2 \mu\text{m}$ FWHM). The MASCOT was placed at the $f/13.5$ Cassegrainian focus of the 1.3m telescope of the McGraw-Hill Observatory on Kitt Peak. The image scale on the 490×328 pixel Texas Instruments chip was 1.6 arcsec per $25 \mu\text{m}$ pixel. Useful images were obtained on the nights of UT 1984 October 22, 24, 27 and UT 1985 January 18, 19, 20 and 21. For instrumental reasons, the telescope was tracked at sidereal rate during all observations. In 1984 October the motion of the comet with respect to the stars was cancelled by moving the software autoguider by one pixel in R.A. at time intervals corresponding to the expected motion divided by the pixel size. Exposures ranged from 600 -1200 seconds. The maximum trailing of the comet image was of order 1 pixel (1.6 arcsec) which was smaller than the atmospheric seeing ($\approx 2 \text{ arcsec}$ FWHM). In October, comet P/Halley appeared projected so close to the galactic plane that as many as 60% of the observations were affected by glare from bright field stars. The affected observations have not been used in the present work. The October data were obtained during non-photometric conditions; relative but uncalibrated photometry among frames on each night was established by measuring several bright field stars on each frame. Absolute calibration was achieved when the nightly October fields were re-exposed in photometric conditions in January. A representative image from 1984 October is shown in Figure 2-1.

In 1985 January the comet was coincidentally projected against a dark interstellar cloud, thus reducing the problems caused by adjacent bright stars. However, the resulting lack of suitable guide stars meant that the exposures had to be kept short in order to minimize trailing due to the motion of the comet with respect to the sidereal rate. The January seeing was in the range 2 - 3 arcsec FWHM.

Figure 2-1 MASCOT CCD image of comet P/Halley taken UT 1984 October 24 8:41 (observation number 6 in Table 2-1). North is to the top, East is to the right in the figure. The box around the image of P/Halley is 16 arcsec square.



2.3 Data Reduction

Bias level and dawn sky flat-field calibration exposures were taken each night. Intrinsic pixel to pixel sensitivity differences were removed, after bias subtraction, by dividing each image by the nightly mean flat field. In October, photometry of comet P/Halley was obtained within square diaphragms of 10 - 15 arcsec width centered on the apparent nucleus of the comet. The diaphragms were large compared with the atmospheric seeing and with any trailing of the image. Because of the diffuse appearance of the comet in January, the diaphragms were increased to 15 - 20 arcsec in width. Measurements showed that the brightness of the comet remained essentially constant in all larger diaphragms, implying that there was negligible contribution to the total brightness from any extended coma beyond the diaphragm. The largest source of error in the photometry was the uncertainty in the determination of the sky background. In regions where star crowding was not a problem, this uncertainty was found to be smaller when using square instead of circular diaphragms, probably because of residual column to column sensitivity differences left after flattening. When faint objects were too close to P/Halley to be excluded from the diaphragm, both the objects and the comet were measured together. Subsequent measurements of the faint objects in all frames where the comet - object separation was large compared to the diaphragm size enabled the comet brightness to be recovered. In some instances it was not possible to either isolate the comet or use a diaphragm sufficiently large to measure the comet and the nearby stars. For images such as this, the background was estimated by fitting a plane to regions outside the coma (as judged from other less crowded fields).

Photometric calibration of the data was obtained from observations of the standard stars Feige 34, BD+25°1981, BD+21°607, BD+54°1216 and HD 19445 (Thuan and Gunn, 1976). These observations showed that each of the nights 1985 January 18-21 was photometric to better than 3%. The observations are listed in Table 2-1. The first 5 columns

Table 2-1
P/Halley Photometry

#	DATE 1984/85	UT [midtime]	EXP [sec]	χ	R_J	$V(1,1,\alpha)$	R^\dagger [AU]	Δ^\S [AU]	α^\ddagger [deg]
1	OCT 22	9:48	900	1.26	20.49 ± 0.30	13.44	5.90	5.52	9.23
2	OCT 22	10:58	1200	1.11	20.84 ± 0.15	13.79	5.90	5.52	9.23
3	OCT 22	11:29	1200	1.07	20.80 ± 0.30	13.75	5.90	5.52	9.23
4	OCT 22	12:29	1100	1.07	21.08 ± 0.30	14.03	5.90	5.52	9.23
5	OCT 24	8:19	900	1.70	20.62 ± 0.50	13.60	5.89	5.48	9.14
6	OCT 24	8:41	900	1.53	20.58 ± 0.20	13.56	5.89	5.48	9.14
7	OCT 24	9:01	600	1.42	20.46 ± 0.20	13.44	5.89	5.48	9.14
8	OCT 24	9:17	600	1.34	20.49 ± 0.15	13.47	5.89	5.48	9.14
9	OCT 24	9:33	600	1.28	20.77 ± 0.20	13.75	5.89	5.48	9.14
10	OCT 24	10:01	600	1.20	20.31 ± 0.15	13.29	5.89	5.48	9.14
11	OCT 24	12:15	600	1.06	20.49 ± 0.20	13.47	5.89	5.48	9.14
12	OCT 27	9:13	600	1.31	21.27 ± 0.20	14.28	5.87	5.42	9.02
13	OCT 27	9:29	661	1.25	21.16 ± 0.20	14.17	5.87	5.42	9.02
14	JAN 18	3:14	600	1.19	19.38 ± 0.10	13.19	5.12	4.30	6.59
15	JAN 19	2:56	600	1.22	19.14 ± 0.10	12.95	5.11	4.30	6.73
16	JAN 19	3:29	600	1.14	19.11 ± 0.30	12.92	5.11	4.30	6.73
17	JAN 19	4:39	600	1.07	19.22 ± 0.15	13.03	5.11	4.30	6.74
18	JAN 19	5:12	600	1.06	19.44 ± 0.10	13.25	5.11	4.30	6.74
19	JAN 19	7:23	600	1.28	19.51 ± 0.10	13.32	5.11	4.30	6.76
20	JAN 19	7:58	600	1.43	19.40 ± 0.20	13.21	5.11	4.30	6.76
21	JAN 20	2:35	600	1.26	19.32 ± 0.10	13.14	5.10	4.30	6.92
22	JAN 20	3:39	600	1.06	19.31 ± 0.25	13.13	5.10	4.30	6.93
23	JAN 20	4:11	600	1.06	19.00 ± 0.10	12.82	5.10	4.30	6.93
24	JAN 20	5:17	600	1.07	19.04 ± 0.15	12.86	5.10	4.30	6.94
25	JAN 20	5:53	600	1.09	19.15 ± 0.10	12.97	5.10	4.30	6.95
26	JAN 20	6:23	600	1.13	19.19 ± 0.25	13.01	5.10	4.30	6.95
27	JAN 20	6:57	600	1.21	19.28 ± 0.10	13.10	5.10	4.30	6.96
28	JAN 21	2:42	600	1.23	19.01 ± 0.15	12.83	5.09	4.30	7.12

† Heliocentric distance.

§ Geocentric distance.

‡ Phase angle in degrees.

list the observation number, the date, the UT midtime of the observation, the exposure duration in seconds, and the airmass, respectively. The R_J magnitudes of the comet appearing in column 6 of Table 2-1 were obtained using extinction coefficients determined nightly from field stars. The uncertainties on the tabulated R_J magnitudes reflect the uncertainties of the sky

brightness near the comet in each image (0.1-0.3 mag), extinction correction uncertainty (0.03 mag) and absolute photometric calibration uncertainty (< 0.1 mag).

To be consistent with the majority of observations published by other observers, all observations are converted to the V magnitude system. The conversion from the R_J magnitudes presented in Table 2-1 has been made assuming solar color $V - R_J = 0.52$ (Allen, 1976). The V magnitudes are plotted as a function of the Julian Date in Figure 2-2. Photometry from Jewitt and Danielson (1984) is also shown, using the relations given there for converting between the Thuan and Gunn (1976) g and r filters and the Johnson filters. A heliocentric distance scale is shown at the top of the figure.

The brightness of comet Halley is seen (Figure 2-2) to increase by almost 5 magnitudes between $R = 11$ AU and $R = 5.1$ AU but also to fluctuate on short timescales (probably due to the rotation of the nucleus), with a range of about 1 mag prior to 1984 October. The general brightness increase is largely due to the changing position of the comet relative to the sun and earth. The solid line in the figure represents an inert "asteroidal" nucleus model in which the magnitude is taken to vary as

$$V(R,\Delta,\alpha) = V(1,1,0) + 2.5 \log (R^2 \Delta^2) + \phi(\alpha) \quad (2.1)$$

where the constant $V(1,1,0)$ is the V magnitude at unit heliocentric distance, $R = 1$, and geocentric distance, $\Delta = 1$, and at 0° phase angle. (Throughout most of the observing period the phase angle remained small, therefore the phase function term in Eq. 2.1, $\phi(\alpha)$, will be neglected). The constant $V(1,1,0)$ will thus be expressed as $V(1,1,\alpha)$ to account for the fact that the phase term is not included. Figure 2-2 shows that the general increase in the brightness of the comet by a factor of 15 from $R = 11$ AU to $R = 5.9$ AU, is consistent with the inverse square law (Eq. 2.1). By implication, the mean cross-section of the comet remained constant over the stated heliocentric distance range, implying that the nucleus was

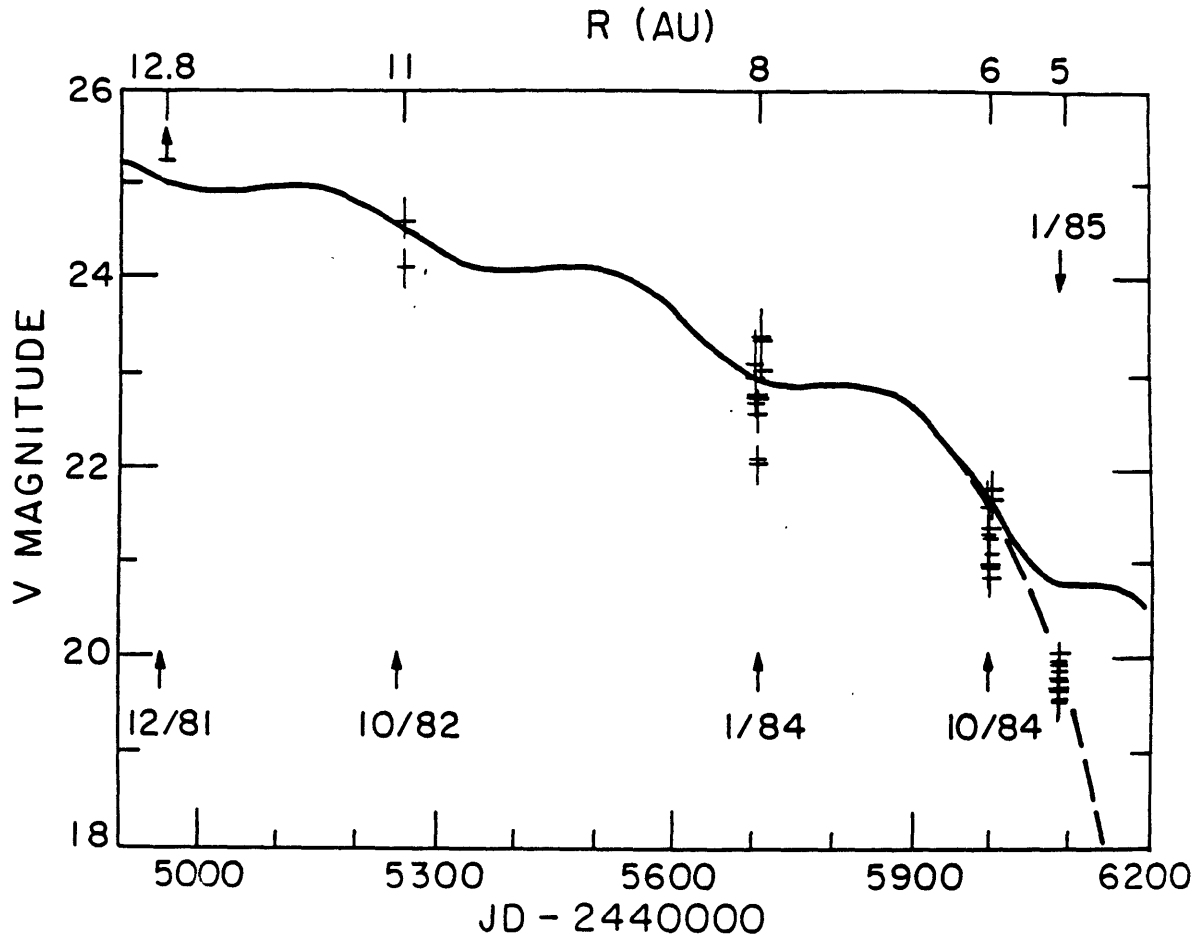


Figure 2-2 The Johnson V magnitudes of comet P/Halley (from Jewitt and Danielson (1984) and the present work) are plotted versus Julian Day Number (JD 2444900.0 = 1981 October 22.5 UT). The measurement from 12/81 represents a pre-recovery magnitude limit. The solid line represents an inert nucleus model with zero phase coefficient (Eq. 2.1). The normalization has been determined from observations prior to 1984 October. Note the enhanced brightness of the comet with respect to the inert nucleus during January 1985. The dashed line represents the total V magnitude (contributions from the nucleus and the coma) for a sublimating H₂O nucleus model as described in the text. The heliocentric distance in AU is indicated at the top of the figure. The scatter in the data at each distance is significant and reflects the rotation of the nucleus.

directly visible prior to $R = 5.9$ AU. Using all available P/Halley observations at $R > 5.9$ AU (i.e. prior to 1984 October; see Tables 2-1 and 2-2, and Jewitt and Danielson, 1984), the weighted mean value of the constant in Eq. (2.1) is found to equal

$$V(1,1,\alpha) = 14.17 \pm 0.03 \quad (2.2)$$

magnitudes. The formal uncertainty is the standard error of the mean of 64 observations. The neglect of the nucleus phase function in Eq. (2.1) may cause $V(1,1,0)$ to differ from the value given in Eq. (2.2) by at most a few times 0.1 mag. By 1985 January the comet was consistently brighter than expected from the "asteroidal" model (Eq. (2.1)), suggesting the presence of a coma about comet Halley at $R = 5.1$ AU. Specifically, about two thirds of the light from the comet at this R was due to coma.

2.4 Discussion

2.4.1 Sublimating Nucleus Model

The new photometry, in combination with the photometry of other observers, will be used to constrain the possible mechanisms which might produce the brightness increase observed in P/Halley at $R = 5.1$ AU. In particular, was the brightness increase seen in 1985 January due to mass loss from the nucleus caused by the sublimation of H_2O ice? Note that the following simple model for the sublimation of a water ice nucleus contains many free parameters for which only estimates can be made: the model is certainly non-unique. The intent is simply to show that a sublimating water ice nucleus model can reasonably account for the presence of coma at $R = 5.1$ AU.

In the absence of gaseous emission features (suggested, for example, by the spectrum

Table 2-2
Other Sources of P/Halley Magnitudes

Date	Heliocentric Distance	Reference
12/81	12.80	Felenbok <i>et al.</i> (1982)
10/82	11.03	Belton & Butcher (1982)
10/82, 11/82	11.04, 10.86	Sicardy <i>et al.</i> (1983) Baudrand <i>et al.</i> (1982)
12/82, 1/83	10.72, 10.51	West & Pedersen (1983)
12/82	10.70	Belton & Butcher (1983)
02/83	10.33	Belton <i>et al.</i> (1983)
12/83, 1/84	8.21, 8.01	Racine (1984) Pedersen & West (1984)
01/84	8.01	West & Pedersen (1984)
02/84	7.96	Belton <i>et al.</i> (1985)
02/84	7.96	Le Fevre <i>et al.</i> (1984)
03/84	7.75	Belton <i>et al.</i> (1984)
09/84	6.13	Spinrad <i>et al.</i> (1984)
10/84, 11/84	5.84, 5.60	Belton <i>et al.</i> (1985)
11/84	5.60	Wyckoff <i>et al.</i> (1985a)
02/85	4.84	Wehinger <i>et al.</i> (1985)

of Wehinger *et al.*, 1985), the optical brightness of the comet is due to scattering both from the nucleus and from solid grains in the coma. The brightness of the nucleus is described by Eq. (2.1), in which $V(I, I, \alpha)$ provides a measure of the product of the optical geometric albedo with the square of the radius of the nucleus.

The amount of scattered light received from the coma is proportional to the total dust grain cross section, $\pi\beta^2$ [m²], where

$$(p_v \beta^2)_{\text{coma}} = 2.235 \times 10^{22} R^2 \Delta^2 10^{0.4[V_0 - V_{\text{coma}}]} \quad (2.3)$$

where Δ^2 assumes that all of the coma is contained within the observing diaphragm (see Appendix 2 for the derivation of this equation). Here R and Δ are in AU, $V_0 = -26.74$ is the V magnitude of the sun (Allen, 1976), p_v is the geometric albedo of the grains in the V filter passband, and β [m] is the radius of a sphere of cross section equal to the total grain cross section. The mass of grains within the projected photometry diaphragm is equal to the product of the total mass loss rate from the nucleus, dM/dt [kg s⁻¹], with the time, t [s], spent in the diaphragm (this relation is valid provided the diaphragm crossing time is short compared with the time for R , hence dM/dt , to change appreciably). The mass of the grains, M_{tot} , is related to the total cross section of grains in an optically thin coma, $\pi\beta^2$ (see Appendix 4 for a discussion of the optical thickness in the coma). Here $\pi\beta^2 = N\sigma$ where N is the number of grains and $\sigma \approx \pi a^2$ is the cross section per grain. N is equal to M_{tot} / m where $m = 4 \pi a^3 \rho / 3$ is the mass of a grain. Assuming $M_{\text{tot}} = (dm/dt) t$ gives:

$$(p_v \beta^2)_{\text{coma}} = \left(\frac{3 p_v}{4 \pi \rho a} \frac{dM}{dt} \right) t \quad (2.4)$$

where $\rho = 1000 \text{ kg m}^{-3}$ is the assumed grain density, and the representative grain size is taken to be $a = 1 \mu\text{m}$. (The absence of a blue continuum in P/Halley (Brooke and Knacke, 1985; Wehinger *et al.*, 1985) suggests that the mean grain size is larger than a wavelength.) The diaphragm crossing-time in Eq. (2.4) may be approximated by $t = x/v$ where x [m] is the projected diaphragm radius at the comet and v [m s⁻¹] is the average speed of the grains

relative to the nucleus. The empirical relation of Bobrovnikoff (1954) as modified by Delsemme (1982), $v \approx 600 R^{-0.5} \text{ m s}^{-1}$ (R in AU), provides a useful approximation to the grain velocity (see also Appendix 6 for a more detailed discussion of grain velocity in a gas flow). The total brightness of the grain coma, in magnitudes, is found by combining equations (2.3) and (2.4)

$$V_{\text{coma}} = 30.7 - 2.5 \log_{10} \left[\frac{p_v \left(\frac{dM}{dt} \right) t}{\rho a R^2 \Delta^n} \right]. \quad (2.5)$$

For measurements where the observing diaphragm does not include all of the coma, we put $n = 1$. This arises because the surface brightness in an optically thin coma varies as the reciprocal of the projected distance from the nucleus (see Appendix 4 for a complete discussion). When the coma is entirely included within the diaphragm the inverse square law holds and $n = 2$. The total mass loss rate in Eq. (2.5) may be obtained from the energy balance equation for a sublimating nucleus in thermal equilibrium:

$$\frac{F_o (1 - A)}{R^2} = \chi \left[\varepsilon \sigma T^4 + L(T) \left(\frac{dm_s}{dt} \right) + \kappa \frac{dT}{dz} \right] \quad (2.6)$$

where F_o is the Solar constant ($1360.74 \text{ J s}^{-1} \text{ m}^{-2}$ at $R = 1 \text{ AU}$), A is the Bond albedo, χ is a "rotation parameter" (equal to 2 for a half isothermal nucleus and equal to 4 for an isothermal nucleus), ε is the infrared emissivity, $\sigma = 5.669 \times 10^{-8} \text{ J s}^{-1} \text{ m}^{-2} \text{ K}^{-4}$ is the Stephan-Boltzman constant, $L(T) [\text{J kg}^{-1}]$ is the latent heat of sublimation, $dm_s/dt [\text{kg s}^{-1} \text{ m}^{-2}]$ is the mass loss rate per unit area, κ is the thermal conductivity [$\text{J s}^{-1} \text{ m}^{-1} \text{ K}^{-1}$] and $dT/dz [\text{K m}^{-1}]$ is the temperature gradient. A rapidly rotating nucleus may be defined as one which has a rotation

period which is short compared to the time required for the sublimation to drop to a level where gas drag is insufficient to remove dust into the coma. In this context, a rapidly rotating nucleus is one which is sublimating into both the daytime and nighttime hemispheres. The slowly rotating nucleus, by analogy, is one which is sublimating primarily on the sunlit hemisphere. For the purpose of these computations the Bond albedo is set equal to p_v . Smoluchowski (1981) suggests that for even slightly porous cometary ice, the thermal conductivity drops to below 1% of that of solid ice. This is consistent with measurements of terrestrial snows (Langham, 1981), which are good insulators. The term describing the conduction of heat into the interior is therefore assumed to be negligible in the nucleus heat balance.

The latent heat as a function of temperature, $L(T)$ [J kg^{-1}], is determined from a fit to data from Delsemme and Miller (1971) made by Cowan and A'Hearn (1982) (see Appendix 3). The mass loss rate per unit area, $dm_s/dt = (dM/dt) / (\chi\pi\beta^2)$, is related to the sublimation vapor pressure, $P(T)$, via

$$\frac{dm_s}{dt} = P(T) \sqrt{\frac{\mu m_h}{2 \pi k T}} \quad (2.7)$$

where $[(2kT/\pi\mu m_h)^{1/2}]/2$ is the average speed of the molecules leaving the surface. The sublimation vapor pressure is obtained from an empirical fit to measurements made by Washburn (1928) (see Appendix 3). Alternatively, the vapor pressure may be computed using the Clausius-Clapeyron equation which gives the approximate relation for the pressure of a vapor in equilibrium with a solid:

$$\frac{dP}{dT} = \frac{L}{T \Delta V} \quad (2.8)$$

where $\Delta V = V_g - V_s \approx V_g$ is the difference between the specific volumes of the gas and solid [$\text{m}^3 \text{kg}^{-1}$]. The specific volume may be obtained from the equation of state for an ideal gas:

$$V_g = \frac{k T}{\mu m_H P(T)} . \quad (2.9)$$

Neglecting the temperature dependence of the latent heat, Eq. (2.8) may be integrated to obtain the vapor pressure as a function of temperature:

$$P(T) = P_o \exp \left[\frac{L \mu m_H}{k T_o} \right] \exp \left[- \frac{L \mu m_H}{k T} \right]. \quad (2.10)$$

This method is used only when direct measurements of the vapor pressure of ices are unavailable.

Equations (2.6) and (2.7) were solved iteratively for dm_j/dt and combined with Eq. (2.5) and the nuclear magnitude (Eq. (2.1)) to produce the model plotted in Figure 2-2 as a dotted line. The parameters and assumptions used in all the model computations are summarized in Table 2-3. Models including both rapid and slow nucleus rotation have been computed, although only a slowly rotating nucleus model has been plotted. Note from the figure that this model fits the observations rather well. The rapid nucleus rotation models, however, do not fit the data. They more closely resemble the asteroidal nucleus model because rapid rotation lowers the mean surface temperature of the nucleus, thereby reducing sublimation. For the same reason, only low albedo nuclei ($A < 0.15$) give significant sublimation near $R = 6$ AU. The constant $V(1,1,\alpha) = 14.17$ (Eq. 2.2), when substituted into Eq. 2.3, gives a nucleus cross section

$$p_v \beta_n^2 = (0.97 \pm 0.03) \times 10^6 \text{ m}^2. \quad (2.11)$$

The cross section given in Eq. 2.11 may be taken to refer to the bare nucleus of P/Halley, since no coma was apparent at $R \geq 8$ AU. An effective nucleus radius, β_n , in the range

$$2.5 \leq \beta_n \text{ [km]} \leq 7.0 \quad (2.12)$$

is computed from Eq. (2.11) using albedos suggested by the model ($0.02 < p_v < 0.15$). Formally, sublimation models which fit the coma photometry can be constructed with $p_v = 0$. However, $p_v = 0.02$ is the practical lower limit on the albedo, here set equal to the albedo of the darkest known Solar System objects. The upper limit on the albedo, (hence the lower limit on the radius of the nucleus), is well constrained, since water ice sublimation models using albedos > 0.15 cannot be made to fit the photometry. Clark (1982) has suggested that only a very small amount of dark particulate material is needed to significantly darken an ice surface (≈ 0.1 to 1% contaminants by weight). The low nucleus albedo suggests that the surface ice is dirty.

2.4.2 Comparison of Model With Other Observations

The agreement between the model and the observations persists when the observations of other investigators are included. Figure 2-3 presents the absolute $V(1,1,\alpha)$ magnitudes of P/Halley calculated using data from this paper, from Jewitt and Danielson (1984), and from the sources listed in Table 2-2. The horizontal line in the figure represents the "asteroidal" nucleus model (Eq. 2.1). Solid lines show two slow-rotation nucleus models with input parameters as listed in Table 2-3. The smaller values quoted in the table (*i.e.*: slow rotation, low albedo) produce the model which shows the earliest onset of coma production. It is

Table 2-3
H₂O Model Parameters

Model Parameter	Symbol	Value*	Units	Notes
nucleus cross section	$p_v \beta^2$	0.97×10^6	m^2	Equation (2.11)
geometric albedo	p_v	0.02 - 0.15		typical for dark bodies
bond albedo	A	0.02 - 0.15		set equal to p_v
infrared emissivity	ϵ	0.85 - 0.90		
phase function	$\phi(a)$	0		assumed
density	ρ, ρ_n	$0.7-1.3 \times 10^3$	$kg\ m^{-3}$	for water ice
grain size	a	$1-1.5 \times 10^{-6}$	m	see text
atomic mass	μ	18		H ₂ O
dust/gas ratio	ψ	1		assumed
spin parameter	χ	2, 4		slow, fast

* Ranges of parameters which produce sublimating water nucleus models consistent with the data.

apparent from Figure 2-3 that measurable coma production may have begun on the nucleus of P/Halley, as far out as $R \approx 5.9$ AU (1984 October). The water model can readily account for the coma observed at $R = 5.9$ AU, *provided the nucleus is both dark and slowly rotating*. The model successfully reproduces the observed rapid brightness increase at smaller heliocentric distances.

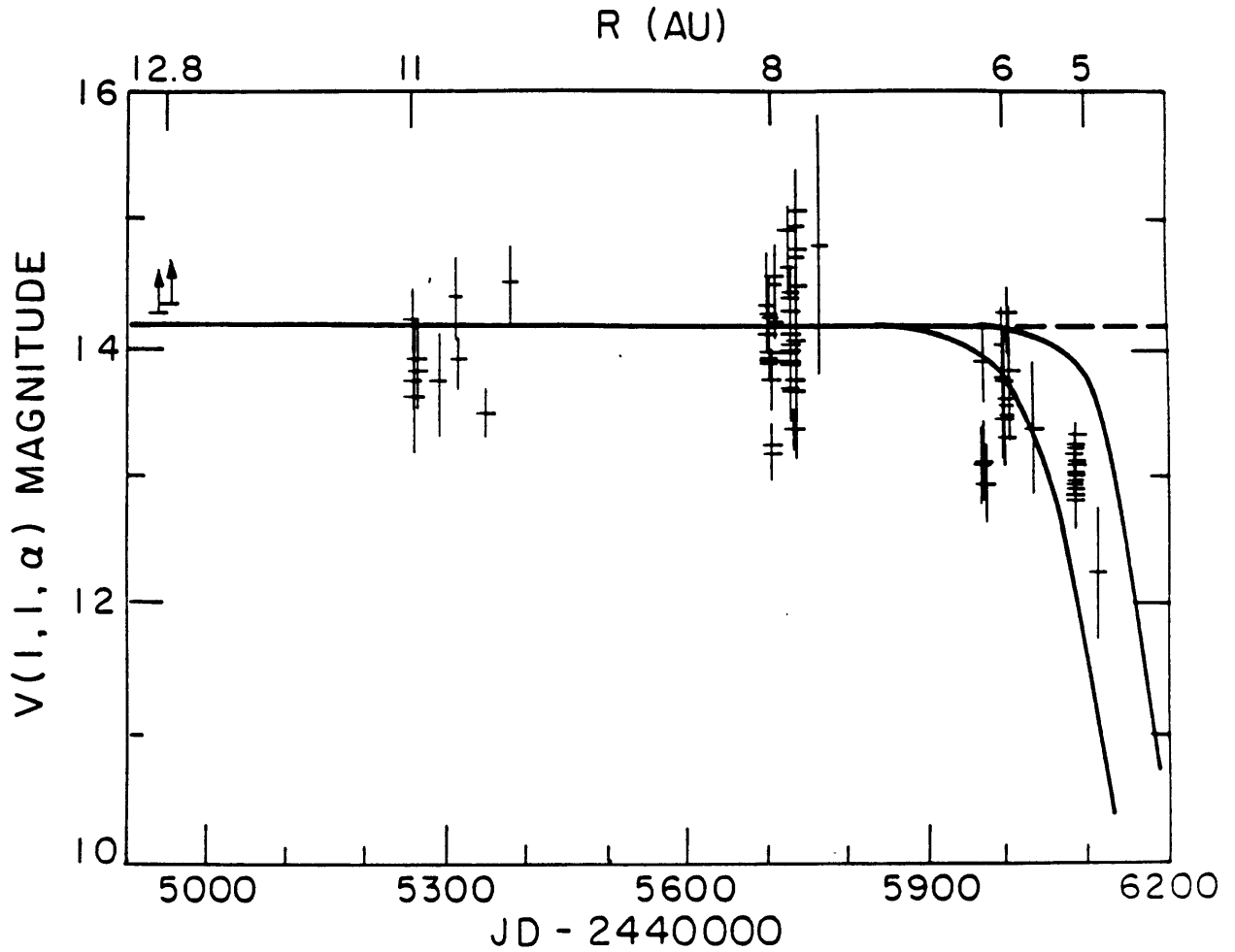


Figure 2-3 The total $V(1,1,\alpha)$ magnitude of P/Halley (magnitude reduced to unit R and Δ) is plotted versus Julian Day Number. Data are from the present work, from Jewitt and Danielson (1984) and from sources listed in Table 2-2. The absolute visual magnitude of the nucleus, $V(1,1,\alpha) = 14.17$, is shown as a horizontal line. The solid lines represent two sublimation models of a low albedo, slowly rotating nucleus with a plausible range of input parameters as described in the text (see Table 2-3).

The October images of the comet discussed in this work showed no evidence of an extended coma down to a limit of ≈ 26.8 mag arcsec⁻². A low surface brightness coma ($V_s > 27$ mag arcsec⁻²) could therefore have gone unnoticed in October. In contrast, the images of P/Halley in 1985 January were somewhat extended and diffuse. Figure 2-4 presents a surface brightness profile of the comet on UT January 20.24 computed by azimuthal averaging of pixels in concentric annuli centered on the nucleus. A star profile from the same CCD image is shown for comparison. The star and comet profiles are normalized to the same peak surface brightness. For comet Halley, 100 surface brightness units correspond to $V_s = 23.7$ mag arcsec⁻². Figure 2-4 clearly shows coma extending several times 10^7 m from the nucleus of P/Halley in 1985 January. The fact that photometry from 1984 October to 1985 February and beyond shows a growing separation from the inert nucleus model (see Figures 2-2 and 2-3), suggests strongly that *sustained* coma production began near 1984 October at $R \approx 5.9$ AU.

Recently, Cruikshank *et al.* (1985) have claimed to measure the color and size of the *nucleus* of comet P/Halley using observations taken at $R = 4.8$ AU (1985 February). However, when compared with Figure 2-3, their photometry is similar to other photometry reported near this time and the comet is brighter than expected from the asteroidal nucleus model (Eq. (2.1)) by about 1.2 magnitudes. Hence we believe that their observations refer as much to the coma as they do to the nucleus, and are consistent with our finding sustained coma production in February.

Another recent paper by Wyckoff *et al.* (1985b) presents photometry derived from continuum spectra of comet P/Halley. They use their data, in addition to a small subset of the P/Halley data published prior to 1985 February, to suggest that the onset of sublimation began near 6 AU. The spectra taken in February, March and April of 1985, were obtained several months after the brightening of the comet seen in 1984 September and October. Assuming a I/p coma profile (where p is the projected distance from the nucleus), and using the estimate

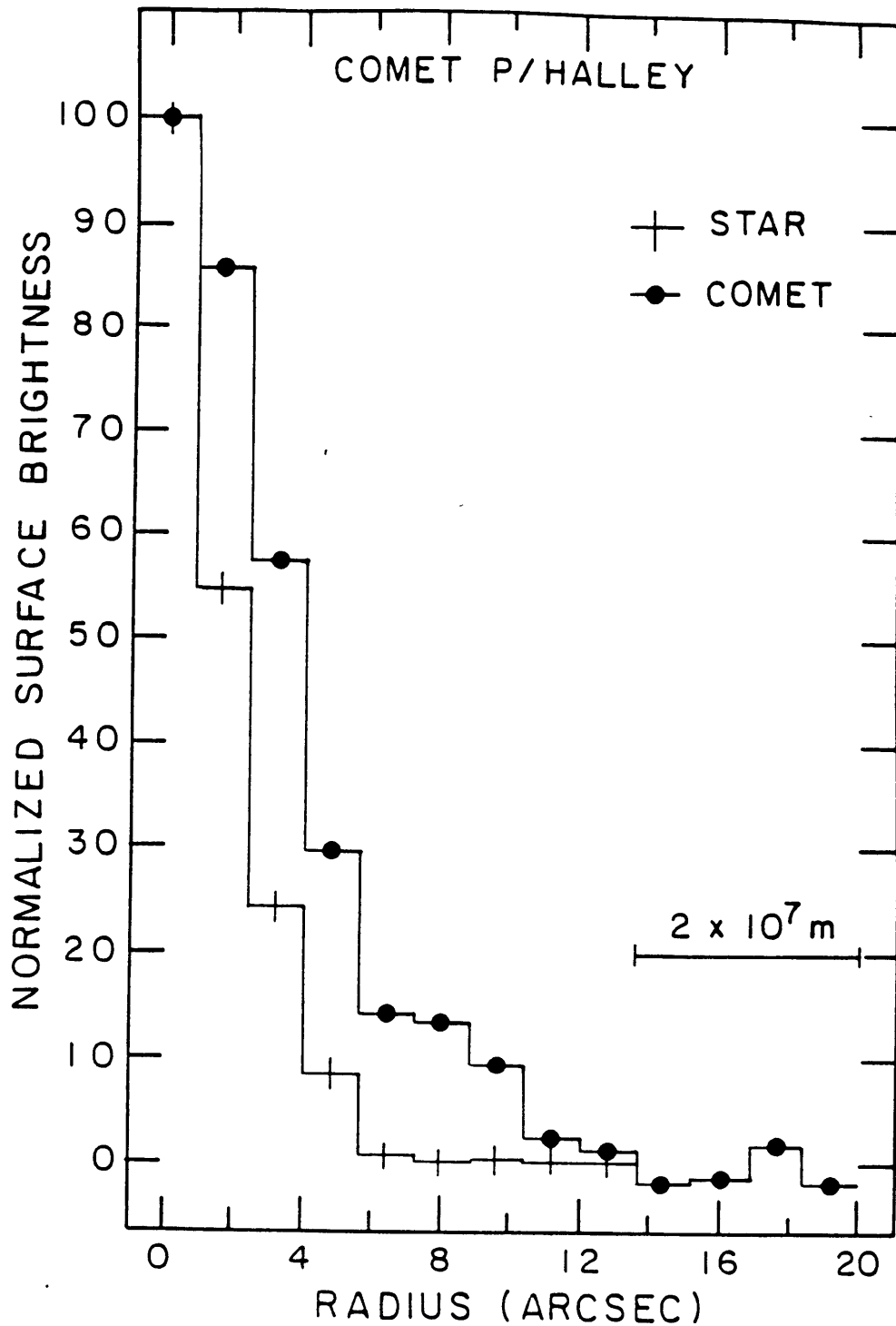


Figure 2-4 Azimuthally averaged surface brightness distribution of comet P/Halley in 1985 January (observation number 25 in Table 2-1). The surface brightness distribution from a field star on the same image is shown for comparison. The curves have been normalized to 100 hundred surface brightness units at the peak. For comet Halley this corresponds to $V_s = 23.7 \text{ mag arcsec}^{-2}$. The average sky brightness near the comet is $\approx 21.8 \text{ mag arcsec}^{-2}$ in the V filter.

that $\approx 60\%$ of the total light was contributed by the coma in January, the correction for their diaphragm size (2.5 arcsec radius) is estimated to be at least 1 mag. Even without correcting for their use of a small diaphragm, the photometry from the spectra is more than 1 mag brighter than the asteroidal model. The present work strengthens the conclusion that the coma formation began around 6 AU and further shows that it is consistent with sublimation from a predominantly water-ice nucleus of low albedo.

The optical cross section derived by Wyckoff *et al.* (1985b) appears to be in error by a factor of π , but otherwise agrees with the value in Eq. (2.11) within the uncertainties of measurement.

2.4.3 Other Coma Producing Mechanisms

Mechanisms, which might produce a grain coma, other than water ice sublimation, will now be briefly considered. Other comets which appear active at large R have comae which may be controlled by the sublimation of substances more volatile than water, such as CO_2 . The model in §2.4.1 was used to compute a light-curve for a coma produced by pure CO_2 ice sublimation using the latent heat measured by Smith (1929) and the vapor pressure as fit to data by Eggerton and Edmondson (1928) (see Appendix 3). When restricting the albedo of the nucleus to fall within the range of known Solar System albedos, the resulting CO_2 nucleus sublimation model does not fit the P/Halley photometry in the sense that the CO_2 model yields a curve which is too shallow to follow the rapid brightening of P/Halley seen after 1984 October. However, if albedos of $p_v > 0.9$ are allowed, the resulting CO_2 sublimation model does follow the rapid brightening of the comet seen around 5.9 AU; however, the fit to the data is not as good as that for H_2O ice. For this reason, and because albedos this high are not likely, there is no evidence that CO_2 controlled the onset of sublimation of P/Halley seen at $R = 5.9$ AU. This does not suggest that small amounts of volatiles other than H_2O are not

present, only that their influence on the mass loss is small.

It has been suggested by Lanzerotti *et al.* (1978) that the dominant process for the erosion of water ice from the surfaces of interplanetary grains at large heliocentric distances is sputtering by energetic solar wind protons. From Figure 2-1 of their paper, the water ice erosion rate at $R = 5.9$ AU corresponds to $dM/dt \approx (1 - 10) \times 10^{-7} \text{ kg s}^{-1}$ when integrated over the surface of a 3 - 7 km radius nucleus. The mass loss rate computed using the present model at the same heliocentric distance is $dM/dt \approx (4 - 40) \times 10^{-3} \text{ kg s}^{-1}$. Hence, sputtering by solar wind protons gives a mass loss rate many orders of magnitude too small to be considered a plausible coma producing mechanism, even in 1984 October.

The amorphous-to-crystalline phase transition in water ice may provide an internal energy source in comets (Klinger, 1980). The transition occurs at a temperature similar to the probable nucleus temperature of P/Halley at the time of its first activity ($T \approx 135$ K). However, the transition does not represent a likely energy source for comet P/Halley since the outer layers of its nucleus have almost certainly been heated above this temperature during previous orbits.

2.5 Conclusions

1. The observed increase in the mean brightness of comet P/Halley, from $R = 11$ AU to $R = 5.9$ AU, is consistent with the increase expected of an "asteroidal" nucleus devoid of coma. Most of the light from the comet at $R > 5.9$ AU was scattered from the bare nucleus.
2. A coma was present at $R = 5.1$ AU (1985 January). About 60% of the light from the comet at $R = 5.1$ AU was due to scattering from this coma. The photometry suggests that sustained coma production began near $R = 5.9$ AU (1984 October).
3. The formation of the dust grain coma beginning at $R \leq 5.9$ AU may be due to the equilibrium sublimation of water ice on the nucleus of the comet, provided the nucleus is both dark (Bond albedo $A < 0.15$) and slowly rotating. It is not necessary to invoke any more exotic processes to account for the activity observed at large R . Sputtering by solar wind protons is unable to account for the brightness increase seen at $R = 5.1$ AU.
4. The rotationally averaged value of the product of the optical geometric albedo of the nucleus with the square of the radius is $0.97 \pm 0.03 \text{ km}^2$ (standard error of the mean of 64 observations). The product varies with rotation in the range 0.5 - 1.5 km^2 . The implied mean nucleus radius is in the range 2.5 - 7.0 km for geometric albedos from 0.02 - 0.15.

References

- Allen, C. W. (1976), *Astrophysical Quantities*, 3rd edition, University of London, The Athlone Press, London, p. 162.
- Baudrand, J., M. Combes, E. Gerard, J. Guerin, J. Lecacheux, B. Sicardy, G. Lelievre, J. P. Lemonnier and J. P. Picat (1982), "Periodic Comet Halley (1982i)", *IAU Circular No. 3753*.
- Belton, M. J. S. and H. Butcher (1982), "Periodic Comet Halley (1982i)", *IAU Circular No. 3742*.
- Belton, M. J. S. and H. Butcher (1983). "Periodic Comet Halley (1982i)", *IAU Circular No. 3776*.
- Belton, M. J. S., P. A. Wehinger and S. Wyckoff (1983). "Periodic Comet Halley (1982i)", *IAU Circular No. 3873*.
- Belton, M. J. S., H. Spinrad, P. A. Wehinger and S. Wyckoff (1984). "Periodic Comet Halley (1982i)", *IAU Circular No. 3934*.
- Belton, M., H. Spinrad, P. Wehinger and S. Wyckoff (1985). "Periodic Comet Halley (1982i)", *IAU Circular No. 4029*.
- Bobrovnikoff, N. T. (1954). "Physical Properties of Comets (in Perkins Observatory Report)", *Astron. J.* **59**, 357-358.
- Brooke, T. Y. and R. Knacke (1985). "Periodic Comet Halley (1982i)", *IAU Circular No. 4041*.
- Clark, R. N. (1982), "Implication of Using Broadband Photometry For Compositional Remote Sensing of Icy Objects", *Icarus* **49**, 244-257.
- Cowan, J. J. and M. F. A'Hearn (1982), "Vaporization in Comets; Outbursts From Comet Schwassmann-Wachmann 1", *Icarus* **50**, 53-62.
- Cruikshank, D. P., W. K. Hartmann and D. J. Tholen (1985), "Colour, Albedo and Nucleus Size of Halley's Comet", *Nature* **315**, 122-124.
- Delsemme, A. H. (1982), "Chemical Composition of Cometary Nuclei", In *Comets*, ed. L. L. Wilkening, University of AZ press, Tucson, AZ, p. 85-130.
- Delsemme, A. H. and D. C. Miller (1971), "Physico-Chemical Phenomena in Comets III. The Continuum of Comet Burnham (1960 II)", *Planet. Space Sci.* **19**, 1229-1257.
- Eggerton, A. C. and W. Edmondson (1928), "Vapor Pressure of Chemical Compounds in the Crystalline State", In *International Critical Tables, Vol. III*. McGraw Hill, NY, p. 207.
- Felenbok, P., J. P. Picat, A. Chevillot, J. Guerin, M. Combes, E. Gerard, J. Lecacheux and G. Lelievre (1982), "Deep Sounding with Electronographic Camera at the Prime Focus of the CFHT: Upper Limit to the Visual Brightness of Comet P/Halley During 1981/1982 Opposition", *Astron. Astrophys.* **113**, L1-L2.

References, contd.

- Herschel, J. F. W. (1847), "Observations of Halley's Comet, With Remarks on its Physical Condition, and that of Comets in General", in *Results of Astronomical Observations Made During the Years 1834, 5, 6, 7, 8 at the Cape of Good Hope*, reprinted 1985, Arcturus Press, England, p. 393-413.
- Jewitt, D. C., G. E. Danielson, J. E. Gunn, J. A. Westphal, D. P. Schneider, A. Dressler, M. Schmidt and B. A. Zimmerman (1982). "Periodic Comet Halley (1982i)", *IAU Circular No. 3737*.
- Jewitt, D. and G. E. Danielson (1984), "Charge-Coupled Device Photometry of Comet P/Halley", *Icarus* **60**, 435-444.
- Klinger, J. (1980), "Influence of a Phase Transition of Ice on the Heat and Mass Balance of Comets", *Science* **209**, 271-272.
- Langham, E. J. (1981), "Physics and Properties of Snowcover", in *Handbook of Snow, Principles, Processes, Management and Use*, eds. D. M. Gray and D. H. Male, Pergamon Press, Toronto, p. 294-298.
- Lanzerotti, L. J., W. L. Brown, J. M. Poate and W. M. Augustyniak (1978), "Low Energy Cosmic Ray Erosion of Ice Grains in Interplanetary and Interstellar Media", *Nature* **272**, 431-433.
- Le Fevre, O., J. Lecacheux, G. Mathez, G. Lelievre, J. Baudrand and J. P. Lemonnier (1984), "Rotation of Comet P/Halley: Recurrent Brightening Observed at the Heliocentric Distance of 8 AU", *Astron. Astrophys.* **138**, L1-L4.
- Meyer, S. S. and G. R. Ricker (1980), "A Dual Charge-Coupled Device (CCD), Astronomical Spectrometer and Direct Imaging Camera. I. Optical and Detector Systems", *S. P. I. E.* **264**, 38-41.
- Pederson, H. and R. M. West (1984). "Periodic Comet Halley (1982i)", *IAU Circular No. 3914*.
- Racine, R. (1984). "Periodic Comet Halley (1982i)", *IAU Circular No. 3914*.
- Sicardy, B., J. Guerin, J. Lecacheux, J. Baudrand, M. Combes, J. P. Picat, G. Lelievre and J. P. Lemonnier (1983), "Astrometry and Photometry of Comet P/Halley in October and November 1982", *Astron. Astrophys.* **121**, L4-L6.
- Smith, A. W. (1929), "Latent Heat of Vaporization", In *International Critical Tables, Vol. V*, McGraw Hill, NY, p. 138.
- Smoluchowski, R. (1981), "Heat Content and Evolution of Cometary Nuclei", *Icarus* **47**, 312-319.
- Spinrad, H., S. Djorgovski and M. J. S. Belton (1984), "Periodic Comet Halley (1982i)", *IAU Circular No. 3996*.

References, contd.

- Thuan, T. X., and J. E. Gunn (1976), "A New Four Color Intermediate Photometric System. *Publ. Astron. Soc. Pacific* **88**, 543-547.
- Washburn, E. W. (1928), "The Vapor Pressures of Ice and Water up to 100°C", In *International Critical Tables, Vol. III.*, McGraw Hill, NY, p. 210-212.
- Wehinger, P. A., S. Wyckoff, C. Foltz, C. Heller, M. Wagner, D. Schleicher and M. Festou (1985), "Periodic Comet Halley (1982i)", *IAU Circular No. 4041*.
- West, R. M. and H. Pedersen (1983), "P/Halley: First Signs of Activity?", *Astron. Astrophys.* **121**, L11-L12.
- West, R. M. and H. Pedersen (1984), "Variability of P/Halley", *Astron. Astrophys.* **138**, L9-L10.
- Wyckoff, S., P. Wehinger, M. Belton, M. Wagner and D. Schleicher (1985a), "Periodic Comet Halley (1982i)", *IAU Circular No. 4029*.
- Wyckoff, S., M. Wagner, P. A. Wehinger, D. G. Schleicher and M. C. Festou (1985b), "Onset of Sublimation in Comet P/Halley", *Nature* **316**, 241-242.

Chapter 3 - Albedo Determination

3.1 Introduction

Knowledge of the albedo of an object is fundamental to the understanding of its interaction with the solar radiation field. The albedo determines how much of the incident solar radiation is absorbed and how much is reflected; it therefore affects the equilibrium temperature of the nucleus. The albedo is determined by the composition as well as the bulk properties (such as porosity and roughness) of the material. Unfortunately, confusion can arise because several definitions of the albedo are used in planetary science.

The Bond albedo, A_B , is defined as the ratio of the total amount of scattered (reflected and refracted) radiation to the total amount of radiation incident upon a surface. The Bond albedo is related to the geometric albedo, p , which is the ratio of the backscattered radiation (at zero phase angle) to that expected from a perfectly diffusing disk (scattered intensity varies as $\cos(\theta)$, where θ is measured from the normal to the surface) of the same size at the same distance. The geometric albedo is directly related to the nucleus radius, r_n , and brightness at phase angle zero, $m(0)$, as well as the heliocentric and geocentric distances (R and Δ , respectively), and the apparent brightness of the sun, m_\odot :

$$p r_n^2 = 2.235 \times 10^{22} R^2 \Delta^2 10^{0.4[m_\odot - m(0)]} \quad (3.1)$$

The derivation of this equation, which is the same as Eq. 2.3, is presented in Appendix 2 (Eq. A2.12). The final definition of albedo applies to scattering from single particles. The single scattering albedo as defined by van de Hulst (1981), is the ratio of the total scattered (reflected, refracted and diffracted) energy to the total energy removed from the incident

radiation by both absorption and scattering. In terms of the scattering and absorption efficiencies, Q_s and Q_a , the single scattering albedo, A_s is

$$A_s = \frac{Q_s}{Q_s + Q_a} \quad (3.2)$$

As discussed by Hanner *et al.* (1981), the single scattering albedo is applicable to small particles whose size is comparable with the wavelength. From the point of view of determining the albedo of cometary dust, the definition of the Bond albedo (or geometric albedo) is appropriate for the surface of the nucleus, whereas the single scattering albedo is used for dust particles in the coma.

3.2 IR Techniques for Measuring Albedo

In the early 1970's two methods were developed to measure the albedos of solar system objects. Allen (1970) was the first to use the method of radiometry to determine the infrared diameter and Bond albedo of the asteroid 4 Vesta. The method utilizes measurements of both the thermally emitted radiation and the scattered solar radiation. Likewise, using a different technique, O'Dell (1971) utilized both thermal flux measurements and optical photometry of the comae of active comets to determine the albedos of the dust grains in the comae. Finally, there is a third method of albedo determination which also applies to the comae of active comets. All of these techniques are discussed below.

3.2.1 The Radiometric Method

Infrared radiometry has been extensively discussed and refined by several authors

(Hansen, 1977, Morrison & Lebofsky, 1979 and Lebofsky *et al.*, 1986) since its first application in 1970. The total thermal emission from an inactive spherical comet nucleus is proportional to the product of the nucleus cross section and the fraction of the incident radiation absorbed, $(1 - A_B)$. The scattered radiation, on the other hand, is proportional to the product of the cross section and the geometric albedo (Eq. 3.1). The Bond albedo is equal to the product of the geometric albedo and the phase integral, q , which describes the angular pattern into which the surface scatters light (see Appendix 2). Measurements in the infrared and optical spectral regions can therefore determine the diameter and albedo of the nucleus. The relation between the absorbed incident radiation and the thermal emission is given in Eq. 3.3:

$$\frac{F_O}{R^2} (1 - A_B) [\pi r_n^2] = \beta \varepsilon \sigma r^2 \int_{\lambda=0}^{2\pi} \int_{\varphi=-\frac{\pi}{2}}^{\frac{\pi}{2}} T^4(\lambda, \varphi) \cos(\varphi) d\varphi d\lambda \quad (3.3)$$

where F_O is the solar flux density ($1360.74 \text{ J s}^{-1} \text{ m}^{-2}$ at $R = 1 \text{ AU}$), r_n is the nucleus radius, ε is the infrared emissivity and $\sigma = 5.669 \times 10^{-8} \text{ J m}^{-2} \text{ s}^{-1} \text{ K}^{-4}$, is the Stephan-Boltzmann constant. The quantity, β , is the infrared beaming factor (see Hansen, 1977 and Lebofsky *et al.* 1986). This coefficient (of order unity) models the increase in temperature seen at small phase angles. The temperature increase is present on rough surfaces where surface depressions receive thermal radiation from nearby topography in addition to the incident solar radiation.

In the standard radiometric model the emitting body is assumed to be spherical. The temperature distribution will therefore be a function of position (λ, φ) on the surface (see Figure 3-1). An approximate expression for the temperature distribution, $T(\lambda, \varphi)$ may be obtained by comparing the incident radiation and thermal emission for small elements of area,

dA , located at the subsolar point and at an arbitrary point on the sunlit hemisphere. For the subsolar point, the absorbing area is dA , and the temperature will be a maximum, T_{max} . For a surface element not at the subsolar point, the effective absorbing area is $\cos(\psi) dA = \cos(\lambda) \cos(\phi) dA$. Approximating the surface elements as planes and

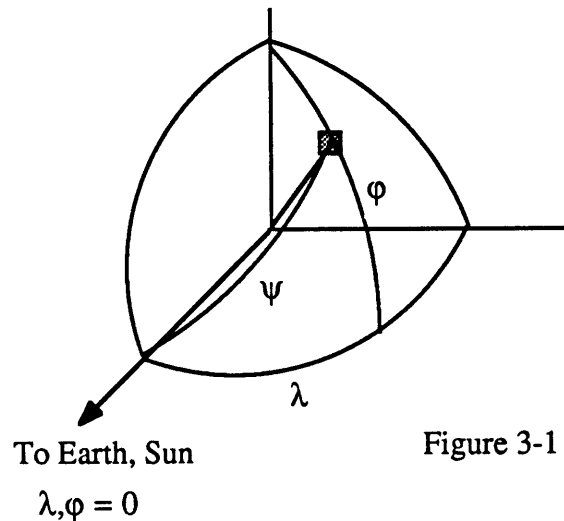


Figure 3-1

assuming all the incident energy is re-radiated, the surface temperature at an arbitrary point is given by:

$$T(\lambda, \phi) = T_{max} \cos^{1/4}(\lambda) \cos^{1/4}(\phi) \quad (3.4)$$

on the sunlit hemisphere. The standard radiometric model assumes that the thermal conductivity is low and that the rotation is slow compared to the time taken to reach thermal equilibrium (several hours) such that all of the emission is in the sunlit hemisphere. Using the radiometric method, the thermal emission from the surface is modelled, with the constraint that the total infrared flux from the model must equal the observed infrared flux. The Bond albedo may then be determined from Eq. 3.3 and from this a geometric albedo.

Measurements of the scattered radiation then yield the nucleus cross section (Eq. 3.1).

Typically, observations are not made over the entire thermal spectrum. However, it is possible to estimate the total thermal energy radiated from a few infrared measurements assuming that the body radiates like a blackbody. The total flux radiated at all wavelengths is given by the integral of the Planck function, B_λ , and is equal to σT^4 . However, it is a property of the Planck function that the maximum value of λB_λ , where

$$\lambda B_\lambda = \frac{2 \pi h c^2}{\lambda^4} \frac{1}{e^{hc/\lambda kT} - 1} \quad (3.5)$$

is directly proportional to σT^4 . The observations need only include the peak of the infrared spectrum to compute the total energy:

$$\int_0^\infty B_\lambda d\lambda = 1.3596 (\lambda F_\lambda)_{\max} \quad (3.6)$$

There are several assumptions inherent in the radiometric method. First, the method assumes that the nucleus is spherical. This is certainly *not* the case for comet P/Halley, with an axis ratio of $\approx 2:1$ (see Chapter 2; Wilhelm *et al.*, 1986). Brown (1985) has investigated the effect of using the standard model on objects with ellipsoidal geometry. He concludes that for small departures from spherical shape the model yields good agreement with the predicted fluxes. However, for significantly aspherical bodies, the radiometric diameters are systematically smaller and the albedos higher than found from the standard model. Second, since measurements are usually insufficient to determine the phase integral (measurements at all phase angles are required), values for the moon and Mercury are typically used ($q \approx 0.6$) to

relate the Bond albedo to the geometric albedo. (The phase integrals for brighter, icy bodies, are typically higher, $0.9 < q < 1.2$ (Morrison, 1977)). Third, the method assumes the measurements are made at zero phase angle, $\lambda = \varphi = 0$; if they are not, a phase function must be assumed. Finally, there must be some information about the rotation period and the conductivity of the surface (low conductivity is usually assumed).

3.2.2 Albedo of Coma Grains - Method of O'Dell

There are relatively few comet nuclei for which the radiometric method is well suited. The method requires that the comet be inactive, without a significant dust coma. Most comets become active at distances sufficiently far from the sun so that the nuclei are too faint for infrared observations. Only a few extremely inactive nuclei at small R have been bright enough to apply the radiometric method, notably, P/Arend-Rigaux and P/Neujmin 1.

O'Dell (1971) pointed out that for an optically thin coma, the optical surface brightness is given by

$$SB_{\text{vis}} = (N l) \pi a^2 Q_s(\lambda) \frac{F_{\odot}(\lambda)}{R^2} \quad (3.7)$$

where N is the column density of grains, l is the path length through the coma, πa^2 is the geometric cross section of the grain, $Q_s(\lambda)$ is the scattering efficiency, and $F_{\odot}(\lambda)$ is the solar flux density. Writing a similar equation for the infrared surface brightness, SB_{IR} , and using Eq. 3.2 for the single scattering albedo, the albedo at a particular wavelength may be determined from

$$\frac{A_s}{1 - A_s} = \frac{(\lambda F_{\lambda})_{\text{max VIS}}}{(\lambda F_{\lambda})_{\text{max IR}}} \quad (3.8)$$

This assumes that the total flux of energy in the visible or IR is proportional to the flux at the peak of the spectrum (as discussed above).

3.2.3 Albedo of Coma Grains - Alternate Method

Under the assumption that the thermal flux received from the comet may be interpreted as radiation from a blackbody radiator, the area of the radiator, in this case the dust coma, may be computed from the thermal measurements alone. The specific intensity of radiation measured from a blackbody, B_λ [$\text{W m}^{-2} \mu\text{m}^{-1} \text{sr}^{-1}$], is a function of both the area of the emitter and the solid angle subtended by the detector, $d\Omega$. The power per unit wavelength radiated from the blackbody which is intercepted by the detector is then:

$$L_\lambda = B_\lambda(T) \frac{A_d}{\Delta^2} A_e \text{ [W } \mu\text{m}^{-1}] \quad (3.9)$$

where A_d is the area of the detector and A_e is the area of the emitter. What is measured at the telescope is the flux density, F_λ [$\text{W m}^{-2} \mu\text{m}^{-1}$]:

$$F_\lambda = \frac{B_\lambda(T) A_e}{\Delta^2} \quad (3.10)$$

Using a measured value of F_λ and a value of T determined from a blackbody fit to the thermal IR data to compute $B(T)$, the emitting area can thus be obtained from Eq. 3.10. Eq. 3.1 can then be used to obtain the geometric albedo.

3.3 Measurements of P/Halley

3.3.1 Present Work

Data were obtained during photometric conditions on the night of 1985 November 11/12 using the NASA Infrared Telescope Facility (IRTF). At the time of the observations, centered around 12:05 UT, P/Halley was at a heliocentric distance, $R = 1.756$ AU, a geocentric distance, $\Delta = 0.786$ AU and a phase angle $\alpha = 9.51$ deg. An InSb detector cooled to solid N₂ temperatures was used for the observations between 1.25 and 3.5 μ m, and a liquid Helium cooled bolometer was used for observations between 4.8 and 20 μ m. A diaphragm of 4mm diameter was used for all observations, corresponding to 7.88 arcsec on the sky. The positions of the chopping for the sky background subtraction were 51 arcsec north and south of the comet. Although such a large chop amplitude increased the noise in the observations, it was selected to minimize the contribution from the coma in the sky position. For a radially outflowing coma, the coma brightness in the sky position relative to the central position is: $B/B_o = \phi / 2p_o$ (see Appendix 4), where ϕ is the radius of the observing diaphragm and p_o is the chop distance. For these observations the coma contribution in the sky position was only 3.8%.

Data were reduced using the standard stars HD 1160 and HD 22686 (Elias *et al.*, 1982) and α Tau (Hanner *et al.*, 1984). The standards were observed at the same airmass as P/Halley ($\chi \approx 1.02$). The P/Halley observations are presented in Table 3-1. The first 3 columns of Table 3-1 list the filter name, the central wavelength and reduced magnitude within the 7.88 arcsec diameter diaphragm for P/Halley. The correction to remove the effect of the coma contamination in the sky position is listed in column 4. All of the data are referred to the effective wavelength of the bandpass, which is a function of the filter/optics transmission, the

sky transmission and the source spectrum. The effective wavelengths for the standard star and the comet may be substantially different for the L, M, N, and Q filters since the cometary radiation is primarily cool thermal emission (few $\times 100$ K) in these filters. Correction factors (as a function of wavelength and temperature) for converting cometary magnitudes to the monochromatic magnitudes at the effective wavelengths of the standard stars have been computed by Hanner *et al.* (1984). The correction factors and the monochromatic magnitudes for P/Halley are listed in columns 5 and 6 of Table 3-1. The L filter correction has not been applied to the data since there is a substantial amount of scattered radiation in this bandpass. The absolute flux densities for α Lyr (mag $\equiv 0.0$ at all λ) from Tokunaga *et al.* (1986) are shown for reference in column 7. The P/Halley flux densities as computed from $F_{\lambda}(\alpha \text{ Lyr}) \times 10^{-0.4[\text{mag}]}$ are listed in column 8 and in column 9 the product λF_{λ} for P/Halley is shown.

In order to compute the geometric albedo in the J, H and K passbands, the temperature of the dust coma of P/Halley was found by fitting a blackbody to the 10.1, 12.5 and 20.0 μm data. The observation at 4.8 μm was not used in the fit because of a possible contribution from scattered solar radiation. At small R many comets show a silicate emission feature at 10.1 μm . As seen in spectra obtained of P/Halley by Herter *et al.* (1986), the feature is approximately 4 μm wide, and does not effect the 12.5 μm measurements. For this reason, in order to determine the temperature of the present P/Halley data, the fits were constrained to pass through the 12.5 μm point. The color temperature of the scattered radiation was determined in the same manner from the 1.25, 1.65 and 2.2 μm measurements. The scattered light measurements are best approximated by a $T \approx 4000$ K blackbody. This corresponds to a star of a mid to late K spectral class and is redder than the sun (class G2). This is consistent with observations of other comets which show that the scattered continuum is reddened with respect to the sun (see Chapter 6, and Jewitt & Meech, 1986). From the fit to the near IR data, the scattered light contribution in the 4.8 μm band can be removed (see Table 3-1) and the thermal data refit for the temperature. Temperatures between $244 \leq T \text{ [K]} \leq 268$ give

Table 3-1

IRTF Observations of Comet P/Halley

Filter	λ_{eff} μm	Mag	Coma [‡]	C_{λ} [§]	Mag _{corr}	F_{λ} [Wm ⁻² μm^{-1}] α Lyr	F_{λ} [Wm ⁻² μm^{-1}] P/Halley	λF_{λ} [Wm ⁻²] P/Halley
J	1.25	10.44 ± 0.03	-0.04	---	10.40	3.07 x 10 ⁻⁹	2.12 x 10 ⁻¹³	(2.65 ± 0.07) x 10 ⁻¹³
H	1.65	9.99 ± 0.03	-0.04	---	9.95	1.12 x 10 ⁻⁹	1.17 x 10 ⁻¹³	(1.94 ± 0.06) x 10 ⁻¹³
K	2.20	9.85 ± 0.03	-0.04	---	9.81	4.07 x 10 ⁻¹⁰	4.85 x 10 ⁻¹⁴	(1.07 ± 0.05) x 10 ⁻¹³
L	3.45	9.51 ± 0.05	-0.04	[0.50]	9.46	7.30 x 10 ⁻¹¹	1.20 x 10 ⁻¹⁴	(4.14 ± 0.20) x 10 ⁻¹⁴
M	4.8	6.74 ± 0.05	-0.04	-0.055	6.65	2.12 x 10 ⁻¹¹	4.64 x 10 ⁻¹⁴	(2.23 ± 0.10) x 10 ⁻¹³ †(2.05 ± 0.10) x 10 ⁻¹³
N	10.1	1.30 ± 0.07	-0.04	-0.03	1.23	1.17 x 10 ⁻¹²	3.77 x 10 ⁻¹³	(3.81 ± 0.25) x 10 ⁻¹²
--	12.5	0.45 ± 0.10	-0.04	---	0.41	5.07 x 10 ⁻¹³	3.48 x 10 ⁻¹³	(4.34 ± 0.40) x 10 ⁻¹²
Q	20.0	-1.03 ± 0.15	-0.04	-0.04	-1.11	7.80 x 10 ⁻¹⁴	2.17 x 10 ⁻¹³	(4.34 ± 0.60) x 10 ⁻¹²

[‡]Correction for coma in sky position.

[§]Correction to monochromatic magnitudes, from Hanner *et al.* 1984.

[†]After removal of scattered component of solar spectrum.

Table 3-2

Derived Comet Halley Albedo

λ (μm)	Solar Flux Density [†] [W m ⁻² μm^{-1}]	Albedo [p_{λ}]
1.25	4.473 x 10 ²	0.06 ± 0.01
1.65	2.279 x 10 ²	0.07 ± 0.02
2.20	0.759 x 10 ²	0.08 ± 0.02

[†]Magnitude of the Sun, as determined from a solar spectrum from Labs and Neckle (Hanner, private communication).

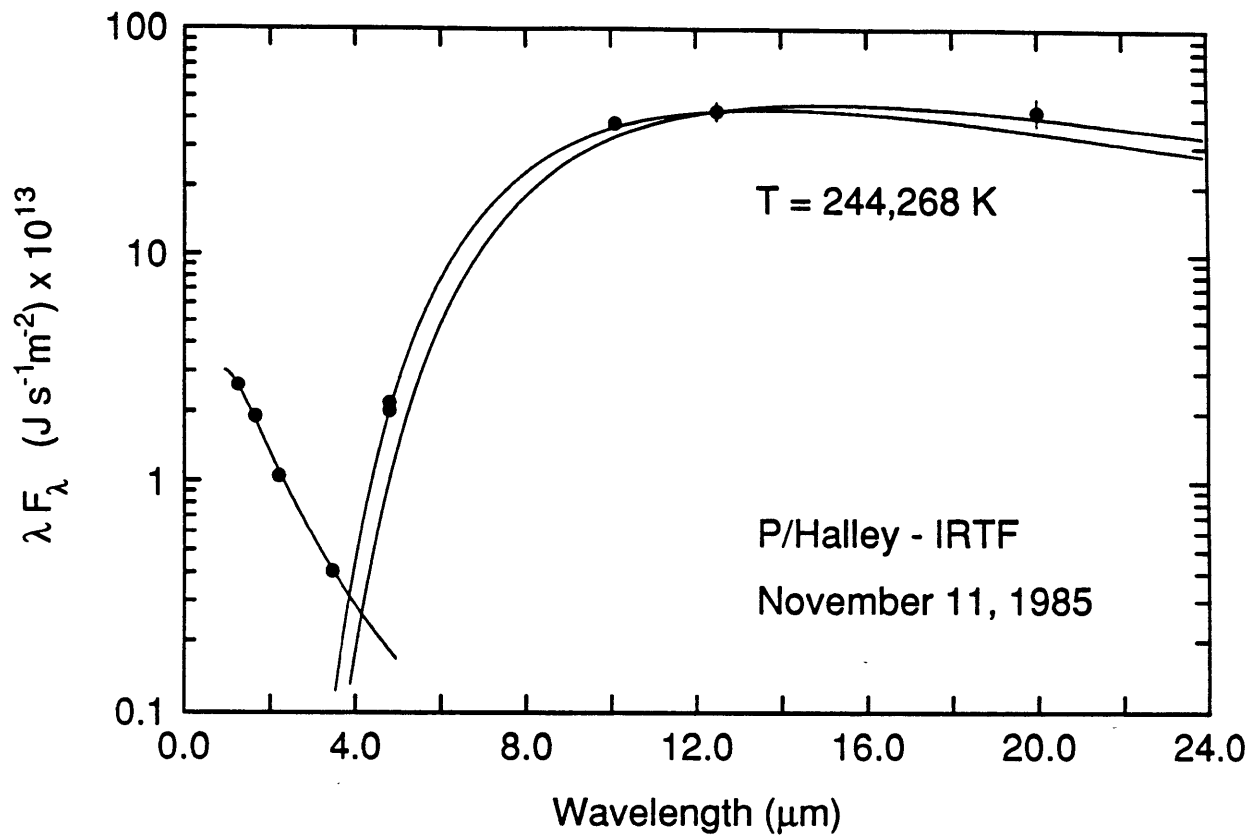


Figure 3-2. Near IR (1.25-3.5 μm) and thermal IR measurements of P/Halley (from Table 3-1) obtained with the IRTF on 1985 November 11. The curve passing through the near IR data is for a blackbody of $T = 4000 \text{ K}$. The near IR data is the radiation scattered from the grains. The scattered radiation has been reddened with respect to the solar continuum. The 2 blackbody curves ($T = 244, 268 \text{ K}$) passing through the thermal data show the range of temperatures which best match the thermal emission from the grains.

acceptable fits to the thermal emission from P/Halley. The temperature 256 ± 12 K is therefore adopted as the temperature of the coma. In Figure 3-2 the P/Halley data are shown with the fits for the scattered and thermal radiation. Both the total $4.8 \mu\text{m}$ measurement and that corrected for just the thermal emission are shown in the figure for comparison.

The albedos in each of the near-IR bandpasses (J, H and K) have been computed using the method described in section 3.2.3 and are listed in Table 3-2. Although the definition of albedo used by O'Dell (1971) typically yields somewhat higher albedos, the albedo of P/Halley is very low no matter which definition is used. This finding is consistent with the result from the H_2O sublimation model presented in Chapter 2 which required that the Bond albedo be lower than 0.15, and with more recent measurements from spacecraft (see Chapter 8).

3.3.2 Other Sources of P/Halley Albedos

There have been at least two other programs to monitor the infrared brightness of P/Halley as a function of R , one at the IRTF and one at the United Kingdom Infrared Telescope (UKIRT) on Mauna Kea. The published flux densities from both programs (Tokunaga *et al.*, 1986; and Green *et al.*, 1986) are consistent with the observations presented here for P/Halley. The albedos derived by Tokunaga *et al.* (1986) are somewhat lower than those presented here; however. The area of the dust in Tokunaga *et al.* (1986) was determined from the thermal emission by considering models for various grain size distributions. According to Hanner (private communication) this method may differ by up to 25% from the simple determination of the area as described above. The IRTF and UKIRT studies show that both the near IR colors and albedos remained constant within their errors as a function of distance (for $1 < R$ (AU) < 4.8). Finally, direct measurements of the reflectivity of the nucleus (unfiltered) with the Giotto spacecraft Multicolor Camera (Delamere *et al.*, 1986;

Keller *et al.*, 1986) found that the mean surface reflectivity is about 3.5%.

3.4 Other Comets

It is not always possible to determine the albedo for either the comet nucleus or the dust grains if the comet is at large R because of the lower surface temperature and the relative insensitivity of the infrared detectors. It is therefore useful to compare the measured albedos of many different comets to see if the low albedo measured for P/Halley is typical of other comets.

Table 3-3 summarizes the known albedo measurements for 13 comets. Some of the albedos were determined using radiometric methods (nuclei), whereas others were determined using the method of O'Dell or the method discussed in section 3.2.3. It is not possible to convert the albedos to one particular system because of insufficient information in the references. However, the albedos computed with the method of O'Dell are typically 2-4 times higher than the albedos computed by the alternate method. The conclusion that may be drawn from Table 3-3 is that the dust and nuclei of comets appear to be very dark, between $0.02 < p_\lambda < 0.15$. Furthermore, when modelling the activity of comets in the absence of any albedo information, a reasonable choice of albedo would be $p_\lambda \approx 0.07$, which is probably not wrong by more than a factor of two.

Table 3-3
Cometary Albedos - Nucleus and Coma

Comet	Position	p_{λ}	λ [μm]	Radius [km]	Reference
Arend-Rigaux	nucleus	0.02±0.01		5 (max)	A'Hearn 1986
		0.05±0.01	1.25	4.8±0.4	Tokunaga & Hanner, 1985
		0.03			Veeder <i>et al.</i> , 1985
		0.02±0.01	0.55	5.1±1.1	Brooke & Knacke, 1986
		0.03±0.01	1.25		"
		0.06±0.03	1.25	4.5±0.2/0.5	Birkett <i>et al.</i> , 1987
		0.028±0.005		5.15±0.2	Millis <i>et al.</i> 1987
Bowell	coma	0.14±0.05	1-2		Jewitt <i>et al.</i> , 1982
	coma	0.10	1.25		Hanner & Campins, 1986
Bradfield	coma	0.10			Ney, 1974
P/Chernykh	coma	0.05±0.03	1.65		Campins <i>et al.</i> , 1982
Churyumov-Gerasimenko	coma	0.04	1.25		Hanner <i>et al.</i> , 1985
Halley	coma	0.06±0.01	1.25		Present work
	coma	<0.1			Cruikshank <i>et al.</i> , 1985
	coma	0.032±0.002	1.25		Tokunaga <i>et al.</i> , 1986
		0.045±0.003	2.20		
	coma	<0.05 to 0.15			Gehrz & Ney, 1986
nucleus	0.035			Delamere <i>et al.</i> , 1986	
P/Kearns-Kwee	coma	0.16±0.05	1.65		Campins <i>et al.</i> , 1982
Kohoutek ('73f)	coma	0.14	1.65		Rieke & Lee, 1974
	coma	0.12	1.25		computed from Ney, 1974
Neujmin 1	nucleus	0.02-0.03		8.8-10.6	Campins <i>et al.</i> , 1987
Panther	coma	0.14±0.05	1-2		Jewitt <i>et al.</i> , 1982
SW1	nucleus	0.13±0.04		40±5	Cruikshank & Brown, 1983
P/Stephan-Oterma	coma	0.07			Veeder & Hanner, 1981
		0.12±0.04	1.65		Campins <i>et al.</i> , 1982
P/Tuttle	coma	0.10±0.02	1.65		Campins <i>et al.</i> , 1982

3.5 Conclusions

1. The albedo of comet P/Halley was measured to be $p_\lambda = 0.06 \pm 0.01$ at $\lambda = 1.25\mu\text{m}$, 0.07 ± 0.02 at $\lambda = 1.65\mu\text{m}$ and 0.08 ± 0.02 at $\lambda = 2.20\mu\text{m}$. These albedos refer to dust grains in the coma.
2. The low albedo of P/Halley is typical of other comets measured in the same manner.
3. The albedos of cometary nuclei and cometary dust lie within the range $0.02 < p_\lambda < 0.15$, so that in the absence of albedo measurement, an albedo estimate of $p_\lambda \approx 0.07$ is probably not wrong by more than a factor of two.
4. The comet Halley albedo did not change appreciably as a function of heliocentric distance.

References

- A'Hearn, M. F. (1986), "Are Cometary Nuclei Like Asteroids?", in *Asteroids Comets Meteors II*, eds. C.-I. Lagerkvist, B. A. Lindblad, H. Lundstedt and H. Rickman, Uppsala universitet, Uppsala, p. 187-190.
- Allen, D. A. (1970), "Infrared Diameter of Vesta", *Nature* **227**, 158-159.
- Birkett, C. M., S. F. Green, J. C. Zarnecki and K. S. Russell (1987), "Infrared and Optical Observations of Low-Activity Comets, P/Arend-Rigaux (1984k) and P/Neujmin 1 (1984c)", *Mon. Not. R. Astr. Soc.* **225**, 285-296.
- Brooke, T. Y. and R. F. Knacke (1986), "The Nucleus of Comet P/Arend-Rigaux", *Icarus* **67**, 80-87.
- Brown, R. H. (1985), "Ellipsoidal Geometry in Asteroid Thermal Models: The Standard Radiometric Model", *Icarus* **64**, 53-63.
- Campins, H., M. F. A'Hearn and L. A. McFadden (1987), "The Bare Nucleus of Comet Neujmin 1", *Astrophys. J.* **316**, 847-857.
- Campins, H., G. H. Rieke and M. J. Lebofsky (1982), "Infrared Photometry of Periodic Comets Encke, Chernykh, Kearns-Kwee, Stephan-Oterma, and Tuttle", *Icarus* **51**, 461-465.
- Cruikshank, D. P. and R. H. Brown (1983), "The Nucleus of Comet P/Schwassmann-Wachmann 1", *Icarus* **56**, 377-380.
- Cruikshank, D. P., W. K. Hartmann and D. J. Tholen (1985), "Colour, Albedo and Nucleus Size of Halley's Comet", *Nature* **315**, 122-124.
- Delamere, W. A., H. J. Reitsema, W. F. Huebner, H. U. Schmidt, H. U. Keller, W.K. H. Schmidt, K. Wilhelm and F. L. Whipple (1986), "Radiometric Observations of the Nucleus of Comet Halley", in *Proceedings of the 20th ESLAB Symposium on the Exploration of Halley's Comet*, eds. B. Battrock, E. J. Rolfe and R. Reinhard, ESA Publications Division, The Netherlands, Vol. II, p. 355-357.
- Elias, J. H., J. A. Frogel, K. Matthews and G. Neugebauer (1982), "Infrared Standard Stars", *Astron. J.* **87**, 1029-1034.
- Gehrz, R. D. and E. P. Ney (1986), "Infrared Temporal Development of P/Halley", in *Proceedings of the 20th ESLAB Symposium on the Exploration of Halley's Comet*, eds. B. Battrock, E. J. Rolfe and R. Reinhard, ESA Publications Division, The Netherlands, Vol. II, p. 101-105.
- Green, S. F., J. A. M. McDonnell, G. S. A. Pankiewicz and J. C. Zarnecki (1986), "The UKIRT Infrared Observational Programme", in *Proceedings of the 20th ESLAB Symposium on the Exploration of Halley's Comet*, eds. B. Battrock, E. J. Rolfe and R. Reinhard, ESA Publications Division, The Netherlands, Vol. II, p. 81-86.

References, contd.

- Hanner, M. S. and H. Campins (1986), "Thermal Emission From the Dust Coma of Comet Bowell and a Model For the Grains", *Icarus* **67**, 51-62.
- Hanner, M. S., R. H. Giese, K. Weiss, R. Zerull (1981), "On the Definition of Albedo and Application to Irregular Particles", *Astron. Astrophys.* **104**, 42-46.
- Hanner, M. S., E. Tedesco, A. T. Tokunaga, G. J. Veeder, D. F. Lester, F. C. Witteborn, J. D. Bregman, J. Gradie and L. Lebofsky (1985), "The Dust Coma of Periodic Comet Churyumov-Gerasimenko (1982 VIII)", *Icarus* **64**, 11-19.
- Hanner, M. S., A. T. Tokunaga, G. J. Veeder, M. F. A'Hearn (1984), "Infrared Photometry of the Dust in Comets", *Astron. J.* **89**, 162-169.
- Hansen, O. L. (1977), "An Explanation of the Radiometric Method for Size and Albedo Determination", *Icarus* **31**, 456-482.
- Herter, T., G. E. Gull and H. Campins (1986), "Airborne Spectrophotometry of P/Halley from 16 to 30 Microns", in *Proceedings of the 20th ESLAB Symposium on the Exploration of Halley's Comet*, eds. B. Battrick, E. J. Rolfe and R. Reinhard, ESA Publications Division, The Netherlands, Vol. II, p. 117-120.
- Jewitt, D. C. and K. J. Meech (1986), "Cometary Grain Scattering Versus Wavelength, or 'What Color is Comet Dust?' ", *Astrophys. J.* **310**, 937-952.
- Jewitt, D. C., B. T. Soifer, G. Neugebauer and K. Matthews (1982), "Visual and Infrared Observations of the Distant comets P/Stephan-Oterma (1980g), Panther (1980u), and Bowell (1980b)", *Astron. J.* **87**, 1854-1866.
- Keller, H. U., C. Arpigny, C. Barbieri, R. M. Bonnet, S. Cazes, M. Coradini, C. B. Cosmovici, W. A. Delamere, W. F. Huebner, D. W. Hughes, C. Jamar, D. Malaise, H. J. Reitsema, H. U. Schmidt, W. K. H. Schmidt, P. Seige, F. L. Whipple and K. Wilhelm (1986), "First Halley Multicolour Camera Imaging Results from Giotto", *Nature* **321**, 320-326.
- Lebofsky, L. A., M. V. Sykes, E. F. Tedesco, G. J. Veeder, D. L. Matson, R. H. Brown, J. C. Gradie, M. A. Feierberg, and R. J. Rudy (1986), "A Refined Standard Thermal Model for Asteroids Based on Observations of 1 Ceres and 2 Pallas", *Icarus* **68**, 239-251.
- Millis, R. L., M. F. A'Hearn and H. Campins (1987), "An Investigation of the Nucleus and Coma of Comet P/Arend-Rigaux", preprint.
- Morrison, D. (1977), "Radiometry of Sattellites and of the Rings of Saturn", in *Planetary Satellites*, ed. J. A. Burns, Univ. of AZ Press, Tucson, AZ, p. 269-301.
- Morrison, D. and L. A. Lebofsky (1979), "Radiometry of Asteroids", in *Asteroids*, ed. T. Gehrels, Univ. of AZ Press, Tucson AZ, p. 184-205.

References, contd.

- Ney, E. P. (1974), "Multiband Photometry of Comets Kohoutek, Bennett, Bradfield, and Encke", *Icarus* **23**, 551-560.
- Ney, E. P. (1982), "Optical and Infrared Observations of Bright Comets in the Range 0.5 μ m to 20 μ m", in *Comets*, ed. L. L. Wilkening, Univ. of AZ Press, Tucson AZ, p. 323-340.
- O'Dell, C. R. (1971), "Nature of Particulate Matter in Comets as Determined From Infrared Observations", *Astrophys. J.* **166**, 675-681.
- Rieke, G. H. and T. A. Lee (1974), "Photometry of Comet Kohoutek (1973f)", *Nature* **248**, 737-740.
- Tokunaga, A. T., W. F. Golisch, D. M. Griep, C. D. Kaminski and M. S. Hanner (1986), "The NASA Infrared Telescope Facility Comet Halley Monitoring Program. I. Preperihelion Results", *Astron. J.* **92**, 1183-1190.
- Tokunaga, A. T. and M. S. Hanner (1985), "Does Comet P/Arend-Rigaux Have a Large Dark Nucleus?", *Astrophys. J.* **296**, L13-L16.
- van de Hulst (1981), *Light Scattering by Small Particles*, General Pub. Co., Toronto, Canada, p. 183.
- Veeder, G. J. and M. S. Hanner (1981), "Infrared Photometry of Comets Bowell and P/Stephan-Oterma" *Icarus* **47**, 381-387.
- Veeder, G. J., M. Hanner, B. Goldberg, D. J. Tholen, and A. T. Tokunaga (1985), "The Nucleus of P/Arend-Rigaux", *Bull. Amer. Astron. Soc.* **17**, 688.
- Wilhelm, K., C. B. Cosmovici, W. A. Delamere, W. F. Huebner, H. U. Keller, H. Reitsema, H. U. Schmidt and F. L. Whipple (1986), "A Three-Dimensional Model of the Nucleus of Comet Halley", in *Proceedings of the 20th ESLAB Symposium on the Exploration of Halley's Comet*, ESA Pub. Div., the Netherlands, Vol. II., p. 367-369.

Chapter 4 - Cometary Phase Functions

4.1 Introduction

Measurement of the scattering properties of particles as a function of phase angle is an important means of learning about the composition and physical properties of the scatterers. The phase functions of cometary grains have been measured in the range $30 \leq \alpha$ [deg] ≤ 150 (Ney and Merrill, 1976; Ney 1982) and are consistent with scattering from μm -sized dielectric spheres. At small phase angles ($\alpha \leq 7$ deg), atmosphereless solar system bodies exhibit a surge in brightness (the so called "opposition effect") caused by the disappearance of interparticle shadows. The exact height and shape of the surge are dependent upon the roughness and porosity of the surface and upon the single scattering albedo of the particles (Lumme and Bowell, 1981). In comets, however, the nucleus is rarely directly visible. Generally, the scattering cross section in active comets lies in small solid particles in the extended coma. An opposition surge may or may not be produced in the coma particles, depending on their shape, composition and size. Some cometary dust grains may be similar to the Brownlee particles (Brownlee, 1978) collected in the Earth's upper atmosphere: aggregates of silicate grains bound together by an amorphous carbon-rich material (Bradley *et al.*, 1984). Hanner *et al.* (1981) and Mukai *et al.* (1982) have shown that enhanced backscattering is possible for slightly absorbing fluffy particles such as these. Resonant backscattering ("glory") may also be produced (Oetking, 1966) if the particles are both spherical and transparent. The Gegenschein may be caused by enhanced backscattering from the zodiacal light particles (Dumont and Sánchez, 1975) which may themselves be cometary debris (Whipple, 1967). It therefore seems reasonable to search for an opposition surge or enhanced backscattering in the grain comae of active comets. Although the scattering function can certainly not be used as a unique diagnostic of the properties of cometary grains, it may be

possible to use it to place useful constraints on the nature of the grains.

There have been several attempts to observe backscattering phase effects in comets. Kiselev and Chernova (1981) obtained broadband photometric measurements as a function of phase angle ($2 \leq \alpha$ [deg] ≤ 25) for the comae of comets Meier (1978f) and P/Ashbrook-Jackson. Based on additional polarization measurements and Mie theory calculations they interpreted the enhanced brightening at small phase angles to be caused by backscattering from large (radius $a \geq 1 \mu\text{m}$) dielectric particles. It is likely that the broadband filters used by Kiselev and Chernova took in considerable gas band emission in the case of comet Meier, so that a simple interpretation of their data may not be possible. Millis *et al.* (1982) made *narrowband* observations of the dust continuum of comet P/Stephan-Oterma as a function of phase angle ($3 \leq \alpha$ [deg] < 30) and reported a factor of two increase in brightness at small phase angles which they interpreted as single particle enhanced backscattering. Finally, similar observations have been obtained for comet Bowell (1982I), by A'Hearn *et al.* (1984), who argued that the backscattering brightness (near $\alpha = 0$ deg) is approximately a factor of 3 greater than at moderate phase angles.

Advantage was taken of the fortuitous passage of P/Halley through small phase angles in November 1985 to examine its brightness as a function of phase, and to study temporal changes in the brightness of the gas bands and continuum. The major problem with any attempted measurements of the phase functions of comets is that the heliocentric distance, R , and the phase angle, α , vary simultaneously, so that a given observed brightness change may be attributed to either variable. Temporal variations intrinsic to the comet may also be present. However, the geometry of P/Halley was particularly suitable for this project since the heliocentric distance remained virtually constant ($1.62 < R$ [AU] < 1.72) while the phase angle changed from $1.3 \leq \alpha$ [deg] ≤ 8.6 . In the remainder of this chapter, observations of P/Halley will be described and the data will be compared to the known backscattering measurements of other comets.

4.2 Observations

Observations were obtained during UT 1985 November 15-22 at the McGraw-Hill Observatory 1.3m telescope at Kitt Peak. The MkII spectrograph and a 2048 channel intensified Reticon detector (Sectman and Hiltner, 1976) were used at the $f/7.5$ Cassegrain focus. All observations were taken with a 300 line/mm grating, giving a dispersion of 2.3\AA per channel. The effective spectrograph resolution over the range of wavelengths $3700 \leq \lambda$ (\AA) ≤ 6900 was $\Delta\lambda \approx 15\text{\AA}$. All observations were taken through an 8 arcsec diameter circular diaphragm which was chopped to a nominal sky position 40 arcsec west of the nucleus. The chop position always contained coma, however, and was used as a second data position. True sky subtraction was achieved by periodically observing the sky 3 deg north of the nucleus. Guiding on the comet was achieved by using an intensified CCD camera to monitor the image of the comet reflected from the spectrograph slit plate. The guiding was accurate to better than ± 1 arcsec. Exposure durations for both the central and 40 arcsec west positions were between 300 - 600 s. Table 4-1 lists the geometry of the comet on each of the 8 nights during which data were obtained.

The Reticon counting rate was kept below $4000 \text{ photon s}^{-1}$ via the use of neutral density filters, in order to avoid coincidence detection problems. The same filters used to observe the comet were also used for the standard stars since the transmission curves of the supposedly neutral filters are known to be slightly wavelength dependent. A single neutral density filter was used on all nights except for UT 1985 November 21 during which the comet brightened significantly. Ironically, as a consequence of the additional neutral density used on this night, the spectra of the comet at its brightest have the smallest signal to noise ratio.

Spectrophotometric calibration was obtained from observations of the standard stars HZ15, Feige 15 and Feige 25 (Stone, 1977). These standards were chosen to be at similar airmass to the comet so as to minimize possible errors in assuming the Kitt Peak mean

Table 4-1
Observing Geometry

UT Date 1985	JD [†] -2440000	R[AU] [§]	Δ [AU] [◇]	α [◇] [deg]
15 Nov	6384.5	1.72	0.74	5.68
16 Nov	6385.5	1.71	0.72	4.02
17 Nov	6386.5	1.69	0.70	2.38
18 Nov	6387.5	1.68	0.69	1.37
19 Nov	6388.5	1.66	0.67	2.41
20 Nov	6389.5	1.65	0.66	4.31
21 Nov	6390.5	1.63	0.65	6.42
22 Nov	6391.5	1.62	0.64	8.63

[†]Julian Day Number for 0^hUT of date; [§]Heliocentric Distance;
[‡]Geocentric Distance; [◇]Phase angle.

All positions were computed with a two-body ephemeris program
using elements from MPC 10155.

extinction coefficients. Wavelength comparison Hg and Kr spectra were taken before and after each observation in order to correct for instrumental flexure. Third order polynomial fits to 16 spectral lines provided good dispersion solutions, with residuals typically less than 1 channel (2.3Å). No significant differences were found in the instrumental response curves computed from each standard star, hence a mean curve was formed from all of the standards observed each night. The standard star magnitudes were reproducible to within $\approx \pm 0.1$ mag over the 8 nights of observation, providing an empirical measure of the photometric quality of the data.

4.3 Analysis and Discussion

In order to study the scattering properties of the dust, the signature of the solar spectrum must be removed from the data. The solar spectrum (Arvesen *et al.*, 1969) was smoothed to match the MkII spectral resolution by convolving it with the instrumental spectral line profile, which was approximated by a gaussian of full width at half maximum (FWHM) equal to $\Delta\lambda = 15\text{\AA}$. Reflectivity spectra were computed by dividing each of the spectra of P/Halley by the convolved solar spectrum. The effectiveness of the division can be seen in Figures 4-1 and 4-2 by the removal of the solar H and K calcium and the hydrogen-alpha lines from the spectra.

The reflectivity spectra show molecular emission bands (due to $\text{CN}(\Delta v=0)$, C_3 , $\text{C}_2(\Delta v=+1)$ and $\text{C}_2(\Delta v=0)$) as well as weaker bands due to $\text{CH}(\Delta v=0)$ and $[\text{OI}]$ superimposed on a strong dust continuum. In order to separate the continuum brightness from the molecular emissions, the continuum brightness was measured in a narrow emission-free region between $5760 \leq \lambda [\text{\AA}] \leq 5820$. The location of this "continuum window" is shown in Figure 4-1, which is an average of 9 reflectivity spectra obtained on UT 1985 November 22. Several of the gas bands are indicated in Figure 4-1, together with their corresponding continuum windows. The wavelengths used for the gas bands and their continuum windows are listed in Table 4-2a. Nightly averages of the reflectivity spectra are presented in Figures 4-2a-e. The spectra are plotted at a fixed absolute scale for ease of comparison. It is evident from the figure that substantial changes occurred in the dust continuum and molecular band components of the spectrum of P/Halley. For example, note the fading of the continuum from UT 1985 November 15 to 16 and from UT 1985 November 21 to 22 and the changes in the strength of the CN band from night to night.

Although there are substantial changes in the strength of the dust continuum, the continuum color does not change significantly from night to night. Measurements of the

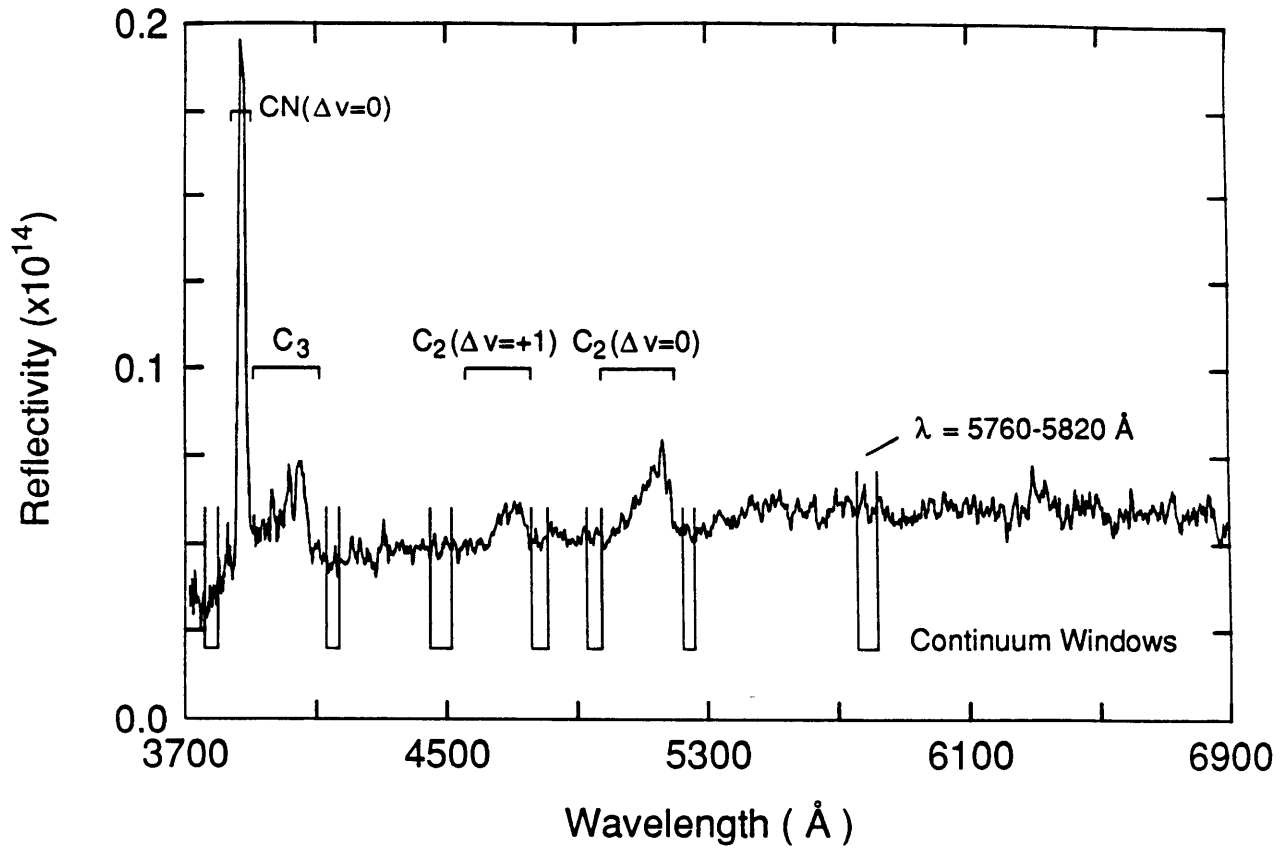


Figure 4-1. Average of 9 P/Halley reflectivity spectra from UT 1985 November 22. Gas emission bands of $CN(\Delta v=0)$, C_3 , $C_2(\Delta v=+1)$ and $C_2(\Delta v=0)$ are marked as are their surrounding continuum regions. An additional continuum window at $\lambda_{cent} = 5790\text{Å}$ is also marked.

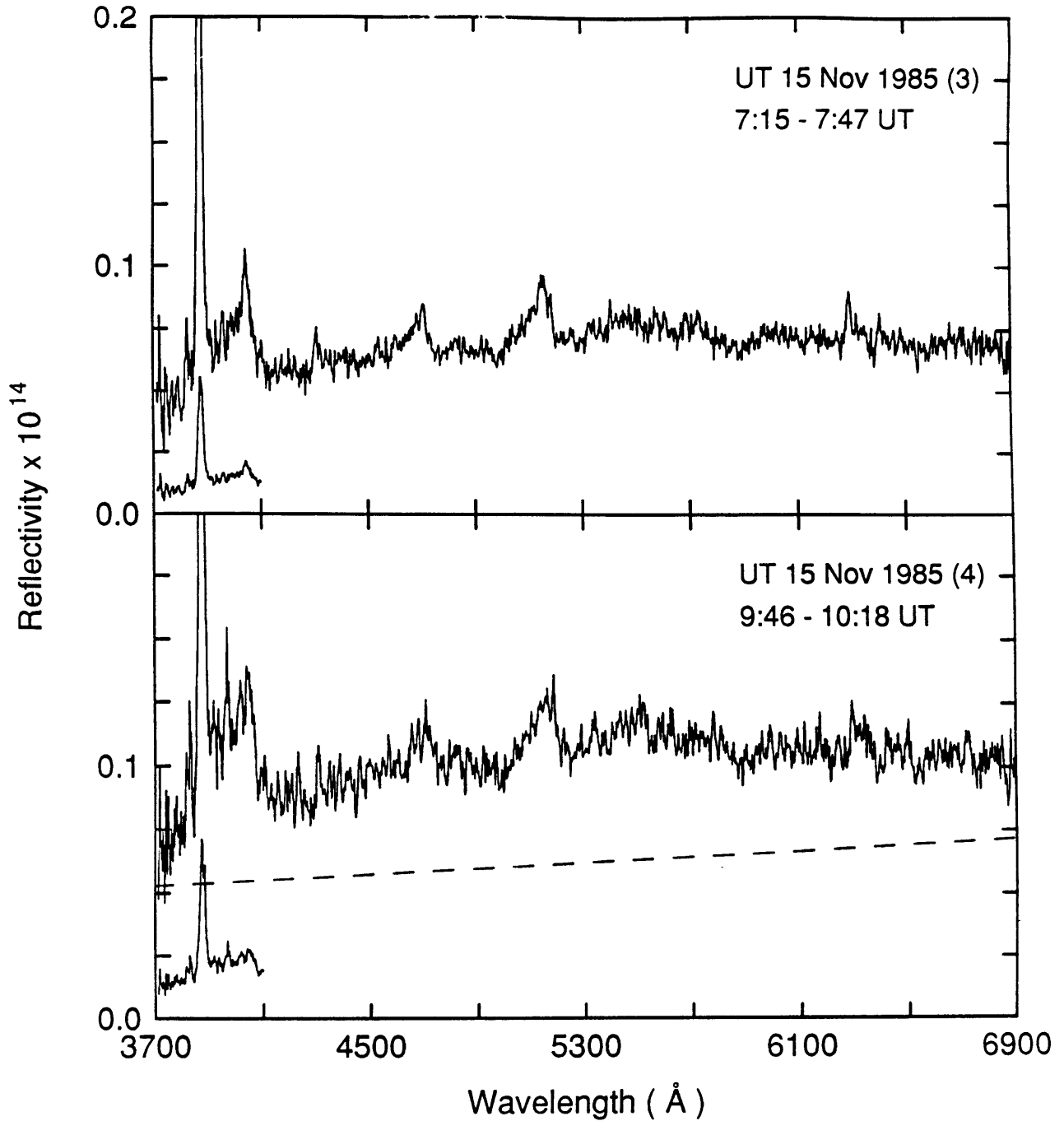


Figure 4-2. (a) Nightly averages of P/Halley reflectivity spectra versus wavelength. Note that all spectra are plotted at the same absolute scale for ease in comparing nightly changes in both the line strength and continuum brightness. The CN band is also plotted at one tenth scale. The UT date and range of times for the spectra used to compute the average reflectivities are indicated. The number in parentheses following the date is the number of spectra used in the average. Outbursts in the continuum brightness are evident on UT 1985 November 15 and 21. For comparison, the mean continuum brightness in the $5760 \leq \lambda (\text{Å}) \leq 5820$ continuum window for all other nights is indicated by the dashed lines.

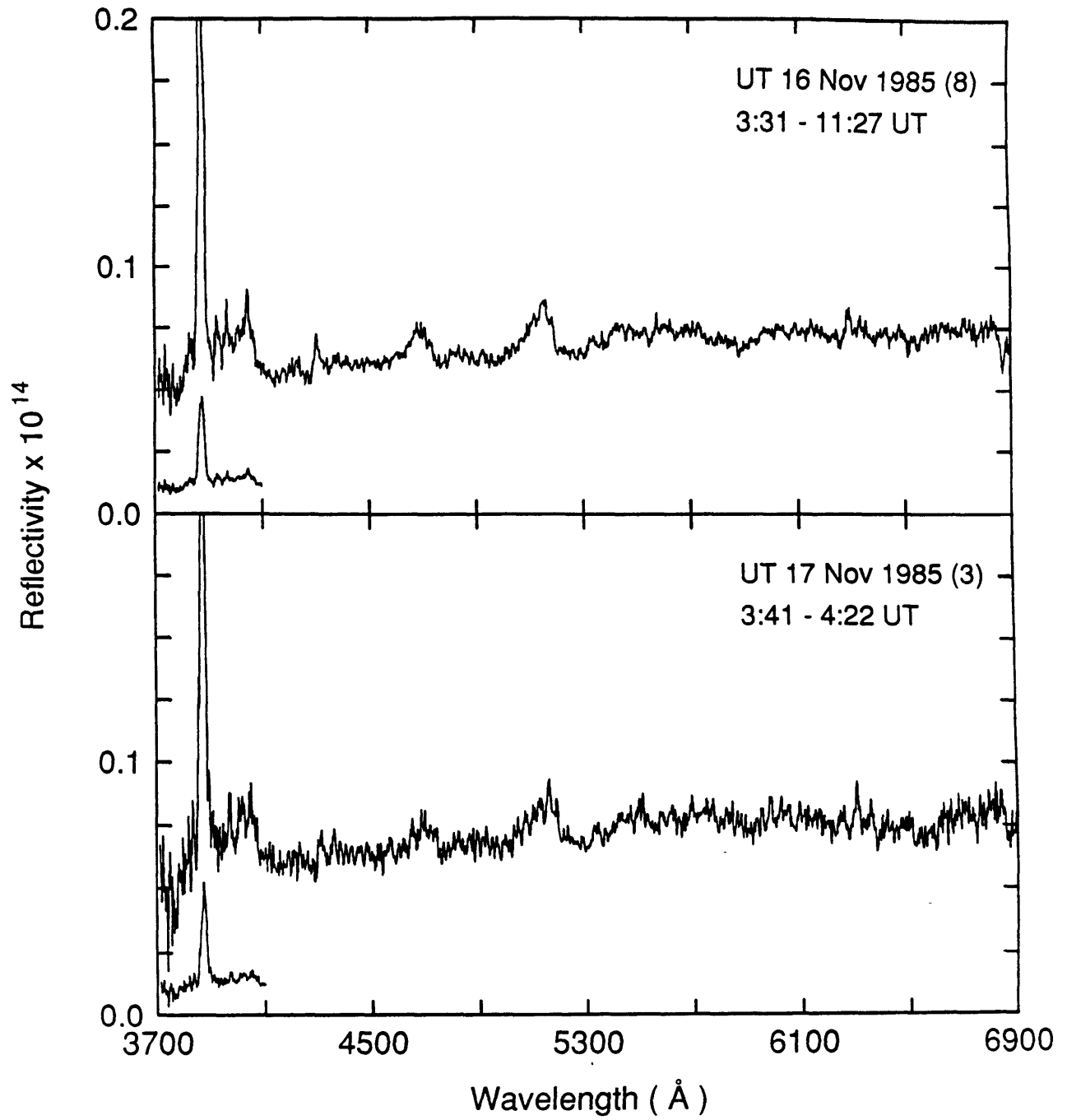


Figure 4-2. (b) See Figure caption for Figure 4-2a.

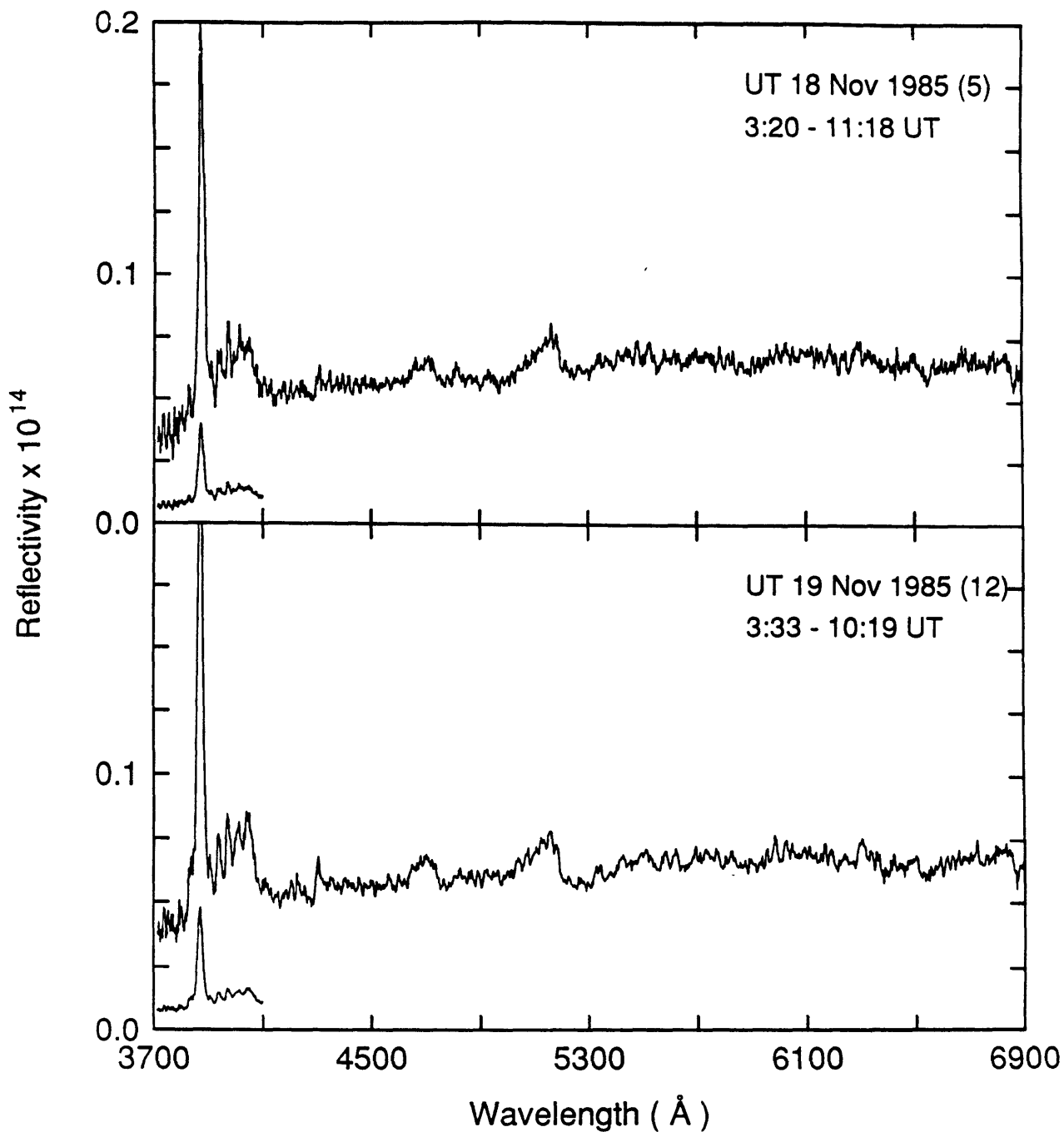


Figure 4-2. (c) See Figure caption for Figure 4-2a.

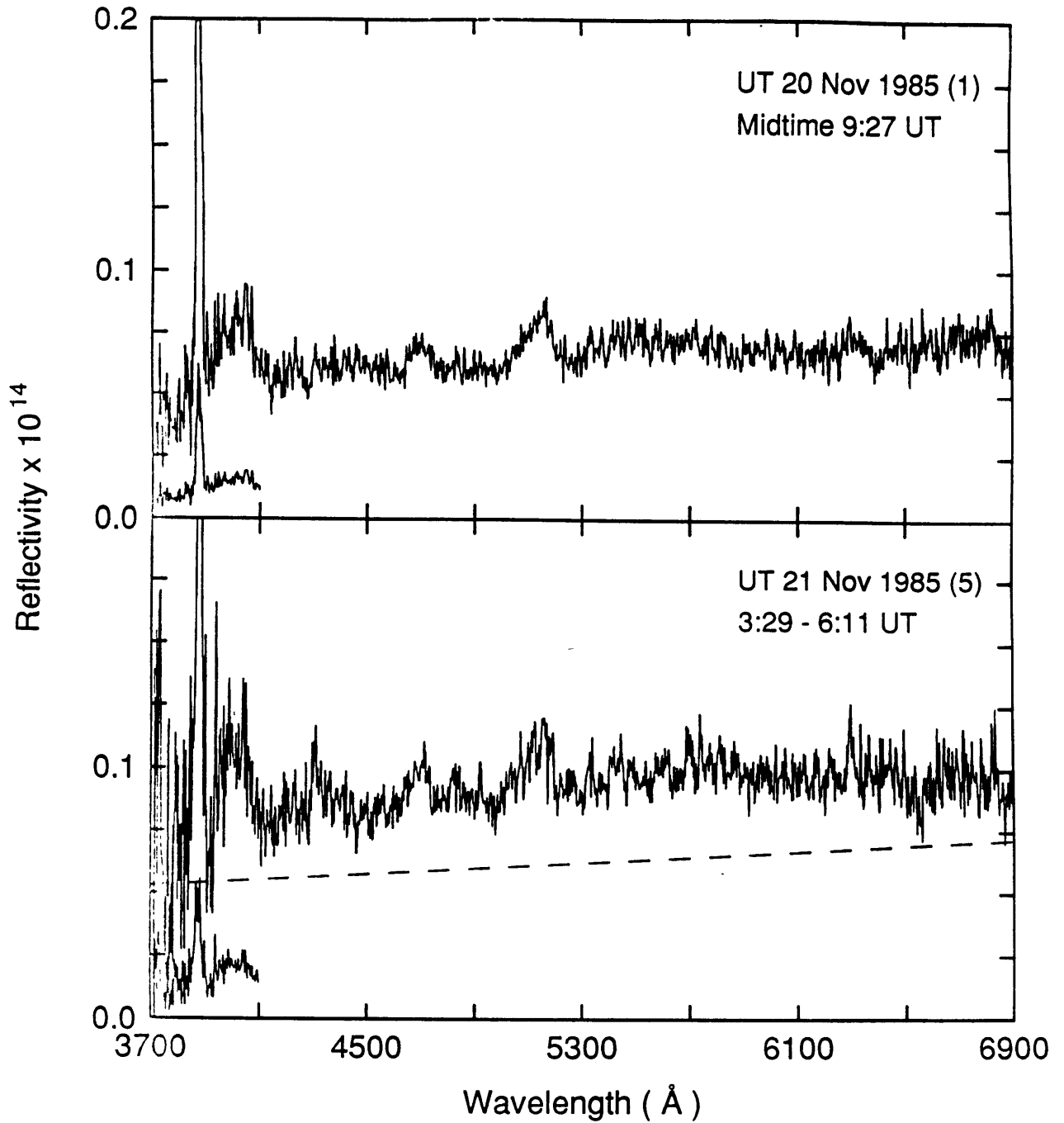


Figure 4-2. (d) See Figure caption for Figure 4-2a. The increased noise in the reflectivity on UT November 21 is due to the large neutral density filter employed (see text).

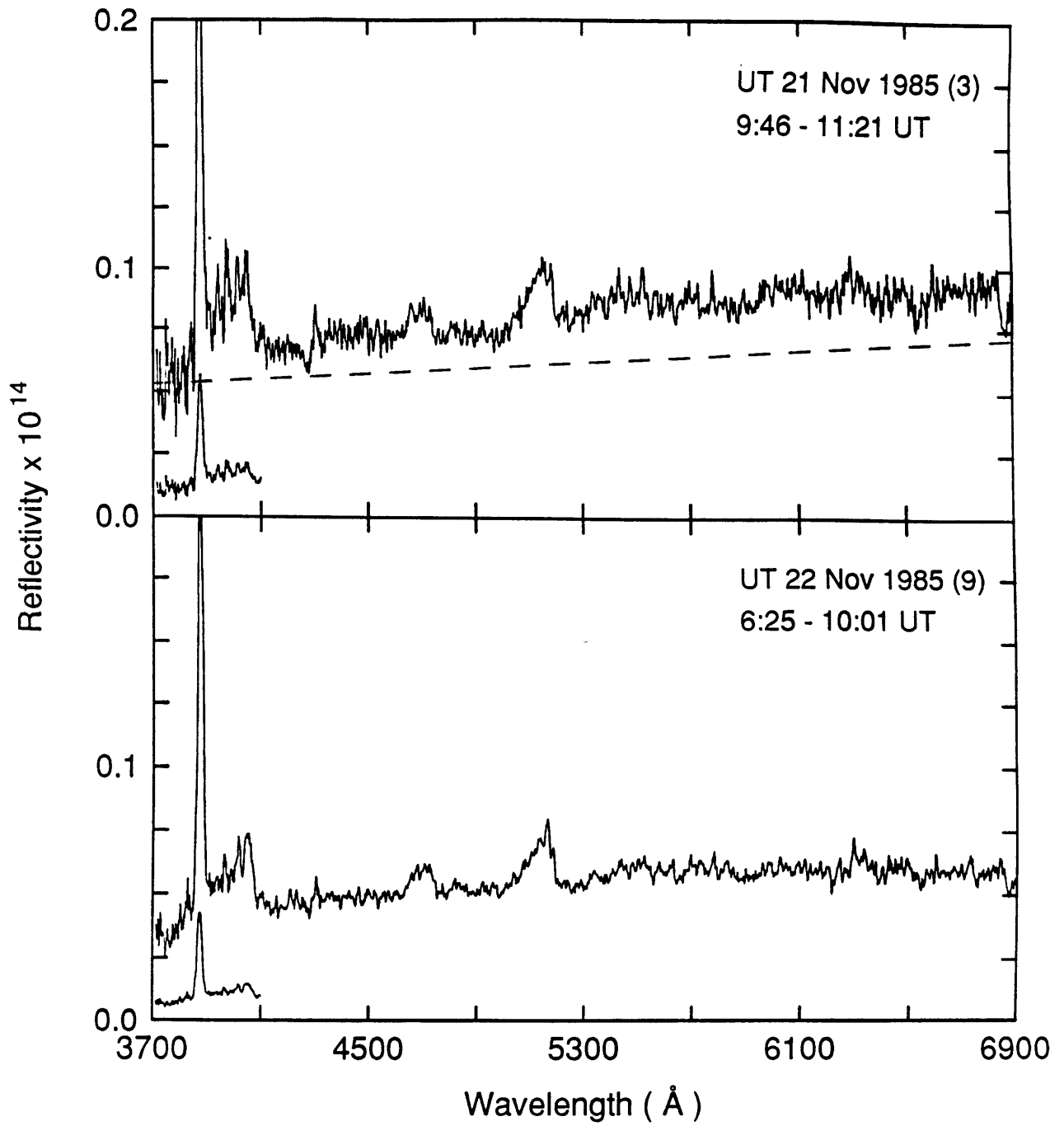


Figure 4-2. (e) See Figure caption for Figure 4-2a.

Species	Emission [†]	Continuum [†]
CN($\Delta v=0$)	3840-3900	3760-3800, 4130-4170
C ₃	3910-4110	3760-3800, 4130-4170
C ₂ ($\Delta v=+1$)	4560-4760	4450-4515, 4760-4810
C ₂ ($\Delta v=0$)	4975-5200	4930-4975, 5225-5260

[†] Wavelength range in Å.

Start (Wavelength in Å)	End (Wavelength in Å)
4390	4450
4750	4825
5200	5250
5760	5820
6235	6265
6380	6475
6780	6820

brightness in 7 continuum windows between $4390 \leq \lambda [\text{Å}] \leq 6820$ (see Table 4-2b) were used to compute the normalized reflectivity gradient, $S'(4390\text{Å}, 6820\text{Å}) = (dS/d\lambda) / S_{mean}$, expressed in percent per 10^3 Å , where $dS/d\lambda$ is the slope of the reflectivity spectrum and S_{mean} is the mean reflectivity in the wavelength interval. The normalized reflectivity gradient

is a measure of the grain color (see Chapter 6 for a discussion of this quantity); positive values indicating grain reddening, or increased scattering efficiency at longer wavelengths. Uncertainties in the color of the sun can introduce systematic errors in the color gradient of about $\pm 2\% / 10^3 \text{ \AA}$, which is roughly equal to the reflectivity gradient measurement error (Chapter 6; Jewitt and Meech, 1986). Emission band contamination of the continuum windows is minimal as all spectra (including those of other active comets) were examined to determine the emission free regions. The measurements show that the continuum of P/Halley is reddened with respect to the sun by $S'(4390 \text{ \AA}, 6820 \text{ \AA}) = (9 \pm 2) \% / 10^3 \text{ \AA}$. This value is consistent with the reddening ($5 \pm 2 < S'[\% / 10^3 \text{ \AA}] < 18 \pm 2$) seen for a sample of nine other comets (Jewitt and Meech, 1986).

4.4 Phase Function

4.4.1 Comet P/Halley

Figure 4-3 shows a plot of the mean continuum flux density, $F_{\lambda=5790 \text{ \AA}} [\text{J s}^{-1} \text{ m}^{-2} \text{ \AA}^{-1}]$, at the central and 40 arcsec West positions as a function of the time of observation. It is evident from Figure 4-3 that the continuum flux density varies among nights by a factor of order 2. There are two distinct outbursts in the continuum centered near JD 2446385.0 and JD 2446390.7, each with a duration of about 1 day. In between the outbursts, the continuum is a relatively smooth function of time. The substantial maxima apparent in the central ("nucleus") diaphragm are muted or absent at the 40 arcsec West position.

The data from the central diaphragm are shown in Figure 4-4a, but this time the continuum magnitude

$$m_{5790} = -2.5 \log (F_{\lambda}) - 28.58 \quad (4.1)$$

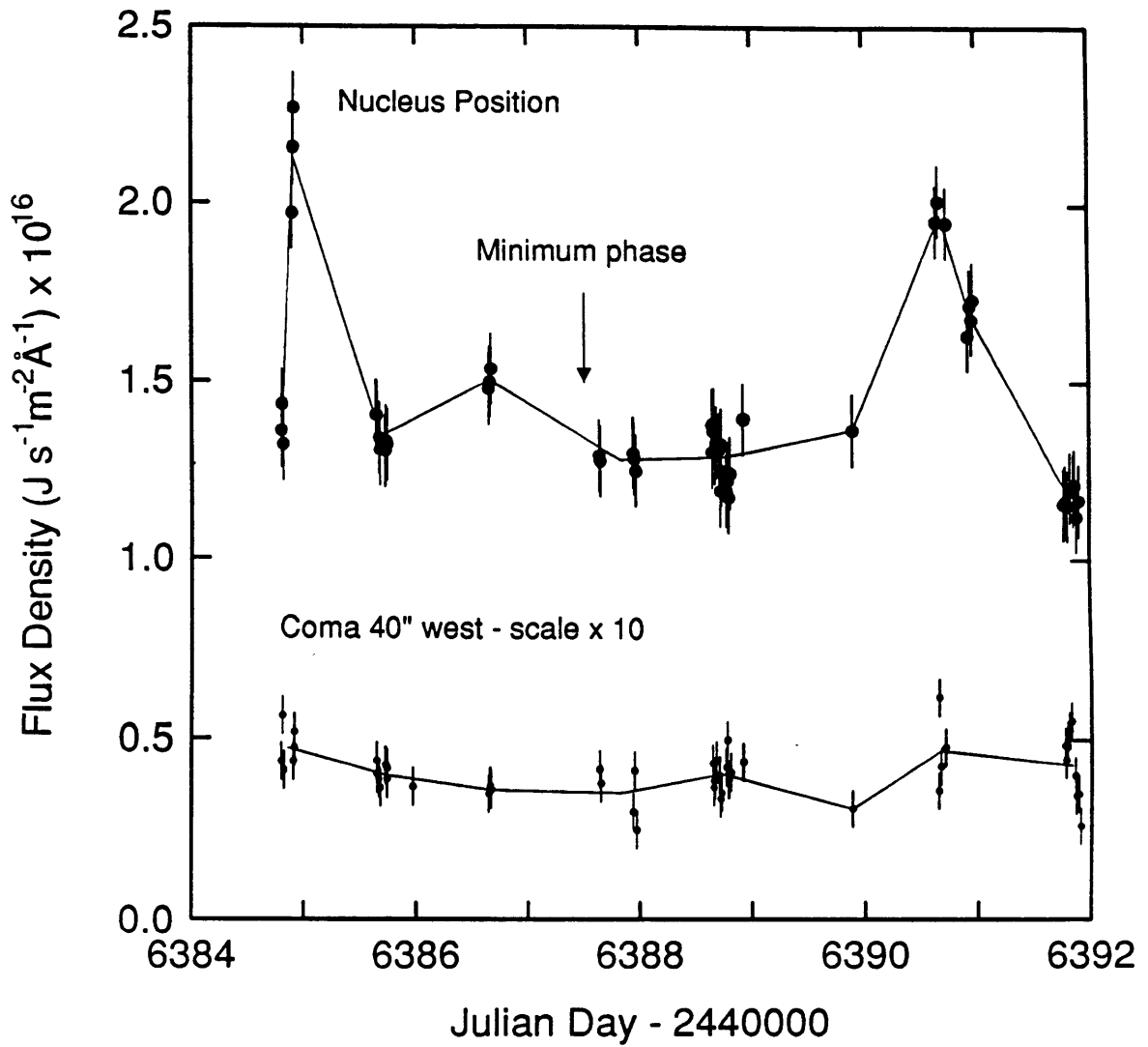


Figure 4-3. Plot of the P/Halley continuum flux density ($5760 \leq \lambda \text{ (\AA)} \leq 5820$) in the central and coma positions as a function of Julian Day (JD 2446384.5 = 1985 November 15 at 0^hUT). Minimum phase angle ($\alpha = 1.37$ deg) occurred near JD = 2446387.5; no phase related brightening is apparent. However, two brightness outbursts in the dust coma are evident near JD = 2446385.0 and JD = 2446390.7, (UT 1985 November 15 and 21) with brightness increases of 0.6 and 0.4 mag, respectively. The continuum flux density versus JD for the coma position (40 arcsec west of the nucleus) shows no delayed brightness surge. The flux density measured at the coma position has been multiplied by 10 in the figure.

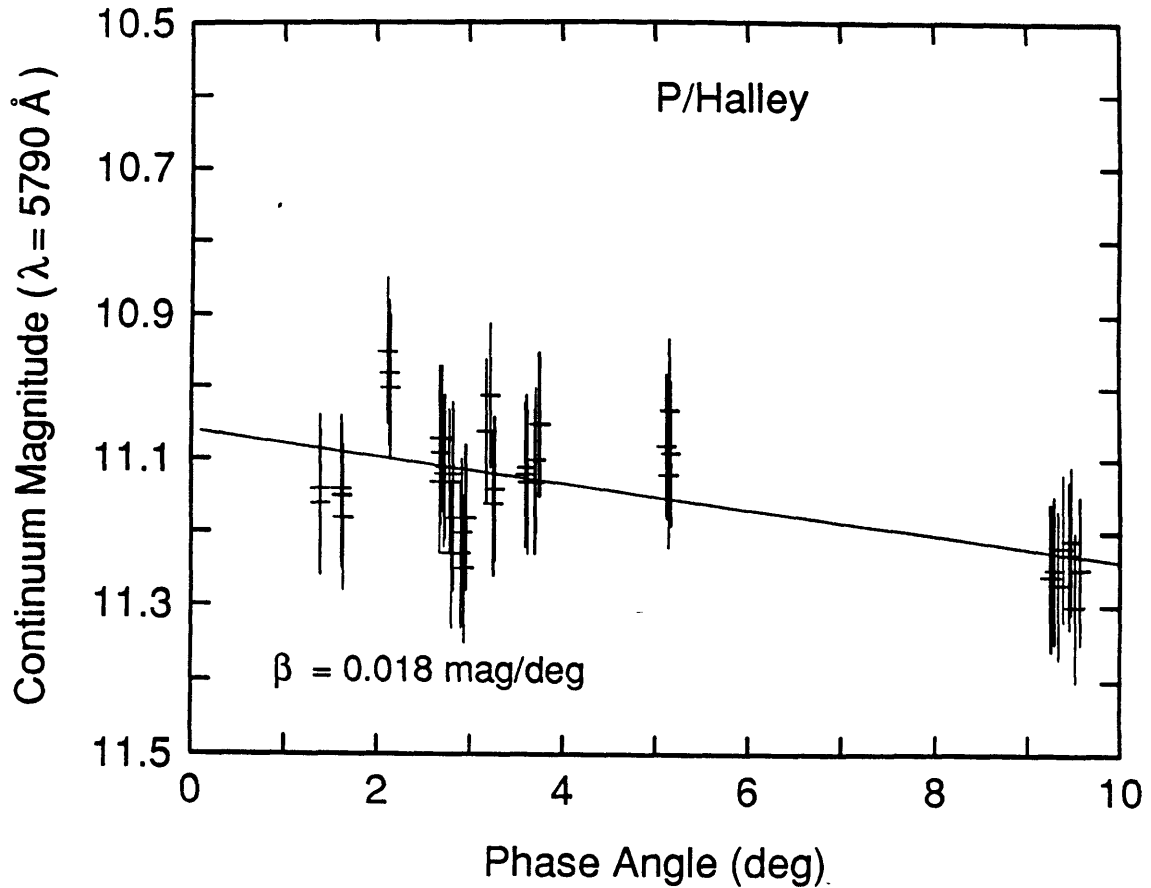


Figure 4-4. (a) Normalized magnitude versus phase angle for P/Halley (data from the present work), where the magnitude is that computed from the continuum window at $\lambda = 5790\text{\AA}$ ($m_{5790\text{\AA}} \approx V$), and only magnitudes measured outside the two "outbursts" have been plotted for clarity. A linear least squares fit for the linear phase coefficient, β , is shown. All comets are consistent with no opposition effect $\geq 0.2 \text{ mag}$ for $0 < \alpha \text{ (deg)} < 10$ and have linear phase coefficients in the range $0.01 \leq \beta [\text{mag deg}^{-1}] \leq 0.04$.

is plotted against the phase angle, α . (For practical purposes, m_{5790} is close to the V magnitude of the continuum). Data judged to be from the two outbursts in Figure 4-3 have been omitted from Figure 4-4a to attempt to emphasize any phase variations which may be present. The data are consistent with a small linear phase coefficient $\beta = 0.02 \pm 0.01$ mag deg⁻¹. There is no evidence for an opposition surge $\geq 20\%$. Most importantly, the factor of 2 to 3 ($\Delta m \approx 1$ mag) backscattering enhancements reported for other comets are clearly not seen in comet Halley over the phase angle range $1 \leq \alpha$ [deg] ≤ 10 . It is possible, although unlikely, that intrinsic activity acted to cancel phase related variations in P/Halley.

To set the P/Halley data in proper context, the following is a critical assessment of the brightness versus phase data for four other comets.

4.4.2 Comet P/Ashbrook-Jackson

Data from Kiselev and Chernova (1981) for comet P/Ashbrook-Jackson have been re-analyzed and are shown in Figure 4-4b. The magnitudes have been reduced to unit R and Δ , where Δ is the geocentric distance in AU, by subtracting $2.5 \log(R^2 \Delta)$ from the data. (Note that Kiselev and Chernova assumed a Δ^2 dependence in their analysis which is appropriate for a point source but not for an extended comet). Additionally, the magnitudes have been normalized so that the brightness at $\alpha = 10$ deg is equal to the brightness of P/Halley at this phase angle ($V \approx 11.24$ mag). Although the P/Ashbrook-Jackson observations were made with the broadband V filter ($\lambda_{eff} = 5480 \text{ \AA}$, $\Delta\lambda = 860 \text{ \AA}$), Larson (1978) found that the comet spectrum was pure continuum, so that gas contamination should not be a problem. Furthermore, the change in R during the interval of observation (4.5 months) was only $\Delta R \approx 0.1$ AU, so that intrinsic brightness variations with R may also be neglected. Even though Kiselev and Chernova have fitted an asteroid-like phase function to the data, showing an opposition surge (linear phase coefficient plus a non-linear term), the

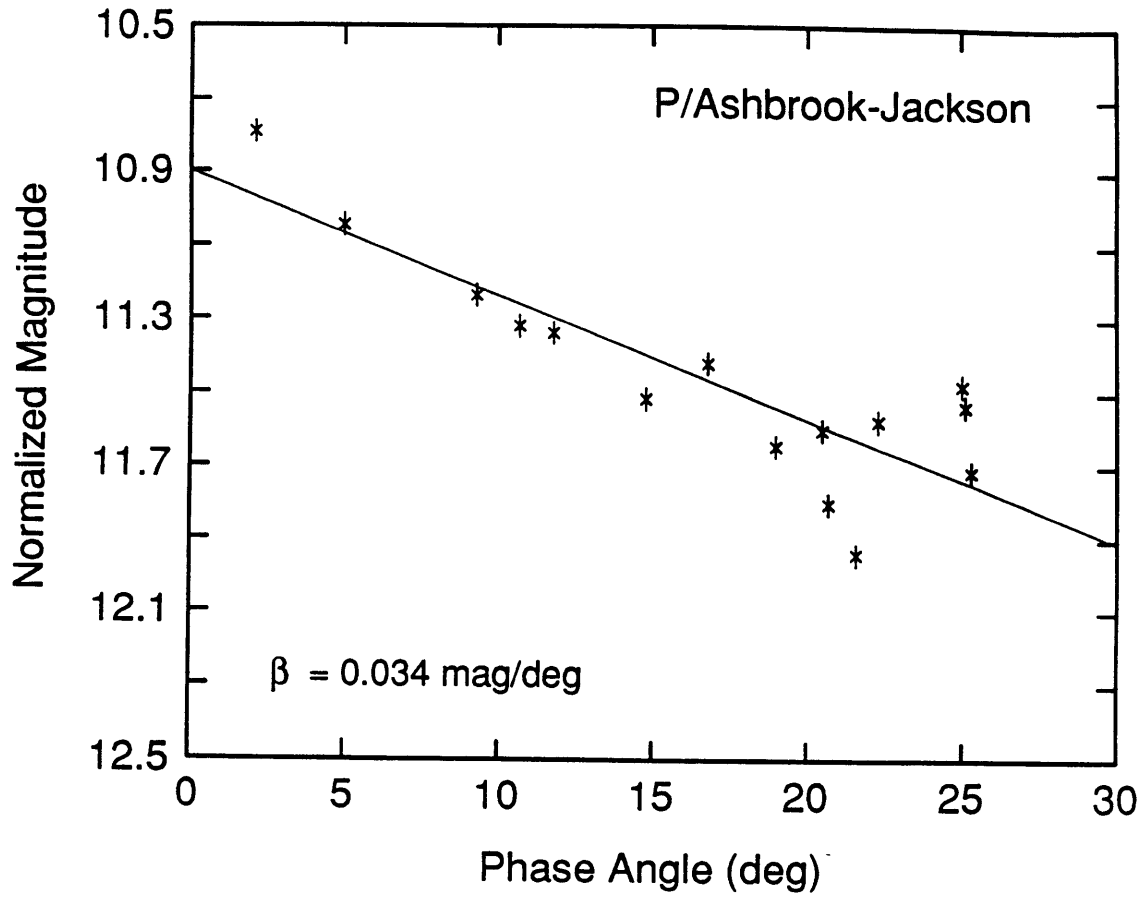


Figure 4-4. (b) Normalized magnitude versus phase angle for P/Ashbrook-Jackson (data from Kiselev & Chernova, 1981), where the errors of 0.03 mag are as reported in Kiselev & Chernova. A linear least squares fit for the linear phase coefficient, β , is shown. All comets are consistent with no opposition effect ≥ 0.2 mag for $0 < \alpha$ (deg) < 10 and have linear phase coefficients in the range $0.01 \leq \beta$ [mag deg⁻¹] ≤ 0.04 .

data may be equally well fitted with a simple linear phase coefficient $\beta = 0.034 \pm .006$ mag deg^{-1} . Any more complicated fit to the Kiselev and Chernova data is unjustified given that the data were sparsely sampled during the 4.5 month observation interval, thus precluding any estimate of the intrinsic cometary activity.

4.4.3 Comet *Bowell*

Data from A'Hearn *et al.* (1984) for comet *Bowell* (1982I) have been used to create the plot in Figure 4-4c. The continuum magnitudes were derived from mean flux densities, F_λ ($\lambda_{\text{eff}} = 5246\text{\AA}$, $\Delta\lambda = 72\text{\AA}$), found in Table I of their paper. The normalized V magnitude plotted in Figure 4-4c was computed via:

$$V = -2.5 \left[\log \left(\frac{\phi_o R^2 \Delta}{\phi} \right) + \log (F_\lambda) \right] + C_o \quad (4.2)$$

where ϕ is the observing diaphragm diameter, $\phi_o = 20$ arcsec is a standard diaphragm diameter and C_o is a normalization constant (so that $V \approx 11.24$ mag at $\alpha = 10$ deg). The observations of comet *Bowell* were taken over a large range of R ($3.7 \leq R [\text{AU}] \leq 5.6$) so that temporal and heliocentric variations may be suspected. However, the cross section of the coma of comet *Bowell* was nearly constant during the interval of observation (e.g. Jewitt, 1984), suggesting that the trend in brightness was due to the changing phase. The best fitting linear phase coefficient is $\beta = 0.035 \pm 0.005$ mag deg^{-1} ; there is no evidence for an opposition surge.

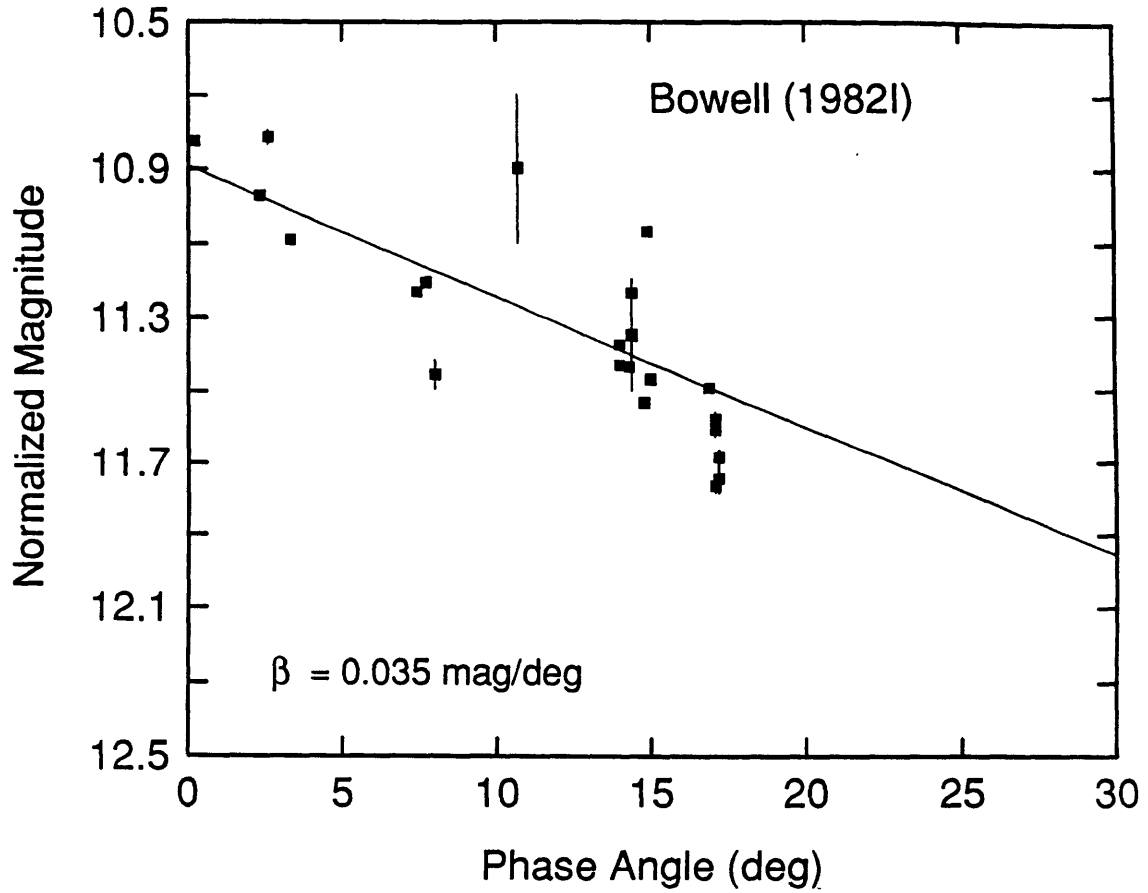


Figure 4-4. (c) Normalized magnitude versus phase angle for Bowell (data from A'Hearn *et al.*, 1984); the errors, where shown, are the errors on $\log(F_\lambda)$ as taken from the original paper. A linear least squares fit for the linear phase coefficient, β , is shown. All comets are consistent with no opposition effect ≥ 0.2 mag for $0 < \alpha$ (deg) < 10 and have linear phase coefficients in the range $0.01 \leq \beta$ [mag deg⁻¹] ≤ 0.04 .

4.4.4 Comet P/Stephan-Oterma

The normalized magnitudes of P/Stephan-Oterma (Millis *et al.* 1982) are presented as a function of phase angle in Figure 4-4d. Unlike the previous authors, Millis *et al.* did attempt to remove the effect of intrinsic activity from their data by examining the ratio of the dust production rate to the C₂ gas production rate as a function of phase angle. The success of their method demands that the ratio of the dust to gas production rates did not change as a function of R . The normalized magnitudes shown in Figure 4-4d were computed from the data found in Table II of Millis *et al.* by assuming that the coma brightness is proportional to the amount of dust in the coma and so to the production rate. A change in the dust/gas production ratio is thus equivalent to a change in the dust brightness, which can be converted to a normalized V magnitude using:

$$V = -2.5 \log (Q_R) + C_1, \quad (4.3)$$

where Q_R is the ratio of the dust production rate to the C₂ gas production rate, and C_1 is the normalization constant to the P/Halley data at $\alpha = 10$ deg. As with the previous comets, there is no evidence for an opposition surge. Instead, a linear phase coefficient represents the data well; for P/Stephan-Oterma $\beta = 0.020 \pm 0.004$ mag deg⁻¹.

4.4.5 Comet P/Encke

Finally, there exists a small set of measurements of comet P/Encke over a large range of phase angles ($7 \leq \alpha$ [deg] ≤ 117). The measurements are summarized in Figure 4-4e which is a plot of the R magnitude reduced to unit R and Δ versus phase angle. The small phase angle data ($\alpha \approx 7$ deg, 15 deg) are from the observations presented in Chapter 5 (Cometary Rotation

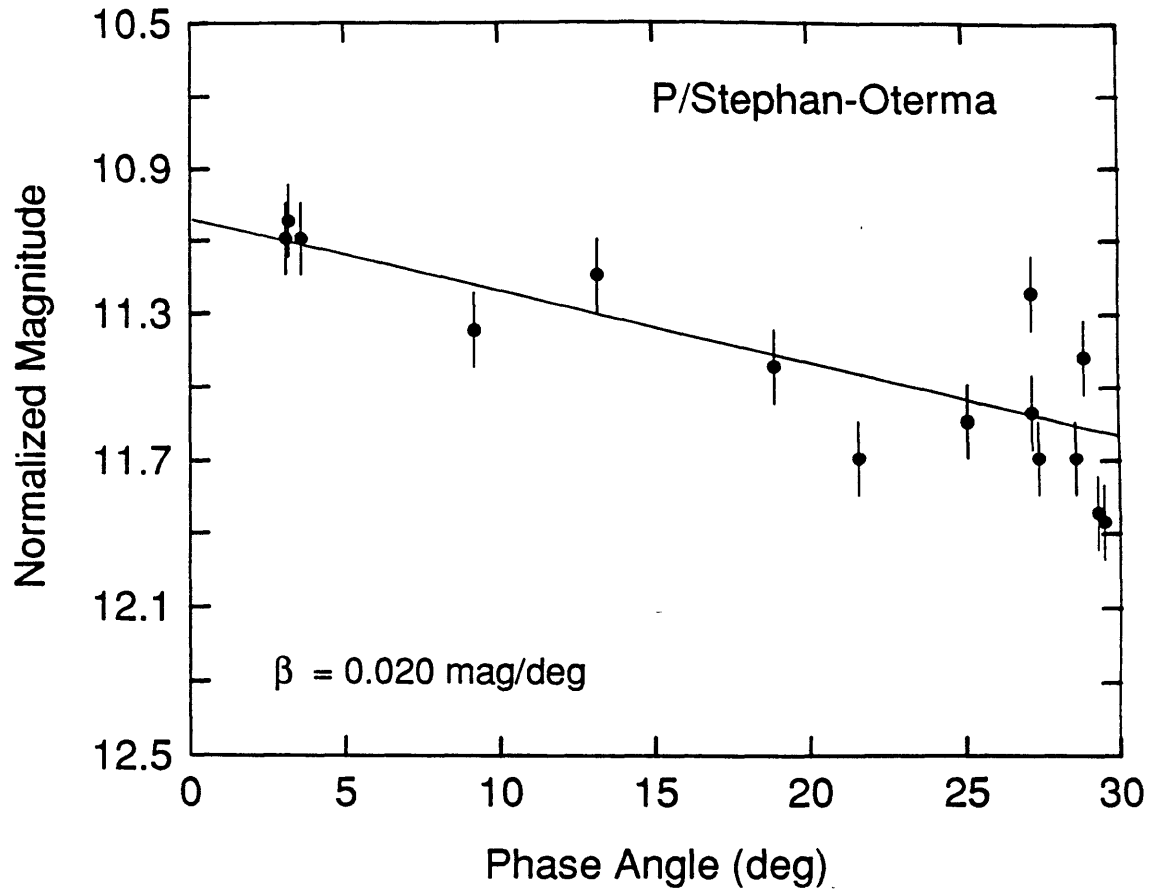


Figure 4-4. (d) Normalized magnitude versus phase angle for P/Stephan-Oterma (data from Millis *et al.*, 1982) where arbitrary 0.1 mag errors are plotted. A linear least squares fit for the linear phase coefficient, β , is shown. All comets are consistent with no opposition effect ≥ 0.2 mag for $0 < \alpha$ (deg) < 10 and have linear phase coefficients in the range $0.01 \leq \beta$ [mag deg⁻¹] ≤ 0.04 .

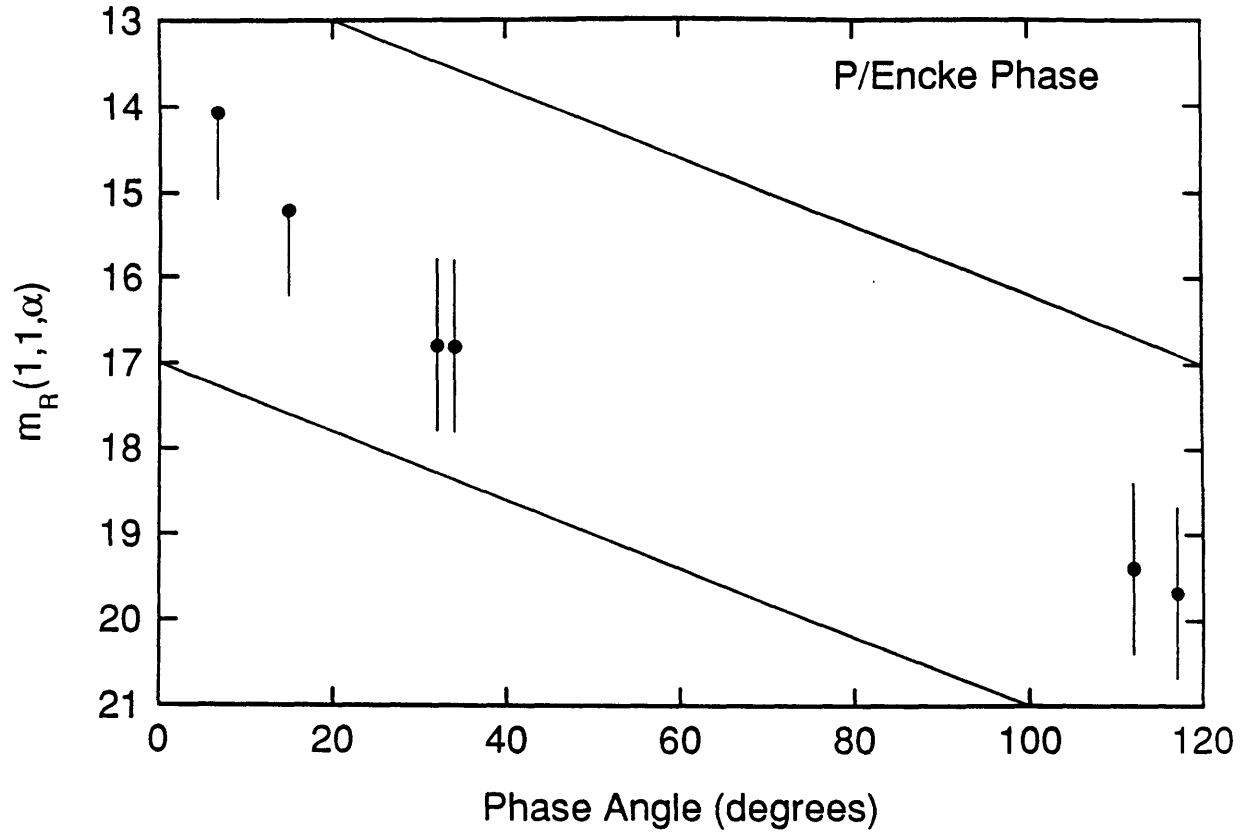


Figure 4-4. (e) Normalized magnitude versus phase angle for P/Encke (data from Chapter 5 and Jewitt & Meech, 1987) where the error bars indicate the uncertainty due to the rotational phase. The half error bars are for data known to be at maximum brightness. A linear least squares fit for the linear phase coefficient, β , is shown. All comets are consistent with no opposition effect ≥ 0.2 mag for $0 < \alpha$ (deg) < 10 and have linear phase coefficients in the range $0.01 \leq \beta$ [mag deg $^{-1}$] ≤ 0.04 .

Periods), whereas the large phase angle data are those of Spinrad as summarized in Jewitt and Meech (1987). The error bars on the data are a result of the uncertainty in the rotational phase of the comet. There are half error bars on two of the data points because the comet was known to be at maximum brightness (see Chapter 5). There are insufficient data to search for an opposition surge, however, the data are consistent with a phase coefficient of $\beta \approx 0.04$ mag deg⁻¹.

4.4.6 Comparison With Other Solar System Bodies

In all the cases discussed above, with the exception of P/Encke, the comets were described as showing either a "backscattering peak" or "enhancement", suggesting an asteroid-like opposition surge in some cases. There is no convincing evidence for an asteroid-like opposition surge, neither in the present data on P/Halley nor in the other comets for which phase curve measurements exist. The present spectrophotometric data set for P/Halley is probably the best suited for searching for the opposition surge, since the data were taken over a small interval in time and R . Frequent sampling allowed gross temporal variations to be easily identified.

In Figure 4-5a all of the normalized phase curves (except for that of P/Encke), including the present data for P/Halley, are plotted versus phase angle. For comparison, a theoretical phase curve for a low albedo asteroid (after Bowell and Lumme, 1979) has been plotted as a solid line. The dashed line shows a linear phase coefficient of 0.03 mag deg⁻¹, normalized to the theoretical curve for $\alpha > 15$ deg. The theoretical phase function has been normalized to the P/Halley magnitude at $\alpha = 10$ deg. It is evident from Figure 4-5a that none of the comet phase curves exhibit the 0.4 mag brightness enhancement over the linear portion of the curve as seen for the model. Models for surfaces with higher albedos have smaller opposition surges because multiple scattering destroys interparticle shadows; however, these

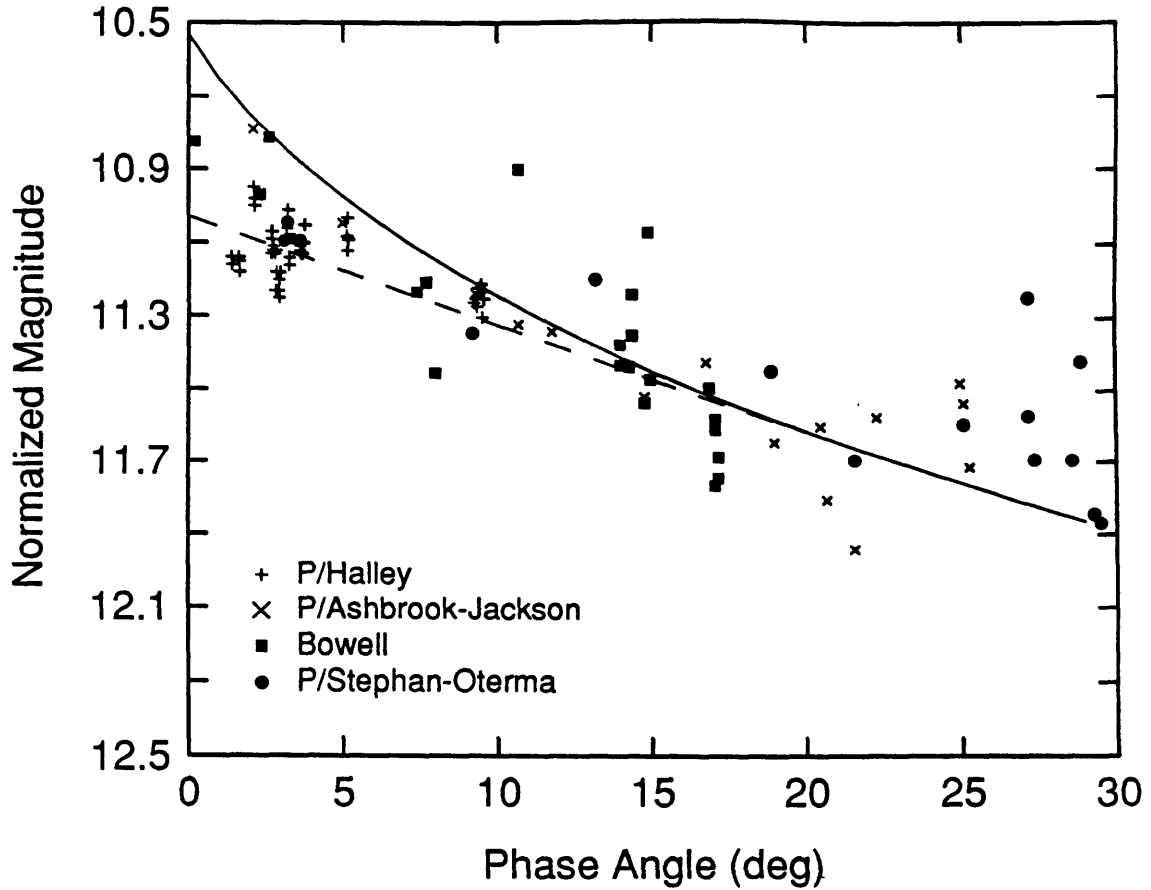


Figure 4-5. (a) Normalized V magnitude versus phase angle for all of the comets shown in Figures 4a-d. A Bowell and Lumme (1979) phase function ($p_V = 0.07$, $\beta = 0.037 \text{ mag deg}^{-1}$) is plotted as the solid line. The dashed line indicates a linear phase coefficient of $0.03 \text{ mag deg}^{-1}$. The comet data do not show the backscattering enhancement of $\Delta V \approx 0.4 \text{ mag}$ over the linear portion of the phase curve which is typically seen for asteroids.

models do not fit the large phase angle portion of the comet phase data as well as the low albedo models. The fact that the asteroid regolith scattering models do not fit the data well may suggest that the phase dependence is not caused by interparticle shadowing and that effects due to the single scattering albedos of the cometary particles are more important. It can therefore be concluded that the comets show a linear phase coefficient $\beta = 0.02 - 0.04 \text{ mag deg}^{-1}$ for phase angles $1 \leq \alpha \text{ [deg]} \leq 30$, but that there is no evidence for an opposition surge greater than about 0.2 mag. In this sense, the backscattering from comets is different from that seen in typical asteroids.

Although it appears unlikely that the phase function of the dust in the coma of P/Halley would be similar to that of a regolith, there are occasions when a regolith opposition effect can be extremely narrow and therefore go unobserved unless the measurements extend to very small phase angles $0 < \alpha \text{ [deg]} < 2$. Such is the case for the phase curves of the Uranian satellites Oberon, Ariel and Titania where the sharp rise in brightness does not occur until the phase angle is less than $\alpha \approx 1 \text{ deg}$ (*c.f.* Brown & Cruikshank, 1983; Hapke, 1986; Lane *et al.*, 1986). According to Hapke (1986), the width of the opposition peak is a function of both the filling factor and the particle size distribution. For power-law particle size distributions with indices $1 \leq k \leq 4$ and a large ratio of the largest to smallest particle sizes such as has been measured for P/Halley (McDonnell *et al.*, 1986), the opposition surge width can be extremely narrow. A comparison of the opposition surges of the Uranian satellites and P/Halley is presented in Figure 4-5b. The data for the satellites have been normalized to the P/Halley data at $\alpha = 2.95 \text{ deg}$. Furthermore, the surge can also be narrow when the particle volume filling factor is low. It is possible that an opposition surge in P/Halley was unobserved by us because it was extremely narrow.

At the other extreme, an opposition surge would be difficult to detect if it were broad and of low amplitude. For example, the Gegenschein is a broad backscattering enhancement from interplanetary particles which are themselves believed to originate in comets. The

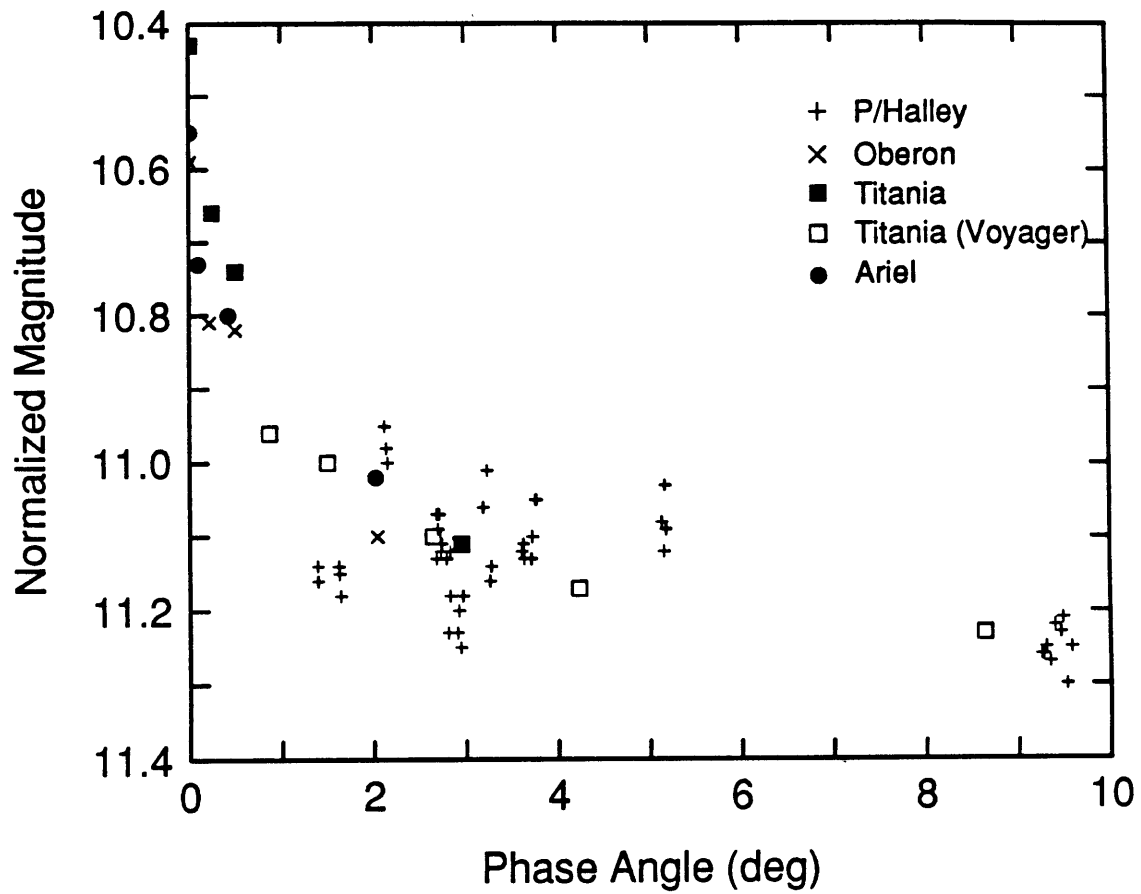


Figure 4-5. (b) Comparison of the opposition surge for the Uranian satellites with the data for P/Halley. The data have been normalized at $\alpha = 2.95$ deg.

Gegenschein is an antisolar brightness excess of about 20% with a diameter approximately 20 degrees between the points of half intensity (Dumont & Sánchez, 1975). Lamy and Perrin (1986) have utilized extensive zodiacal light brightness measurements in order to obtain the scattering phase function per unit volume of the interplanetary dust. They concluded that the backscattering enhancement was only a factor of 2 over the minimum value near phase angle $\alpha = 80$ deg; furthermore, the models do not suggest a strong surge at small phase angles ($\alpha \leq 10$ deg). Leinert (1975) found similar brightness gradients in the Gegenschein of about 1-2% per deg, within approximately $\alpha \leq 10$ deg of the center. This corresponds to about a 0.1 - 0.2 mag brightness enhancement within the phase angle range observed for P/Halley.

In Figure 4-5c the phase function of the zodiacal dust (Dumont & Sánchez (1975); Leinert (1975)) is compared with the brightness versus phase data for the comets. As in Figure 4-5a, all data are normalized to $V = 11.24$ at $\alpha = 10$ deg. The very small amplitude of the Gegenschein is apparent from the figure. Considerable scatter among the phase curves of the comets makes a comparison with the zodiacal dust rather difficult. However, it appears that the phase curves of the comets are steeper than the phase curve of the interplanetary dust, especially for phase angles $\alpha \geq 10$ deg.

In summary, the backscattering phase functions of the comets are different from a majority of asteroid and satellite phase functions (including that of the moon, see Gehrels *et al.*, 1964) which show a pronounced opposition surge (see Figure 4-5a). Furthermore, there appear to be differences between the phase functions of the interplanetary dust and the cometary dust (see Figure 4-5c). On the other hand, a similarity to surfaces with very narrow backscattering enhancements such as Oberon, Ariel and Titania cannot be ruled out (see Figure 4-5b). The slopes of the phase curves shown in Figure 4-5a are compatible with a simple extrapolation to small phase angles of the phase curves presented for angles $30 \leq \alpha$ [deg] ≤ 150 by Ney (1982) for comet West. It should also be noted that there is no evidence for glory-like backscatter in the present data. Further measurements of scattering from the

comae of comets at small to moderate phase angles, while taking account of the intrinsic variability of the coma brightness, will allow more detailed comparison of the scattering properties of comet dust, the interplanetary dust and asteroid surfaces.

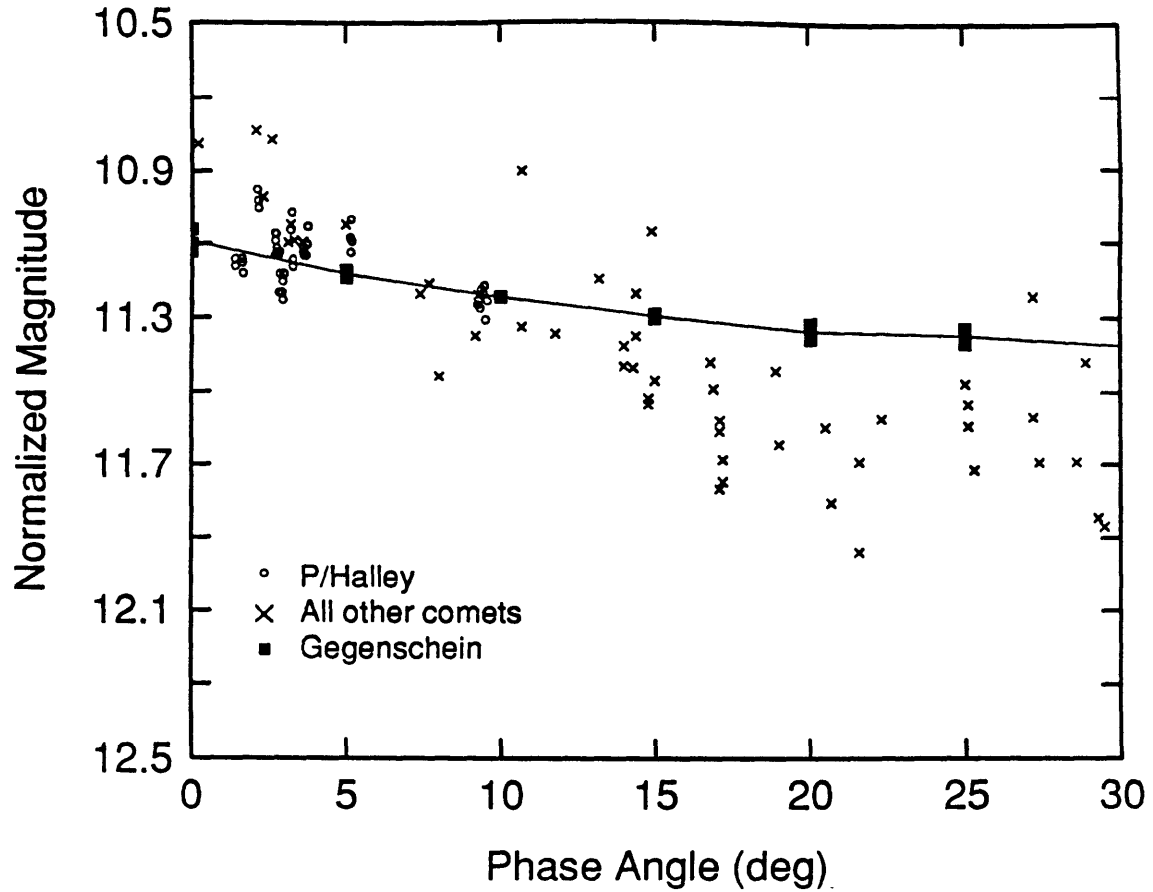


Figure 4-5. (c) Comparison of the normalized V magnitude versus phase angle for all of the comets with the phase dependence of the zodiacal light (data from Dumont & Sánchez, 1975; Leinert, 1975). The data on P/Halley are plotted with open circles, whereas all other comets are plotted with crosses. The zodiacal dust data are plotted as filled boxes.

4.5 Conclusions

1. No opposition effect $\geq 20\%$ is detected in the continuum of P/Halley in the phase angle range $1 < \alpha$ [deg] < 10 . Instead, the backscattered continuum is adequately represented by a linear phase coefficient, $\beta = 0.02 \pm 0.01$ mag deg⁻¹.
2. No evidence for opposition effects greater than 20% was found in a re-examination of published data on comets P/Ashbrook-Jackson, Bowell and P/Stephan-Oterma. The backscattering phase functions of these comets are best described by small (but significant) linear phase coefficients, $\beta = 0.02 - 0.04$ mag deg⁻¹.
3. The cometary phase coefficients are similar to those of low albedo asteroids. However, the comets differ from low albedo asteroids in that they lack observable opposition surges. The backscattering phase functions of comets are steeper than the phase function of the zodiacal light in the range $0 < \alpha$ [deg] < 30 .
4. Reflectivity spectra of comet P/Halley show a strong dust continuum with bands of $CN(\Delta v=0)$, C_3 , $C_2(\Delta v=+1)$ and $C_2(\Delta v=0)$ superimposed. The dust continuum of P/Halley is reddened with respect to the sun by $S' = (9 \pm 2) \% / 10^3 \text{ \AA}$ in the wavelength interval $4390 \leq \lambda$ [Å] ≤ 6820 . This value is typical of other comets.

References

- A'Hearn, M. F., P. V. Birch, P. D. Feldman and R. L. Millis (1985), "Comet Encke: Gas Production and Lightcurve", *Icarus* **64**, 1-10.
- A'Hearn, M. F., D. G. Schleicher, P. D. Feldman, R. L. Millis, and D. T. Thompson (1984), "Comet Bowell 1980b", *Astron. J.* **89**, 579-591.
- Arvesen, J. C., R. N. Griffin, and B. D. Pearson (1969), "Determination of Extraterrestrial Solar Spectral Irradiance From a Research Aircraft", *Appl. Optics* **8**, 2215-2232.
- Bowell, E. and K. Lumme (1979), "Colorimetry and Magnitudes of Asteroids", in *Asteroids*, ed. T. Gehrels, Univ. of AZ Press, Tucson, p. 132-169.
- Bradley, J. P., D. E. Brownlee, and P. Fraundorf (1984), "Carbon Compounds in Interplanetary Dust: Evidence for Formation by Heterogeneous Catalysis", *Science* **223**, 56-58.
- Brown, R. H. and D. P. Cruikshank (1983), "The Uranian Satellites: Surface Compositions and Opposition Brightness Surges", *Icarus* **55**, 83-92.
- Brownlee, D. E. (1978), "Microparticle Studies By Sampling Techniques", in *Cosmic Dust*, ed. J. A. M. McDonnell, John Wiley and Sons, NY, p. 295-336.
- Dumont, R. and F. Sánchez (1975), "Zodiacal Light Photopolarimetry", *Astron. Astrophys.* **38**, 405-412.
- Gehrels, T., T. Coffeen and D. Owings (1964), "Wavelength Dependence of Polarization. III. The Lunar Surface", *Astron. J.* **69**, 826-852.
- Hanner, M. S., R. H. Giese, K. Weiss, and R. Zerull (1981), "On the Definition of Albedo and Application to Irregular Particles", *Astron. Astrophys.* **104**, 42-46.
- Hapke, B. (1986), "Bidirectional Reflectance Spectroscopy 4. The Extinction Coefficient and the Opposition Effect", *Icarus* **67**, 264-280.
- Jewitt, D. (1984), "Coma Expansion and Photometry of Comet Bowell (1980b)", *Icarus* **60**, 373-385.
- Jewitt, D. and K. J. Meech (1986), "Cometary Grain Scattering Versus Wavelength, or 'What Color is Comet Dust?'", *Astrophys. J.* **310**, 937-952.
- Jewitt, D. and K. J. Meech (1987), "CCD Photometry of Comet P/Encke", *Astron. J.* **93**, 1542-1548.
- Kiselev, N. N. and G. P. Chernova (1981), "Phase Functions of Polarization and Brightness and the Nature of Cometary Atmosphere Particles", *Icarus* **48**, 473-481.
- Lamy, P. L. and J. -M. Perrin (1986), "Volume Scattering Function and Space Distribution of the Interplanetary Dust Cloud", *Astron. Astrophys.* **163**, 269-286.

References, contd.

- Lane, A. L., C. W. Hord, R. A. West, L. W. Esposito, K. E. Simmons, R. M. Nelson, B. D. Wallis, B. J. Buratti, L. J. Horn, A. L. Graps and W. R. Pryor (1986), "Photometry From Voyager 2: Initial Results From the Uranian Atmosphere, Satellites and Rings", *Science* **233**, 65-70.
- Larson, S. (1978), "Spectroscopic Observations of Comets", *IAU Circ. No.* 3293
- Leinert, C. (1975), "Zodiacal Light - A Measure of the Interplanetary Environment", *Space Sci. Rev.*, **18**, 281-339.
- Lumme, K., E. Bowell (1981), "Radiative Transfer in the Surfaces of Atmosphereless Bodies. I. Interpretation of Phase Curves", *Astron. J.* **86**, 1705-1721.
- McDonnell, J. A. M., W. M. Alexander, W. M. Burton, E. Bussoletti, D. H. Clark, R. J. L. Grard, E. Grün, M. S. Hanner, D. W. Hughes, E. Igenbergs, H. Kuczera, B. A. Lindblad, J. -C. Mandeville, A. Minafra, G. H. Schwehm, Z. Sekanina, M. K. Wallis, J. C. Zarnecki, S. C. Chakaveh, G. C. Evans, S. T. Evans, J. G. Firth, A. N. Littler, L. Massonne, R. E. Olearczyk, G. S. Pankiewicz, T. J. Stevenson and R. F. Turner (1986), "Dust Density and Mass Distribution Near Comet Halley From Giotto Observations", *Nature* **321**, 338-341.
- Millis, R. L., M. F. A'Hearn and D. T. Thompson, D. T. (1982), "Narrowband Photometry of Comet P/Stephan-Oterma and the Backscattering Properties of Cometary Grains", *Astron. J.* **87**, 1310-1317.
- Mukai, S., T. Mukai, R. H. Giese, K. Weiss, K. and R. H. Zerull (1982), "Scattering of Radiation by a Large Particle with a Random Rough Surface", *Moon & Planets* **26**, 197-208.
- Ney, E. P. (1982), "Optical and Infrared Observations of Bright Comets in the Range 0.5 μ m to 20 μ m", in *Comets*, ed. L. L. Wilkening, Univ. of AZ Press, Tucson, p. 323-340.
- Ney, E. P. and K. M. Merrill (1976), "Comet West and the Scattering Function of Cometary Dust", *Science* **194**, 1051-1053.
- Oetking, P. (1966), "Photometric Studies of Diffusely Reflecting Surfaces with Applications to the Brightness of the Moon", *J. Geophys. Research* **71**, 2505-2513.
- Shectman, S. and W. A. Hiltner (1976), "A Photon-Counting Multichannel Spectrometer", *Pub. Astron. Soc. Pac.* **88**, 960-965.
- Stone, R. P. S. (1977), "Spectral Energy Distributions of Standard Stars of Intermediate Brightness. II.", *Astrophys. J.* **218**, 767-769.
- Whipple, F. L. (1967), "On Maintaining the Meteoritic Complex", in *The Zodiacal Light and the Interplanetary Medium*, ed. J. L. Weinberg, NASA SP-150, p. 409-426

Chapter 5 - Cometary Rotation Periods

5.1 Introduction

The nucleus rotation period is a fundamental property of a comet. Knowledge of the period is extremely important if the behavior of a comet is to be modelled as a function of heliocentric distance. The rotation period determines the rate at which solar energy is deposited on the surface of the nucleus; it therefore controls the surface temperature distribution and the rate of mass loss from the nucleus. Additionally, as first discussed by Whipple (1950,1951), the non-gravitational motions of comets can be interpreted as reactions to jet forces from the irregular sublimation of rotating nuclei. The period of rotation and the sense of rotation (prograde, retrograde) both effect the interpretation of the non-gravitational accelerations.

5.1.1 Period Determination

Unlike asteroids, whose rotation periods may be easily measured by direct observations of the brightness as a function of time, comets present some difficulties. Until very recently, most comet observations were made when the comet is bright and close to the sun (for heliocentric distances $R < 3$ or 4 AU). At such small distances the nucleus is actively sublimating, expelling dust and ice into the coma. A typical nucleus cross section (few km^2) is many orders of magnitude smaller than the cross section of grains in the coma which scatter the incident sunlight; therefore even though the coma is optically thin, it is difficult to directly determine the rotation period of the nucleus. Additionally, active comets are known to exhibit non-periodic changes in brightness, presumably due to outbursts. A solution to the problem of determining the rotation period is to either *infer* a nucleus rotation period from periodic

variations in the coma brightness, or to observe relatively inactive comets in which the nucleus cross section is a significant fraction of the coma cross section. Finally, if observations are made of nuclei at distances beyond which water-ice sublimation is active ($R > 6$ AU) it may be possible to observe the nucleus directly. Typically, because of their small cross sections and low albedos, cometary nuclei are faint ($m_R > 19$ mag), so that observations require both large aperture telescopes and sensitive detectors (CCD's).

The first systematic investigation of cometary rotation periods was made by Whipple (1982) who developed the "halo method" of period determination. In this method, it is assumed that the nucleus activity arises from discrete sources and that these sources become active as the nucleus rotation carries them into the sunlit hemisphere. The periodic injection of material into the coma therefore produces a series of halos or parabolic envelopes which expand outward from the nucleus. Measurements of the envelope radius divided by the velocity yield the time of formation. Successive halos will be separated by a multiple of the rotation period. There are several major weaknesses inherent in this method. First, the expansion velocity of the halos is generally not well known. Second, there may be multiple active areas on the nucleus, the number of which may not be constant with time. Third, Whipple has made extensive use of visual observations and these are of uncertain accuracy. Given these weaknesses, the method is probably untrustworthy.

Whipple (1982) has applied this technique to 47 comets. Unfortunately, the accuracy of this method of period determination has been little tested. The most direct method of nucleus rotation determination involves the use of photoelectric photometry. The only known photoelectric photometry of the brightness variations of a comet which may be compared to the halo method results (prior to the work presented in this Chapter) is by Fay and Wisniewski (1978) for comet P/d'Arrest. Fay and Wisniewski find a complicated four-peaked light curve with a period of 5.17 ± 0.01 hr for comet P/d'Arrest, whereas the halo method yields a period of either 6.7 or 7.9 hr. It is difficult to interpret a four-peaked

lightcurve as resulting from the rotation of an irregularly shaped nucleus (which, by rotational symmetry, should produce a two-peaked lightcurve); however, observational errors may have contributed to the difference in appearance between the peaks. Observations were obtained with a simple aperture photometer; therefore centering errors can be important and it would have been difficult to exclude faint field stars from the diaphragm. Therefore, based on this one measurement of comet P/d'Arrest, one cannot make any statements concerning the validity of the Whipple halo method of period determination.

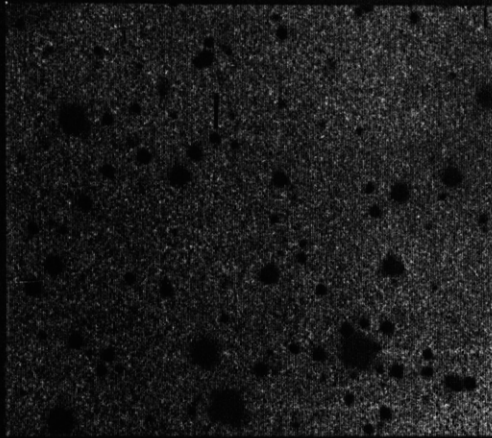
In the following sections observations of 4 cometary nuclei at large heliocentric distances and one relatively inactive comet at smaller heliocentric distances will be presented. Periods have been determined for comets P/Arend-Rigaux, P/Neujmin 1 and P/Encke and constraints have been placed on the periods for comets P/Tempel 2 and P/Halley. The periods are all long compared to the time for the surface to reach thermal equilibrium, so for the purposes of modelling the sublimation from the nucleus, the comets may be considered "slow" rotators. Figure 5-1 presents a composite of all of the nuclei discussed in this Chapter. The image of P/Arend-Rigaux shows the comet when it was at a larger R than when the rotation period was determined.

5.2 Observations

5.2.1 Comet P/Arend-Rigaux

Comet P/Arend-Rigaux is an extremely inactive comet; on some apparitions it has developed no coma at all. This is consistent with the calculations by Marsden (1968) which show that the comet has no measurable non-gravitational acceleration. For these reasons, it is an attractive object from which to obtain a rotation period. During the perihelion passage in 1984 December the comet was near opposition, and several groups monitored the brightness

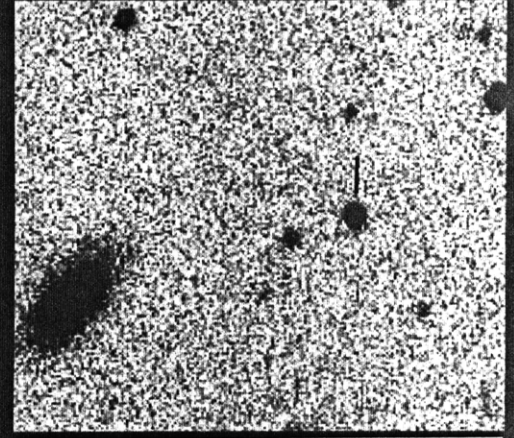
Figure 5-1. Five comet nuclei. (i) Comet P/Neujmin at $R = 5.03$ AU, exposure made with the Kitt Peak 2.1m telescope (observation #16 from Table 5-5). The scale of the image is 150 arcsec on a side. (ii) Comet P/Tempel 2 at $R = 3.99$ AU (observation #37 from Table 5-8); taken with the KPNO 2.1m. Image is about 150 arcsec on a side. (iii) Comet P/Encke at $R = 4.07$ AU (observation #23 from Table 5-6) taken with the KPNO 4m. Image is approximately 60 arcsec on a side. (iv) Comet P/Arend-Rigaux at $R = 3.98$ AU, $\Delta = 3.62$ AU. Image taken 1986 March 6 with the KPNO 2.1m. Image is 150 arcsec on a side. (v) Comet P/Halley at $R = 8.2$ AU, $\Delta = 7.2$ AU taken by D. Jewitt (private communication) using the PFUEI CCD camera at the Palomar 5m telescope during 1984 January. The comet is centered within a circle of radius 10 arcsec. All images were taken through the Mould R filter with the exception of P/Halley which was taken through the Thuan - Gunn r filter ($\lambda = 0.65 \mu\text{m}$, $\Delta\lambda \approx 0.1 \mu\text{m}$).



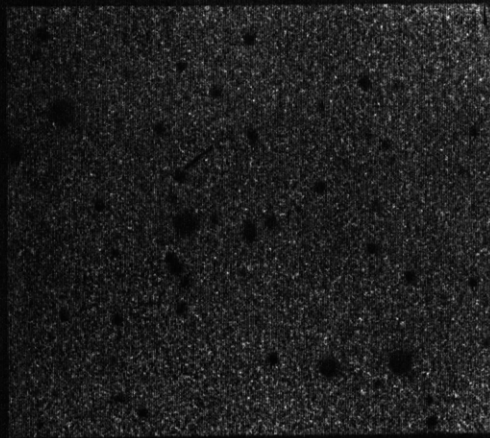
P/Neujmin 1 (R = 5.04)



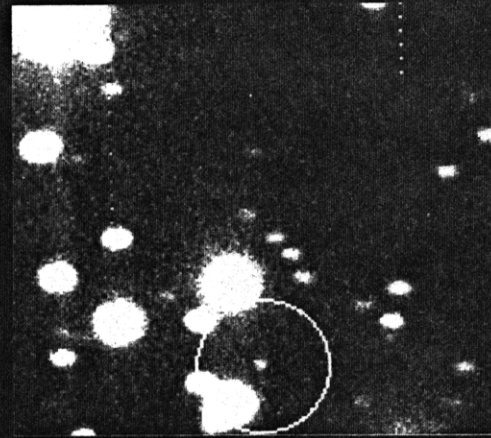
P/Tempel 2 (R = 3.99)



P/Encke (R = 4.07)



P/Arend-Rigaux (R = 3.98)



P/Halley (R = 8.16)

of the comet. The present observations were taken using the MASCOT CCD camera (Meyer & Ricker, 1980) at the f/13.5 Cassegrain focus of the 1.3m telescope at MIT's McGraw-Hill observatory (MHO). The instrument was used in its direct imaging mode with an image scale of 1.6 arcsec per 25 μm pixel. Images were obtained on the nights of UT 1985 January 18, 19, 20, and 21 during photometric conditions. Table 5-1 presents the geometry of the observations. All observations were made through the Johnson R_J filter (central wavelength $\lambda_{cent} \approx 0.7 \mu\text{m}$, $\Delta\lambda \approx 0.2 \mu\text{m}$). The photometry was calibrated using the standard stars Feige 34, BD+54°1981, BD+21°607, BD+54°1216 and HD 19445 (Thuan & Gunn, 1976). Extinction was determined from measurements of several field stars in each frame. From observations of the standard stars, each night was found to be photometric to better than 3%. The seeing was in the range 1.5 to 2.0 arcsec FWHM. The images show a bright, condensed nucleus in addition to a low surface brightness coma. The brightness of the comet was measured in a diaphragm of projected radius 8 arcsec ($3.3 \times 10^6\text{m}$ at the comet). Measurements were also made in an annulus of inner radius 8 arcsec and outer radius of 12 arcsec in order to monitor variations in the coma. The mean R_J surface brightness in the annulus was $21.4 \text{ mag arcsec}^{-2}$. Sky measurements were made 50 arcsec to the south of the nucleus in a region free of coma. The photometric measurements for both the diaphragm

Table 5-1

Geometry of Comet P/Arend-Rigaux

Date	Tel. Diameter	Seeing [arcsec]	No. of obs.	R (AU)	Δ (AU)	α°
85/01/18	1.3	2 - 3	1	1.538	0.567	10.1
85/01/19	1.3	2 - 3	12	1.541	0.569	9.3
85/01/20	1.3	2 - 3	24	1.545	0.571	8.6
85/01/21	1.3	2 - 3	24	1.549	0.574	8.0

Photometry of P/Arend-Rigaux

Table S-2

N	Date	UT [†]	Tel [m]	Exp [sec]	Time [†]	Airmass	m_R^*	$m_R^R(1,1,0)^{\S}$	$m_R^R(\text{coma})$
---	------	-----------------	---------	-----------	-------------------	---------	---------	---------------------	----------------------

1	85 / 01 / 18	12:29	1.3	70	12.4847	1.66	13.61	12.88	15.15
2	85 / 01 / 19	9:15	1.3	70	33.2486	1.04	13.61	12.91	15.25
3	85 / 01 / 19	9:22	1.3	70	33.3600	1.04	13.60	12.90	15.37
4	85 / 01 / 19	9:49	1.3	70	33.8203	1.07	13.63	12.93	15.41
5	85 / 01 / 19	10:00	1.3	70	34.0061	1.09	13.66	12.96	15.42
6	85 / 01 / 19	10:10	1.3	70	34.1606	1.10	13.61	12.91	15.35
7	85 / 01 / 19	10:23	1.3	70	34.3817	1.12	13.65	12.95	15.38
8	85 / 01 / 19	10:42	1.3	70	34.7033	1.16	13.71	13.01	15.28
9	85 / 01 / 19	11:01	1.3	70	35.0236	1.22	13.71	13.01	15.11
10	85 / 01 / 19	11:17	1.3	70	35.2792	1.27	13.78	13.08	15.26
11	85 / 01 / 19	11:31	1.3	70	35.5139	1.32	13.76	13.06	15.36
12	85 / 01 / 19	11:47	1.3	70	35.7487	1.40	13.79	13.09	15.26
13	85 / 01 / 19	12:08	1.3	70	36.1361	1.52	13.73	13.03	15.20
14	85 / 01 / 20	7:59	1.3	70	55.9758	1.03	13.80	13.11	15.30
15	85 / 01 / 20	8:03	1.3	70	56.0481	1.03	13.80	13.11	15.30
16	85 / 01 / 20	8:28	1.3	70	56.4681	1.02	13.89	13.20	15.28
17	85 / 01 / 20	8:36	1.3	70	56.6019	1.02	13.90	13.21	15.14
18	85 / 01 / 20	8:52	1.3	70	56.8628	1.03	13.87	13.18	15.32
19	85 / 01 / 20	9:07	1.3	70	57.1208	1.03	13.87	13.18	15.24
20	85 / 01 / 20	9:22	1.3	70	57.3589	1.04	13.82	13.13	15.27
21	85 / 01 / 20	9:35	1.3	70	57.5792	1.06	13.77	13.08	15.17
22	85 / 01 / 20	9:48	1.3	70	57.8069	1.07	13.79	13.10	15.41
23	85 / 01 / 20	10:03	1.3	70	58.0453	1.09	13.71	13.02	15.21
24	85 / 01 / 20	10:12	1.3	70	58.1969	1.11	13.72	13.03	15.33
25	85 / 01 / 20	10:27	1.3	70	58.4492	1.14	13.68	12.99	15.34
26	85 / 01 / 20	10:38	1.3	70	58.6406	1.17	13.64	12.95	15.30
27	85 / 01 / 20	10:50	1.3	70	58.8378	1.20	13.63	12.94	15.33
28	85 / 01 / 20	10:59	1.3	70	58.9847	1.22	13.57	12.88	15.19
29	85 / 01 / 20	11:10	1.3	70	59.1722	1.26	13.60	12.91	15.19
30	85 / 01 / 20	11:23	1.3	70	59.3767	1.31	13.59	12.90	15.21
31	85 / 01 / 20	11:36	1.3	70	59.6078	1.37	13.52	12.83	15.18
32	85 / 01 / 20	11:56	1.3	70	59.9314	1.47	13.60	12.91	15.16
33	85 / 01 / 20	12:06	1.3	70	60.0953	1.53	13.62	12.93	15.36
34	85 / 01 / 20	12:15	1.3	70	60.2547	1.60	13.60	12.91	15.16
35	85 / 01 / 20	12:25	1.3	70	60.4081	1.67	13.58	12.89	15.23
36	85 / 01 / 20	12:31	1.3	70	60.5228	1.73	13.61	12.92	15.16
37	85 / 01 / 20	12:35	1.3	70	60.5911	1.77	13.57	12.88	15.40
38	85 / 01 / 21	4:44	1.3	70	76.7342	1.61	13.74	13.08	15.23
39	85 / 01 / 21	4:49	1.3	70	76.8247	1.57	13.80	13.14	15.44
40	85 / 01 / 21	5:05	1.3	70	77.0747	1.47	13.74	13.08	15.55
41	85 / 01 / 21	5:23	1.3	70	77.3856	1.37	13.73	13.07	15.29
42	85 / 01 / 21	5:37	1.3	70	77.6225	1.31	13.70	13.04	15.46
43	85 / 01 / 21	5:56	1.3	70	77.9261	1.24	13.67	13.01	15.53

Table 5-2, (contd.)

Photometry of P/Arend-Rigaux

N	Date	UT [‡]	Tel [m]	Exp [sec]	Time [†]	Airmass	m_R^*	$m_R(1,1,0)^{\S}$	$m_R(\text{coma})$
44	85 / 01 / 21	6:16	1.3	70	78.2675	1.18	13.66	13.00	15.67
45	85 / 01 / 21	6:36	1.3	70	78.6006	1.13	13.66	13.00	15.71
46	85 / 01 / 21	6:54	1.3	70	78.8961	1.10	13.61	12.95	15.55
47	85 / 01 / 21	7:16	1.3	70	79.2664	1.06	13.57	12.91	15.55
48	85 / 01 / 21	7:28	1.3	70	79.4689	1.05	13.56	12.90	15.47
49	85 / 01 / 21	7:42	1.3	70	79.7067	1.04	13.56	12.90	15.26
50	85 / 01 / 21	7:58	1.3	70	79.9675	1.03	13.50	12.84	15.60
51	85 / 01 / 21	8:16	1.3	70	80.2744	1.02	13.57	12.91	15.47
52	85 / 01 / 21	8:40	1.3	70	80.6606	1.02	13.53	12.87	15.45
53	85 / 01 / 21	9:43	1.3	70	81.7228	1.07	13.60	12.94	15.37
54	85 / 01 / 21	9:53	1.3	70	81.8883	1.08	13.64	12.98	15.45
55	85 / 01 / 21	10:04	1.3	70	82.0739	1.10	13.63	12.97	15.49
56	85 / 01 / 21	10:19	1.3	70	82.3186	1.13	13.68	13.02	15.28
57	85 / 01 / 21	10:32	1.3	70	82.5269	1.16	13.71	13.05	15.46
58	85 / 01 / 21	10:47	1.3	70	82.7822	1.20	13.74	13.08	15.43
59	85 / 01 / 21	10:59	1.3	70	82.9900	1.23	13.79	13.13	15.46
60	85 / 01 / 21	11:52	1.3	70	83.8656	1.46	13.77	13.11	15.09
61	85 / 01 / 21	12:04	1.3	70	84.0664	1.54	13.81	13.15	15.22

[‡] UT start of integration.
[†] Time in hours since UT 1985 January 18 at 0^h UT (JD 2446083.5).
^{*} Photometric errors = 0.04 mag.
[§] $m_R(1,1,0) = m_R - 2.5 \log(R^2 \Delta) - \beta \alpha$; where $\beta = 0.04 \text{ mag deg}^{-1}$.

centered on the nucleus (m_R) and the annulus ($m_R[\text{coma}]$) are presented in Table 5-2 (these data also appear in Jewitt and Meech, 1985). The photometric uncertainty of the inner diaphragm measurements is 4%. The errors result from uncertainties in the sky subtraction, extinction correction and in the centering of the image. Additionally, there may be a systematic zero point uncertainty of up to 10% (0.1 mag).

The P/Arend-Rigaux photometry is shown in Figure 5-2. Both the inner diaphragm and the annulus coma magnitudes are shown in the figure. The brightness within the inner diaphragm varies by a factor of 1.4 (0.38 mag) whereas the coma brightness is relatively stable, suggesting that the brightness variations are not due to coma activity.

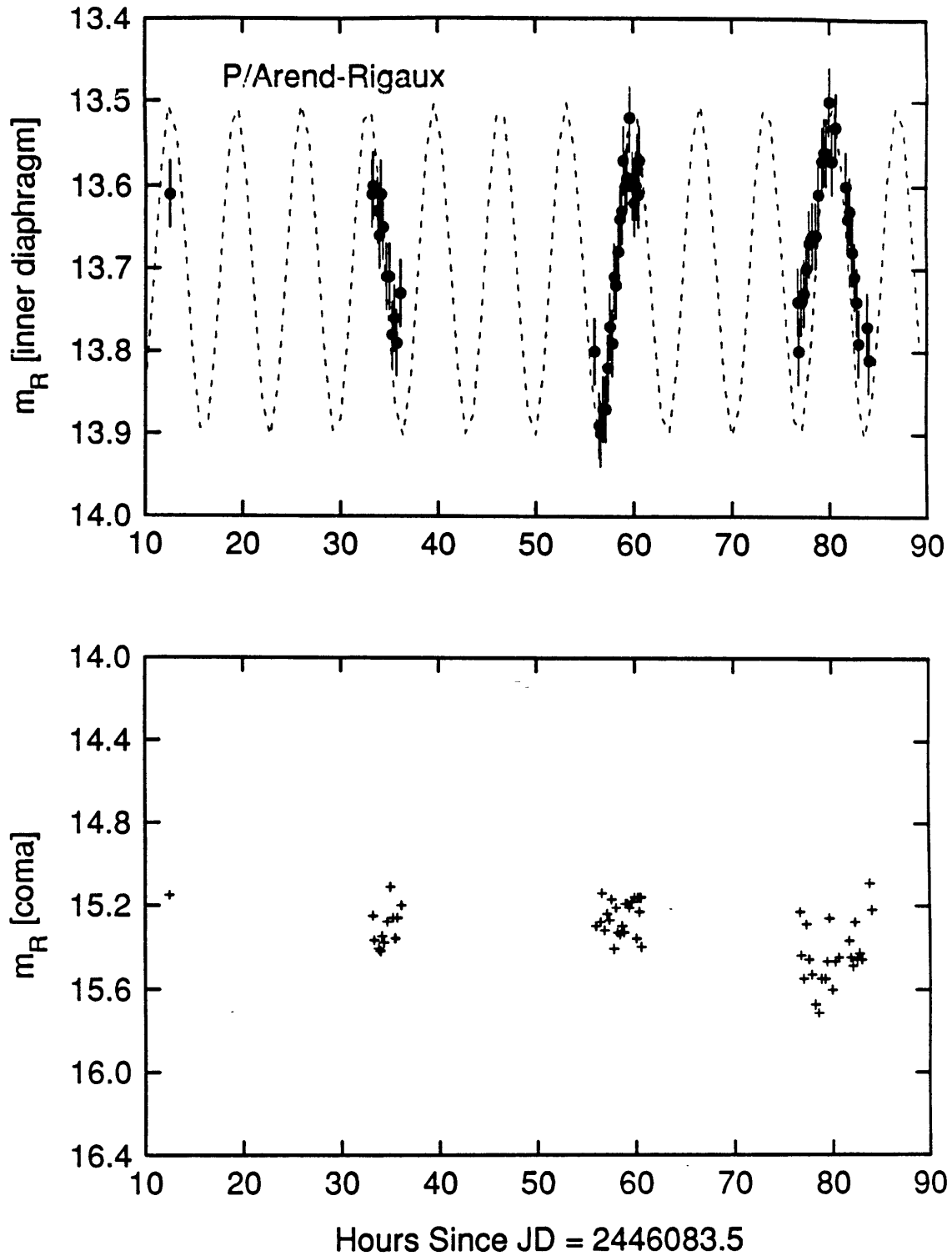


Figure 5-2. CCD photometry for P/Arend-Rigaux from MIT's 1.3m telescope at McGraw-Hill observatory. The m_R magnitude for both the inner diaphragm and outer annulus (coma) is plotted as a function of time. The magnitude scale for the coma position was selected so as to indicate the true relative brightness changes between the coma and the inner diaphragm. A sine curve of period 6.77 hours ($T/2$; see Table 5-12) has been plotted to emphasize the periodic nature of the variations.

5.2.2 Comets P/Neujmin 1 and P/Encke

Photometric observations were obtained at the Kitt Peak (KPNO) 4m telescope in 1985 September and at the Kitt Peak 2.1m telescope in 1986 October-November. The geometry of the observations is shown in Tables 5-3 and 5-4. All observations were taken with a single 800 x 800 pixel Texas Instruments CCD (TI#2). The image scale at the prime focus of the 4m was 0.29 arcsec per 15 μ m pixel, while at the Cassegrainian focus of the 2.1m the scale was 0.38 arcsec per pixel. Potential non-linearity at the lowest signal levels (important only in integrations much less than a minute) was eliminated by pre-flashing the chip with light from an internal source prior to each exposure. The resultant readout noise per pixel (including the pre-flash photon noise) was approximately 25 electrons at the 4 m and only 15 electrons at the 2.1 m. Dark emission was found to be negligible at the $T = 170$ K operating temperature of the CCD. The pixel to pixel sensitivity variations were removed from the data frames using nightly sequences of dome flats and bias frames. The resulting sensitivity of the detector was uniform to better than 1% over the full field of view.

Table 5-3

Geometry of Comet P/Neujmin 1

Date	Tel. Diameter	Seeing [arcsec]	No. of obs.	R (AU)	Δ (AU)	α°
85/09/21	4	$\approx 1 - 2$	7	3.874	3.965	14.7
85/09/22	4	≈ 1.2	4	3.881	3.958	14.7
85/09/23	4	≈ 1.0	4	3.888	3.951	14.7
86/03/06	2.1	≈ 1.3	1	5.034	4.715	11.1
86/10/30	2.1	0.8 - 1.2	6	6.450	6.286	8.8
86/10/31	2.1	1.6 - 2.0	5	6.455	6.275	8.8
86/11/01	2.1	≈ 1.5	4	6.461	6.264	8.8

Table 5-4
Geometry of Comet P/Encke

Date	Tel. Diameter	Seeing [arcsec]	No. of obs.	R (AU)	Δ (AU)	α°
1985 / 09 / 22	4 m	≈ 1.2	9	4.059	3.143	6.6
1985 / 09 / 23	4 m	≈ 1.0	16	4.060	3.152	6.9
1986 / 10 / 30	2.1 m	0.8 - 1.2	9	3.153	2.442	14.4
1986 / 10 / 31	2.1 m	1.6 - 2.0	6	3.147	2.449	14.6
1986 / 11 / 01	2.1 m	≈ 1.5	7	3.141	2.456	14.9
1986 / 11 / 03	2.1 m	≈ 2	6	3.129	2.471	15.4

Both comets appeared stellar, with no discernable trace of coma or tail. They were identified by noting their motion with respect to field stars. Observations at the 2.1m telescope were taken with the telescope tracking at cometary rates. The tracking held the position of the comet fixed on the CCD to better than 0.3 pixels (0.1 arcsec) during a typical integration. Technical problems at the 4m prevented guiding while the telescope was tracking at non-sideral rates. The resulting trailing of the comet across the CCD was ≤ 1 arcsec during a typical exposure. This motion is small compared to the size of the diaphragm used for photometry, so that the photometry is unaffected. Images were taken through the Mould R filter ($\lambda_{cent} = 0.65 \mu\text{m}$, $\Delta\lambda = 0.09 \mu\text{m}$, FWHM). Photometric measurements were made using circular diaphragms. For comet P/Encke at the 4m telescope a photometry diaphragm of 7.0 arcsec diameter and a sky annulus with inner and outer diameters of 7.0 and 11.6 arcsec was used. Measurements from the 2.1 m used a 6.1 arcsec diameter diaphragm and a 6.1 to 15.2 arcsec sky annulus. The photometry was invariant with respect to the sizes of the diaphragms for diaphragms larger than the seeing disk (0.8 - 2.0 arcsec FWHM). For comet P/Neujmin 1 a photometry diaphragm of 6.1 arcsec diameter was used with a sky annulus of

inner and outer diameters of 6.1 and 9.1 arcsec, respectively.

Most of the observations were taken during photometric conditions. Comparison of the brightness of several reference stars per frame indicated that the sky transparency was constant to within $\pm 1\%$ during all observations. The major photometric uncertainty was in the determination of the sky brightness near the comet. The photometry for P/Neujmin 1 is presented in Table 5-5 and that for P/Encke is in Table 5-6 (the P/Encke observations also appear in Jewitt and Meech, 1987a). A single measurement of comet P/Neujmin 1 obtained at the KPNO 2.1m telescope in March 1986 with the same instrument and under photometric conditions is also shown in Table 5-5 for completeness. Absolute calibration of the photometry was achieved through observations of standard stars from Christian *et al.* (1985). Repeated near-simultaneous measurements showed that the measurement uncertainty was $\sigma(m_R) = \pm 0.05$ mag in the 4m data and $\sigma(m_R) = \pm 0.07$ mag in the 2.1m data. With comet Encke at $m_R = 19.5 - 20.5$ mag, these uncertainties imply that field objects at $m_R = 23 - 24$ mag were fully rejected from the photometry diaphragm. Similarly, for P/Neujmin 1, objects of $m_R = 21 - 22$ mag were rejected. The ability to do real time flattening was crucial so that the observations of comets could be avoided during those times when the motion carried them close to faint field galaxies and stars. The observations for P/Neujmin 1 and P/Encke are presented in Figures 5-3 and 5-4, respectively.

Table 5-5
Photometry of P/Neujmin 1

N	Date	UT [‡]	Tel [m]	Exp [sec]	Time [†]	Airmass	$m_R \pm \sigma(m_R)$	$m_{R(1,1,0)}$ [§]
1	85 / 09 / 21	08:40	4	600	8.6655	2.64	18.43 ± 0.05	11.91
2	85 / 09 / 21	09:10	4	300	9.1667	2.14	18.51 ± 0.05	11.99
3	85 / 09 / 21	09:25	4	100	9.4167	1.96	18.56 ± 0.05	12.04
4	85 / 09 / 21	10:26	4	100	10.4333	1.48	18.71 ± 0.05	12.19
5	85 / 09 / 21	11:34	4	50	11.5742	1.20	19.03 ± 0.05	12.51
6	85 / 09 / 21	11:38	4	50	11.6308	1.19	19.06 ± 0.05	12.54
7	85 / 09 / 21	12:26	4	75	12.4258	1.09	19.00 ± 0.05	12.48
8	85 / 09 / 22	09:44	4	100	33.7352	1.74	18.52 ± 0.05	12.00
9	85 / 09 / 22	10:42	4	100	34.7019	1.38	18.52 ± 0.05	12.00
10	85 / 09 / 22	10:48	4	100	34.7947	1.32	18.49 ± 0.05	11.97
11	85 / 09 / 22	11:28	4	100	35.4588	1.20	18.68 ± 0.05	12.16
12	85 / 09 / 23	09:38	4	100	57.6394	1.76	18.81 ± 0.05	12.29
13	85 / 09 / 23	09:51	4	100	57.8508	1.65	18.74 ± 0.05	12.22
14	85 / 09 / 23	11:01	4	150	59.0161	1.29	18.44 ± 0.05	11.92
15	85 / 09 / 23	11:36	4	100	59.6033	1.18	18.42 ± 0.05	11.90
16	86 / 03 / 06	07:11	2.1	300	07.1836	1.87	19.82 ± 0.07	12.51
17	86 / 10 / 30	08:18	2.1	600	08.3008	2.16	20.49 ± 0.07	12.10
18	86 / 10 / 30	09:48	2.1	600	09.7969	1.40	20.69 ± 0.07	12.30
19	86 / 10 / 30	10:13	2.1	600	10.2086	1.29	20.66 ± 0.07	12.27
20	86 / 10 / 30	10:43	2.1	600	10.7247	1.19	20.58 ± 0.07	12.19
21	86 / 10 / 30	11:41	2.1	600	11.6786	1.07	20.41 ± 0.07	12.02
22	86 / 10 / 30	12:29	2.1	600	12.4864	1.01	20.30 ± 0.07	11.91
23	86 / 10 / 31	08:42	2.1	600	32.6964	1.83	20.53 ± 0.07	12.14
24	86 / 10 / 31	09:19	2.1	600	33.3194	1.54	20.39 ± 0.07	12.00
25	86 / 10 / 31	10:17	2.1	600	34.2786	1.27	20.39 ± 0.07	12.00
26	86 / 10 / 31	11:31	2.1	600	35.5186	1.08	20.68 ± 0.07	12.29
27	86 / 10 / 31	11:57	2.1	600	35.9442	1.04	20.74 ± 0.07	12.35
28	86 / 11 / 01	12:00	2.1	600	60.0011	1.03	20.65 ± 0.07	12.26
29	86 / 11 / 01	12:11	2.1	600	60.1772	1.02	20.69 ± 0.07	12.30
30	86 / 11 / 01	12:21	2.1	600	60.3558	1.02	20.61 ± 0.07	12.22
31	86 / 11 / 01	12:32	2.1	600	60.5356	1.01	20.73 ± 0.07	12.34

[‡] UT start of integration.

[†] Obs (1-15) - time in hours since UT 1985 September 21 at 0^h UT (JD = 2446329.5).

Obs (17-31) - time in hours since UT 1986 October 30 at 0^h UT (JD = 2446733.5).

[§] $m_{R(1,1,0)} = m_R - 5 \log(R\Delta) - \beta \alpha$; where $\beta = 0.034 \text{ mag deg}^{-1}$ (from Jewitt & Meech, 1987b)

Photometry of P/Encke

Table 5-6

N	Date	UT [†]	Tel [m]	Exp [sec]	Time [†]	Air [‡] mass	$m_R \pm \sigma(m_R)$	$m_R(1,1,0)$ [§]
---	------	-----------------	---------	-----------	-------------------	-----------------------	-----------------------	---------------------------

1	85 / 09 / 22	06:01	4	200	6.0161	1.36	20.00 ± 0.05	14.21
2	85 / 09 / 22	06:43	4	200	6.7127	1.42	19.95 ± 0.05	14.16
3	85 / 09 / 22	06:55	4	200	6.9133	1.47	19.84 ± 0.05	14.05
4	85 / 09 / 22	07:02	4	200	7.0238	1.49	19.80 ± 0.05	14.01
5	85 / 09 / 22	07:35	4	150	7.5899	1.62	19.80 ± 0.05	14.01
6	85 / 09 / 22	07:40	4	150	7.6706	1.64	19.68 ± 0.05	13.89
7	85 / 09 / 22	08:23	4	150	8.3775	1.95	19.59 ± 0.05	13.80
8	85 / 09 / 22	08:28	4	150	8.4636	2.00	19.74 ± 0.05	13.95
9	85 / 09 / 22	08:58	4	150	8.9689	2.34	19.59 ± 0.05	13.80
10	85 / 09 / 23	02:53	4	150	26.8814	1.83	20.41 ± 0.05	14.60
11	85 / 09 / 23	03:00	4	150	26.9975	1.74	20.46 ± 0.05	14.65
12	85 / 09 / 23	03:19	4	150	27.3183	1.65	20.24 ± 0.05	14.43
13	85 / 09 / 23	03:24	4	150	27.3931	1.61	20.17 ± 0.05	14.36
14	85 / 09 / 23	03:54	4	150	27.9017	1.50	20.14 ± 0.05	14.33
15	85 / 09 / 23	03:59	4	150	27.9791	1.48	20.17 ± 0.05	14.36
16	85 / 09 / 23	04:34	4	150	28.5681	1.40	19.98 ± 0.05	14.17
17	85 / 09 / 23	04:39	4	150	28.6522	1.38	19.98 ± 0.05	14.17
18	85 / 09 / 23	05:16	4	150	29.2664	1.35	19.93 ± 0.05	14.12
19	85 / 09 / 23	05:23	4	150	29.3778	1.35	19.70 ± 0.05	13.89
20	85 / 09 / 23	06:13	4	150	30.2236	1.39	19.62 ± 0.05	13.81
21	85 / 09 / 23	06:30	4	150	30.5044	1.41	19.65 ± 0.05	13.84
22	85 / 09 / 23	07:08	4	150	31.1411	1.52	19.61 ± 0.05	13.80
23	85 / 09 / 23	08:04	4	150	32.0622	1.79	19.58 ± 0.05	13.77
24	85 / 09 / 23	08:57	4	150	32.9419	2.39	19.63 ± 0.05	13.82
25	85 / 09 / 23	09:03	4	150	33.0486	2.54	19.67 ± 0.05	13.86

† UT midtime of integration.
 ‡ Hours elapsed since UT 1985 September 22, 0^h UT (JD 2446330.5).
 § $m_R(1,1,0) = m_R - 5 \log(R\Delta) - \beta \alpha$; where $\beta = 0.04 \text{ mag deg}^{-1}$ (from Jewitt and Meech, 1987a).

Table 5-6, (contd.)

Photometry of P/Encke

N	Date	UT [‡]	Tel [m]	Exp [sec]	Time [†]	Airmass	$m_R \pm \sigma(m_R)$	$m_R(1,1,0)$ [§]
26	86 / 10 / 30	02:45	2.1	200	2.7736	1.23	19.84 ± 0.07	14.83
27	86 / 10 / 30	03:05	2.1	300	3.0881	1.20	19.82 ± 0.07	14.81
28	86 / 10 / 30	04:06	2.1	300	4.0983	1.17	19.67 ± 0.07	14.66
29	86 / 10 / 30	04:12	2.1	300	4.1975	1.18	19.74 ± 0.07	14.73
30	86 / 10 / 30	05:13	2.1	300	5.2156	1.26	19.62 ± 0.07	14.61
31	86 / 10 / 30	07:28	2.1	300	7.4661	1.86	19.78 ± 0.07	14.77
32	86 / 10 / 30	07:34	2.1	300	7.5583	2.22	19.87 ± 0.07	14.86
33	86 / 10 / 30	07:39	2.1	300	7.6556	2.28	19.70 ± 0.07	14.69
34	86 / 10 / 30	07:58	2.1	300	7.9675	2.56	19.79 ± 0.07	14.78
35	86 / 10 / 31	02:14	2.1	500	26.2294	1.30	19.97 ± 0.07	14.95
36	86 / 10 / 31	02:56	2.1	500	26.9356	1.21	19.79 ± 0.07	14.77
37	86 / 10 / 31	06:06	2.1	300	30.0922	1.45	19.67 ± 0.07	14.65
38	86 / 10 / 31	06:14	2.1	500	30.2275	1.48	19.64 ± 0.07	14.62
39	86 / 10 / 31	06:43	2.1	500	30.7133	1.65	19.69 ± 0.07	14.67
40	86 / 10 / 31	07:13	2.1	500	31.2150	1.92	19.81 ± 0.07	14.79
41	86 / 11 / 01	01:47	2.1	300	49.7964	1.34	19.79 ± 0.07	14.76
42	86 / 11 / 01	01:57	2.1	600	49.9436	1.32	19.67 ± 0.07	14.64
43	86 / 11 / 01	03:05	2.1	600	51.0802	1.20	19.70 ± 0.07	14.67
44	86 / 11 / 01	03:53	2.1	600	51.8839	1.18	19.64 ± 0.07	14.61
45	86 / 11 / 01	04:04	2.1	600	52.0706	1.18	19.63 ± 0.07	14.60
46	86 / 11 / 01	05:15	2.1	600	53.2575	1.28	19.74 ± 0.07	14.71
47	86 / 11 / 01	05:24	2.1	600	53.3950	1.31	19.80 ± 0.07	14.77
48	86 / 11 / 03	01:44	2.1	300	97.7419	1.31	19.73 ± 0.07	14.67
49	86 / 11 / 03	01:51	2.1	300	97.8506	1.29	19.76 ± 0.07	14.70
50	86 / 11 / 03	02:14	2.1	600	98.2258	1.26	19.80 ± 0.07	14.74
51	86 / 11 / 03	02:24	2.1	600	98.4011	1.24	19.80 ± 0.07	14.74
52	86 / 11 / 03	02:45	2.1	600	98.7461	1.22	19.73 ± 0.07	14.67
53	86 / 11 / 03	02:56	2.1	600	98.9414	1.20	19.88 ± 0.07	14.82

[‡] UT midtime of integration.

[†] Hours elapsed since UT 1986 October 30, 0^h UT (JD 2446733.5).

[§] $m_R(1,1,0) = m_R - 5 \log(R\Delta) - \beta \alpha$; where $\beta = 0.04 \text{ mag deg}^{-1}$ (from Jewitt and Meech 1987a).

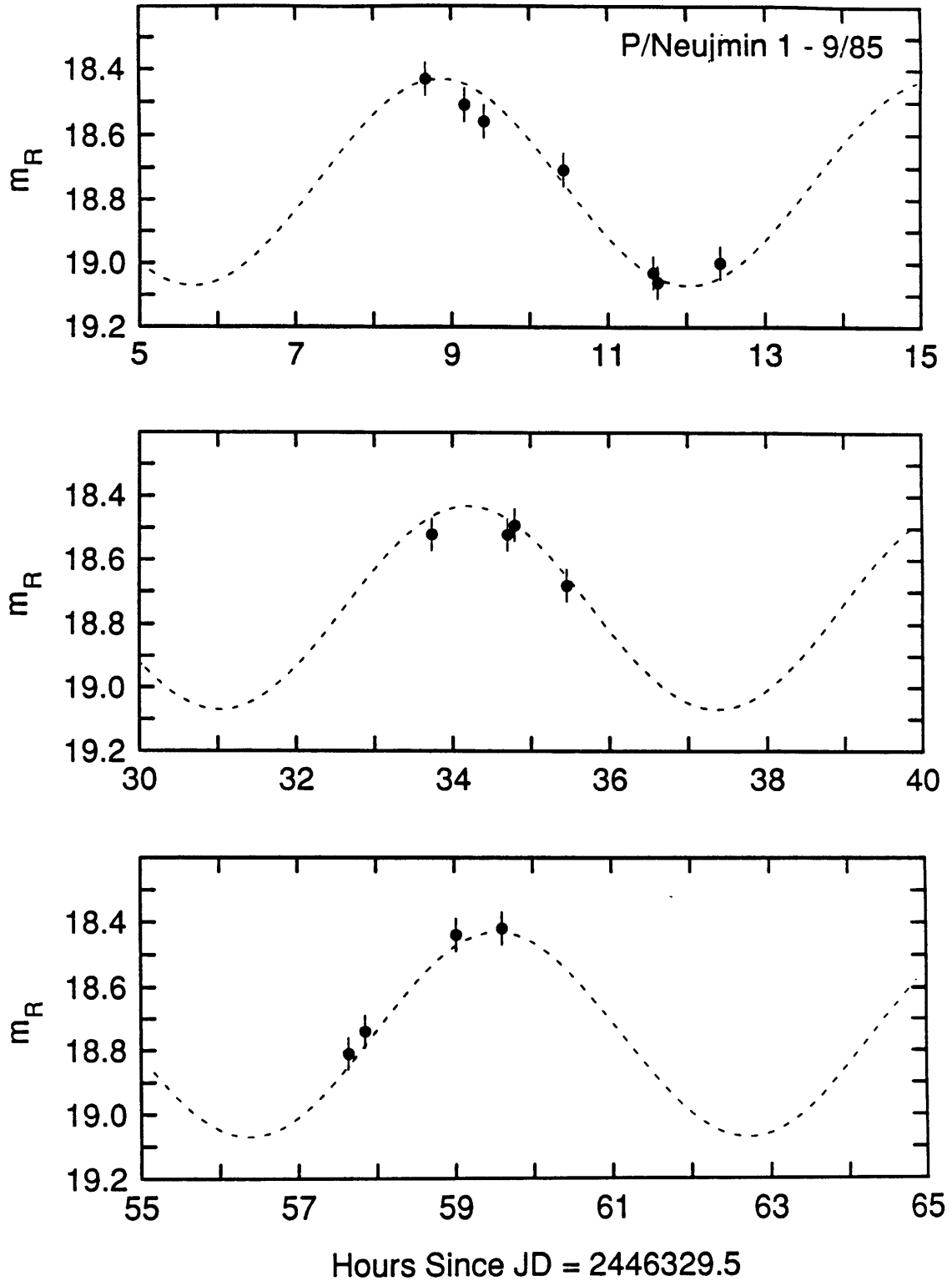


Figure 5-3. CCD photometry of comet P/Neujmin 1 obtained with the KPNO 4m telescope during 1985 September. A sine curve of period $T/2 = 6.34$ hours and arbitrary amplitude is superimposed on the data.

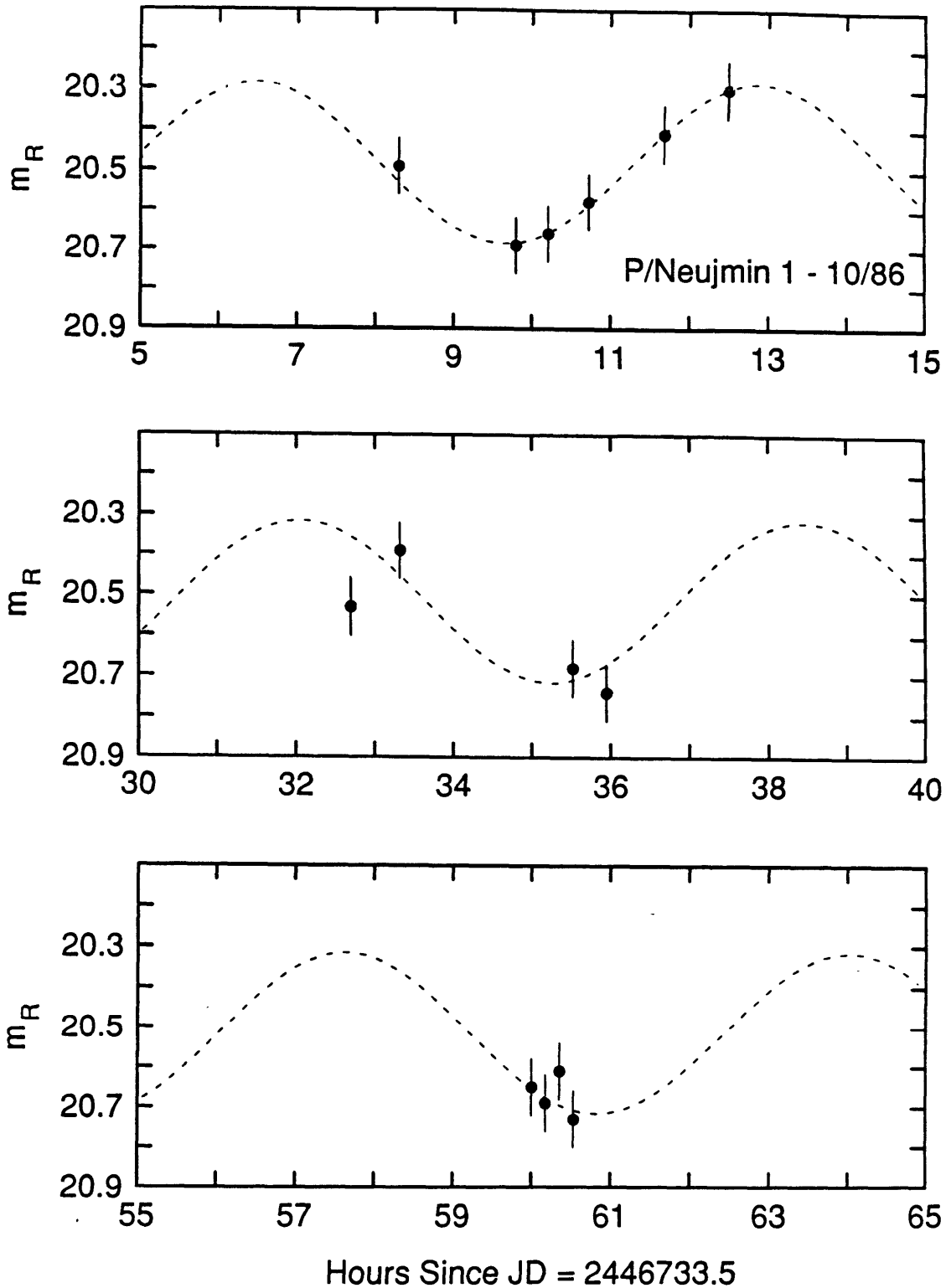


Figure 5-3. (continued) CCD photometry of comet P/Neujmin 1 obtained with the KPNO 2.1m telescope during 1986 October. A sine curve of period $T / 2 = 6.34$ hours and arbitrary amplitude is superimposed on the data.

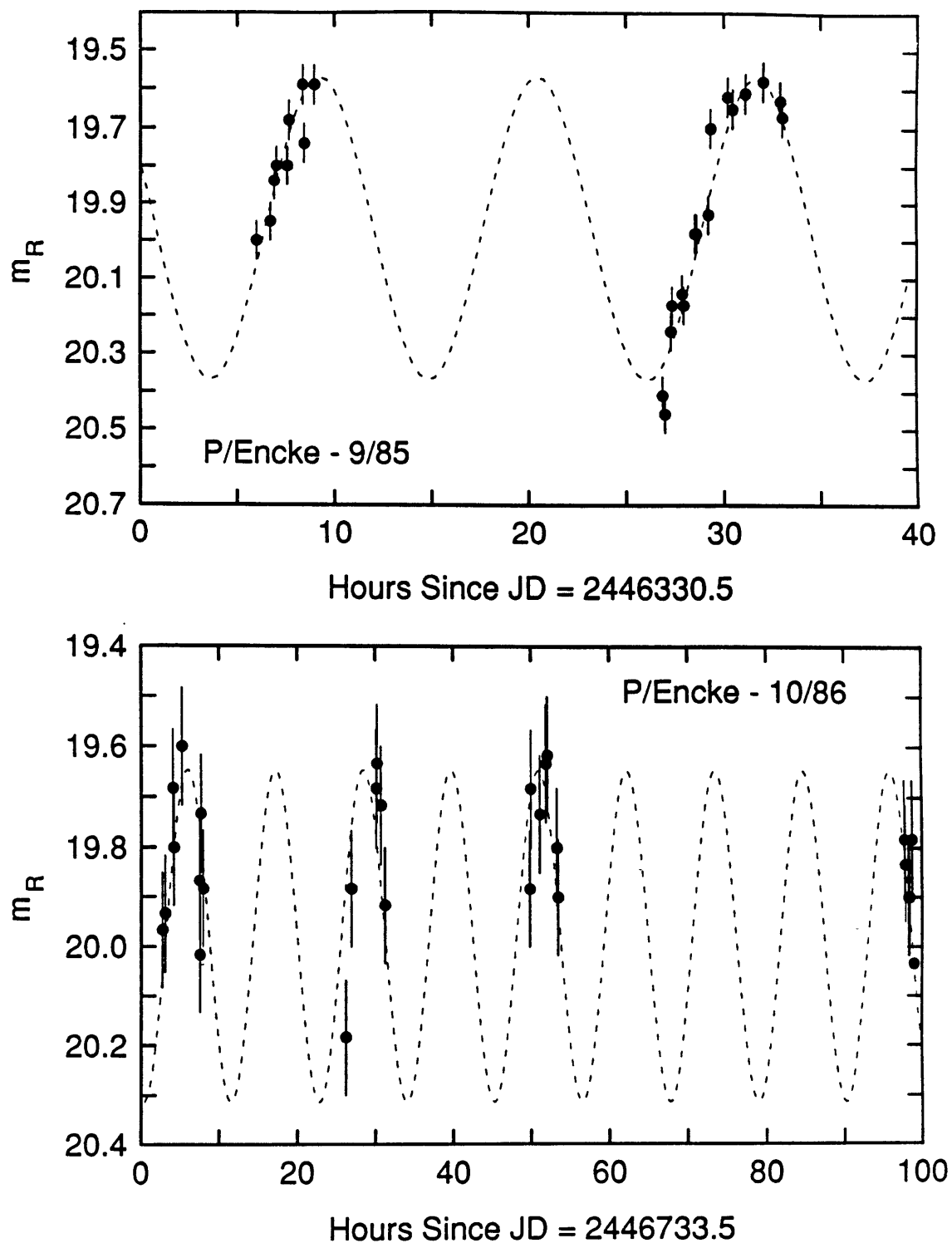


Figure 5-4. CCD photometry of comet P/Encke. The upper panel shows data obtained with the KPNO 4m telescope in 1985 September, and the lower panel shows the data obtained with the KPNO 2.1m telescope in 1986 October. The Mould R filter is plotted versus time in both panels. A sine curve of arbitrary amplitude and of period 11.24 hours ($T/2$) has been plotted for emphasis.

5.2.3 Comet P/Tempel 2

Observations of comet P/Tempel 2 were obtained during 1987 March 31 - April 3 UT using the KPNO 2.1m telescope with CCD TI#2 at the f/7.5 Cassegrain focus. The geometry of the observations is presented in Table 5-7.

Date	Tel. Diameter	Seeing [arcsec]	No. of obs.	R (AU)	Δ (AU)	α°
87/03/31	2.1 m	1 - 1.5	13	3.992	3.160	8.9
87/04/01	2.1 m	≈ 1.1	15	3.988	3.166	9.2
87/04/02	2.1 m	<1 - 1.5	15	3.985	3.172	9.4
87/04/03	2.1 m	≈ 1.1	20	3.982	3.179	9.6

The image scale was 0.38 arcsec pixel⁻¹. All observations were taken through the Mould R filter. The telescope was guided at cometary rates. The nights of 31 March and 02 April were photometric; cirrus was present intermittently during the other two nights. On each of the nights of 01 April and 03 April, however, there were photometric periods (as judged by the stability of the brightness of field stars), during which observations of standard stars from Landolt (1983) were obtained. The comet was identified by its motion with respect to field stars; it appeared stellar in all images. Photometric measurements were made within a circular diaphragm of radius 6.1 arcsec and the sky brightness was measured in an annulus of inner and outer radii 6.1 and 9.1 arcsec, respectively. The photometry for P/Tempel 2 is presented in Table 5-8 and plotted in Figure 5-5.

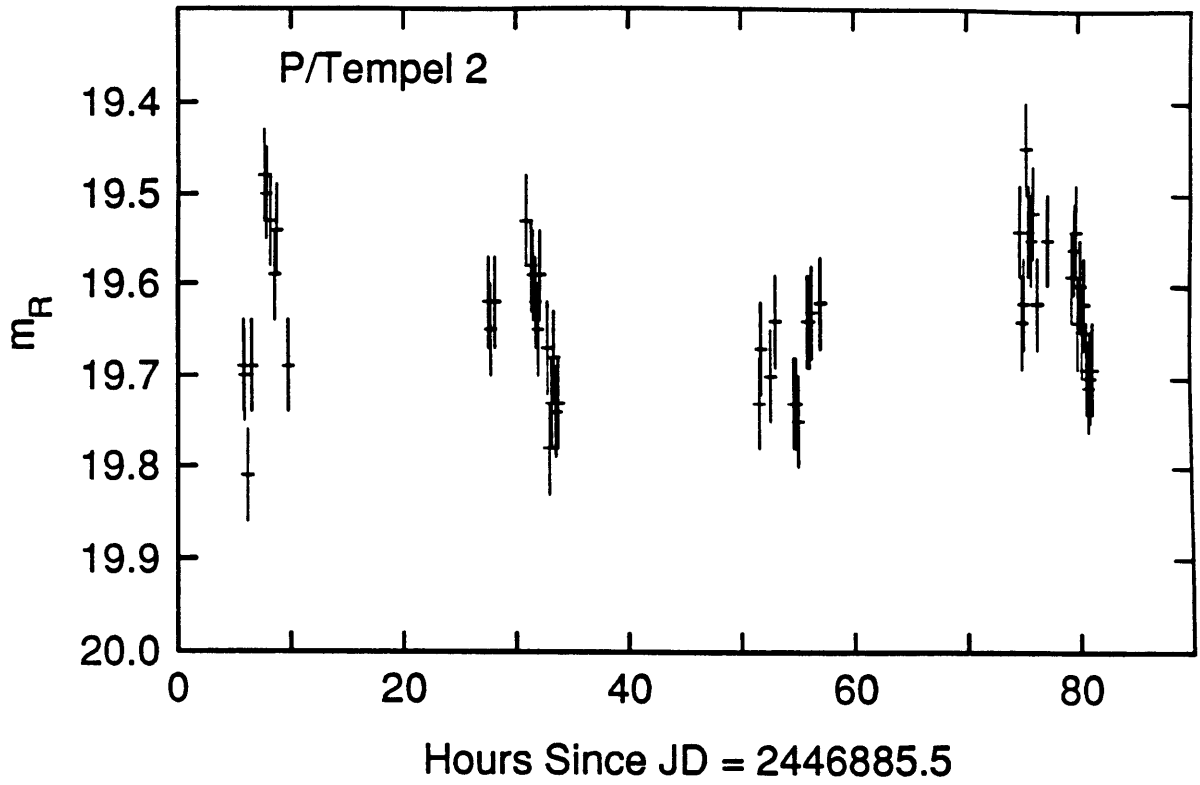


Figure 5-5. CCD photometry of comet P/Tempel 2, obtained in 1987 April at the KPNO 2.1m telescope. The Mould R magnitude is plotted versus time. The most likely rotation period for the comet is $T = 8.93$ hours.

Table 5-8
Photometry of P/Tempel 2

N	Date	UT [†]	Tel [m]	Exp [sec]	Time [‡]	Airmass	$m_R \pm \sigma(m_R)$	$m_R(1,1,0)^{\S}$
1	87 / 03 / 31	05:49	2.1	300	5.8138	1.02	19.69 ± 0.07	13.83
2	87 / 03 / 31	05:55	2.1	600	5.9088	1.03	19.70 ± 0.05	13.84
3	87 / 03 / 31	06:10	2.1	600	6.1669	1.03	19.81 ± 0.05	13.95
4	87 / 03 / 31	06:32	2.1	600	6.5319	1.05	19.69 ± 0.05	13.83
5	87 / 03 / 31	07:40	2.1	600	7.6700	1.17	19.48 ± 0.05	13.62
6	87 / 03 / 31	07:51	2.1	600	7.8467	1.21	19.50 ± 0.05	13.64
7	87 / 03 / 31	08:12	2.1	600	8.2078	1.28	19.53 ± 0.05	13.67
8	87 / 03 / 31	08:35	2.1	600	8.5767	1.37	19.59 ± 0.05	13.73
9	87 / 03 / 31	08:45	2.1	600	8.7517	1.42	19.54 ± 0.05	13.68
10	87 / 03 / 31	09:46	2.1	600	9.7677	1.90	19.69 ± 0.05	13.83
11	87 / 03 / 31	10:22	2.1	600	10.3727	2.45	19.87 ± 0.05	14.01
12	87 / 03 / 31	10:33	2.1	600	10.5497	2.69	19.94 ± 0.05	14.08
13	87 / 03 / 31	10:44	2.1	600	10.7250	2.96	20.11 ± 0.05	14.25
14	87 / 04 / 01	03:37	2.1	600	27.6144	1.11	19.62 ± 0.05	13.75
15	87 / 04 / 01	03:48	2.1	600	27.8000	1.10	19.65 ± 0.05	13.78
16	87 / 04 / 01	04:11	2.1	600	28.1850	1.06	19.62 ± 0.05	13.75
17	87 / 04 / 01	06:59	2.1	600	30.9783	1.10	19.53 ± 0.05	13.66
18	87 / 04 / 01	07:24	2.1	600	31.4139	1.14	19.58 ± 0.05	13.71
19	87 / 04 / 01	07:36	2.1	600	31.5963	1.18	19.59 ± 0.05	13.72
20	87 / 04 / 01	07:47	2.1	600	31.7758	1.21	19.62 ± 0.05	13.75
21	87 / 04 / 01	08:00	2.1	600	32.0025	1.25	19.65 ± 0.05	13.78
22	87 / 04 / 01	08:11	2.1	600	32.1814	1.29	19.59 ± 0.05	13.72
23	87 / 04 / 01	08:50	2.1	600	32.8336	1.47	19.67 ± 0.05	13.80
24	87 / 04 / 01	09:01	2.1	600	33.0183	1.55	19.78 ± 0.05	13.91
25	87 / 04 / 01	09:12	2.1	600	33.2033	1.63	19.73 ± 0.05	13.86
26	87 / 04 / 01	09:23	2.1	600	33.3883	1.72	19.68 ± 0.05	13.81
27	87 / 04 / 01	09:35	2.1	600	33.5763	1.83	19.74 ± 0.05	13.87
28	87 / 04 / 01	09:46	2.1	600	33.7658	1.97	19.73 ± 0.05	13.86
29	87 / 04 / 02	03:37	2.1	600	51.6217	1.11	19.73 ± 0.05	13.85
30	87 / 04 / 02	03:48	2.1	600	51.8014	1.09	19.67 ± 0.05	13.79
31	87 / 04 / 02	04:37	2.1	600	52.6292	1.03	19.70 ± 0.05	13.82
32	87 / 04 / 02	05:06	2.1	600	53.0922	1.02	19.64 ± 0.05	13.76
33	87 / 04 / 02	06:42	2.1	600	54.7025	1.08	19.73 ± 0.05	13.85
34	87 / 04 / 02	06:53	2.1	600	54.8828	1.09	19.73 ± 0.05	13.85
35	87 / 04 / 02	07:04	2.1	600	55.0653	1.11	19.75 ± 0.05	13.87
36	87 / 04 / 02	07:55	2.1	600	55.9206	1.25	19.64 ± 0.05	13.76
37	87 / 04 / 02	08:06	2.1	600	56.1000	1.29	19.64 ± 0.05	13.76
38	87 / 04 / 02	08:16	2.1	600	56.2792	1.33	19.63 ± 0.05	13.75
39	87 / 04 / 02	09:03	2.1	600	57.0533	1.59	19.62 ± 0.05	13.75
40	87 / 04 / 02	10:08	2.1	600	58.1297	2.34	19.59 ± 0.05	13.71
41	87 / 04 / 02	10:19	2.1	600	58.3181	2.57	19.60 ± 0.05	13.72
42	87 / 04 / 02	10:30	2.1	600	58.4986	2.84	19.61 ± 0.05	13.73
43	87 / 04 / 02	10:41	2.1	600	58.6808	3.16	19.70 ± 0.05	13.82

Table 5-8, (contd.)

Photometry of P/Tempel 2

N	Date	UT [‡]	Tel [m]	Exp [sec]	Time [†]	Airmass	$m_R \pm \sigma(m_R)$	$m_R(1,1,0)$ [§]
44	87 / 04 / 03	02:46	2.1	600	74.7744	1.22	19.54 ± 0.05	13.64
45	87 / 04 / 03	02:57	2.1	600	74.9558	1.19	19.64 ± 0.05	13.74
46	87 / 04 / 03	03:08	2.1	600	75.1331	1.16	19.62 ± 0.05	13.72
47	87 / 04 / 03	03:21	2.1	600	75.3536	1.14	19.45 ± 0.05	13.55
48	87 / 04 / 03	03:32	2.1	600	75.5269	1.11	19.54 ± 0.05	13.64
49	87 / 04 / 03	03:48	2.1	600	75.7919	1.09	19.55 ± 0.05	13.65
50	87 / 04 / 03	03:58	2.1	600	75.9658	1.07	19.52 ± 0.05	13.62
51	87 / 04 / 03	04:20	2.1	600	76.3250	1.04	19.62 ± 0.05	13.72
52	87 / 04 / 03	05:14	2.1	600	77.2292	1.02	19.55 ± 0.05	13.65
53	87 / 04 / 03	07:26	2.1	600	79.4381	1.17	19.59 ± 0.05	13.69
54	87 / 04 / 03	07:37	2.1	600	79.6169	1.20	19.56 ± 0.05	13.66
55	87 / 04 / 03	07:48	2.1	600	79.7953	1.24	19.54 ± 0.05	13.64
56	87 / 04 / 03	07:59	2.1	600	79.9822	1.28	19.64 ± 0.05	13.74
57	87 / 04 / 03	08:10	2.1	600	80.1669	1.32	19.60 ± 0.05	13.70
58	87 / 04 / 03	08:21	2.1	600	80.3475	1.37	19.65 ± 0.05	13.75
59	87 / 04 / 03	08:32	2.1	600	80.5275	1.42	19.62 ± 0.05	13.72
60	87 / 04 / 03	08:42	2.1	600	80.7067	1.48	19.69 ± 0.05	13.79
61	87 / 04 / 03	08:53	2.1	600	80.8859	1.55	19.71 ± 0.05	13.81
62	87 / 04 / 03	09:04	2.1	600	81.0628	1.63	19.70 ± 0.05	13.80
63	87 / 04 / 03	09:14	2.1	600	81.2411	1.72	19.69 ± 0.05	13.79

[‡] UT of the start of the integration.

[†] Time in hours since UT 1987 March 31 at 0^h UT (JD = 2446885.5).

[§] $m_R(1,1,0) = m_R - 5 \log(R\Delta) - \beta \alpha$; where $\beta = 0.04 \text{ mag deg}^{-1}$.

5.2.4 Comet P/Halley

Observations of comet P/Halley were made during 1984 October and 1985 January with the MASCOT CCD camera using the MHO 1.3m telescope. The geometry of the observations is presented in Table 5-9. A detailed discussion of the observations has been presented in Chapter 2 section 2.2 and in Meech, Jewitt and Ricker (1986) and will not be repeated here. The observations are presented in Table 5-10 and are plotted in Figure 5-6.

Table 5-9
Geometry of Comet P/Halley

Date	Tel. Diameter	Seeing [arcsec]	No. of obs.	R (AU)	Δ (AU)	α°
84 / 10 / 22	1.3	≈ 2	4	5.908	5.535	9.3
84 / 10 / 24	1.3	≈ 2	7	5.891	5.485	9.2
84 / 10 / 27	1.3	≈ 2	2	5.865	5.411	9.0
85 / 01 / 18	1.3	2 - 3	1	5.123	4.303	6.6
85 / 01 / 19	1.3	2 - 3	6	5.114	4.304	6.8
85 / 01 / 20	1.3	2 - 3	7	5.104	4.305	7.0
85 / 01 / 21	1.3	2 - 3	1	5.095	4.307	7.2

Table 5-10

Photometry of P/Halley

N	Date	UT [‡]	Tel [m]	Exp [sec]	Time [†]	Airmass	$m_R \pm \sigma(m_R)$	$m_R(1,1,0)$ [§]
1	84 / 10 / 22	9:48	1.3	900	9.8069	1.26	20.49 ± 0.30	12.75
2	84 / 10 / 22	10:58	1.3	1200	10.9705	1.11	20.84 ± 0.15	13.10
3	84 / 10 / 22	11:29	1.3	1200	11.4858	1.07	20.80 ± 0.30	13.06
4	84 / 10 / 22	12:29	1.3	1100	12.4875	1.07	21.08 ± 0.30	13.34
5	84 / 10 / 24	8:19	1.3	900	56.3156	1.70	20.62 ± 0.50	12.91
6	84 / 10 / 24	8:41	1.3	900	56.6908	1.53	20.58 ± 0.20	12.87
7	84 / 10 / 24	9:01	1.3	600	57.0144	1.42	20.46 ± 0.20	12.75
8	84 / 10 / 24	9:17	1.3	600	57.2836	1.34	20.49 ± 0.15	12.78
9	84 / 10 / 24	9:33	1.3	600	57.5514	1.28	20.77 ± 0.20	13.06
10	84 / 10 / 24	10:01	1.3	600	57.0150	1.20	20.31 ± 0.15	12.60
11	84 / 10 / 24	12:15	1.3	600	60.2553	1.06	20.49 ± 0.20	12.78
12	84 / 10 / 27	9:13	1.3	600	129.2125	1.31	21.27 ± 0.20	13.60
13	84 / 10 / 27	9:29	1.3	661	129.4875	1.25	21.16 ± 0.20	13.49
14	85 / 01 / 18	3:14	1.3	600	3.2406	1.19	19.38 ± 0.10	12.54
15	85 / 01 / 19	2:56	1.3	600	26.9261	1.22	19.14 ± 0.10	12.30
16	85 / 01 / 19	3:29	1.3	600	27.4872	1.14	19.11 ± 0.30	12.27
17	85 / 01 / 19	4:39	1.3	600	28.6528	1.07	19.22 ± 0.15	12.38
18	85 / 01 / 19	5:12	1.3	600	29.2067	1.06	19.44 ± 0.10	12.60
19	85 / 01 / 19	7:23	1.3	600	31.3903	1.28	19.51 ± 0.10	12.67
20	85 / 01 / 19	7:58	1.3	600	31.9758	1.43	19.40 ± 0.20	12.56
21	85 / 01 / 20	2:35	1.3	600	50.5894	1.26	19.32 ± 0.10	12.48
22	85 / 01 / 20	3:39	1.3	600	51.6564	1.06	19.31 ± 0.25	12.47
23	85 / 01 / 20	4:11	1.3	600	52.1908	1.06	19.00 ± 0.10	12.16
24	85 / 01 / 20	5:17	1.3	600	53.2892	1.07	19.04 ± 0.15	12.20
25	85 / 01 / 20	5:53	1.3	600	53.8756	1.09	19.15 ± 0.10	12.31
26	85 / 01 / 20	6:23	1.3	600	54.3833	1.13	19.19 ± 0.25	12.35
27	85 / 01 / 20	6:57	1.3	600	54.9450	1.21	19.28 ± 0.10	12.44
28	85 / 01 / 21	2:42	1.3	600	74.6958	1.23	19.01 ± 0.15	12.17

[‡] UT midtime of integration

[†] Obs (1-13) hours since 1984 October 22 at 0^h UT (JD = 2445995.5)

Obs (14-28) hours since 1985 January 18 at 0^h UT (JD = 2446083.5)

[§] $m_R(1,1,0) = m_R - 5 \log(R\Delta) - \beta \alpha$; where $\beta = 0.018 \text{ mag deg}^{-1}$ (see Chapter 4).

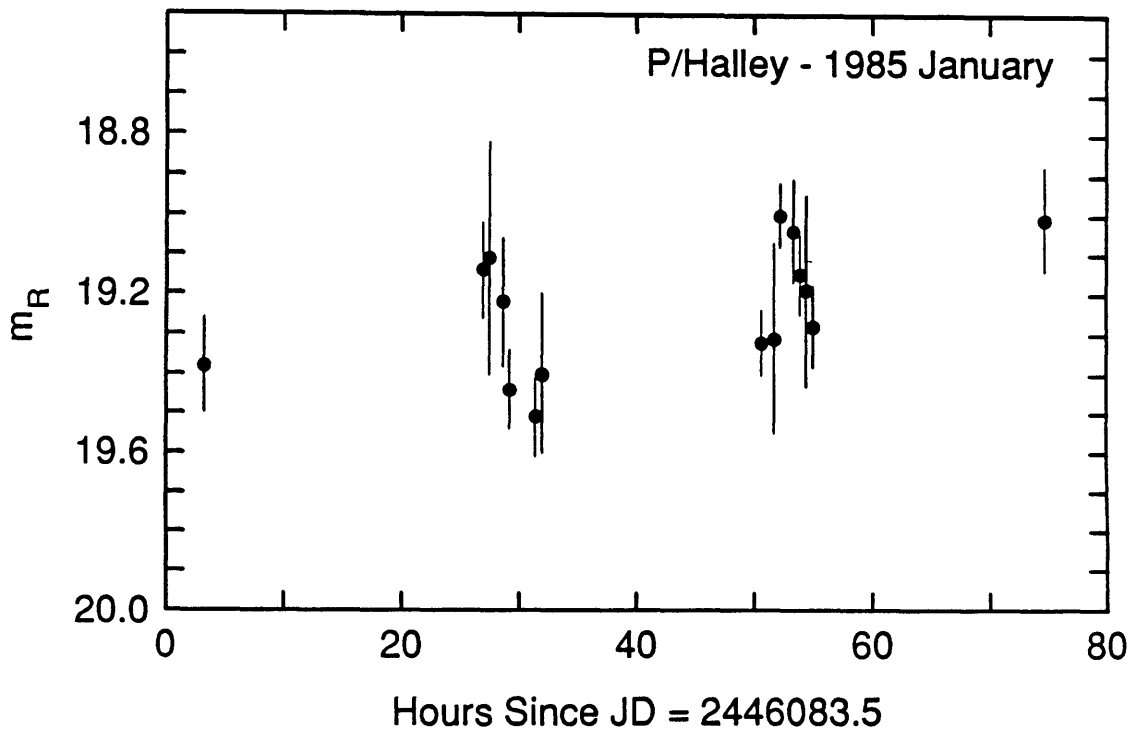
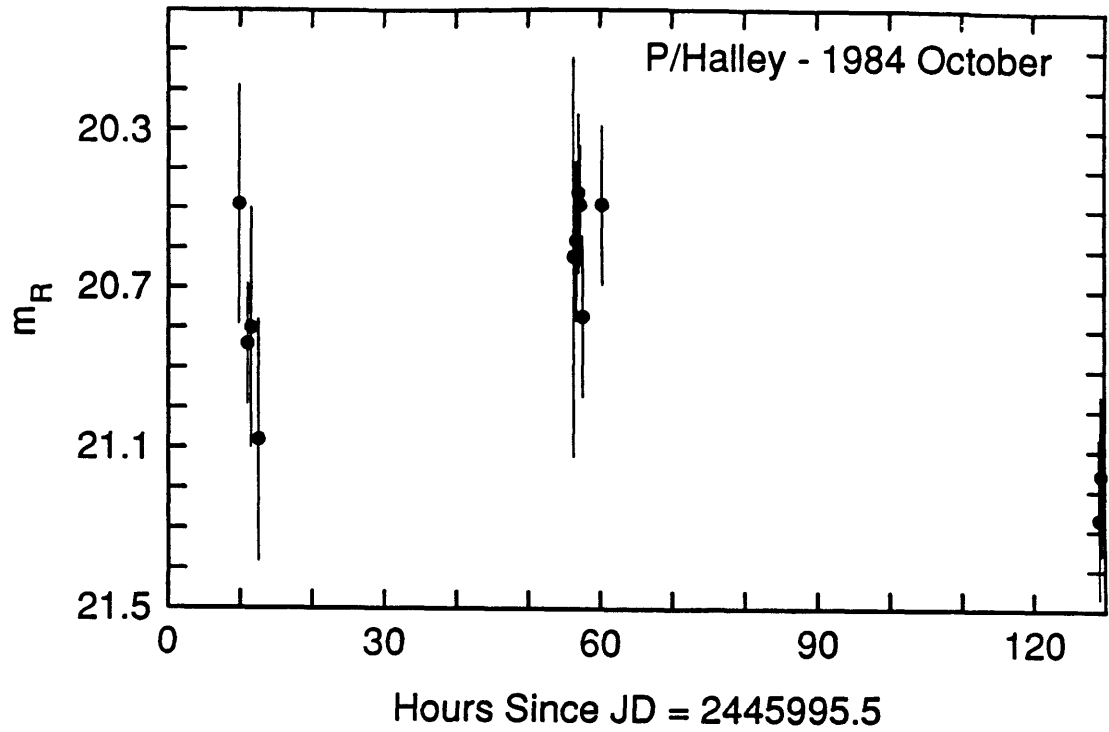


Figure 5-6. CCD Photometry of comet P/Halley obtained during 1984 October and 1985 January with the McGraw-Hill 1.3m telescope. The data are consistent with periods greater than about 18 hours, but undersampling prevents the determination of the period.

5.3 Analysis

Although there is no reason to assume that the rotational brightness variations will be sinusoidal in nature, this is a reasonable approximation to the behavior. For each data set χ^2 is computed as a function of period for the best fitting sinusoid in a range of periods from $T = 1$ to 30 hours. Note that although periods may be longer than 30 hours, the time base of the observations is insufficient for period searches longer than about 30 hours. The results of the minimum χ^2 searches are plotted in Figures 5-7 and 5-9 through 5-11 and the minimum frequencies indicated in the figures ($2\pi/T$) are listed in Table 5-11. For comets P/Neujmin 1 and P/Encke where observations were obtained during 2 separate observing runs, the period search has been conducted separately for each data set. In addition, the data were combined by correcting for the finite light travel time, where $t = t_{obs} - \Delta/c$ where t_{obs} is the time of the observation and $c = 2.997 \times 10^8 \text{ m s}^{-1}$ is the speed of light, and the data were reduced to the brightness for $R = 1$, $\Delta = 1 \text{ AU}$ and $\alpha = 0 \text{ deg}$ (see Eq. 2.1). The reduced magnitude is listed for all comets in Tables 5-2, 5-5, 5-6, 5-8 and 5-10. Only comet P/Arend-Rigaux had a measurable coma which extended beyond the observing diaphragm and the brightness had to be scaled as $R^2\Delta$. The results of the combined fits for P/Neujmin 1 and P/Encke are shown in Figures 5-9b and 5-10b. A similar combined search was not conducted for comet P/Halley because of the onset of sustained sublimation which had reduced the amplitude of the nucleus variations to 30% of the 1984 October range by 1985 January. The best estimates for the periods of all the comets are listed in Table 5-12 and discussed below.

As a check of the validity of the first period search technique, a second period search was conducted for each data set using the "string-length" method of Dworetzky (1983). For each trial period the data are ordered according to phase and the total length of the line segments joining successive points in the phase diagram is computed:

Table 5-11
Rotation Frequencies [$2\pi / T$] From Figures 5-7 to 5-11

Comet		ω_1 [rad hr ⁻¹]	ω_2	ω_3	ω_4
P/Arend-Rigaux		0.6576	0.9280		
P/Tempel 2		1.4071	1.6798		
P/Neujmin 1	(4m)	0.9939	1.2598	0.7332	
	(2.1m)	0.9827	1.2312	1.4842	1.7546
	(both)	0.9917	1.2489		
P/Encke	(4m)	0.2825	0.5628		
	(2m)	0.2776	0.5556	0.8333	1.1111
	(both)	0.27	0.55		
P/Halley	(Oct)	0.3775	0.4941	0.7550	1.3417
	(Jan)	0.6729	0.9566		

$$L = \sum_{i=1}^{i=n-1} [(m_i - m_{i-1})^2 + (\phi_i - \phi_{i-1})^2]^{1/2} + [(m_0 - m_n)^2 + (\phi_0 - \phi_n)^2]^{1/2} \quad (5.1)$$

The quantity ϕ_i is the trial phase and m_i is the magnitude which has been scaled so as to give equal weight to both quantities in Eq. 5.1. The period which yields the minimum string length value should be the best estimate of the period. This technique of phase dispersion minimization assumes no specific form for the light curve. In practice, the string-length results are noisier than the minimum χ^2 search because no constraint is placed on the light curve shape. Reassuringly, however, the two methods yield consistent results. The periods as determined using the string-length method are also listed in Table 5-12.

Table 5-12

Measured Nucleus Rotation Periods

Comet	χ^2 Period [hrs]	String Period [hrs]	Other Measurements	
P/Arend-Rigaux	13.54±0.05	13.54±0.05	13.5 27.31 13.47±0.02	A'Hearn, 1986 Wisniewski <i>et al.</i> , 1986 Millis <i>et al.</i> , 1987
P/Neujmin 1	12.67±0.06	12.73±0.06	25.27	Wisniewski <i>et al.</i> , 1986
P/Encke	22.47±0.07	22.4±0.1	-----	
P/Tempel 2	8.93±0.1 7.48±0.1	8.87±0.1 7.51±0.1	-----	
P/Halley (Oct)	9.37±0.1 16.64±0.1 25.43±0.1 33.28±0.1	16.6±0.2 25.5±0.2 33.0±0.2	24.3±0.3 > 10 > 24 53.97±0.03	LeFevre <i>et al.</i> , 1984 West & Pedersen, 1984 Jewitt & Danielson, 1984 Belton <i>et al.</i> , 1986
(Jan)	13.13±0.1 18.67±0.1	19.0±0.2 31.2±0.6	> 24 48.12 53.04 52.8±2.4 53.5±1 177.6 350.4	Sekanina, 1985 Morbey, 1985 Sekanina & Larson, 1986 Kaneda <i>et al.</i> , 1986 Sagdeev <i>et al.</i> , 1986 Millis & Schleicher, 1986 Festou <i>et al.</i> , 1987

5.4 Discussion

5.4.1 P/Arend-Rigaux

The results of both period searches show minima at frequencies of $\omega_1 = 0.658$ and $\omega_2 = 0.928$ rad hr⁻¹, which correspond to periods of $T_1 / 2 = 9.56$ hr and $T_2 / 2 = 6.77$ hr (where the rotation period, T , is *twice* the lightcurve period because of rotational symmetry). These two periods are aliased by the 24 hr sampling interval. From the χ^2 plot in Figure 5-7, the

minimum corresponding to ω_1 is only slightly deeper than the minimum corresponding to ω_2 . It is therefore difficult to distinguish which is the correct period based on this data alone. Several other groups obtained data at nearly the same time. Millis *et al.* (1987) find a period near 13.5 hours. Therefore,

$$T_2 = 13.54 \pm 0.05 \text{ hr} \quad (5.2)$$

is adopted as the true period of rotation. A sinusoid of this period is superimposed on the data in Figure 5-2. It is interesting to note that Wisniewski *et al.* (1986) claim to have found a four peaked light curve for the rotation just as was the case for comet P/d'Arrest; their period is exactly twice T_2 .

Comet P/Arend-Rigaux had an extended low surface brightness coma during the observations; it is therefore reasonable to ask whether the brightness variations could be due to the intrinsic activity of the comet. If the brightness changes were caused by the injection of dust into the coma, the ejected dust would pass from the inner to the outer diaphragm on a timescale $t_{cross} = d / v$, where v [m s^{-1}] is the grain ejection velocity (approximated by the Bobrovnikoff relation $v \approx 600 R^{-0.5}$, R in AU (Delsemme, 1982)), and d [m] is the projected diaphragm radius. The diaphragm crossing time is of the order of $t_{cross} \approx 10^4$ s. No time-delayed brightness enhancements are seen in the outer diaphragm photometry (see Figure 5-2). Thus, it can be concluded that the variations are not due to ejection of refractory grains into the coma. As discussed in Jewitt and Meech (1985), the variations could be caused by volatile grains, but in this case the variations would likely be modulated by the rotation of the nucleus. In Figure 5-8 the surface brightness of the coma is plotted at both maximum and minimum brightness. The figure shows that the brightness variations are primarily confined to the inner coma. Finally, as shown by Millis *et al.* (1987), the variations are caused by an irregularly shaped nucleus and not by albedo variations on the surface.

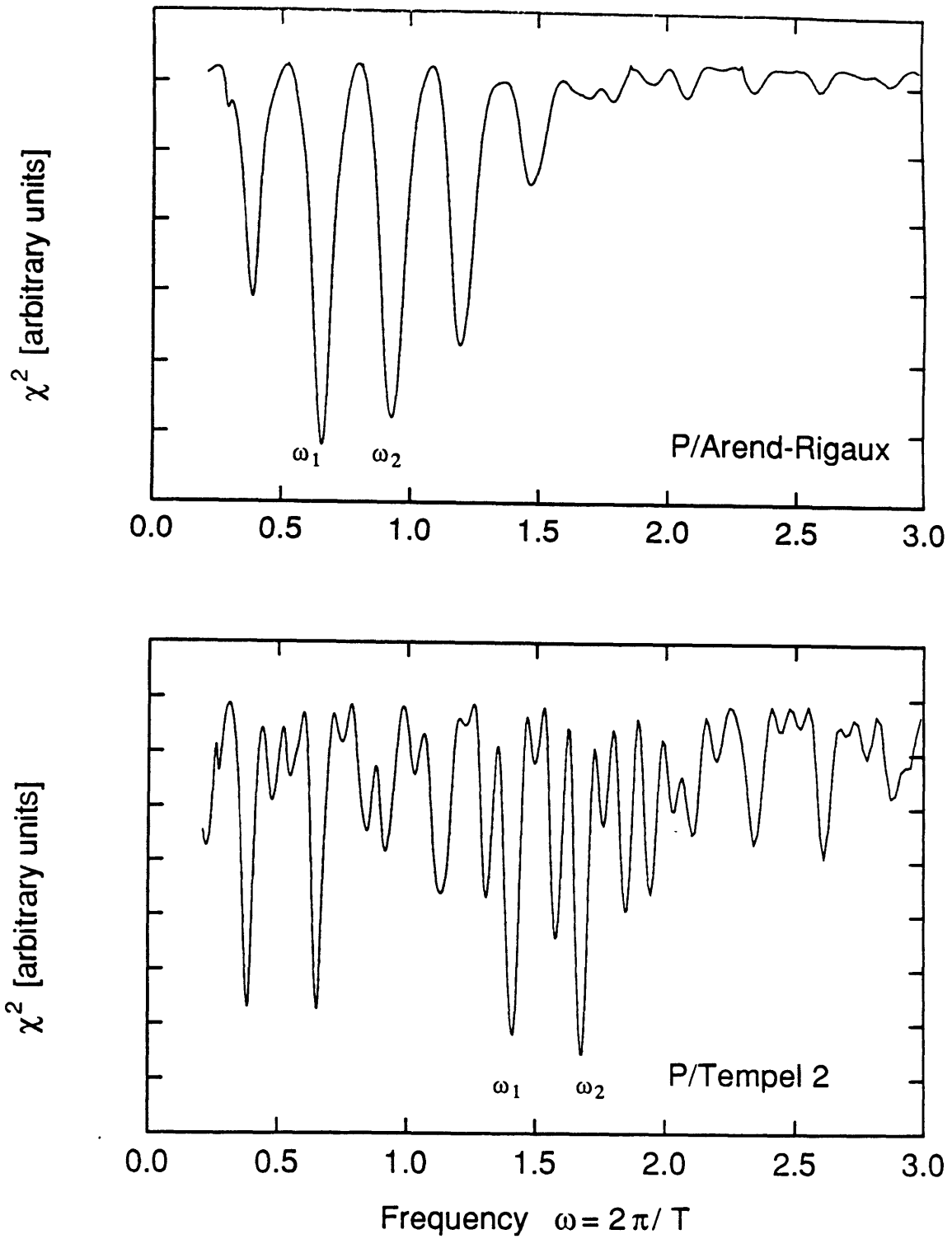


Figure 5-7. Results of least squares period searches for comets P/Arend-Rigaux and P/Tempel 2. χ^2 versus frequency (rad hr^{-1}) is plotted. The locations of the deepest minima are listed in Table 5-11.

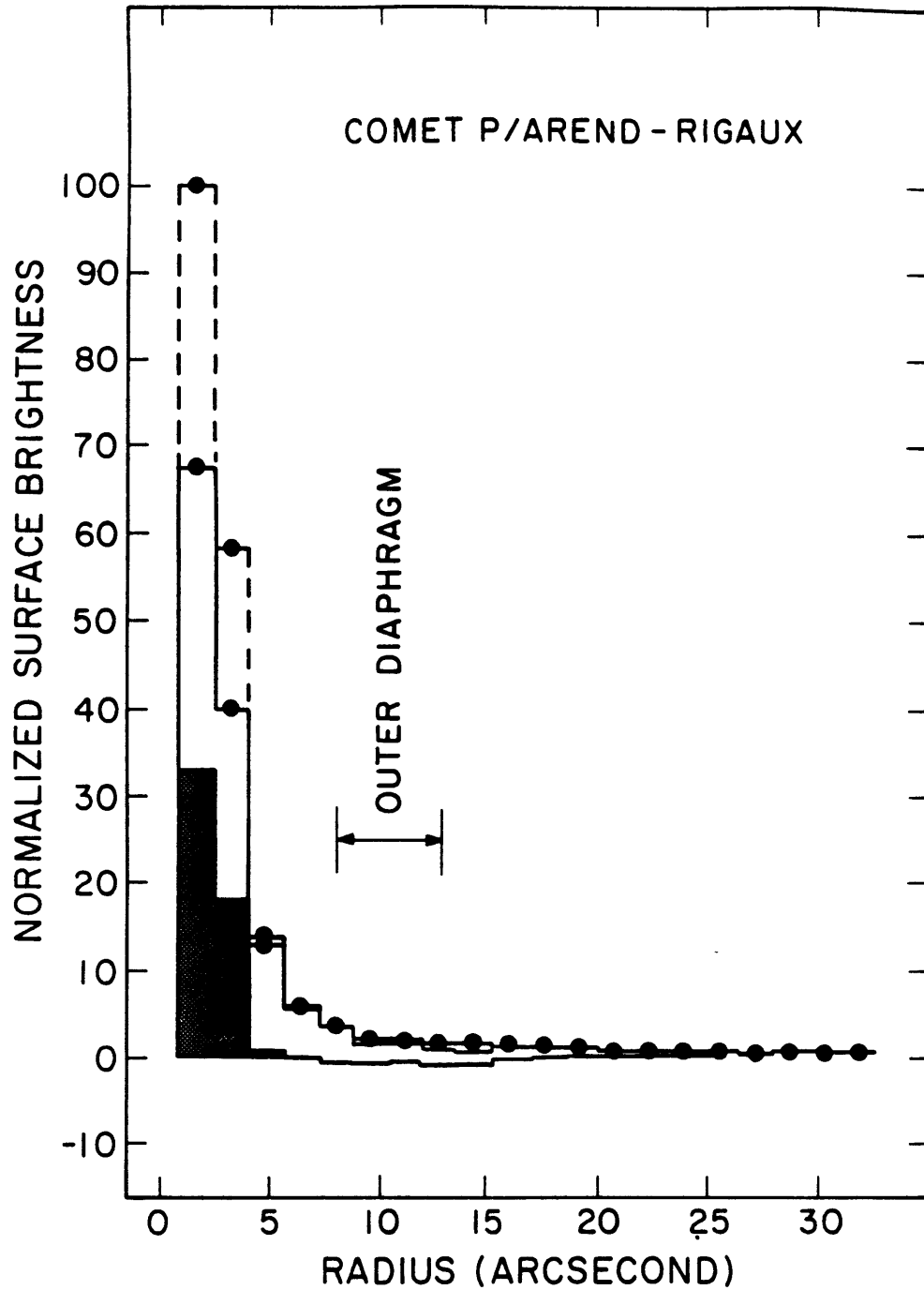


Figure 5-8. Surface brightness (in linear, arbitrary units) of comet P/Arend-Rigaux versus projected distance from the nucleus (in arcsec). The surface brightness (indicated by dots) is the average within concentric annuli about the nucleus. One hundred units of surface brightness correspond to $17.37 \text{ R mag arcsec}^2$. The uppermost profile corresponds to 1985 January 21, 07:58 UT (maximum brightness), the middle profile to 1985 January 21, 11:52 UT (minimum brightness), and the lower profile (shaded) is the difference between the first two curves. Error bars are mostly too small to be plotted on the scale of this figure. The figure shows that the photometric variations in comet P/Arend-Rigaux are confined to the innermost region of the coma.

5.4.2 P/Neujmin 1

The results of both period searches show minima at several different frequencies. These are listed in Table 5-11. There are relatively few data points for P/Neujmin 1 compared to P/Arend-Rigaux; for this reason the period for the individual observing runs is not well determined - there are several deep minima aliased by the 24 hour sampling interval (see Figure 5-9a). The combined data set period search yields two deep minima at frequencies near $\omega_1 = 0.99$ and $\omega_2 = 1.25$ rad hr⁻¹ (see Figure 5-9b). The deepest minimum, at

$$T_1 = 12.67 \pm 0.06 \text{ hr} \quad (5.3)$$

is adopted as the rotation period of the nucleus. The fact that the same period was determined at two separate heliocentric distances suggests that the variations in brightness were not caused by irregular activity since this would change as a function of distance.

The only other known measurement of the rotation period of this comet is by Wisniewski *et al.* (1986), who again find a complicated 4 peaked light curve. Their period, $T = 25.27$ (see Table 5-12) is twice the period adopted here.

5.4.3 P/Encke

The results of the period searches show minima at frequencies near $\omega_1 = 0.28$ and $\omega_2 = 0.56$ rad hr⁻¹ for both the period searches for the individual observing runs and the combined data set (see Figures 5-10a and 5-10b). The minima are approximately the same depth for the separate solutions, whereas ω_1 is the deeper minimum in the combined solution. It is difficult to distinguish between the two periods T_1 and $T_2 = T_1 / 2$; the period

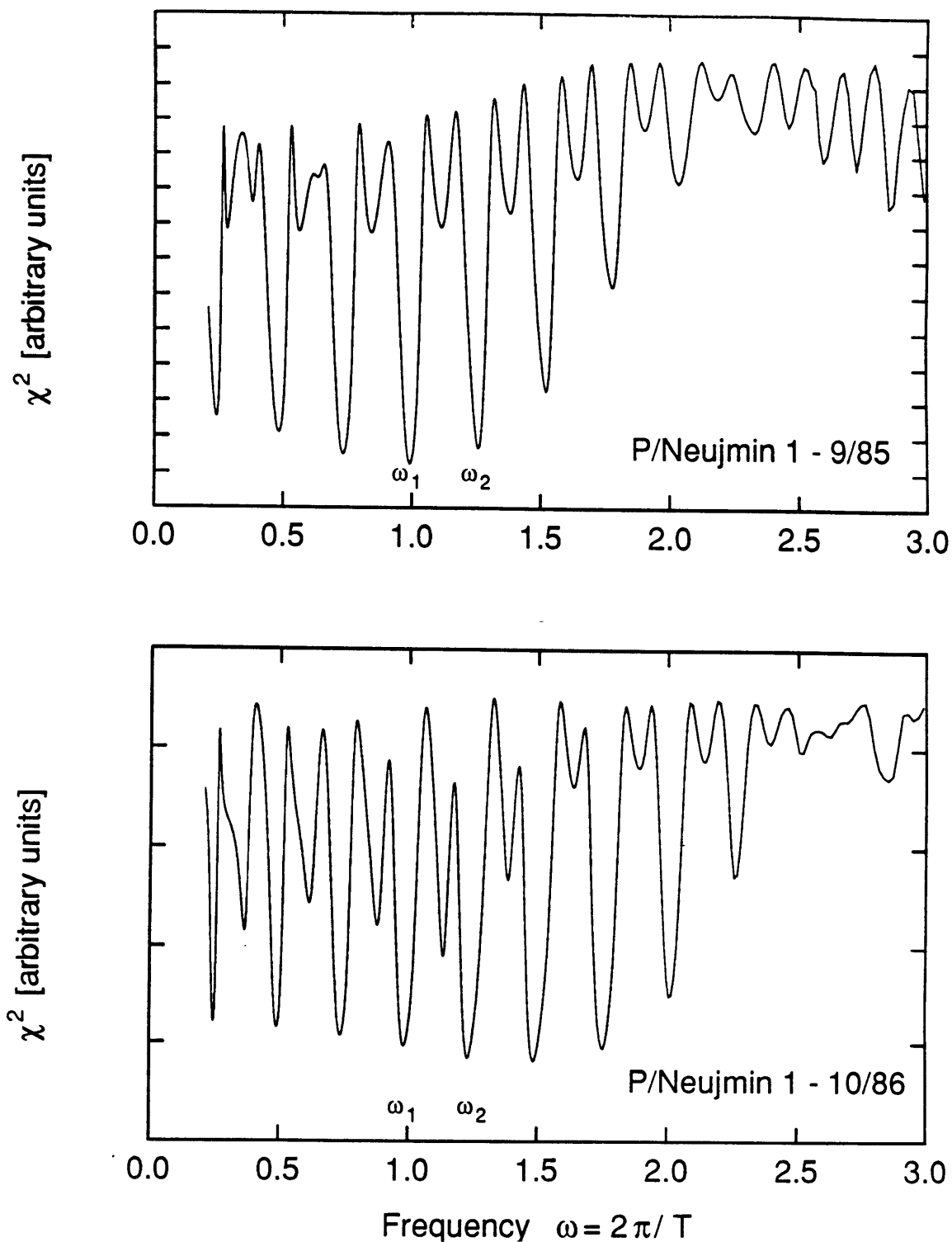


Figure 5-9. (a) Results of a least squares period search for comet P/Neujmin 1. χ^2 versus frequency (rad hr^{-1}) is plotted. Period searches were computed separately for the 1985 September and 1986 October data. The deep minima are separated by the 24 hour daily sampling alias. Although several minima appear equally deep during each month, the location of the deepest is the same during the two runs. The locations of these deepest minima are listed in Table 5-11.

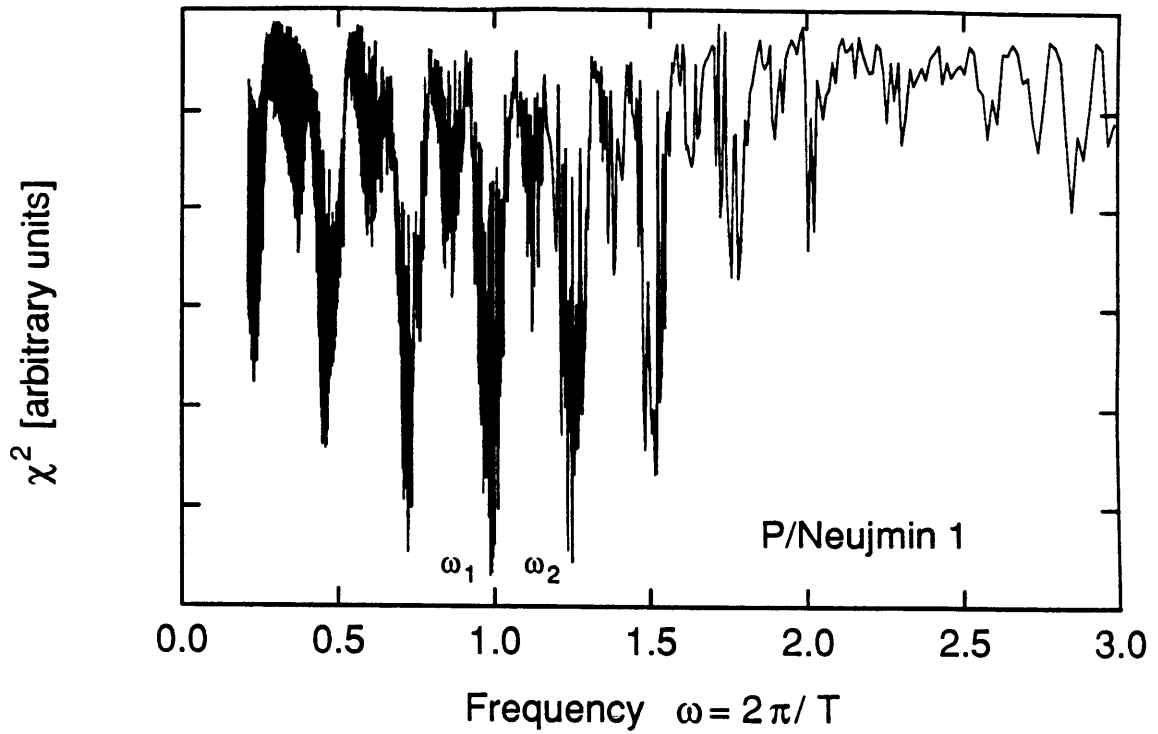


Figure 5-9. (b) Results of a least squares period search for P/Neujmin 1 using the combined 1985 September, 1986 March and 1986 October data. The data have been corrected for light travel time [$t = t_{obs} - \Delta / c$] and reduced to $m_R(1,1,0)$ at unit R , Δ and at phase angle $\alpha = 0$. The frequencies marked ω_1 and ω_2 in Figure 5-8a and listed in Table 5-11 are the deepest in the combined data set.

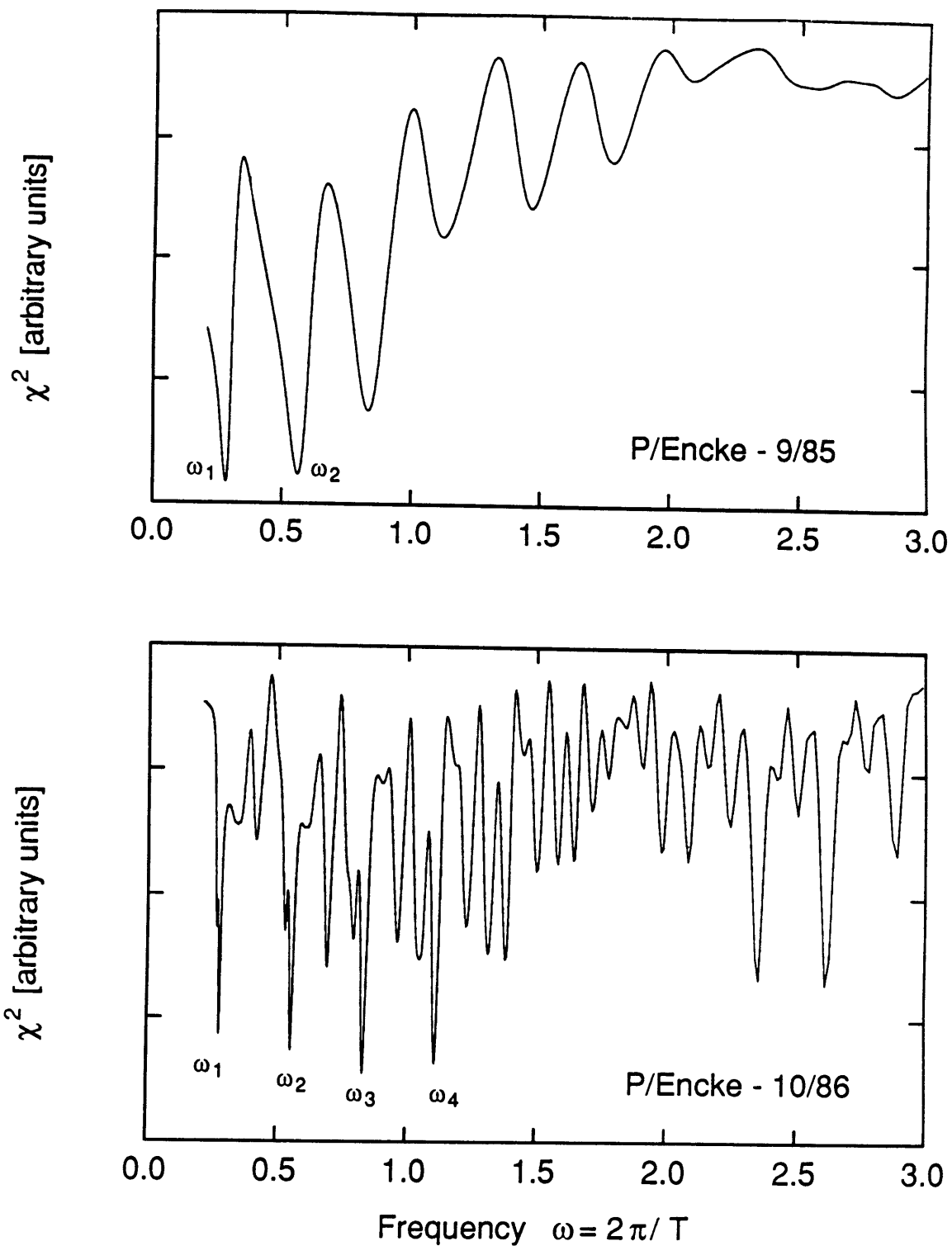


Figure 5-10. (a) Results of a least squares period search for comet P/Encke. χ^2 versus frequency (rad hr^{-1}) is plotted. Period searches were computed separately for the 1985 September and 1986 October data. The deep minima are separated by the 24 hour daily sampling alias. The locations of these deepest minima are listed in Table 5-11.

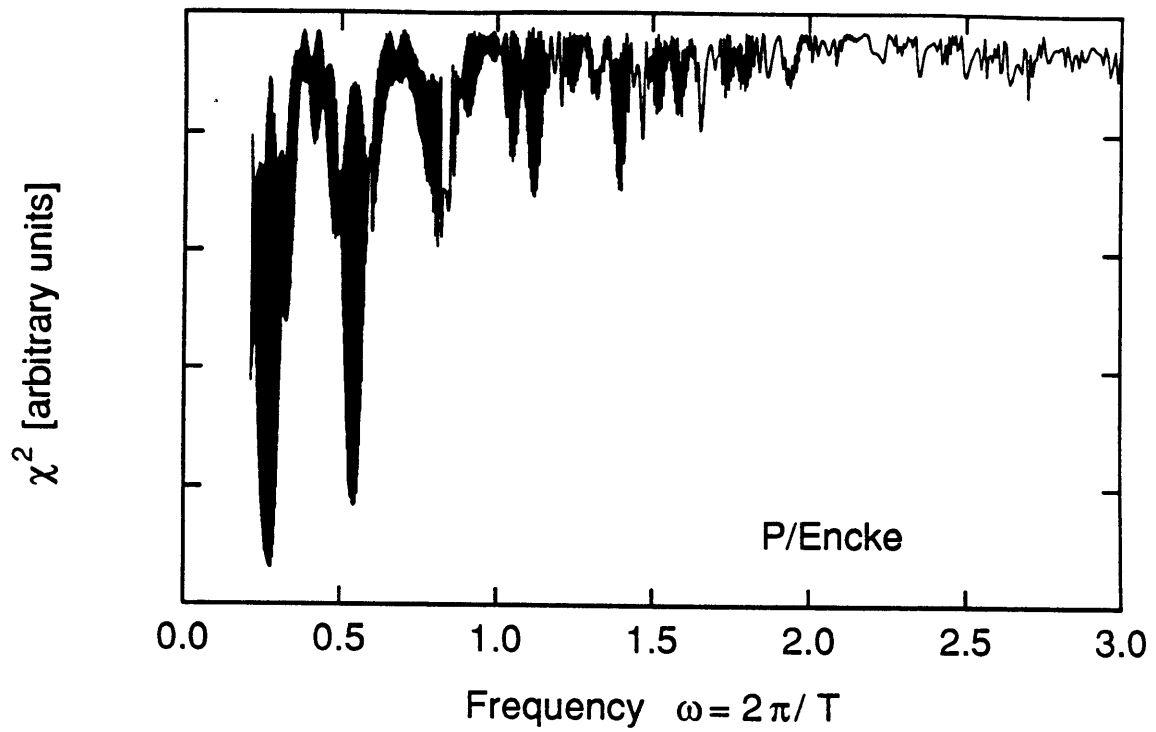


Figure 5-10. (b) Results of a least squares period search for P/Encke using the combined 1985 September and 1986 October data. The data have been corrected for light travel time [$t = t_{obs} - \Delta / c$] and reduced to $m_R(1,1,0)$ at unit R , Δ and at phase angle $\alpha = 0$.

$$T_2 = 22.47 \pm 0.07 \text{ hr} \quad (5.4)$$

is adopted as the rotation period of the nucleus since it gives a 2 peaked lightcurve as expected for a rotating body. As in the case of comet P/Neujmin 1, the fact that the same period was determined at two separate heliocentric distances suggests that the variations in brightness were not caused by irregular activity.

The rotation period was determined by Whipple (1982) using the halo method. The halo method period for P/Encke, $T_{halo} = 6.5$ hr, does not agree well with the value found here. There is no minimum in either Figures 5-10a or 5-10b at $\omega \approx 1.93$ rad hr⁻¹ corresponding to this period. Whipple and Sekanina (1979) have also modelled the secular variation in the non gravitational acceleration of this comet as resulting from precession of the polar axis due to anisotropic mass loss from an oblate nucleus with a rotation period of 6.25 ± 0.25 hr. The Whipple and Sekanina period determination is based on the halo method.

5.4.4 P/Tempel 2

The results of both period searches for this comet yield minima at the frequencies $\omega_1 = 1.41$ and $\omega_2 = 1.68$ rad hr⁻¹, corresponding to nucleus rotation periods $T_1 = 8.9 \pm 0.1$ and $T_2 = 7.5 \pm 0.1$ hr (see Table 5-12 and Figure 5-7). The two periods are aliased by the 24 hr sampling interval, and without further observations, the true period cannot be determined. The possible period, however, may be compared with the halo method determination (Whipple, 1982) of $T = 4.8$ hr.

5.4.5 P/Halley

The period searches in the two P/Halley data sets yield numerous χ^2 minima (see Figure 5-11). Selected frequencies for some of the deepest minima are listed in Table 5-11. Only minima corresponding to periods greater than 5 hours are listed since continuous observations during intervals of 5 hours rule out any periods of shorter duration. Unfortunately, no single period was found which provided good agreement with the data from both 1984 October and 1985 January. Although it was concluded in Chapter 2 that the invariance of the reduced magnitude [$m_R(1,1,0)$] implied that the bare nucleus was visible at $R > 5.9$ AU, it could be argued that the brightness fluctuations were due to the transient ejection of matter from the nucleus (Sekanina, 1985). However, the observed decrease in the range of the brightness fluctuations, from 1.0 mag at $R \geq 8$ AU, to 0.8 mag at $R = 5.9$ AU, to 0.3 mag at $R = 5.1$ AU, strongly suggests that the mechanism producing the fluctuations is nucleus rotation but diluted by increasingly large amounts of coma. It is possible that fluctuations in the relatively strong coma in 1985 January modify the apparent period.

A controversy presently exists as to what is the correct rotation period for P/Halley. Prior to the onset of activity in comet P/Halley as it approached perihelion, numerous other investigators attempted unsuccessfully to determine the rotation period (e.g. Le Fevre *et al.*, 1984; West and Pedersen, 1984; Sekanina, 1985; Morbey, 1985). Most likely, photometric errors and incomplete sampling were the two main reasons for the failure to find the nucleus rotation period. On the one hand, aggregates of observations by different observing groups are susceptible to relative systematic errors of measurement and are therefore very difficult to compare. For example, Le Fevre *et al.* (1984) report brightness variations consistently about a factor of 2 greater than those reported by either West and Pedersen (1984) or Jewitt and Danielson (1984). The large amplitude is probably caused by observational error; no other investigators saw brightness variations this large. On the other hand, subsets of observations

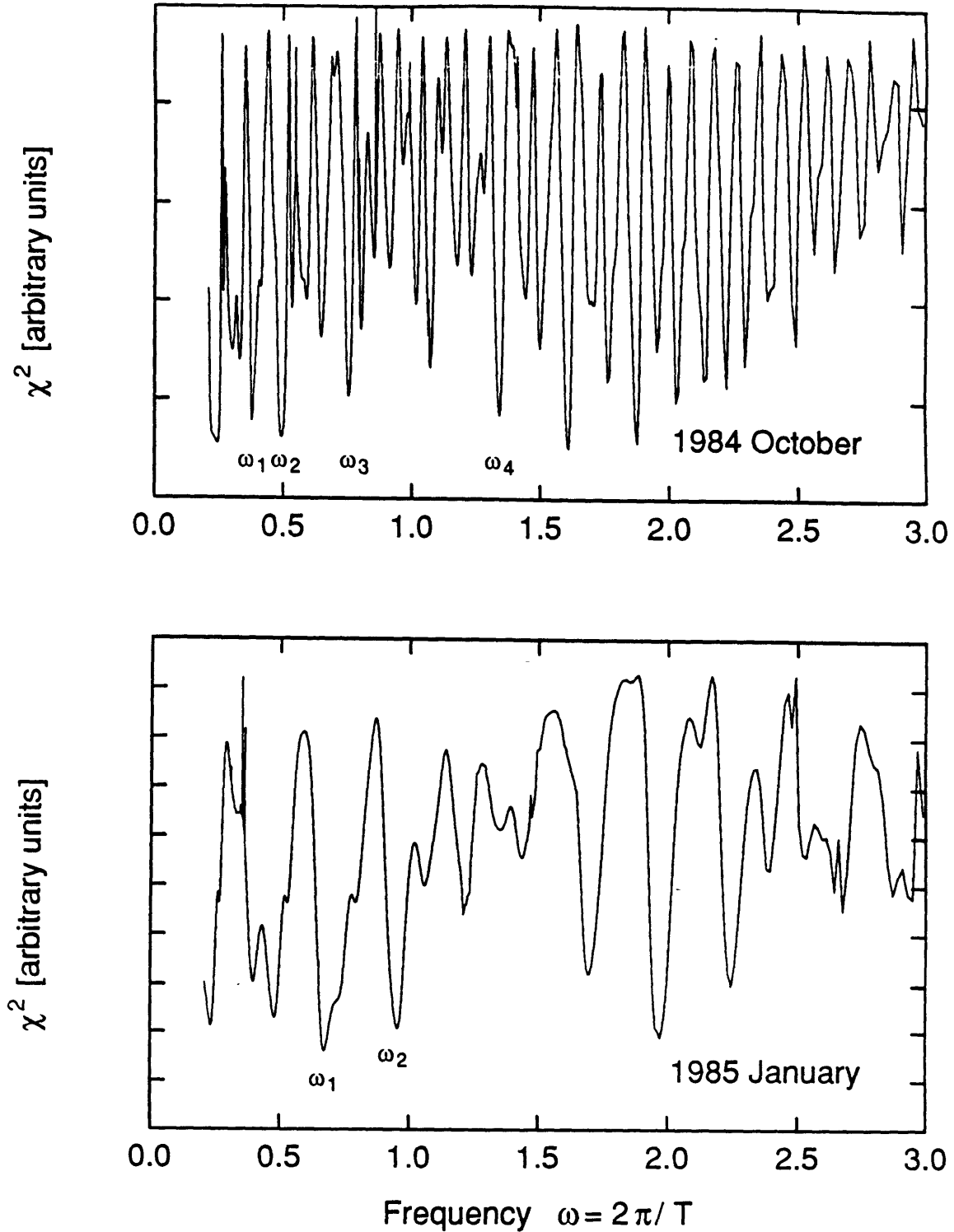


Figure 5-11. Results of a least squares period search for comet P/Halley. χ^2 versus frequency (rad hr^{-1}) is plotted. Period searches were computed separately for the 1984 October and 1985 January data. The deep minima are separated by the 24 hour daily sampling alias. The locations of these deepest minima are listed in Table 5-11. None of the deep minima from the two runs are coincident. The data were not combined to search for a fit because during 1985 January sublimation had begun and the nucleus was only contributing 30% to the total brightness.

taken using a single detector and telescope are free of systematic errors but are too small to firmly establish the period.

Sekanina and Larson (1986) have used the morphology of the images of P/Halley from 1910 to infer a rotation period near 53 hours. Belton *et al.* (1986) have combined all pre-perihelion photometry of high quality and suggested a similar period of either 53.97 or 54.12 hours. These periods are in agreement with those determined by the spacecraft flybys: $T = 52.9 \pm 1$ hr (Kaneda *et al.*, 1986) and $T = 53.5 \pm 1$ hr (Sagdeev *et al.*, 1986).

More recently, Millis and Schleicher (1986) have reported nightly brightness fluctuations in the coma of P/Halley near perihelion, during 1986 March and April. They obtained their observations with a conventional single-channel photometer and several interference filters isolating both gas bands and continuum windows. These investigators found strong evidence for a periodicity of 177.6 hours (7.4 days) in their data. They interpret the brightness fluctuations as due to changes in cometary activity as more and less active areas on the nucleus are brought into the sunlit hemisphere by rotation. It is interesting to note that the spectrophotometric observations of P/Halley presented in Chapter 4 also show a variation of the type reported by Millis and Schleicher. The photometry from Chapter 4 shows a slow day-to-day brightness variation (only seen in the molecular emission bands). Figure 5-12 shows the variation of the CN($\Delta v=0$) flux as a function of JD. (The variation of the C₂($\Delta v=0$) band is remarkably similar). The observations, however, cover a timebase too short to independently determine the period.

There has been considerable discussion attempting to reconcile the 7.4 day period found by Millis and Schleicher and the 2.2 day period seen elsewhere (Wilhelm, 1987; Sekanina, 1986). Sekanina (1986) proposes that the rotation period is 7.4 days and that the comet precesses with a period of 2.2 days. Wilhelm (1987), on the other hand, argues that the rotation period is 2.2 days and the precession period is 14.8 days. Finally, Festou *et al.* (1987) propose a rotation period of 14.6 days with a precession of 2.088 days! It is apparent

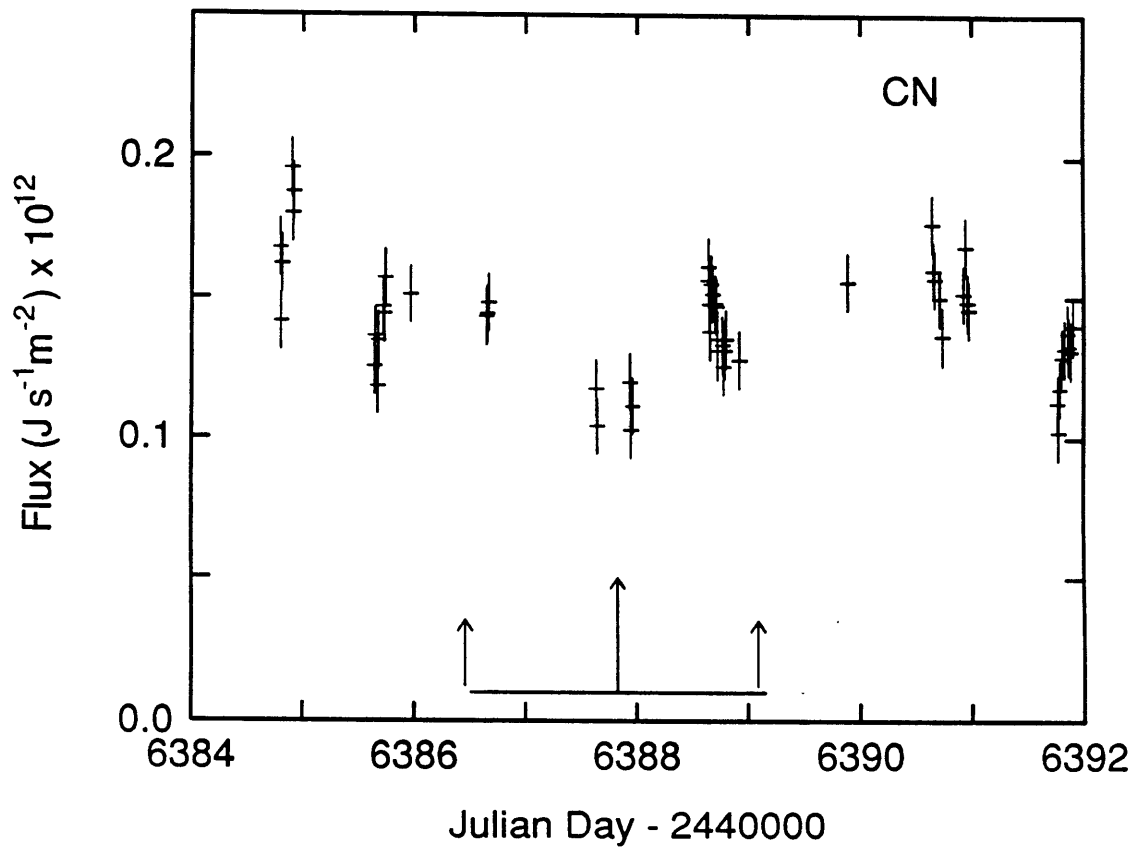


Figure 5-12. Temporal variation in the CN($\Delta v=0$) gas band as observed during 1985 November with the MkII spectrograph at MIT's McGraw-Hill observatory (see Chapter 4).

that the period of rotation for P/Halley is still controversial; however, it is safe to conclude that the period, whatever it is, is long. The best hope of settling the matter will be to observe the comet as it recedes from the sun, when the coma no longer contributes most of the light.

5.5 Comets as Slow Rotators

Ideally, to decide on the basis of the measured rotation periods whether or not comets are slow rotators in the sense defined in Chapter 2 (i.e. the rotation is slow compared to the time for sublimation to drop sufficiently so that dust is not dragged into the coma), the thermal properties of the nucleus must be known. Unfortunately, little is known about the thermal properties. The spacecraft measurements of P/Halley suggest a very low density (Whipple, 1986) and a low thermal conductivity (Combes *et al.*, 1986). The suggestion of a very porous, low density surface for a comet is reminiscent of asteroid and lunar regoliths. Radiometric techniques can very successfully determine asteroid diameters assuming that little energy is radiated into the dark hemisphere from the regolith. The measurements of the rotation periods of comets show that the comets tend to have slightly longer periods than do asteroids of comparable sizes (Jewitt & Meech, 1987b). If a comparison between the asteroid and comet thermal properties is at all valid, the implication is that the comets are slow rotators. In fact, because the sublimation is such a strong function of temperature (see Eqs. 2.6, 2.7 and 2.10), only a small temperature drop is required to dramatically reduce the sublimation.

There is observational evidence that in fact the comets do sublimate primarily in the sunlit hemisphere. Non-gravitational accelerations are observed for nearly all comets; if sublimation were isotropic, there would be no net accelerations. Also there are many observations of sunward jets and fans which give evidence of very strong sunward sublimation. For P/Halley, the activity as observed from Giotto was almost exclusively from the sunward hemisphere (Whipple, 1986).

5.6 Conclusions

1. The rotation periods of P/Arend-Rigaux, P/Neujmin 1 and P/Encke have been determined to be 13.54 ± 0.05 hr, 12.67 ± 0.06 hr and 22.47 ± 0.07 hr respectively.
2. Constraints have been placed on the rotation periods of comets P/Tempel 2 and P/Halley. The period of P/Tempel 2 may be either 8.93 or 7.48 hours. P/Halley has a long rotation period, > 18 hours; however, the question of whether it is 2.2 days with a precession period of 7.4 days or whether it is 7.4 days with a precession period of 2.2 days is still very much controversial. Of course it may be that neither of these periods is correct.
3. Comets have rotation periods which may be considered long from the perspective of computing sublimating ice models.

References

- A'Hearn, M. F. (1986), "Are Cometary Nuclei Like Asteroids?", in *Asteroids Comets Meteors II*, eds. C.-I. Lagerkvist, B. A. Lindblad, H. Lundstedt and H. Rickman, Uppsala Univ., Uppsala, p. 187-190.
- Belton, M. J. S., P. Wehinger, S. Wyckoff and H. Spinrad (1986), "A Precise Spin Period for P/Halley", in *Proceedings of the 20th ESLAB Symposium on the Exploration of Halley's Comet*, ESA Pub. Div., The Netherlands, Vol. I, p. 599-603.
- Christian, C. A., M. Adams, J. V. Barnes, H. Butcher, D. S. Hayes, J. R. Mould, M. Siegel (1985), "Video Camera/CCD Standard Stars (KPNO Video Camera/CCD Standards Consortium)", *Pub. Ast. Soc. Pac.* **97**, 363-372.
- Combes, M., V. I. Moroz, J. F. Crifo, J. M. Lamarre, J. Charra, N. F. Sanko, A. Soufflot, J. P. Bibring, S. Cazes, N. Coron, J. Crovisier, C. Emerich, T. Encrenaz, R. Gispert, A. V. Grigoryev, G. Guyot, V. A. Krasnopolsky, Yu. V. Nikolsky and F. Rocard (1986), "Infrared Sounding of Comet Halley from Vega 1", *Nature* **321**, 266-268.
- Delsemme, A. H. (1982), "Chemical Composition of Cometary Nuclei", in *Comets*, ed. L. L. Wilkening, Univ. of AZ Press, Tucson, AZ, p. 85-130.
- Dworetzky, M. M. (1983), "A Period-Finding Method For Sparse Randomly Spaced Observations or "How Long is a Piece of String", *Mon. Not. Roy. Astr. Soc.* **203**, 917-924.
- Fay, T. D. and W. Wisniewski (1978), "The Light Curve of the Nucleus of Comet d'Arrest", *Icarus* **34**, 1-9.
- Festou, M. C., P. Drossart, J. Lecacheux, T. Encrenaz, F. Puel and J. L. Kohl-Moreira (1987), "The Light Curve of P/Halley and the Rotation of its Nucleus", *Astron. Astrophys.* (submitted).
- Kaneda, E., M. Takagi, K. Hirao, M. Shimizu and O. Ashihara, (1986), "Ultraviolet Features of Comet Halley Observed by Suisei", in *Proceedings of the 20th ESLAB Symposium on the Exploration of Halley's Comet*, ESA Pub. Div., The Netherlands, Vol. I, p. 397-402.
- Jewitt, D. and G. E. Danielson (1984), "Charge-Coupled Device Photometry of Comet P/Halley", *Icarus* **60**, 435-444.
- Jewitt, D. and K. Meech (1985), "Rotation of the Nucleus of Comet P/Arend-Rigaux", *Icarus* **64**, 329-335.
- Jewitt, D. and K. Meech (1987a), "CCD Photometry of Comet P/Encke", *Astron. J.* **93**, 1542-1548.
- Jewitt, D. C. and K. J. Meech (1987b), "P/Neujmin 1, P/Tempel 2 and the Shapes of Cometary Nuclei", in preparation.

References, contd.

- Landolt, A. U. (1983), "UBVRI Photometric Standard Stars Around the Celestial Equator", *Astron. J.* **88**, 439-460. (Contributions of the Louisiana State Univ. Obs., #174).
- Le Fevre, O., J. Lecacheux, J., G. Mathez, G. Lelievre, J. Baudrand and J. P Lemonnier (1984), "Rotation of Comet P/Halley: Recurrent Brightening Observed at the Distance of 8 AU", *Astron. Astrophys.* **138**, L1-L4.
- Marsden, B. G. (1968), "Comets and Non-Gravitational Forces", *Astron. J.* **73**, 367-379.
- Meech, K. J., D. Jewitt and G. R. Ricker (1986), "Early Photometry of Comet P/Halley: Development of the Coma", *Icarus* **66**, 561-574.
- Meyer, S. S. and G. R. Ricker (1980), "A Dual Charge-Coupled Device (CCD), Astronomical Spectrometer and Direct Imaging Camera. I. Optical and Detector Systems", *S.P.I.E.* **264**, 38-41.
- Millis, R. L., M. F. A'Hearn and H. Campins (1987), "An Investigation of the Nucleus and Coma of Comet P/Arend-Rigaux", preprint.
- Millis, R. L. and D. G. Schleicher (1986), "Rotational Period of Comet Halley", *Nature* **324**, 646-649.
- Morbey, C. L. (1985), "Brightness Variations in Comet P/Halley Determined by the Least Scatter Algorithm", *Astron. Exp.* **1**, 133-136.
- Sagdeev, R. Z., V. A. Krasikov, V. A. Shamis, V. I. Tarnopolski, K. Szegö, I. Tóth, B. Smith, S. Larson and E. Merényi (1986), "Rotation Period and Spin Axis of Comet Halley", in *Proceedings of the 20th ESLAB Symposium on the Exploration of Halley's Comet*, ESA Pub. Div., The Netherlands, Vol. II, p.335-338.
- Sekanina, Z. (1985), "Light Variations of Periodic Comet Halley Beyond 7 AU", *Astron. Astrophys.* **148**, 299-308.
- Sekanina, Z. (1986), "Nucleus of Halley's Comet as a Torque-Free Rigid Rotator: Reconciling the 2.2-Day and 7.4-Day Periods", *JPL Preprint No.* 86.
- Sekanina, Z. and S. M. Larson (1986), "Coma Morphology and Dust-Emission Pattern of Periodic Comet Halley. IV. Spin Vector Refinement and Map of Discrete Dust Sources for 1910", *Astron. J.* **92**, 462-482.
- Thuan, T. X. and J. E. Gunn (1976), "A New Four Color Intermediate Photometric System", *Publ. Astron. Soc. Pac.* **88**, 543-547.
- West, R. M. and H. Pedersen (1984), "Variability of P/Halley", *Astron. Astrophys.* **138**, L9-L10.
- Whipple, F. L. (1950), "A Comet Model. I. Acceleration of Comet Encke", *Astrophys. J.* **111**, 374-394.

References, contd.

- Whipple, F. L. (1951), "A Comet Model. II. Physical Relations For Comets and Meteors", *Astrophys. J.* **113**, 464-474.
- Whipple, F. L. (1982), "The Rotation of Comet Nuclei", in *Comets*, ed. L. L. Wilkening, Univ. of Arizona Press, Tucson, AZ, p. 227-250.
- Whipple, F. L. (1986), "The Cometary Nucleus - Current concepts", in *Proceedings of the 20th ESLAB Symposium on the Exploration of Halley's Comet*, ESA Pub. Div., The Netherlands, Vol. II., p. 367-369.
- Whipple, F. L. and Z. Sekanina (1979), "Comet Encke: Precession of the Spin Axis, Nongravitational Motion, and Sublimation", *Astron. J.* **84**, 1894-1909.
- Wilhelm, K. (1987), "Rotation and Precession of Comet Halley", *Nature* **327**, 27-30.
- Wisniewski, W. Z., T. Fay and T. Gehrels (1986), "Light Variations of Comets", in *Asteroids Comets Meteors II*, eds. C.-I. Lagerkvist, B. A. Lindblad, H. Lundstedt and H. Rickman, Uppsala Univ., Uppsala, p. 337-339.

Chapter 6 - Grain Sizes in Cometary Comae

6.1 Introduction

Most of the light observed from comets is scattered from the grains in the coma; the physical characteristics of the grains determine the nature of the scattered radiation. Comet dust may be material which has not been substantially thermally or chemically altered since the formation of the solar system; therefore it is important to be able to use ground-based measurements to infer grain properties. There have been very few detailed studies of the scattering properties of cometary grains; most of the work to date has concentrated in the thermal infra-red. Optical spectrophotometric measurements have been made by Remillard and Jewitt (1985) and by Newburn and Spinrad (1985). Both investigations conclude that comet dust is slightly reddened with respect to the solar continuum. This chapter discusses optical spectrophotometric measurements of the scattering from grains and compares the scattering in the optical to that in the near and thermal infrared. Light scattered from cometary grains is reddened with respect to the solar continuum and the amount of reddening is observed to decrease with increasing wavelength, consistent with the scattering from particles with radii $a > 2 \mu\text{m}$. The work presented in this chapter is a brief summary of Jewitt and Meech (1986); it is discussed here because of its relevance to nucleus sublimation models (Chapter 8).

6.2 Observations

Optical observations of the spectra of nine comets were taken using an intensified image dissector scanner (IIDS) on the 2.1m telescope at Kitt Peak on the night of 1985 February 16 and 17 UT. A journal of observations is presented in Table 6-1. The IIDS was placed at the

f/7.7 Cassegrainian focus, giving a focal plane image scale of $12.3 \text{ arcsec mm}^{-1}$. A reflection grating of 300 line mm^{-1} was used in the first order giving a dispersion of about 3.4 \AA per channel and a wavelength range from 3500 \AA to 7000 \AA . All observations were taken through a circular diaphragm of 8.4 arcsec projected diameter. The instrumental resolution through this diaphragm was measured to be 13 \AA full width at half maximum (FWHM). Sky subtraction with the IIDS was performed using simultaneous observations of the sky by chopping 100 arcsec EW from the object position. When gas emission bands were noticed at the sky positions, separate sky observations were taken at positions 0.5 deg from the comet. Possible instrumental asymmetries between the object and sky beams were cancelled by periodically chopping the comet from one beam to the other.

On both nights the seeing and the guiding uncertainties (1.5 arcsec and 1 arcsec FWHM, respectively) were small in comparison with the spectrometer diaphragm. Absolute flux calibration of the spectra was achieved using observations of the stars Feige 34, BD+8°2015, Hiltner 600, Ross 640, EG 247 and Grw +70°5824 at similar airmasses (Oke, 1974; Stone, 1977). Spectra of an internal Helium-Neon-Argon source were taken throughout each night to provide wavelength calibration and quartz-halogen continuum spectra were taken for use as flat-fields. Each of the spectra was divided by the nightly average flat fields prior to linearizing the wavelength scale. The Kitt Peak mean extinction was applied to all observations. Intercomparison of the standard star spectra showed that the flux calibration was internally consistent to better than 5% in each channel. Systematic differences among the spectra of the standard stars were less than $\pm 6\%$ from 3500 \AA to 6500 \AA wavelength (*i.e.*: gradient errors were $< \pm 2\%$ per 1000 \AA). Slightly larger systematic effects were occasionally seen from 6500 \AA to 7000 \AA ; therefore, this region is not included in the analysis. The flux calibrated spectra for three of the comets are shown in order of increasing heliocentric distance in Figure 6-1. The degree of success of the sky subtraction of the IIDS may be judged from the removal of the night sky line at 5577 \AA . The figure shows a range of cometary spectra

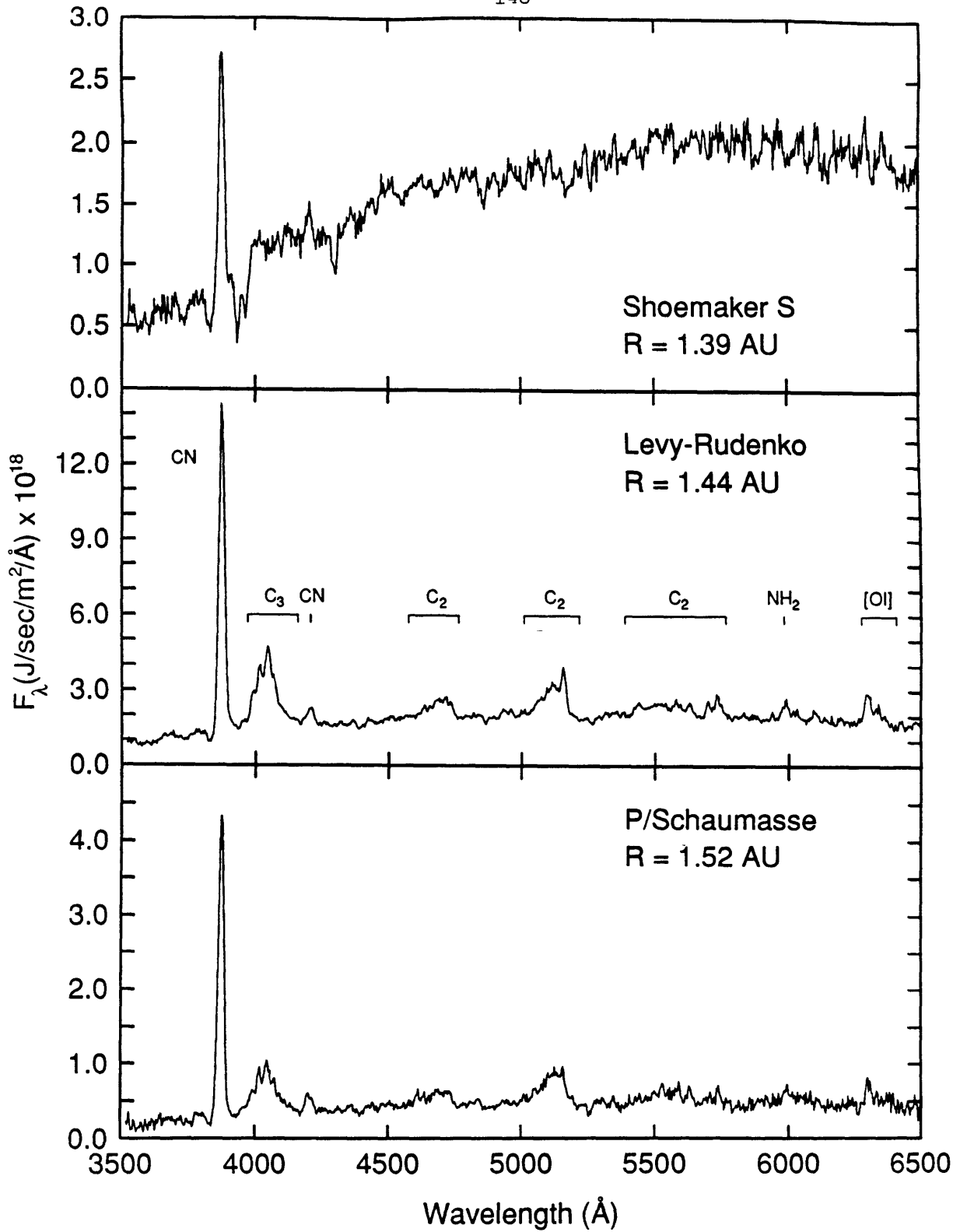


Figure 6-1 Optical spectra of three of the comets observed with the IIDS. The sky subtracted flux density F_λ ($\text{J s}^{-1} \text{m}^{-2} \text{\AA}^{-1}$) within a circular diaphragm of 8.4 arcsec diameter is plotted versus the wavelength λ (\AA) for each comet. No smoothing has been performed on the measured flux densities. Some of the gas emission bands have been identified in the figure.

Table 6-1
Journal of IIDS Observations

Date 1985	Comet	UT [†]	Airmass [‡]	Exp [sec]	Sky chop	R [AU]	Δ [AU]	α [deg]
Feb 16	P/Shoemaker (1984s)	06:20	1.27	1080	EW100	1.39	0.56	36.3
Feb 16	Levy-Rudenko	08:31	1.28	1200	S2160	1.44	0.64	36.2
Feb 16	P/Tsuchinshan-1	10:25	1.14	1800	N1800	1.58	0.62	13.2
Feb 16	P/Schaumasse	12:06	1.40	1200	N1920	1.52	1.18	40.6
Feb 17	P/Arend-Rigaux	03:57	1.27	1800	EW100	1.67	0.72	13.6
Feb 17	P/Gehrels-3	05:53	1.30	1600	EW100	3.46	2.96	15.2
Feb 17	P/Faye	07:20	1.25	2600	EW100	2.62	1.67	8.0
Feb 17	P/Wolf-Harrington	08:30	1.67	2000	EW100	2.13	1.23	14.8
Feb 17	P/Smirnova-Chernykh	11:57	1.64	1200	EW100	3.76	3.63	15.2

[†] Universal Time of the middle of the integration.

[‡] Airmass at the midtime.

from emission-band dominated to continuum dominated. Some of the emission features are identified in the figure.

6.3 Analysis

The physical quantity of interest is the scattering efficiency of the solid grains, $Q_s(\lambda)$. For practical reasons, however, the spectra are described in terms of the reflectivity, $S(\lambda)$, which is proportional to $Q_s(\lambda)$ for an optically thin coma. The spectra were used to compute the reflectivity by dividing the comet flux densities at each wavelength by the solar spectrum of Arvesen *et al.* (1969), which was smoothed by a Gaussian of FWHM equal to the spectrograph resolution. The color of the dust is related to the slope of the continuum

reflectivity. Therefore, only those regions determined to be free from gaseous emission bands were used in this analysis. The wavelength intervals (or continuum windows) 3520-3700 Å, 4390-4450 Å, 5760-5820 Å, 6150-6200 Å and 6380-6500 Å were determined to be free of molecular bands in each of the comet spectra (by inspection). The reflectivities within these continuum windows are plotted in Figure 6-2 for the spectra shown in Figure 6-1. The plotted reflectivities are normalized to the mean of the reflectivities in the wavelength range $5760 < \lambda [\text{Å}] < 5820$. Figure 6-2 shows that the reflectivities of the comets increase with increasing wavelength, indicating that the cometary grains are red.

In order to easily compare the spectra, which have very different brightnesses, a normalized reflectivity gradient between wavelengths λ_1 and λ_2 was defined in Jewitt and Meech (1986) as a convenient measure of the grain color:

$$S'(\lambda_1, \lambda_2) = \frac{[dS / d\lambda]}{S_{\text{mean}}} \quad (6.1)$$

in which $dS/d\lambda$ is the rate of change of the reflectivity with respect to wavelength in the interval λ_1 to λ_2 , and S_{mean} is the mean reflectivity in the observed wavelength range:

$$S_{\text{mean}} = N^{-1} \sum S_i(\lambda) \quad (6.2)$$

The $S'(\lambda_1, \lambda_2)$ are expressed in $\% / 10^3 \text{ Å}$. Grain reddening is indicated by $S'(\lambda_1, \lambda_2) > 0$. Least squares fits to the reflectivities in the continuum windows were computed for each of the 9 comets. These values are listed in Table 6-2, and the results of the least squares fits are plotted in Figure 6-2. The formal errors of the least squares fits are small compared with the possible systematic errors ($\pm 2\% / 10^3 \text{ Å}$), in all comets except P/Gehrels 3 and

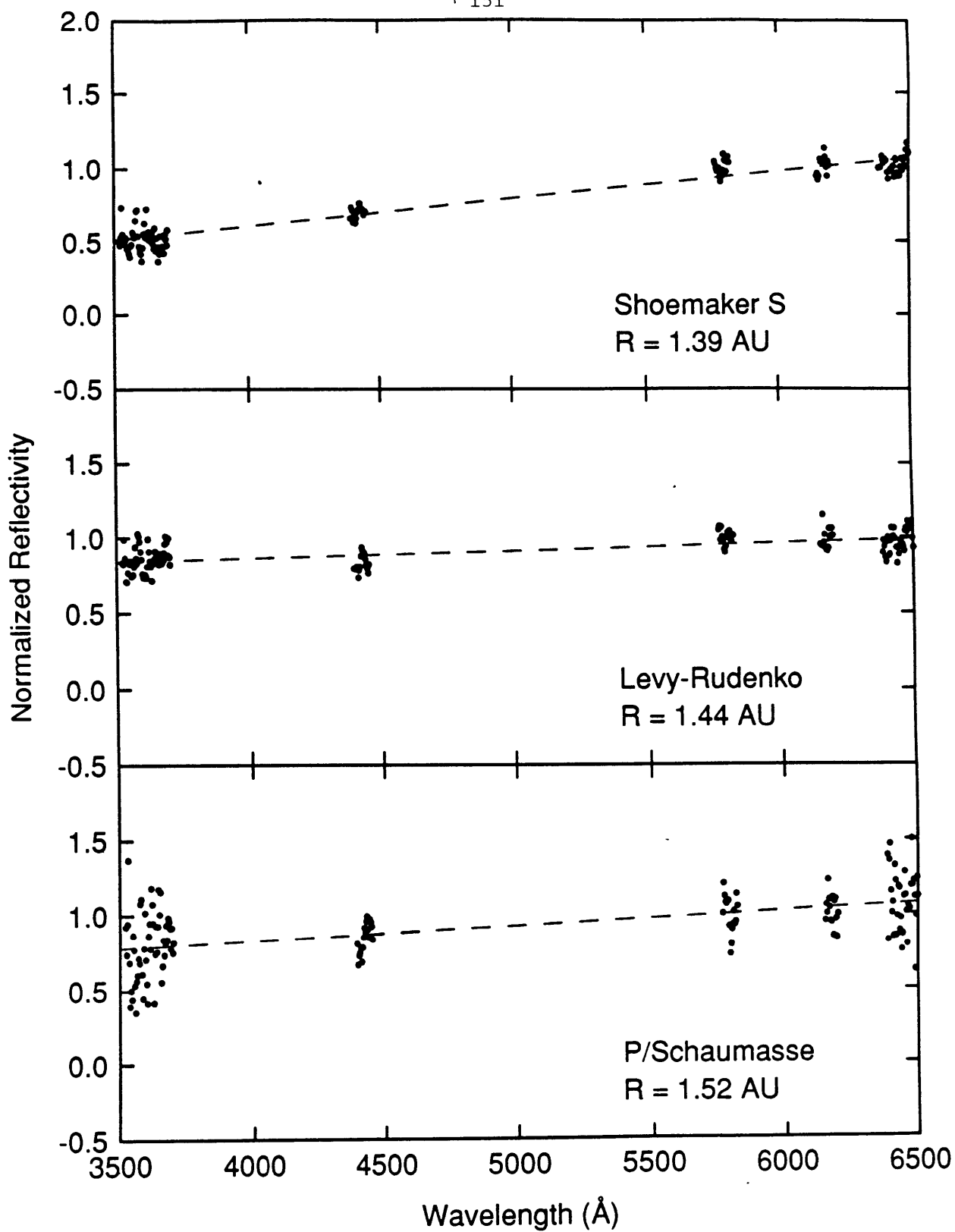


Figure 6-2 Optical reflectivities computed by dividing the spectra from Figure 6-1 by the solar spectrum. The reflectivities are normalized to unity in the continuum interval $5760 < \lambda \text{ (Å)} < 5820$. Only those wavelengths observed to be free of molecular emission bands in all nine comets are plotted in the figure. Dashed lines on each plot are the linear least-squares fits to the normalized reflectivities. The comets are plotted at a fixed scale for comparison.

Table 6-2

Optical Reflectivities

Comet	$S'(\lambda_1, \lambda_2)$ [%/10 ³ Å]	m_{5790}	$m(1,1,0)$
P/Shoemaker 1984S	18 ± 2	15.67	14.14
P/Levy-Rudenko	5 ± 2	15.67	13.92
P/Schaumasse	10 ± 2	17.29	14.56
P/Tsuchinshan-1	7 ± 2	15.91	14.92
P/Arend-Rigaux	14 ± 2	15.84	14.52
P/Wolf-Harrington	16 ± 2	16.45	13.98
P/Faye	14 ± 2	16.94	13.97
P/Gehrels-3	11 ± 6	19.07	14.60
P/Smirnova-Chernykh	16 ± 3	17.59	12.71
P/Halley [†]	9 ± 2	11.06	10.34

[†] Measurement from Chapter 4.

P/Smirnova-Chernykh. The optical normalized reflectivity gradients of the 9 comets vary from (5 ± 2) to (18 ± 2) %/10³ Å. Also listed in Table 6-2 is the brightness in the continuum window centered between $5760 \leq \lambda [\text{Å}] \leq 5820$ as computed from:

$$m_{5790} = -2.5 \log (F_{\lambda}) - 28.58 \quad (6.3)$$

where the constant was chosen such that the m_{5790} magnitudes are approximately equal to the V magnitude. The table also lists the brightness corrected to unit R and Δ , assuming a linear phase coefficient of $\beta = 0.04 \text{ mag deg}^{-1}$:

$$m(1,1,0) = m_{5790} - 2.5 \log (R^2 \Delta) - \beta \alpha . \quad (6.4)$$

6.4 Scattering as a Function of Wavelength

In order to obtain useful physical information about the physical nature of the scattering grains, it is necessary to look at the normalized reflectivity gradient as a function of wavelength since the scattering depends on both the particle size and the wavelength. As discussed in Jewitt and Meech (1986), the normalized reflectivity gradients in the near infrared may be computed from broadband photometry. The justification for using the broadband measurements is discussed in Jewitt and Meech (1986) where a comparison is made between the reflectivities computed using broadband photometry and near infrared CVF spectra. The normalized reflectivity gradients, $S'(\lambda_1, \lambda_2)$ [% / 10^3 \AA], in the J-H and H-K near infrared wavelength intervals were computed using:

$$S'(\lambda_1, \lambda_2) = (20 / \Delta\lambda) \frac{10^{0.4\Delta m} - 1}{10^{0.4\Delta m} + 1} \quad (6.5)$$

in which Δm equals the comet color minus the solar color (both in magnitudes), and $\Delta\lambda = \lambda_2 - \lambda_1$, the difference in the effective wavelengths of the broadband JHK filter pairs, measured in microns. Eq. 6.5 is derived under the approximation that the reflectivity is a linear function of λ in the infrared.

The normalized reflectivity gradients in the optical, combined with those in the near-infrared as presented in Jewitt and Meech (1986), are shown in Figure 6-3. Each horizontal line segment represents one comet reflectivity, where the endpoints of the line indicates the bandpass used. The circles (with 1 sigma error bars) indicate the mean value for each wavelength region. The scatter among the $S'(\lambda_1, \lambda_2)$ is much larger than the typical uncertainties, and is indicative that there are real differences between the grain populations in different comets. As shown in Jewitt and Meech (1986), these differences do not appear to be

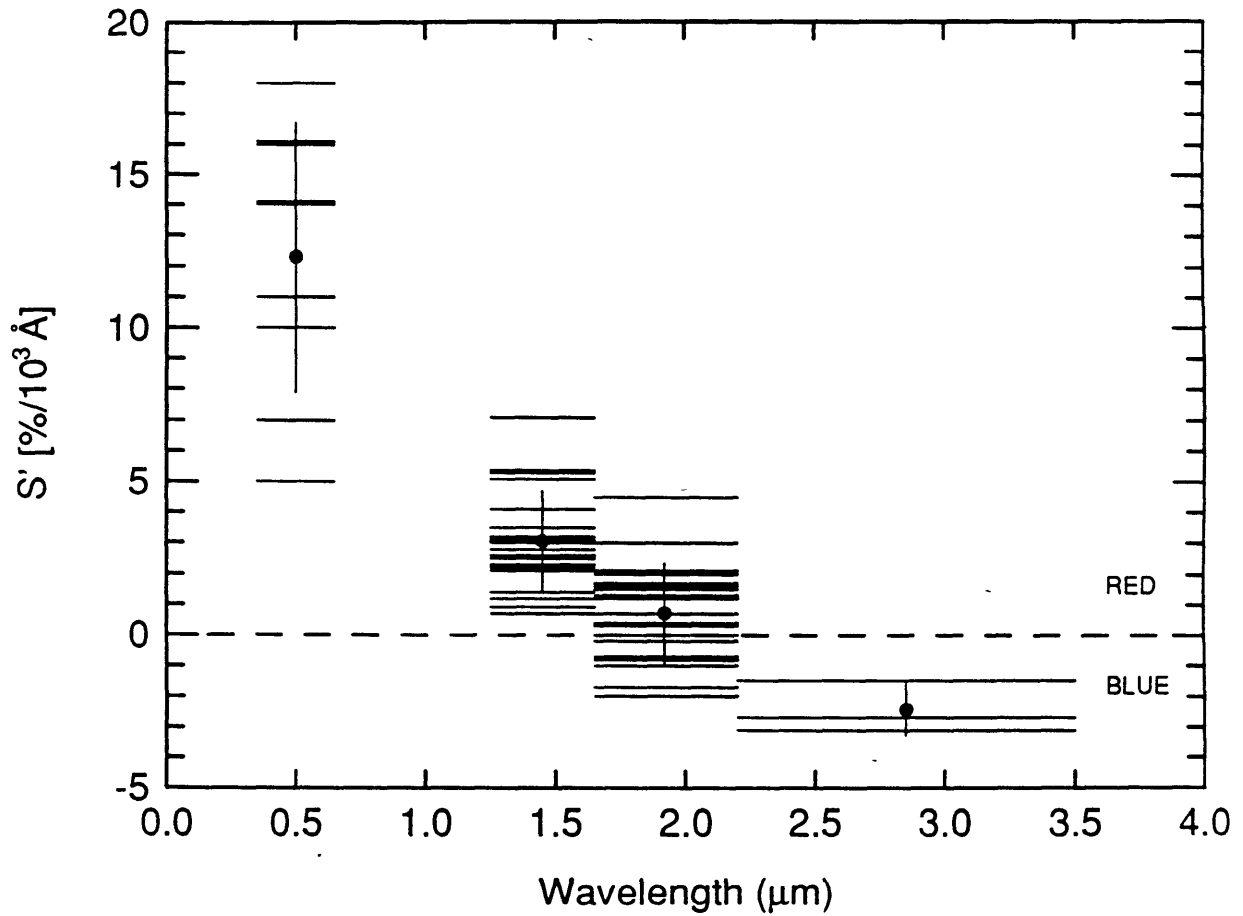


Figure 6-3 The normalized reflectivity gradient, $S'(\lambda_1, \lambda_2)$, measured in $\%/10^3 \text{ \AA}$, is shown as a function of the wavelength of observation λ (in μm). Each comet is represented by a horizontal bar connecting the end point wavelengths λ_1 and λ_2 . Neutral scattering is indicated by the dashed horizontal line at $S'(\lambda_1, \lambda_2) = 0$. Reddening of the scattered radiation is indicated by $S' > 0$ while enhanced blue scattering is indicated by $S' < 0$. The mean S' within each measured wavelength interval is plotted with a black dot and the 1σ standard deviation on the mean is shown with a vertical line. The figure shows that the color of the scattered radiation varies systematically with the wavelength of observation.

correlated with cometary brightness, heliocentric distance or phase angle. It is quite clear from this figure that the reflectivity gradient decreases as a function of increasing wavelength. The horizontal dashed line at zero represents neutral scattering. The mean values of the reflectivity gradients for each wavelength region (from Jewitt and Meech, 1986) are presented in Table 6-3 below. The first entry in the table is from Feldman and A'Hearn (1985); this seems to continue the trend into the UV which is seen in the optical and near IR.

λ_1	λ_2	$S'(\lambda_1, \lambda_2)$	$\pm \sigma$	# of Comets
0.26	0.31	≈ 45	---	5
0.35	0.65	13	5	9
1.25	1.65	3.2	1.6	19
1.65	2.20	0.5	1.3	18
2.20	3.50	< -2.4	0.7	3

As seen in Figure 6-3, for $\lambda > 2 \mu\text{m}$, the scattered radiation is blue. Blue, or Rayleigh scattering occurs when the particles are much smaller than the wavelength of radiation. This suggests that the mean particle sizes for the comets in the figure is near $2 \mu\text{m}$. A simple argument concerning the interference between a tangential ray and a ray passing through the center of a non-opaque homogeneous sphere (Van de Hulst, 1957) illustrates this. For a sphere of radius a , the number of wavelengths contained in a distance $2a$ is $N_r = 2a / \lambda$ for the tangential ray and $N_c = 2a / (\lambda n_r)$ for a ray passing through the center, where n_r is the real index of refraction. The phase difference between the two rays will be $\Delta\phi = 2\pi \Delta N = 2\pi X(n_r - 1)$, where $X = 2\pi a / \lambda$ is the size parameter. Constructive interference occurs if $\Delta\phi = 2\pi m$; the largest maximum is when $m = 1$, when $X_{max} = \pi / (n_r - 1)$. Grains small

compared to a wavelength have $X \ll X_{max}$, and satisfy the Rayleigh approximation $Q_s = k X^4 \propto \lambda^{-4}$, so that the scattered radiation is relatively blue. For larger grains satisfying $X > X_{max}$, the scattering efficiency falls from the maximum asymptotically towards the large-particle limit ($Q_s = 1$) and scattered radiation in this regime is relatively red. The neutral scattering observed near $\lambda \approx 2 \mu\text{m}$ in comets would result if the grains satisfied $X \approx X_{max}$, or equivalently, $a \approx \lambda / [2(n_r - 1)]$. A typical index of refraction for glassy terrestrial rocks is $n_r = 3/2$ (Pollack *et al.*, 1973), which gives $a \approx \lambda$. Therefore, the approximate particle radius $a \approx 2 \mu\text{m}$ would give a wavelength dependence of the scattering similar to what is observed. Scattering at wavelengths $\lambda < 2 \mu\text{m}$ would correspond to the $X > X_{max}$ regime and could qualitatively account for the reddened optical continua. Scattering at wavelengths $\lambda > 2 \mu\text{m}$, corresponding to $X < X_{max}$, would produce blue continua, as suggested by the available K-L measurements. As discussed in Jewitt and Meech (1986), several other methods (radiation pressure analysis on the trajectories of the particles in comet tails, thermal IR measurements of the emissions from grains, grain phase functions) yield similar results for typical grain sizes.

This simple interpretation of Figure 6-3 has obvious shortcomings. Specifically, there will be a distribution of grain sizes present in the coma, and the particles will have complicated morphologies, much like the Brownlee particles collected from the Earth's upper atmosphere (Brownlee, 1978). Also, no reference is made to the expected angle dependence of the scattered radiation, nor to the wavelength dependence of the complex refractive index. More detailed Mie scattering calculations are presented in Jewitt and Meech (1986) to compute the cross-section weighted mean particle size for many different refractive indices and power-law grain size distributions. Using grain size distributions inferred from the dynamical analysis of the effect of radiation pressure on cometary tails, the resulting mean particle radius computed from Mie theory is near $2.2 \mu\text{m}$.

Recent *in situ* spacecraft observations have allowed direct comparison of the particle size distributions in comae with the results presented here. Micron sized grains were detected in

the coma of P/Giacobini - Zinner by the ICE spacecraft (Gurnett *et al.*, 1986). Measurements from the *Giotto* and *Vega* spacecraft suggest a power-law grain size distribution with an index of ≈ 3.5 (McDonnell *et al.*, 1986; Simpson *et al.*, 1986). Grains were detected with radii as small as 10^{-8} m, however, the cross section weighted mean for the inferred distribution and observed range of particle sizes yields $a_{mean} > 1 \mu\text{m}$, which is consistent with the ground-based continuum reflectivity measurements.

6.5 Conclusions

1. The normalized rate of change of the reflectivity of cometary grains with respect to the wavelength of observation, decreases as the wavelength increases. The continuum color changes progressively from red to neutral as the wavelength increases from the optical ($\lambda \approx 0.5 \mu\text{m}$) into the near infrared ($\lambda > 2 \mu\text{m}$).
2. The observed wavelength dependence of the reflectivity gradient is consistent with an origin by scattering from μm sized or larger, slightly absorbing spheres. Although optically small grains ($a < \lambda$) are undoubtedly present in the comae of the observed comets, the scattering cross section lies in particles which are optically large ($a > \lambda$).

References

- Arvesen, J. C., R. N. Griffin, B. D. Pearson (1969), "Determination of Extraterrestrial Solar Spectral Irradiance from a Research Aircraft", *Appl. Optics* **8**, 2215-2232.
- Brownlee, D. E. (1978), "Microparticle Studies by Sampling Techniques", in *Cosmic Dust*, ed. J. A. M. McDonnell, J. Wiley, NY, 295-336.
- Feldman, P. D., and M. F. A'Hearn (1985), "Ultraviolet Albedo of Cometary Grains", in *Ices in the Solar System*, ed. J. Klinger, F. Benest, A. Dollfus and R. Smoluchowski, D. Reidel Pub. Co., Dordrecht, p. 453-461.
- Gurnett, D. A., T. F. Averkamp, F. L. Scarf and E. Grun (1986), "Dust Particles Detected Near Giacobini-Zinner by the ICE Plasma Wave Instrument", *Geophys. Res. Letters* **13**, 291-294.
- Jewitt, D. and K. J. Meech (1986), "Cometary Grain Scattering Versus Wavelength, or, 'What Color is Comet Dust?' ", *Astrophys. J.* **310**, 937-952.
- McDonnell, J. A. M., W. M. Alexander, W. M. Burton., E. Bussoletti, D. H. Clark, R. J. L. Grard, E. Grün, M. S. Hanner, D. W. Hughes, E. Igenbergs, H. Kuczera, B. A. Lindblad, J. -C. Mandeville, A. Minafra, G. H. Schwehm, Z. Sekanina, M. K. Wallis, J. C. Zarnecki, S. C. Chakaveh, G. C. Evans, S. T. Evans, J. G. Firth, A. N. Littler, L. Massonne, R. E. Olearczyk, G. S. Pankiewicz, T. J. Stevenson and R. F. Turner (1986), "Dust Density and Mass Distribution Near Comet Halley From Giotto Observations", *Nature* **321**, 338-341.
- Newburn, R. L. and H. Spinrad (1985), "Spectrophotometry of Seventeen Comets. II. The Continuum", *Astron. J.* **90**, 2591-2608.
- Oke, J. B. (1974), "Absolute Spectral Energy Distributions for White Dwarfs", *Astrophys. J. Supp.* **27**, 21-35.
- Pollack, J. B., O. B. Toon and B. N. Khare (1973), "Optical Properties of Some Terrestrial Rocks and Glasses", *Icarus* **19**, 372-389.
- Remillard, R. A., and D. C. Jewitt (1985), "A Comparison of the Continuum Spectra of Four Comets", *Icarus* **64**, 27-36.
- Simpson, J. A., R. Z. Sagdeev, A. J. Tuzzolino, M. A. Perkins, L. V. Ksanfomality, D. Rabinowitz, G. A. Lentz, V. V. Afonin, J. Erö, E. Keppler, J. Kosorokov, E. Petrova, L. Szabó and G. Umlauf (1986), "Dust Counter and Mass Analyser (DUCMA) Measurements of Comet Halley's Coma From Vega Spacecraft", *Nature* **321**, 278-280.
- Stone, R. P. S. (1977), "Spectral Energy Distributions of Standard Stars of Intermediate Brightness. II.", *Ap. J.* **218**, 767-769.
- Van de Hulst, H. C. (1957), *Light Scattering by Small Particles*. John Wiley & Sons, New York.

Chapter 7 - Effects of Radiation Pressure on the Coma

7.1 Introduction

One of the implicit assumptions used in the sublimation model in Chapter 1 is that the dust grains flow radially outward in the coma, producing a surface brightness profile which varies as the reciprocal of the projected distance from the center. This morphology has long been an assumption of cometary science, but there has been little attempt at observational verification. In an optically thin coma, the surface brightness is directly related to the number density of grains in the coma, hence it is related to the dynamics within the coma. Not only is the variation of surface brightness as a function of distance from the center important in the understanding of the coma dynamics but the knowledge of its behavior is essential if observations using different sized apertures are to be scaled properly for comparison.

The radial surface brightness profile in an optically thin spherical coma is given by :

$$B(p) = K_1 \int N(r) dl \quad (7.1)$$

where $N(r)$ is the number density of grains as a function of distance from the nucleus, l is the distance along the line of sight through the coma, and K_1 is a constant which depends on the size and scattering efficiency of the grains. The projected distance from the nucleus in the plane of the sky, p , is related to l and r , the radial distance, by $p = (r^2 - l^2)^{1/2}$. If $N(r)$ is known, models of the surface brightness distribution may be calculated from Eq. 7.1. In the case where the grains move at a constant velocity, v , from a nucleus with a constant production rate of dust, integration of Eq. 7.1 gives:

$$B(p) = K_2 / p. \quad (7.2)$$

This derivation of this equation is discussed in some detail in Appendix 4. The restriction that the grains move at a constant velocity is not valid in a small region near the nucleus where the grains, which are dragged into the coma by the sublimating gases, have not yet reached their terminal velocities. However, the terminal velocity of the dust is reached within about 10^4 - 10^5 m from the nucleus (see Appendix 6 for a discussion on the terminal grain velocity in a gas flow). For typical comet observations, say near a geocentric distance $\Delta \approx 1$ AU, the angle subtended by this region is $\theta \approx 0.1$ arcsec. This acceleration zone, X_A , is typically unobservable because of the effects of seeing.

This chapter discusses one of the first systematic studies of the surface brightness profiles of a random sample of comets. The need to obtain accurate coma photometry at surface brightnesses equal to a small fraction of the brightness of the night sky constitutes a formidable observational challenge, and is no doubt partly responsible for the dearth of published profile measurements. Linear two dimensional photometers, of a kind available only in the last decade, are virtually a prerequisite for this work. A simple radial outflow model for the dust modified by the effects of radiation pressure will be shown to accurately model most of the comets in the study. The work presented in this chapter is a brief summary of Jewitt and Meech (1987).

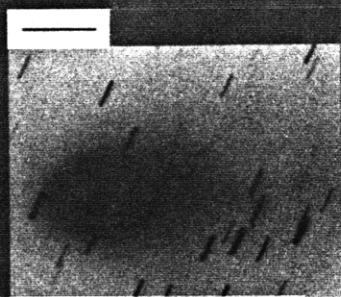
7.2 *Observations*

The present observations were taken using the 4m and 2.1m telescopes at Kitt Peak National Observatory. In September 1985, the 4m was used with an 800 x 800 pixel Texas Instruments CCD (TI #2) at the f/2.6 prime focus. The image scale was 0.29 arcsec per 15 μm pixel, giving a field of view 230 arcsec on a side. In March 1986, the 2.1m was used

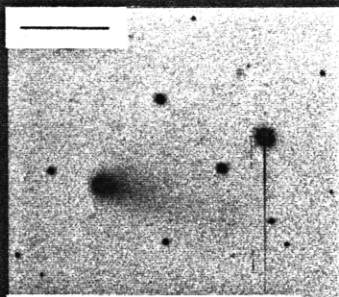
with a similar CCD of the same specifications (TI #3) placed at the $f/7.7$ Cassegrainian focus. The 2.1m image scale was 0.38 arcsec per 30 μm pixel and the field of view was 150 arcsec on a side. Both chips had a root mean square readout noise of about 18 electrons. Sensitivity variations among the pixels on each CCD were removed using flat field exposures taken each night on the illuminated interior of the observatory dome. The reduced images were photometrically calibrated using standard stars from the lists by Oke and Gunn (1983) and Christian *et al.* (1985).

Images of comets P/Halley, P/Giclas, P/Maury, P/Whipple, P/Gunn, P/Giacobini-Zinner, P/Shoemaker 3, P/Kojima, P/Daniel and P/Gehrels 3 were obtained. These comets were all small in comparison with the field of view, so that the instantaneous brightness of the night sky could be determined from the individual CCD images. A journal of observations is presented in Table 7-1. The seeing on each night was 1–1.5 arcsec FWHM at the 4m and 2–2.5 arcsec FWHM at the 2.1m. The telescopes were autoguided on field stars and differentially tracked at cometary rates during each integration; however, neither of the telescopes were able to consistently reproduce the motions of the comets to better than ≈ 1 arcsec. Consequently, the innermost regions of each comet ($p < 3$ arcsec) are affected by image smear as well as by seeing. The two comets known (from spectroscopy) to possess significant gaseous emission (P/Giacobini-Zinner and P/Halley) were imaged using a narrow band continuum filter centered at $\lambda_{cent} = 7007 \text{ \AA}$ ($\Delta\lambda = 89 \text{ \AA}$ FWHM). The remaining comets were imaged through the Mould R ($\lambda = 6500 \text{ \AA}$, $\Delta\lambda = 1280 \text{ \AA}$) filter. Comets P/Maury, P/Giclas, P/Daniel, P/Gehrels 3 and P/Gunn were also imaged in the Mould V ($\lambda = 5460 \text{ \AA}$, $\Delta\lambda = 870 \text{ \AA}$) filter. The V and R filter profiles were found to be identical within the uncertainties of measurement (consistent with the continuum nature of these comets). CCD images of each of the ten comets are presented in Figure 7-1. The comets are arranged in order of increasing R in the figure. The scale bars indicate 30 arcsec in the plane of the sky.

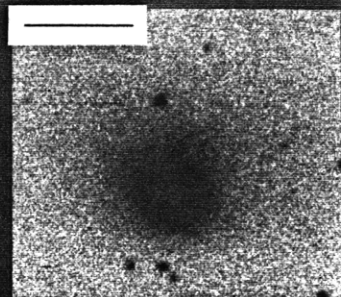
Figure 7-1 CCD images of ten comets arranged in order of increasing R . All of the images were taken through the Mould R filter except for P/Giacobini-Zinner and P/Halley which were imaged through continuum filters. The scale bars represent 30 arcseconds on the plane of the sky. North is to the top and East to the left in these images. See Table 7-1 for details concerning each image.



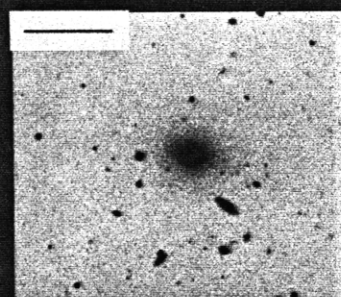
P/Giacobini-Zinner



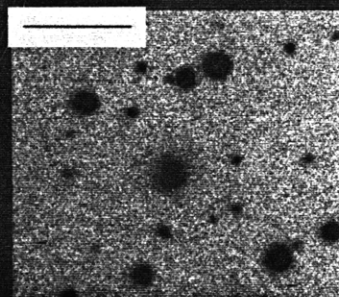
P/Giclas



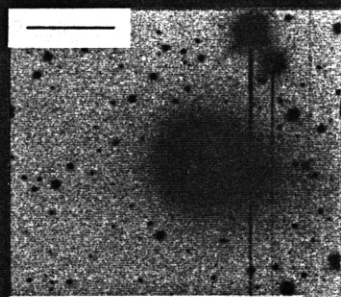
P/Shoemaker 3



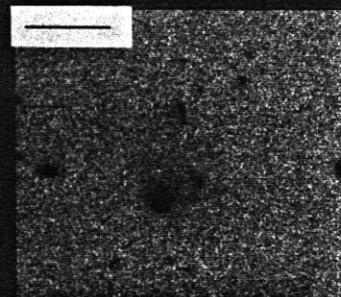
P/Maury



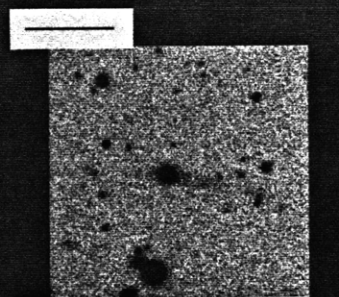
P/Kojima



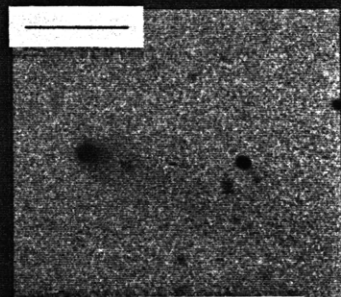
P/Halley



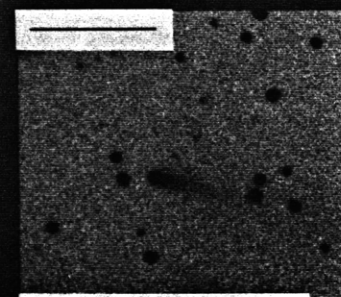
P/Daniel



P/Whipple



P/Gehrels 3



P/Gunn

Table 7-1

Journal of Profile Observations

Comet	Date	UT [†]	Tel [§] [m]	Filter	Airmass	Exp [sec]	R [AU]	Δ [AU]	θ [deg]	Scale [m arcsec ⁻¹]
<i>1985</i>										
P/Halley	9/21	10:04	4	7005 Å	1.54	100	2.47	2.35	23.9	1.71×10^6
P/Giclas	9/21	10:17	4	R	1.13	15	1.84	1.04	25.5	7.56×10^5
P/Maury	9/22	05:10	4	R	1.29	150	2.21	1.31	14.6	9.53×10^5
P/Whipple	9/22	07:14	4	R	1.69	150	3.36	2.52	10.9	1.83×10^6
P/Gunn	9/22	10:09	4	R	1.21	120	4.64	4.37	12.4	3.18×10^6
P/Giacobini-Zinner	9/23	12:20	4	7005 Å	1.18	30	1.06	0.51	69.6	3.71×10^5
<i>1986</i>										
P/Shoemaker 3	3/05	05:32	2.1	R	1.02	600	1.98	1.05	14.0	7.64×10^5
P/Kojima	3/05	06:13	2.1	R	1.11	450	2.42	1.65	17.9	1.20×10^6
P/Daniel	3/06	08:25	2.1	R	1.01	300	2.55	1.66	12.0	1.21×10^6
P/Gehrels 3	3/06	10:31	2.1	R	1.71	300	3.58	2.59	2.6	1.88×10^6

[†] UT of the middle of the integration.

[§] Telescope diameter in meters.

Radial surface brightness profiles were computed by averaging the coma signal within concentric annuli about each photometric center. The averaging algorithm took proper account of those pixels which straddled the boundaries between annuli. Bad pixel values were replaced by the average of the signals in adjacent pixels. Uncertainties in the coma profiles were dominated by the uncertainty in the brightness of the night sky. Statistical uncertainties in the local sky level were typically of order 0.1%, on scales of a few tens of pixels on the CCD. However, on scales of a few hundred pixels (comparable to the projected dimensions of the larger comets), the sky level was observed to vary with a considerably larger range, probably resulting from small differences between the flat field and the sky illumination.

Images of stellar fields showed that the detector response was independent of position on the CCD to better than 1% peak to peak over the full width of the chip. Also, measurements of the sky brightness at different positions around each comet were consistent to better than 0.6% peak to peak in every case. Therefore the 1σ sky brightness uncertainty was estimated as $\pm 1\%$ of the mean sky brightness. This is probably an overestimate of the sky uncertainty around the smaller comets. In Figure 7-2 the surface brightness in magnitudes arcsec⁻² is plotted versus the log of the projected distance from the center ($\log[p]$) for 4 of the comets in Figure 7-1. On a log-log scale such as in the figure, the surface brightness profile corresponding to the canonical radial outflow model described in the introduction would have a slope of $m = -1$. The logarithmic gradient :

$$m \equiv \frac{d \ln[B(p)]}{d \ln[p]} \quad (7.3)$$

is therefore a convenient way to parameterize the curves.

The surface brightness units are R filter magnitudes arcsec⁻², except for comets P/Halley and P/Giacobini - Zinner, for which the magnitudes are in the AB₇₉ system of Oke and Gunn (1983). Practically, AB₇₉ \approx V for an object with a flat spectrum. The brightness of the night sky near each comet is indicated in the figure by a horizontal bar on the right hand axis. The error bars in the figure illustrate the effect on the profiles of changing the adopted sky brightness by $\pm 1\%$. The plotted errors are thus systematic in nature; the statistical errors in each profile may be estimated from the local scatter of the individual measurements. Diagonal lines in the lower left of each panel of Figure 7-2 indicate gradients $m = -1$ and $m = -3/2$ for visual reference.

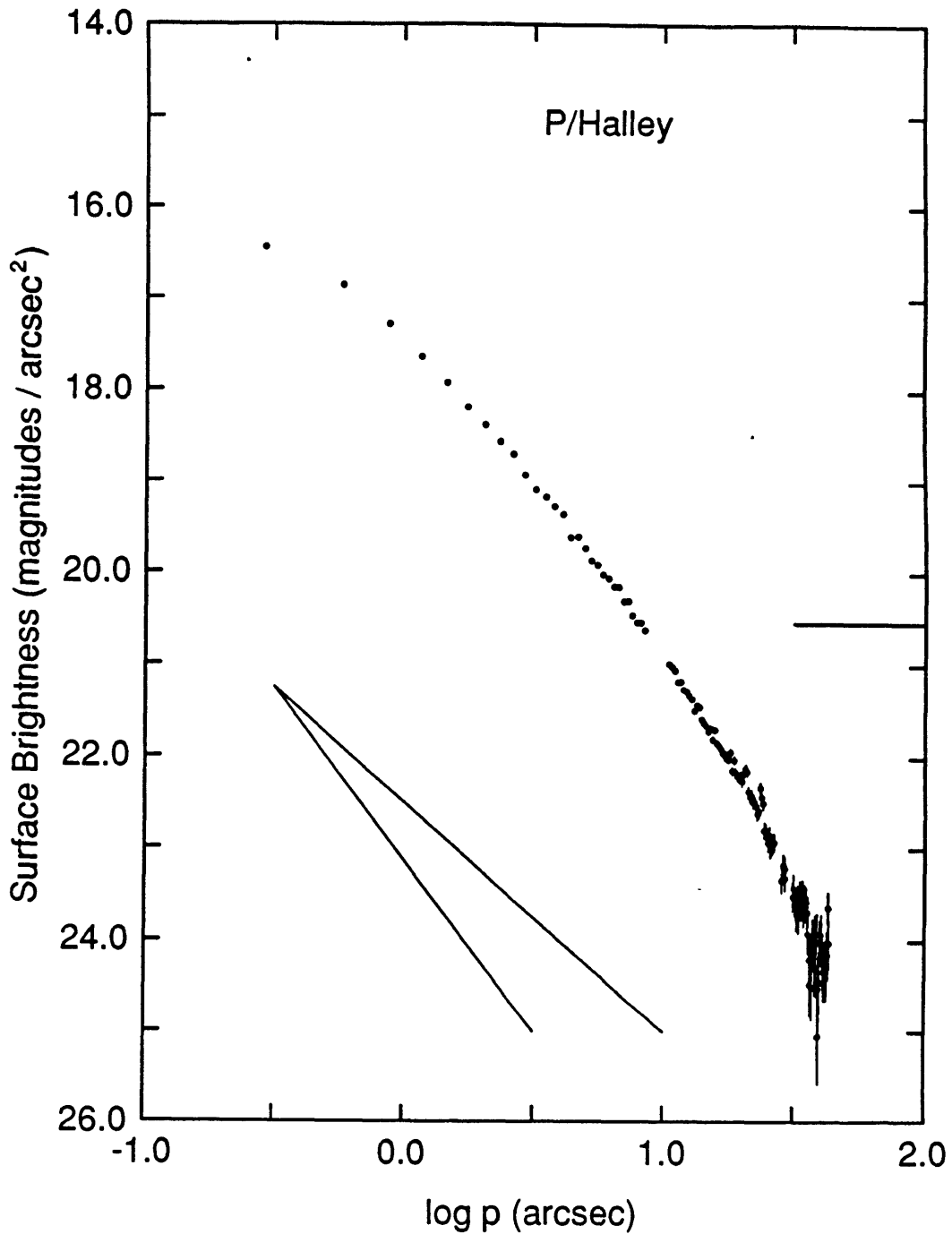


Figure 7-2 The continuum surface brightness profiles of four comets. The surface brightness (in R filter magnitudes per square arcsecond) is plotted versus the logarithm of the radius (in arcseconds) of the center of the annulus within which the surface brightness was determined. The brightness of the night sky is marked in each panel by a short horizontal bar on the right hand axis. Diagonal lines in the lower left of each plot indicate gradients $m = -1$ and $m = -3/2$. Continuous lines drawn through the data represent radiation pressure models computed according to the procedures described in the text. Error bars illustrate the *systematic* uncertainty in each profile which would be caused by a $\pm 1\%$ error in the determination of the surface brightness of the night sky.

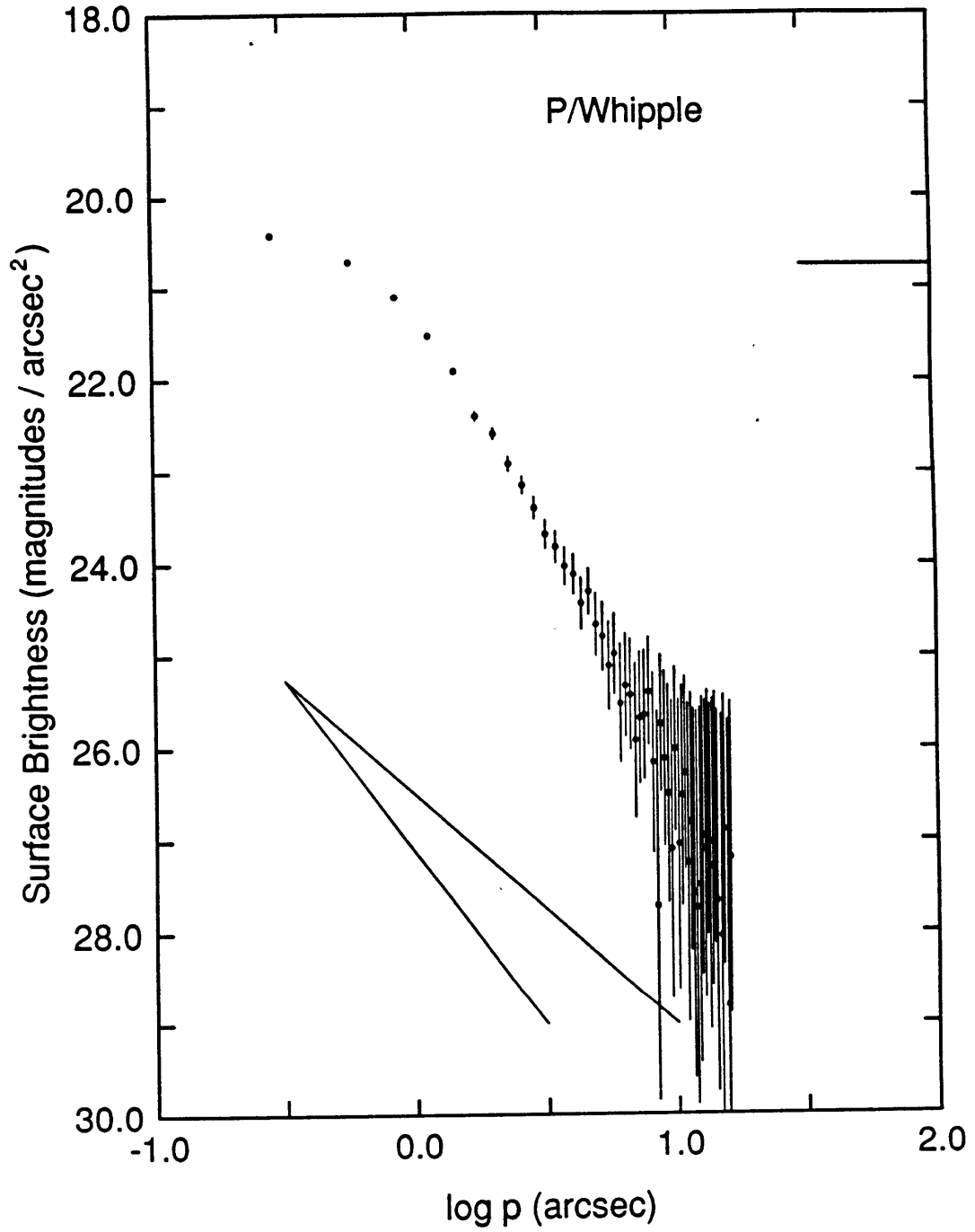


Figure 7-2 (continued). See the caption for P/Halley.

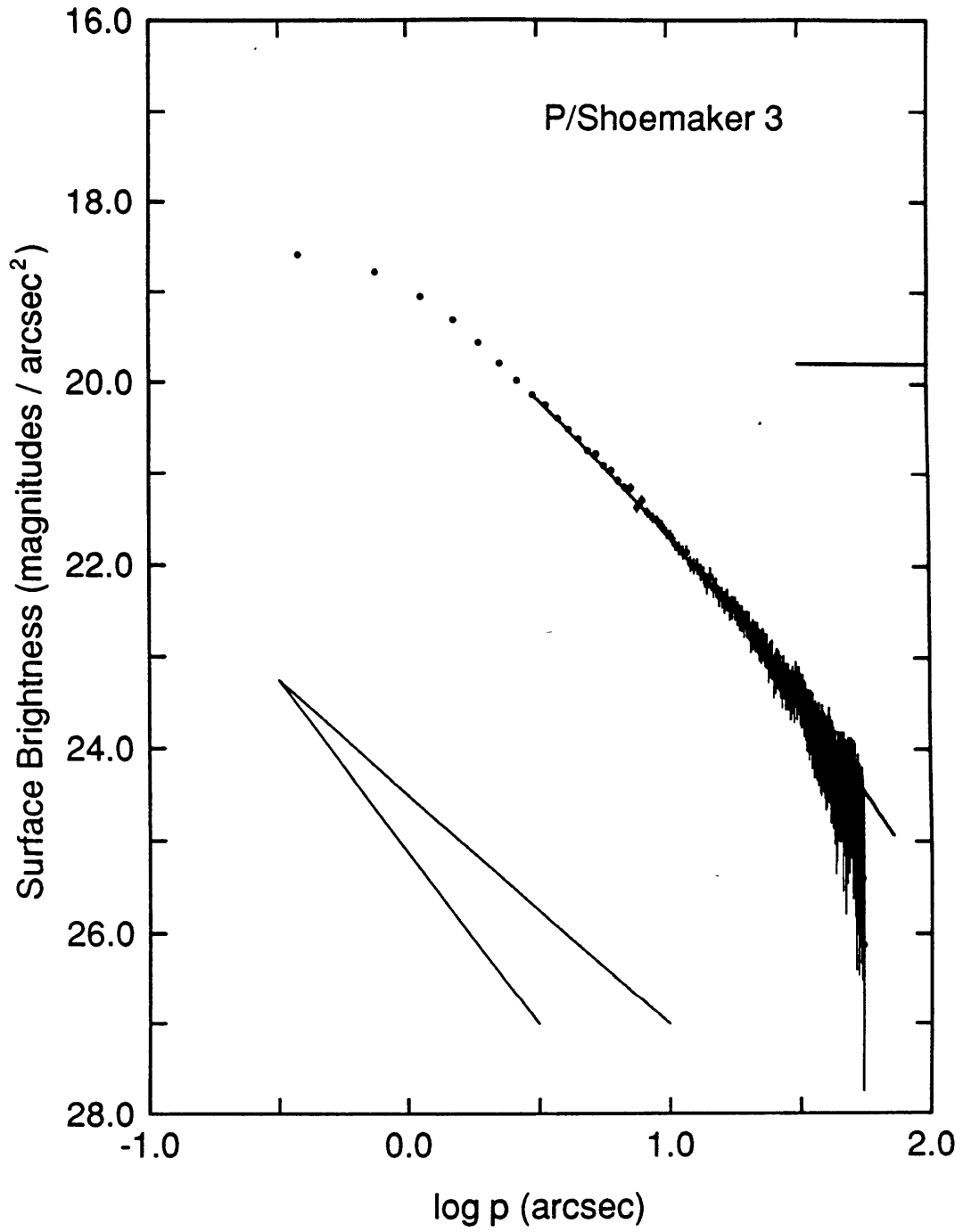


Figure 7-2 (continued). See the caption for P/Halley.

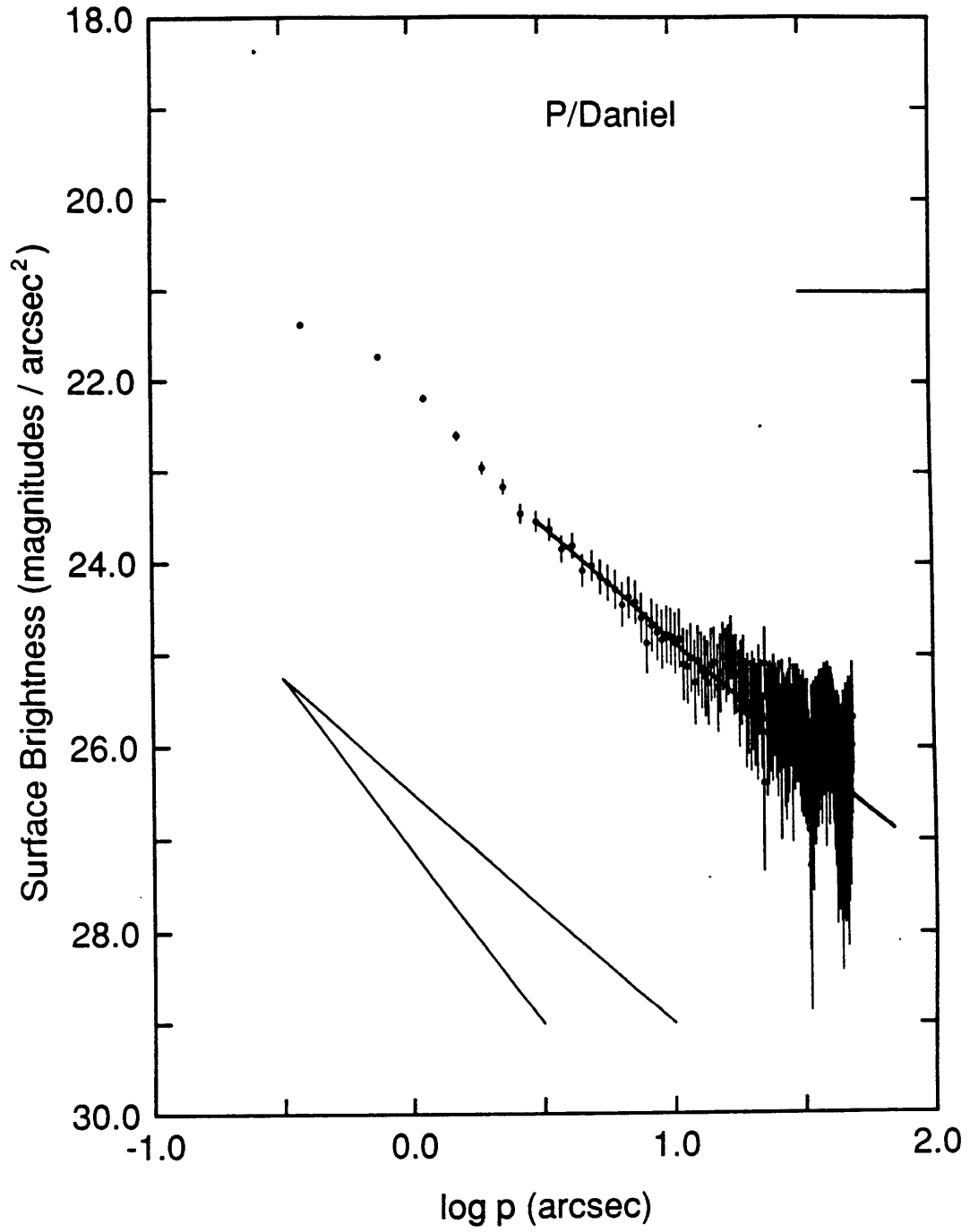


Figure 7-2 (continued). See the caption for P/Halley.

7.3 Interpretation and Discussion

Of the 10 comets observed, only three have profiles with the expected $m = -1$ slope (P/Maury, P/Gunn and P/Daniel), all of the others have steeper slopes. It is to be expected that at some point the profile will become steep because of the effects of radiation pressure which will accelerate particles moving originally in the sunward direction into the tail. The distance, X_R , at which this occurs will be:

$$X_R = \frac{v_{gr}^2}{2 \beta g_O} \quad (7.4)$$

where v_{gr} is the terminal grain velocity and β is the ratio of the radiation pressure acceleration to the solar gravitational acceleration, g_O , at a distance R from the sun as discussed in Appendix 5. The parameter $\beta \propto Q_{pr} / \rho a$ where a is the particle size, ρ is the particle density and Q_{pr} is the radiation pressure scattering efficiency. For distances $X_A < p < X_R$ both gas drag and radiation pressure effects should be minimal and the comae should follow the expected $m = -1$ profile. The value of X_R can yield information about the value β , if the particle velocities can be estimated.

The empirical Bobrovnikoff/Delsemme law ($v_B = 600 R^{-0.5}$, Delsemme, 1982) is often used to provide a reasonable approximation to the grain terminal speed (*i.e.* $v_{gr} \approx v_B$), since the optically dominant micron-sized grains should be well coupled to the gas, at least near $R \approx 1$ AU. The coma of a comet at $R = 1$ AU, containing grains with $\beta \approx 1$ would have a length scale $X_R \approx 3 \times 10^7$ m. Viewed from geocentric distance $\Delta = 1$ AU, this length subtends 40 arcsec, and so is comparable to the dimensions of the observed comets. On scales $p \gg X_R$ the coma becomes highly distorted by radiation pressure and is traditionally called the type II (dust) tail. The shape and orientation of the tail may be used in syndyne/synchrone analyses

to constrain the characteristics of the tail grains and their source, however this will not be discussed in this chapter.

A Monte Carlo computer program is described in Jewitt and Meech (1987) which was written to calculate surface brightness profiles of cometary comae by accounting for solar radiation pressure and for various adopted nucleus steady state source functions. The profiles computed from the radiation pressure model depend on the length X_R and on the phase angle α . The effects of grain size distributions were simulated by summing the models over broad distributions in X_R . The effect of the radiation pressure on the models is seen in Figure 7-3, which is a plot of the model surface brightness versus projected distance from the nucleus. The different curves in the figure represent models for different values of X_R . When $X_R = \infty$, there is effectively no radiation pressure acting on the coma, and the $m = -1$ slope is seen. As the radiation pressure effect increases, X_R decreases and there is a slope change or "knee" in the curves. In the limit that all grains are immediately accelerated into the tail, m approaches $-3/2$. These profiles cannot be interpreted, however, without knowledge of the phase angle. The effect of changing the phase angle for a model at fixed X_R (here, 20 arcsec at $R=\Delta=1$ AU) is seen in Figure 7-4. At $\alpha = 0^\circ$, radiation pressure acts parallel to the line of sight, and the profile gives $m = -1$. At $\alpha = 90^\circ$, the knee gives the value of the angle subtended by X_R .

Profiles of the model comae are plotted in Figure 7-2 as solid lines passing through the data. The data for all comets are well fit by the models, with the exception of P/Halley, P/Giacobini-Zinner and P/Whipple, which are too steep to be fit. The best fitting parameters are presented in Table 7-2 (from Jewitt & Meech, 1987). The table lists values of X_R and v_{gr}^2 / β for each comet to which a fit is possible (comet P/Gunn is omitted from the table since its uncertain profile does not strongly constrain X_R). The Bobrovnikoff velocity for the distance of each comet, v_B , and $v_I = (v_{gr}^2 / \beta)^{1/2}$ are also listed. Studies of the tails of comets (Saito *et al.*, 1985) indicate that in general $\beta < 1$ for most comets; therefore v_I is an upper limit to the coma grain velocity.

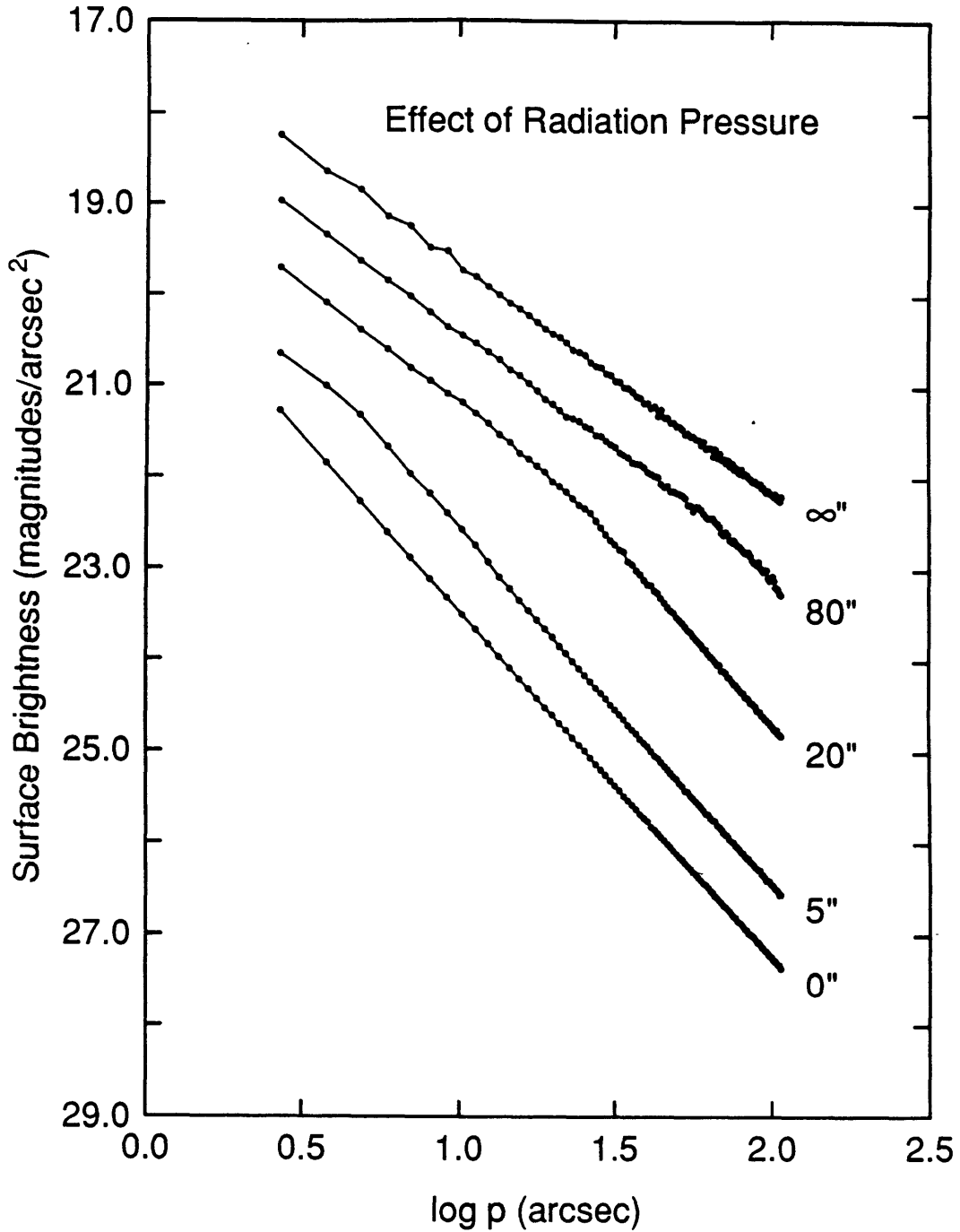


Figure 7-3 Sample surface brightness profiles of Monte Carlo model comae (from Jewitt & Meech, 1987) are shown as a function of the dimension X_R (expressed in arcseconds). The parameter provides a measure of the importance of radiation pressure to the shape of the coma. Successive profiles have been vertically offset for clarity and the zero point of the vertical axis was arbitrarily chosen. The models have 1 arcsec resolution and refer to a comet at $R = \Delta = 1$ AU viewed from phase angle $\alpha = 90^\circ$. Calculated points are shown by dots, while connecting lines have been added for clarity. Note that the gradient $m \rightarrow -1$ as $X_R \rightarrow \infty$ and $m \rightarrow -1.5$ as $X_R \rightarrow 0$.

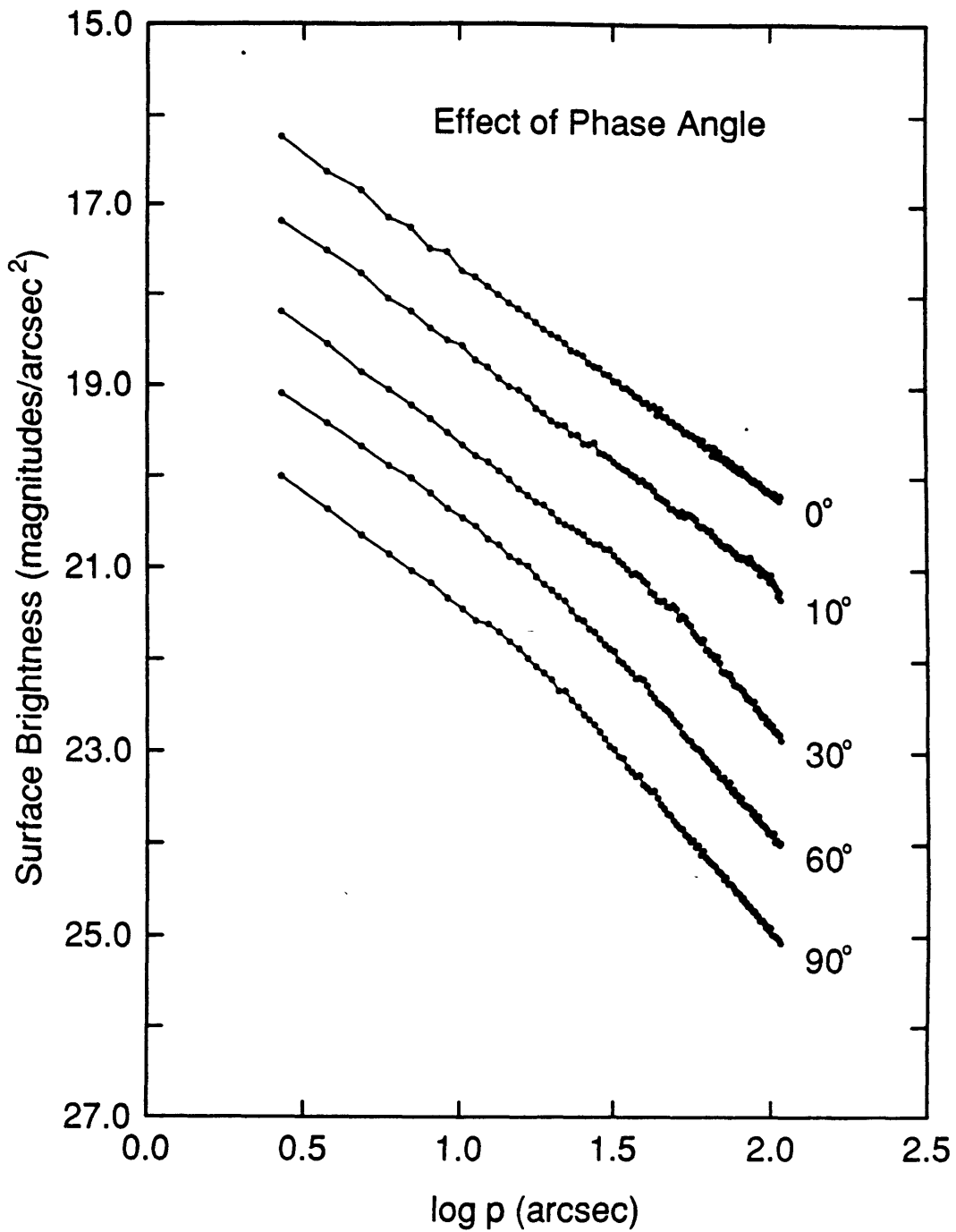


Figure 7-4 The surface brightness profile of a particular Monte Carlo model coma (from Jewitt & Meech, 1987) as a function of the phase angle, α . Successive profiles have been vertically offset for clarity and the zero point of the vertical axis was arbitrarily chosen. The calculations refer to a comet at $R = \Delta = 1$ AU, with $X_R = 1.5 \times 10^7$ m (corresponding to 20 arcsec). Profiles computed for other values of X_R show a qualitatively similar dependence on the phase angle.

Comet	X_R [m]	v_{gr}^2 / β [m ² s ⁻²]	v_B [ms ⁻¹]	v_1 [ms ⁻¹]
P/Giclas	$< 1.6 \times 10^6$	$< 5.6 \times 10^3$	440	< 75
P/Shoemaker 3	$(7.4 - 15) \times 10^6$	$(2.2 - 4.5) \times 10^4$	430	150 - 210
P/Maury	$> 2.3 \times 10^6$	$> 5.6 \times 10^3$	400	> 75
P/Kojima	$< 1.4 \times 10^6$	$< 2.8 \times 10^3$	385	< 50
P/Daniel	$> 3.1 \times 10^6$	$> 5.6 \times 10^3$	375	> 75
P/Gehrels 3	$< 2.4 \times 10^7$	$< 2.3 \times 10^4$	320	< 150

The Bobrovnikoff velocities are inferred from visual observations of expanding halos and probably refer to the gas. The fact that the values of v_1 in Table 7-2 are all $< v_B$ implies that the dust is not well coupled to the gas.

There are several possible reason for the failure of the models to fit three of the comets (P/Halley, P/Giacobini-Zinner and P/Whipple). One assumption of the model is that the coma has a constant source function, *i.e.* the coma is in steady state. In the case of P/Halley, this is certainly not always the case. Images taken in March 1986 (see Figure 8-4a) show dramatic night to night changes, which imply changes on a shorter timescale. The *Giotto* spacecraft images, too, showed that much of the activity was confined to jets of material leaving the nucleus (*e.g.* Keller *et al.*, 1986). Variations in the source function should produce ripples in the coma, provided the timescale for change is of the order $\tau \approx v_{gr} / (\beta g_O)$. Variations on much shorter or longer timescales would produce ripples either too small or too large to be discerned from the profile. It is very likely that the radiation pressure models fail to match the profile of P/Halley simply because the assumption of steady state is violated. However, lacking profiles as a function of time, this hypothesis cannot be verified.

Another assumption implicit in the model is that the grains do not change their scattering properties as a function of distance from the nucleus. A possible mechanism for changing the scattering properties has been developed by Delsemme and Miller (1971) who proposed that icy grains escape from the nucleus and form a halo. The grains subsequently sublimate as they travel outward from the nucleus, causing a rapid drop in the surface brightness of the coma. This idea has been pursued by several investigators. Jewitt *et al.* (1982) observed the profiles of three comets and found that the icy halo model represented the observations for only two of the comets. More recently, from the study of several surface brightness profiles, Baum and Kreidl (1984, 1986) and Baum *et al.* (1986) have come to the conclusion that because the surface brightness falls off more rapidly than the expected $1/p$, the grains in the comae must be fading due to sublimation of ice. Whereas the existence of icy grains in cometary comae is certainly expected, the results of Baum *et al.* (1986) and Baum and Kreidl (1984, 1986) do *not* prove the existence of ice grains as they claim. They do not take account of the effects of radiation pressure which is certainly present (as evidenced by the existence of dust tails), nor do they model the effect of the viewing geometry (specifically the phase angle). Both of these factors greatly influence the shape of the profile as seen in the figures above from Jewitt and Meech (1987). Additionally, as shown by Hanner (1981), the maximum distances reached by dirty water ice grains near $R = 1$ AU are of order $10^4 - 10^5$ m, whereas as seen from Table 7-1 and Figure 7-1 this scale length is not resolvable due to the effects of seeing.

It therefore seems likely that until time series observations of cometary surface brightness profiles are obtained (to determine source function variability), combined with models which correctly account for the effects of radiation pressure and viewing geometry, the existence of icy grains cannot be proven from surface brightness observations.

7.4 Conclusions

1. The continuum radial surface brightness profiles of ten comets have been measured from charge coupled device images, with surface photometry accurate to about 1% of the brightness of the night sky. Except in a limited central region, a majority of the coma profiles are steeper than the canonical $m = -1$ profile anticipated from a symmetric, steady state coma source.
2. Seven of the ten measured comets (P/Giclas, P/Shoemaker 3, P/Maury, P/Kojima, P/Daniel, PGehrels 3, and P/Gunn) show profiles which are consistent with simple models which account for the effects of solar radiation pressure (profiles of P/Maury, P/Daniel and P/Gunn are also consistent with the absence of radiation pressure, within the uncertainties of measurement). The photometric gradients decrease from $m = -1$ for $p < X_R$ to $m = -3/2$ for $p > X_R$, where X_R is the extent of the coma in the direction towards the sun, as a result of solar radiation pressure.
3. The scale lengths, X_R , computed from the profiles imply grain terminal speeds which are less than the Bobrovnikoff speed.
4. Profiles of three comets (P/Halley, P/Whipple and P/Giacobini-Zinner) have $m < -3/2$ and cannot be fitted by the steady state radiation pressure models considered here. The steep profiles probably reflect variations in the strength of the nucleus source. Such variations in P/Halley are *known* from independent photometry.
5. Several processes, including solar radiation pressure, the sublimation of ice grains and variable mass loss from the nucleus may all give rise to coma profiles with gradients different from $m = -1$. The present data provide no clear evidence for a significant population of icy grains in these comets. The effects of ice grains on the measured surface brightness profiles are not easily separated from the effects of radiation pressure and of possible source variations.

References

- Baum, W. A., and T. J. Kreidl (1984), "Sublimation Rates of Grains in Cometary Comae" *Bull. Amer. Astron. Soc.* **16**, 643.
- Baum, W. A., and T. J. Kreidl, (1986), "Volatiles in Cometary Grains", in *Asteroids, Comets, Meteors II*, ed. C. Lagerkvist, B. Lindblad, H. Lundstedt and H. Rickman, Uppsala universitet, Uppsala, p. 397-402.
- Baum, W. A., T. J. Kreidl and D. G. Schleicher (1986), "Ices in Cometary Grains", *Bull. Amer. Astron. Soc.* **18**, 794.
- Christian, C. A., M. Adams, J. V. Barnes, H. Butcher, D. S. Hayes, J. R. Mould, and M. Siegel (1985), "Video Camera/CCD Standard Stars (KPNO Video Camera / CCD Standards Consortium)", *Pub. Astron. Soc. Pac.* **97**, 363-372.
- Delsemme, A. H. (1982) "Chemical Composition of Cometary Nuclei", in *Comets*, ed. L. L. Wilkening, Univ. of AZ Press, Tucson, 85-130.
- Delsemme, A. H., and D. C. Miller (1971), "Physical-Chemical Phenomena in Comets. III. The Continuum of Comet Burnham (1960 II)", *Planet. Space Sci.* **19**, 1229-1257.
- Hanner, M. S. (1981), "On the Detectability of Icy Grains in the Comae of Comets", *Icarus* **47**, 342-350.
- Jewitt, D. C. and K. J. Meech (1987), "Surface-Brightness Profiles of 10 Comets", *Astrophys. J.* **317**, 992-1001.
- Jewitt, D. C., B. T. Soifer, G. Neugebauer, K. Matthews and G. E. Danielson (1982), "Visual and Infrared Observations of the Distant Comets P/Stephan-Oterma (1980g), Panther (1980u), and Bowell (1980b)", *Astron. J.* **87**, 1854-1866.
- Keller, H. U., C. Arpigny, C. Barbieri, R. M. Bonnet, S. Cazes, M. Coradini, C. B. Cosmovici, W. A. Delamere, W. F. Huebner, D. W. Hughes, C. Jamar, D. Malaise, H. J. Reitsemä, H. U. Schmidt, W. K. H. Schmidt, P. Seige, F. L. Whipple and K. Wilhelm (1986), "First Halley Multicolour Camera Imaging Results From Giotto", *Nature* **321**, 320-326.
- Oke, J. B. and J. E. Gunn (1983), "Secondary Standard Stars For Absolute Spectrophotometry", *Astrophys. J.* **266**, 713 - 717.
- Saito, K., S. Isobe, K. Nishioka and T. Ishii (1981), "Substances of Cometary Grains Estimated From Evaporation and Radiation Pressure Mechanisms", *Icarus* **47**, 351-360.

Chapter 8 - Modelling Comet P/Halley - All Observations

8.1 Introduction

The preceding five chapters have discussed in detail observations and methods of obtaining information about specific properties of the nucleus and coma (e.g. dust albedo, phase function, rotation period, dust particle sizes, and radiation pressure effects in the coma). The simple H₂O-ice sublimation model used in Chapter 2 to explain the onset of sublimation in comet P/Halley near $R = 6$ AU will now be re-examined in view of these measurements. New photometry is added to the data from Chapter 2 to form a lightcurve covering the distance range $1 < R < 11$ AU and spanning ≈ 20 magnitudes (a factor of 10^8 in brightness). This is the first comet lightcurve to cover such a large range in brightness.

8.2 Observations

Historically, analysis of the cometary brightness as a function of R relied on visual observations made when the comet was bright at small R ; often the observations were made by many different observers and telescopes. These observations were made with different effective diaphragms; corrections to a standard system were very difficult. For this reason, the observations comprising the lightcurve presented here are those made primarily by the author using CCD detectors and employing consistent observing techniques. The techniques and instrumentation are very similar to those used by Jewitt and Danielson (1984), whose data are also included in the lightcurve. The NASA Infrared Telescope comet Halley monitoring program (Tokunaga *et al.*, 1986; Tokunaga, 1986(a-c); Hanner *et al.*, 1987) also produced a large number of P/Halley magnitudes made in a self consistent manner. Therefore, the IRTF measurements are also included in the lightcurve.

Table 8-1
Geometry of P/Halley Observations

Dates	Telescope	R [AU]	Δ [AU]	α [deg]	Ref. [†]
1981 Dec	Palomar 5m	12.7	11.8	2	1
1982 Oct	Palomar 5m	11.0	10.9	5	1
1984 Jan	Palomar 5m	8.2	7.2	2	1
1984 Oct	MHO 1.3m	5.9	5.5	9	2
1985 Jan	MHO 1.3m, IRTF	5.1	4.3	7	2,3
1985 Mar	IRTF	4.5	4.7	12	3
1985 Aug	MHO 1.3m, IRTF	2.8	3.2	18	3,4
1985 Sept	IRTF, KPNO 4m	2.4-2.6	2.5-2.8	21-23	3,4
1985 Oct	IRTF	2.0	1.3	24	3
1985 Nov	IRTF, MHO 1.3m	1.5-1.9	0.6-1.1	1-24	3,4
1985 Dec	IRTF	1.3-1.4	0.7-0.8	45-49	3
1986 Jan	IRTF	0.9	1.3	49	3
1986 Mar	KPNO 2.1m, IRTF	0.8-1.1	0.7-1.1	59-65	4,5
1986 May	IRTF	2.0	1.7	30	6
1986 July	IRTF	2.5	2.9	20	6
1986 Oct	KPNO 2.1m	3.9	4.6	9	4
1986 Nov	IRTF	4.1	4.6	11	6
1987 Mar	KPNO 2.1m	5.4	4.6	7	4

† 1 - Jewitt & Danielson (1984)	2 - Meech <i>et al.</i> (1986)
3 - Tokunaga <i>et al.</i> (1986)	4 - This work
5 - Hanner <i>et al.</i> (1987)	6 - Tokunaga (1986a,b,c)

The lightcurve is shown in Figure 8-1. The date, telescope, R , Δ , and phase angle for each observing run contributing data to the figure are listed in Table 8-1. Details of the observational techniques are provided in Jewitt and Danielson (1984), Tokunaga *et al.* (1986), Hanner *et al.* (1987) and in Chapters 2 and 5 of this thesis. Additional data from MIT's McGraw-Hill observatory in 1985 August were obtained and reduced in a similar fashion to the observations discussed in Chapter 2. The observing conditions in August were slightly non-photometric, hence the magnitudes in the figure are lower limits only. The 1985 September, 1986 March and 1986 October observational details may be found in Chapters 5 and 9. For all photometric measurements made after the coma developed (1985 January), the

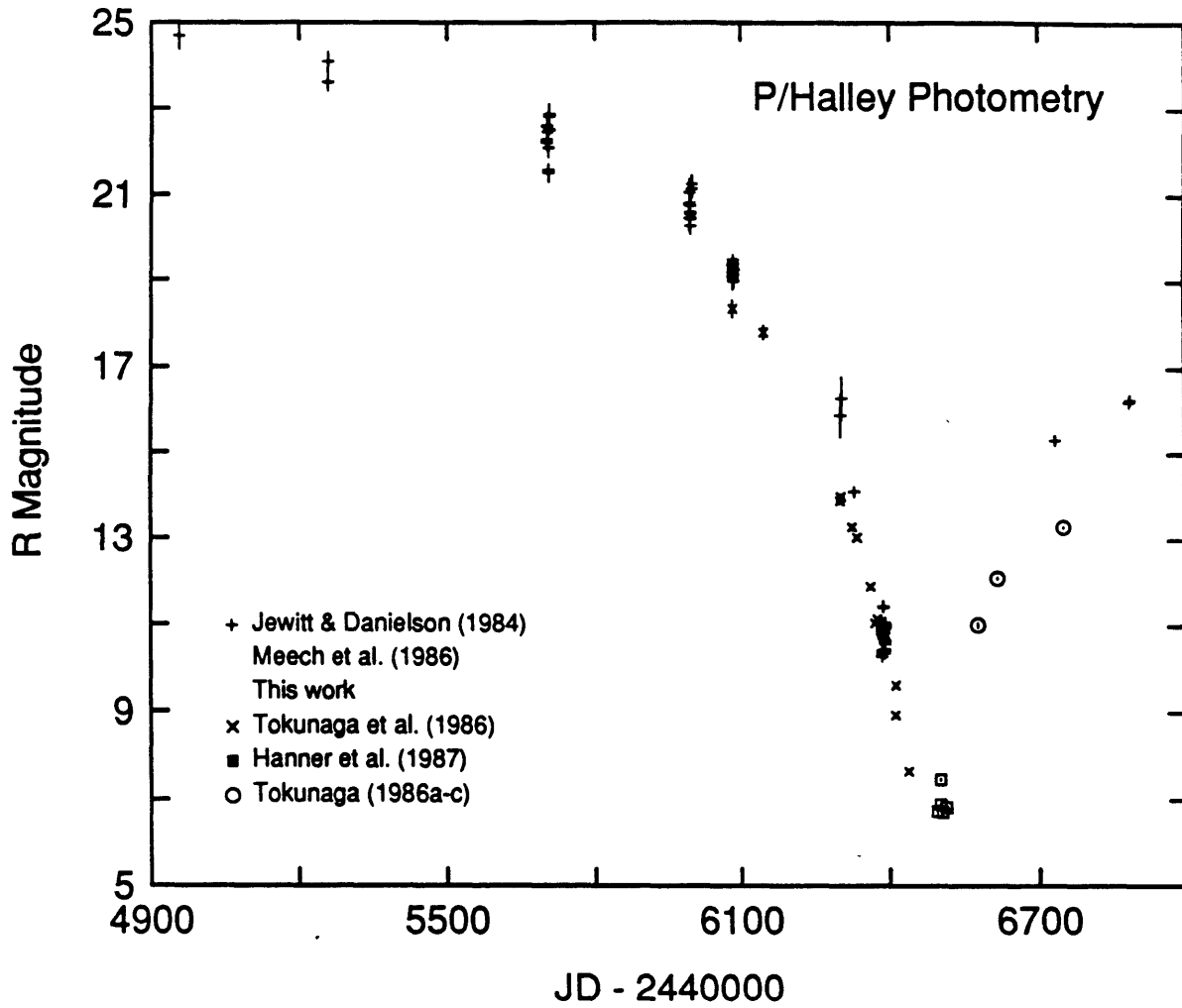


Figure 8-1. Halley lightcurve from recovery at $R = 11$ AU to $R = 5.4$ AU postperihelion. The m_R magnitude is plotted versus JD. The sources of data used in the figure are listed in Table 8-1.

sky brightness was measured separately, offset from the nucleus to avoid coma contamination. The continuum magnitudes ($m_{5790} \approx V$) obtained from spectroscopic data taken in 1985 November are discussed in Chapter 4. All magnitudes have been reduced to the m_R bandpass ($\lambda_{cent} = 0.65 \mu\text{m}$, $\Delta\lambda \approx 0.1 \mu\text{m}$) by assuming solar colors (Allen, 1976). All measurements inside of $R \approx 2.5$ AU were made through continuum interference filters to avoid contamination from emission lines. Only the J magnitudes were used from the infra-red data to avoid the possibility of thermal contamination. At these near infra-red wavelengths, gas emission bands are not a problem. All magnitudes obtained with coma present have been corrected to a 10 arcsec diameter diaphragm assuming a $1/p$ coma: $\Delta m = -2.5 \log(\phi_o/\phi)$, where $\phi_o = 10$ arcsec and ϕ is the photometry diaphragm (arcsec).

The morphological development of the coma from recovery through perihelion and beyond is illustrated in Figure 8-2. Figure 8-2a shows six pre-perihelion images; all except the image at $R = 1.9$ AU are CCD images. The geometric parameters relevant for the figure are listed in Table 8-3. In the figure the comet appears stellar through $R = 5.9$ AU, although at this distance weak but sustained coma production had begun (see Chapter 2). At $R = 2.8$ AU the coma is readily apparent (note, the first 4 sections of Figure 8-2a all have the same angular scale). Once sustained sublimation began the brightness increased rapidly (see Figure 8-1) and the coma increased in size. At $R = 1.9$ AU the plasma tail began to form. The Schmidt photo in Figure 8-2a is one of the first to show a tail. For approximately 2 months near perihelion the comet displayed a spectacular plasma tail which varied on timescales from minutes to days. Two examples of the structure of the plasma tail are shown in Figure 8-2b. Photometric measurements near perihelion obtained brightness estimates for only a very small region inside the coma.

The central region of the coma just one month past perihelion is shown in the first image of Figure 8-2c. Care must be taken when obtaining photometric measurements from images with strong coma to properly center the diaphragm. The center is located in the CCD image

Figure 8-2. (a) Pre-perihelion development of comet P/Halley. All of the relevant parameters pertaining to the figure are listed in Table 8-3. One of the recovery images on 1982 Oct 16 taken by D. Jewitt is shown in the upper left of the figure. The line segments and the box marking the positions of the comet in the first two frames are 7 arcsec in length. At $R = 5.9$ AU the coma was first beginning to develop, although it is not visible in the third frame. The box surrounding P/Halley is 16 arcsec in length. The bottom row shows the rapidly developing coma. The last frame shows one of the earliest photos of the developing plasma tail at $R = 1.9$ AU. North is to the top and East to the left for all frames.

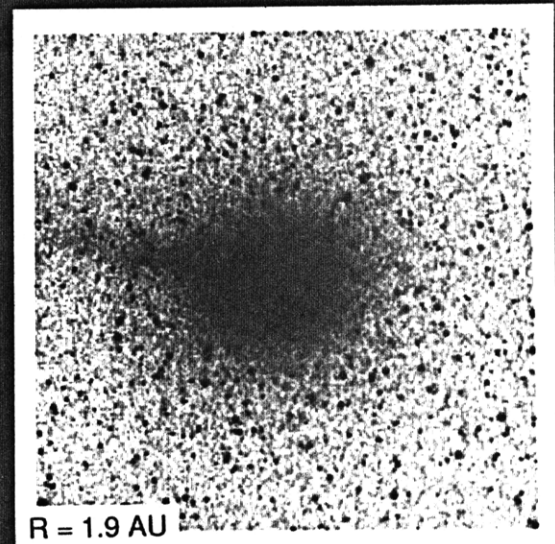
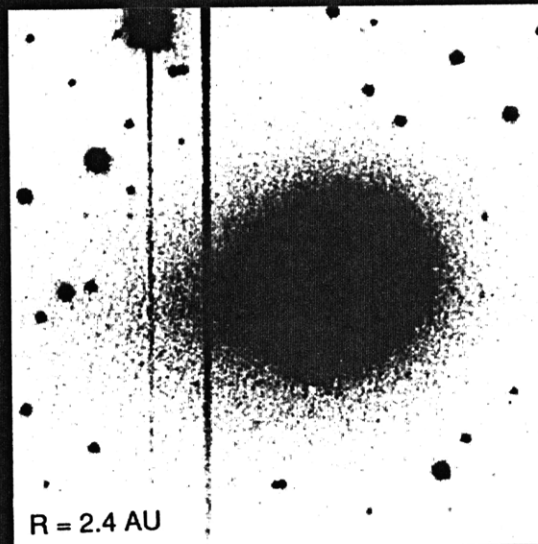
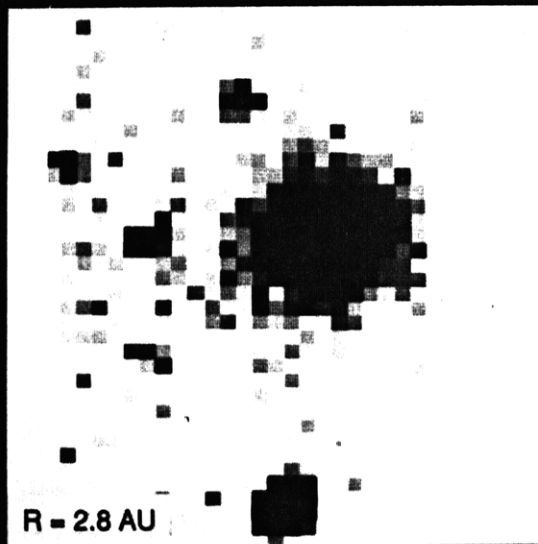
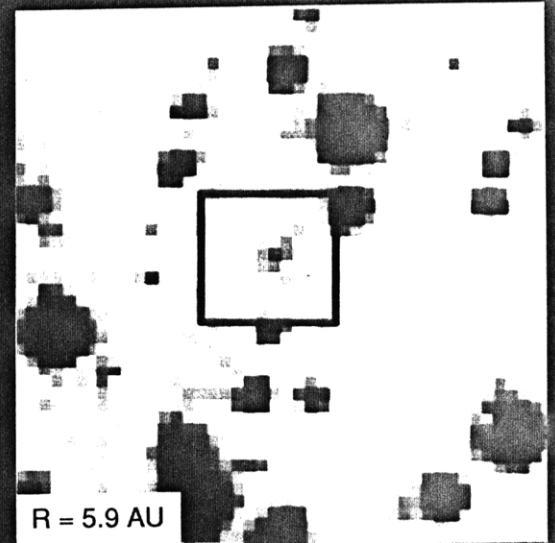
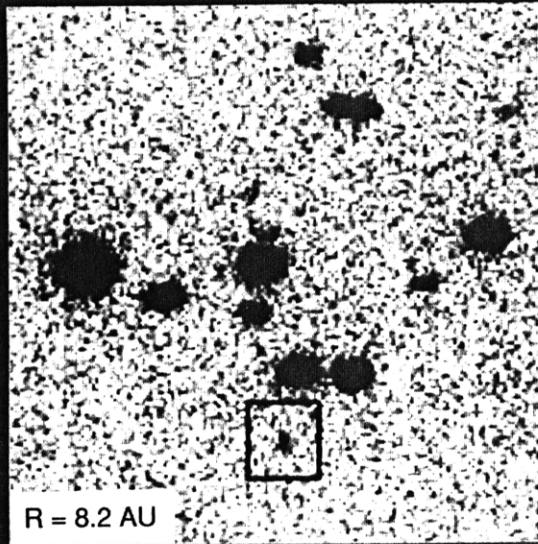
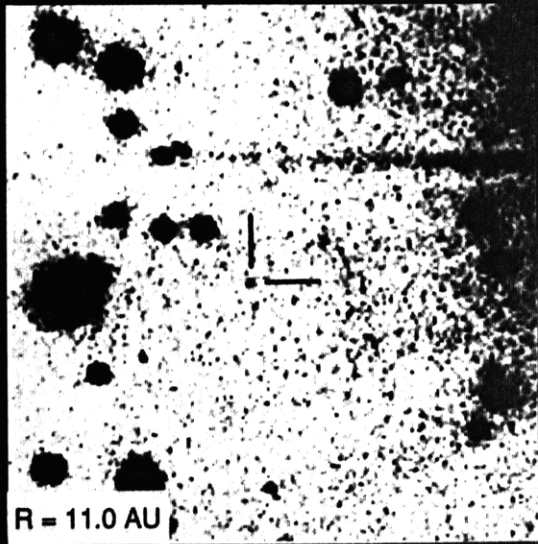


Figure 8-2. (b) Changing P/Halley plasma tail just after perihelion (which occurred on 1986 Feb 9). The figure shows how the morphology of the tail changed between two observing runs. Dramatic changes were even apparent in the tail on nightly timescales. The long dimension of the figure is ≈ 2.5 deg. Other relevant observational parameters are presented in Table 8-3.

P/Halley

1986 March 22

1986 April 30

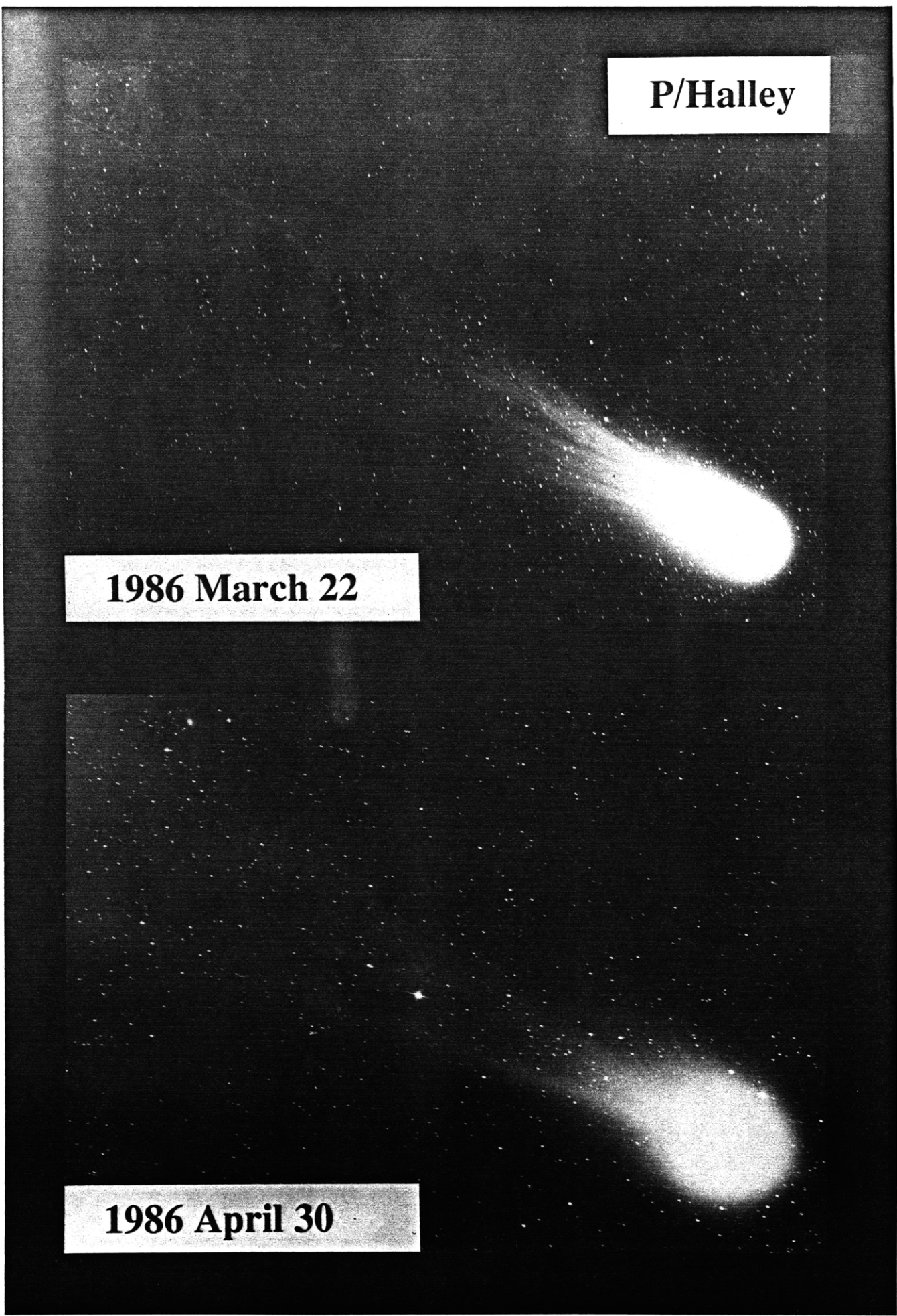
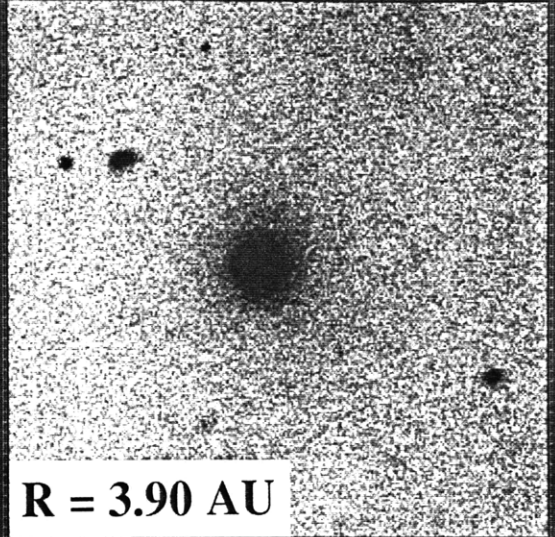


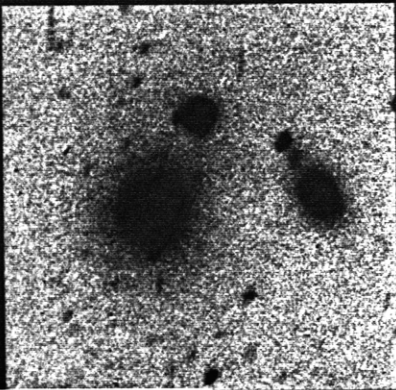
Figure 8-2. (c) Post-perihelion development of comet P/Halley. All of the relevant parameters pertaining to the figure are listed in Table 8-3. Note the brightness asymmetry around perihelion passage by comparing this figure to Figure 8-2a. In particular, the image taken at $R = 5.65$ AU post-perihelion exhibits substantial coma whereas the image taken at $R = 5.89$ AU pre-perihelion was only just developing a coma.



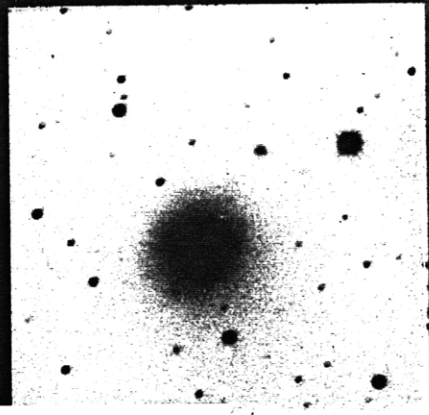
R = 0.82 AU



R = 3.90 AU



R = 5.39 AU



R = 5.65 AU

by displaying only the highest data numbers. For the image at $R = 0.82$ AU the photometric center is displaced approximately half the way from the apparent center to the edge of the coma in the direction of the star. There is pronounced sunward emission from the comet. The other images in Figure 8-2c depict the comet at increasing post-perihelion heliocentric distances (see also Table 8-3). Comparing the appearance of the comet at $R = 5.65$ AU post-perihelion (Figure 8-2c) to the image at $R = 5.9$ AU pre-perihelion (Figure 8-2a) shows a striking brightness asymmetry.

One possible cause of a perihelion brightness asymmetry such as seen for P/Halley, could be due to the penetration of a thermal wave into the nucleus. This would make the nucleus hotter post-perihelion at a particular R compared to the same R pre-perihelion. The spacecraft observations of P/Halley, however, suggest that this is not the case. The nucleus was observed to be covered with a crust of very low thermal conductivity (Combes, *et al.*, 1986) which suggests that insufficient heat would penetrate into the interior to cause such a large brightness asymmetry. Weissman (1986) postulates that the asymmetry is a seasonal effect caused by the comet's northern hemisphere suddenly becoming exposed to sunlight just past perihelion, rapidly heating previously unheated regions of the nucleus. According to Weissman, the rapid heating causes severe thermal stress which cracks the dusty surface, creating large active areas. A brightness asymmetry has been observed in other comets in addition to P/Halley. If the asymmetry was always such that the comet was brighter post-perihelion, then this would suggest that the cause was a thermal wave. However, the mechanism of seasonal variation would be favored if approximately equal numbers of comets were brighter pre-perihelion as were brighter post-perihelion. There is presently insufficient observational data to distinguish between the two mechanisms.

8.3 Discussion

8.3.1 Comparison of Pre- and Post-Encounter Information

Table 8-2 presents all the information used in the H₂O model developed in Chapter 2 and of the values known after the spacecraft encounter. Inspection of the table shows that the values of those parameters which were well-constrained by observations at large R are consistent with those values obtained during the encounter. Specifically, observations prior to the onset of sustained sublimation yielded a value for the product of the cross section times the albedo (see Eq. 2.3). When combined with the albedo as constrained from the model, this gives the average nucleus radius as $2.8 < \beta_n[\text{km}] < 8$. Spinrad (1986), used the approximate nucleus dimensions as observed from Giotto to estimate a volume for the nucleus of P/Halley. This yields a radius for a sphere of the same volume of $\beta_n \approx 6.2$ km. When using the nucleus/dust albedos derived from ground-based measurements prior to the encounter, (see Chapter 3), the average radius is in close agreement with the value of Spinrad (1986). The rotation lightcurve, although unable to yield a definitive period, suggested a long period (see Chapter 5), and from the amplitude a nucleus axis ratio of $\approx 2.5:1$. Again, both values agree with the post-encounter nucleus properties. The primary result of the sublimation model, namely that the vaporization was controlled by water ice, was upheld after the encounter (Mumma *et al.*, 1986; Krankowsky *et al.*, 1986; Woods *et al.*, 1986).

One of the surprising results of the encounter was the very low nucleus density, $\rho_n \approx 80\text{-}300$ kg m⁻³ (Whipple, 1986), which is similar to that of Terrestrial snow. Other characteristics determined from the encounter, such as the extremely localized, uneven mass loss from the nucleus were not explicitly incorporated in the models in Chapter 2, even though completely uniform sublimation was not expected. The sublimation models were never intended to reproduce the detailed behavior of the comet, only the general characteristics

Table 8-2
Halley Model Parameters

Property	Var.	Halley Model	Reference	Current Values	Reference
Albedo x Cross Section	$p_v \beta_n^2$	$(1.24 \pm 0.03) \times 10^6 \text{ m}^2$	Meech <i>et al.</i> 1986	Not measured	
Geometric Albedo	p_v	0.02-0.15	Meech <i>et al.</i> 1986	0.04 ($\lambda=0.5\text{-}0.9\mu\text{m}$)	Sagdeev <i>et al.</i> 1986 Chap. 3
Emissivity	ϵ	0.85-0.90	A		
Phase Coefficient	β	0	A	0.018 dust [0.04 nucleus]	Meech & Jewitt '87
Nucleus Radius	β_n	2.8-8 km	Meech <i>et al.</i> 1986	16 x 10 x 9 km 16 x 8 x 7.5 km $\beta_n \approx 6.2 \text{ km}$	Wilhelm <i>et al.</i> 1986 Whipple, 1986 Spinrad, 1986
Grain Size	a	1-1.5 μm	A	\approx few μm mean many sub μm	Jewitt & Meech, '86 McDonnell <i>et al.</i> 1986
Grain Density	ρ	700-1300 kg m^{-3}	A		
Nucleus Density	ρ_n	700-1300 kg m^{-3}	A	80 - 300 kg m^{-3}	Whipple, 1986
Thermal Conductivity	κ	negligible	A	low {Ortho/Para} low {high temp}	Mumma <i>et al.</i> 1986 Combes <i>et al.</i> 1986
Mass Loading	ψ	1 0.05-1	A Newburn & Spinrad, 1985	0.2 0.22 - 0.45	McDonnell, '86a Hanner, 1987 & Whipple, 1986
Grain Velocity	v	Bobrovnikoff	A	\ll Bob. v	Chapter 7
Brightness Range	Δm	$R > 6\text{AU} \rightarrow 1$ $R = 5.9\text{AU} \rightarrow .8$ $R = 5.1\text{AU} \rightarrow .3$	Meech <i>et al.</i> 1986, Jewitt & Danielson, 1984	Not Measured	
Axis Ratio	$a:b$	$\approx 2.5 : 1$	Meech <i>et al.</i> 1986	2:1	Whipple, 1986
Period	T	"slow" > 18 hours	Meech <i>et al.</i> 1986	Most Activity sunward 2.2 vs 7.4 dy	Whipple, 1986 See Chap. 5
Optical Depth in Coma	τ	optically thin	A	$\tau < 0.3$	Keller <i>et al.</i> 1986

Table 8-2, contd.

Halley Model Parameters

Property	Var.	Halley Model	Reference	Current Values	Reference
Composition	--	H ₂ O	A	H ₂ O (80%) CO (17-20%) CO ₂ (3.5%)	Mumma <i>et al.</i> 1986 Krankowsky <i>et al.</i> 1986 Woods <i>et al.</i> 1986
Sublimation	--	Uniform	A	jets, 0.3-0.5 active	Reitsema <i>et al.</i> 1986 Larson <i>et al.</i> 1986
Dust Density vs. distance	--	1/r ² dependence	A	≈ 1/r ² near nucleus	McDonnell <i>et al.</i> 1986b Levasseur-Regourd <i>et al.</i> 1986

A = assumed in the modelling

which are manifestations of the water-ice composition.

Given improved values for some of the nucleus characteristics (see Table 8-2) in addition to more brightness data, the H₂O sublimation models have been re-computed. One of these models is shown superposed on the data in Figure 8-3. Pre-perihelion, the model compares well with the general brightness increase from recovery through perihelion; however, it does not (nor is it expected to) reproduce short-term variations. The post-perihelion data are significantly brighter than predicted by the model. The seasonal effects suggested by Weissman (1986) cannot be included in the model in the absence of reliable information concerning the nucleus spin state. In principle, it would be possible to arbitrarily change the fraction of the surface area of the nucleus sublimating post-perihelion in order to fit the data. In the absence of an understanding of the mechanism causing the asymmetry, a forced fit is unjustified. Further refinements to the model are also unjustified because many of the parameters are already poorly constrained (e.g. the fraction of the nucleus sublimating, the gas

mass loading etc.). Furthermore, it would be impossible to model the rapid brightness variations caused by irregular outgassing seen in the comet near perihelion. Figure 8-4a shows the dramatic changes in the appearance of the inner coma of P/Halley during four consecutive nights in 1986 March (see Table 8-3 for observational information). The changing direction of dust emission is even more clearly shown in Figure 8-4b which shows contour plots of the images in Figure 8-4a. Figure 8-5 shows an image of P/Halley obtained at $R = 6.65$ AU post-perihelion from CTIO (see Table 8-3) which shows a strongly asymmetric coma. As seen in Chapter 7, asymmetric comae (which result from radiation pressure and from asymmetric ejection) will affect the surface brightness profile. However, since brightness estimates are made within a very small diaphragm (5 arcsec radius) even such strong asymmetries are little noticed.

Therefore, it can be concluded that while such simplified models *cannot* ever reproduce the observed lightcurve in detail, they are extremely useful for understanding general characteristics and basic nucleus properties.

8.3.2 *The Visual Lightcurve*

Since this is the first comet lightcurve to be observed over such large ranges in heliocentric distance and brightness with sophisticated electronic detectors, it is of interest to compare this lightcurve with that observed visually. The visual lightcurve has traditionally been used for analysis of the behavior of other comets (see for example Delsemme, 1985; Meisel & Morris, 1982; Whipple, 1978; Whipple & Sekanina, 1979). An impressive lightcurve has been published by Green and Morris (1986) combining observations at large R (> 5 AU) made with electronic detectors with visual observations made at smaller heliocentric distances. In Figure 1 of their paper they plot the quantity $H \equiv \text{mag} - 5 \log (\Delta)$ (a quantity which has no physical meaning since the Δ dependence of the coma brightness changes with

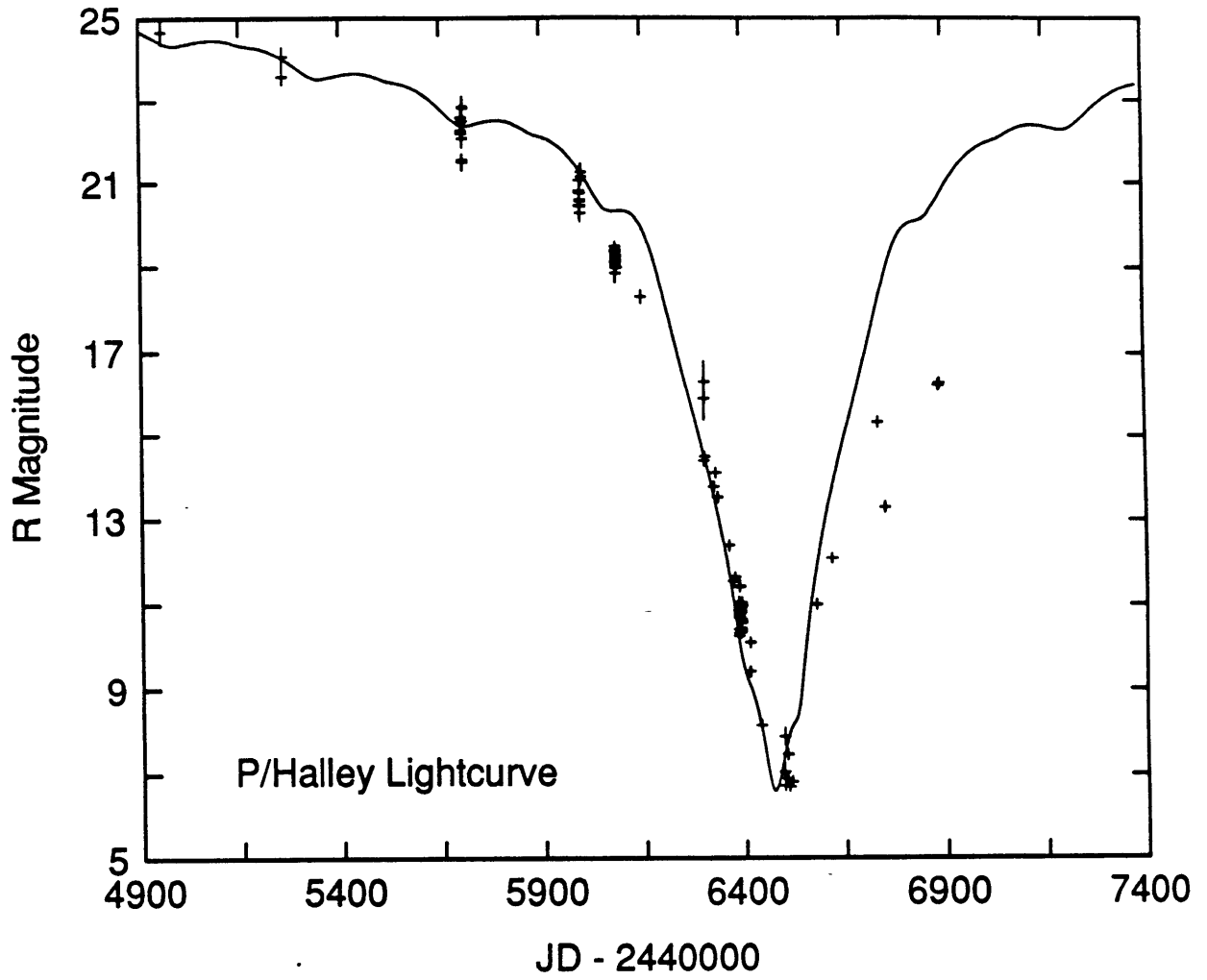
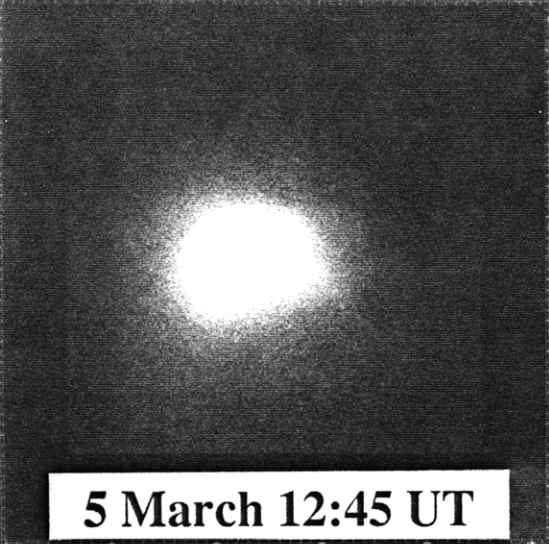


Figure 8-3. P/Halley lightcurve and H₂O sublimation model (see text for discussion).

Figure 8-4. (a) Images taken on consecutive nights in 1986 March showing the dramatic changes in the inner coma over the 4 nights. In particular, the shape of the coma changes in addition to the direction of maximum emission. North is to the left and East to the top in all of these images.

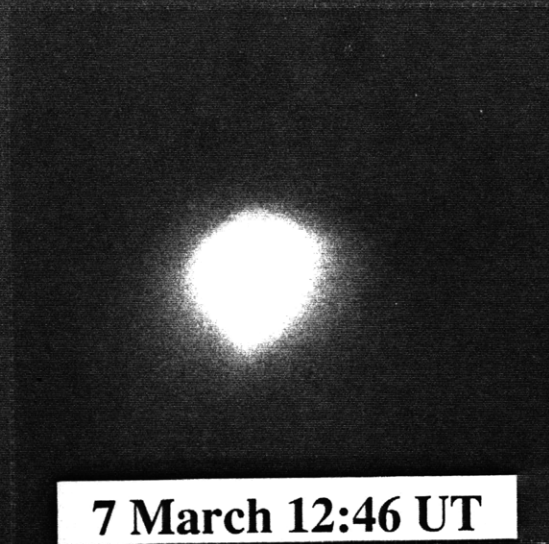
P/Halley - 1986



5 March 12:45 UT



6 March 12:54 UT



7 March 12:46 UT



8 March 12:25 UT

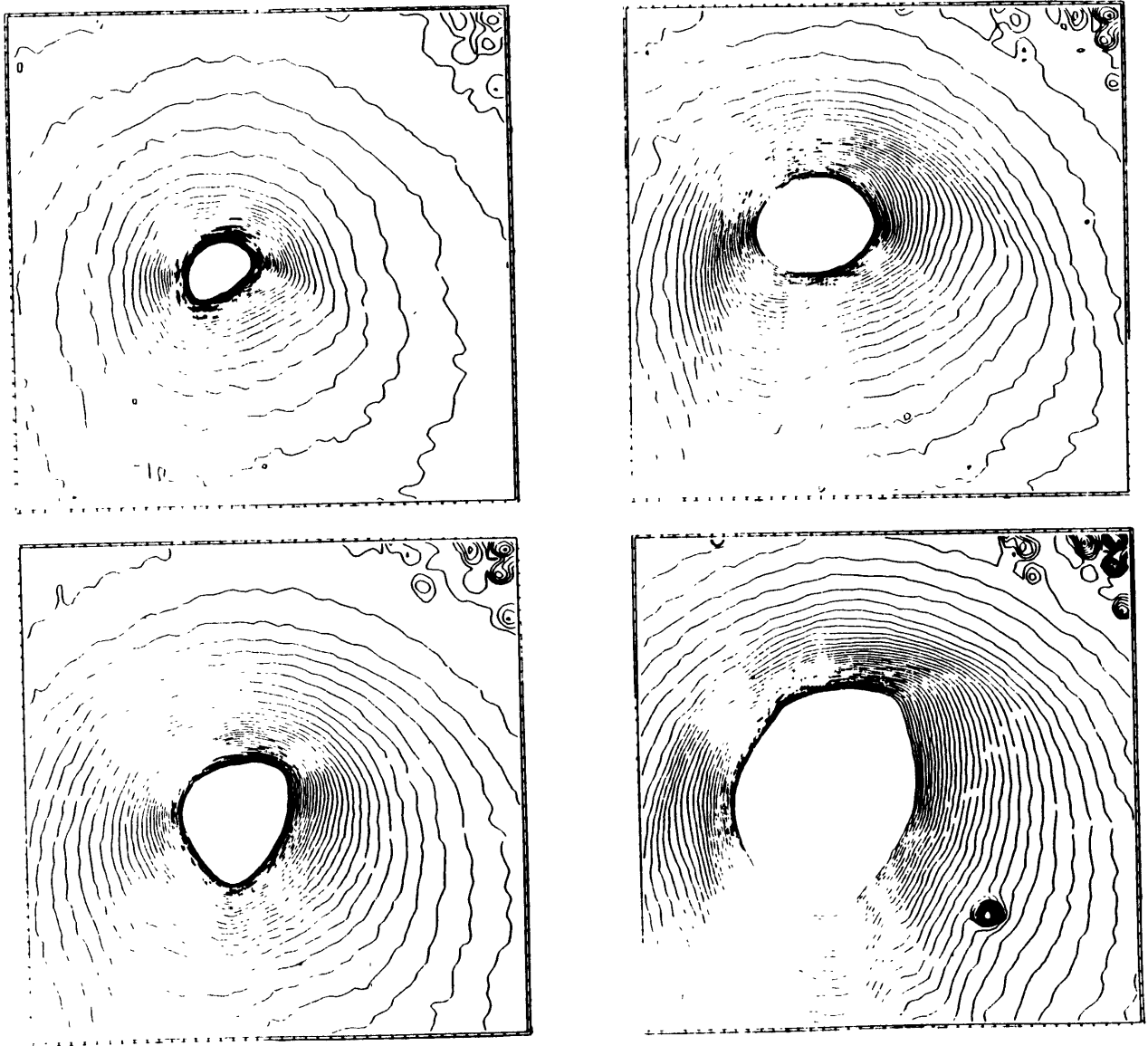
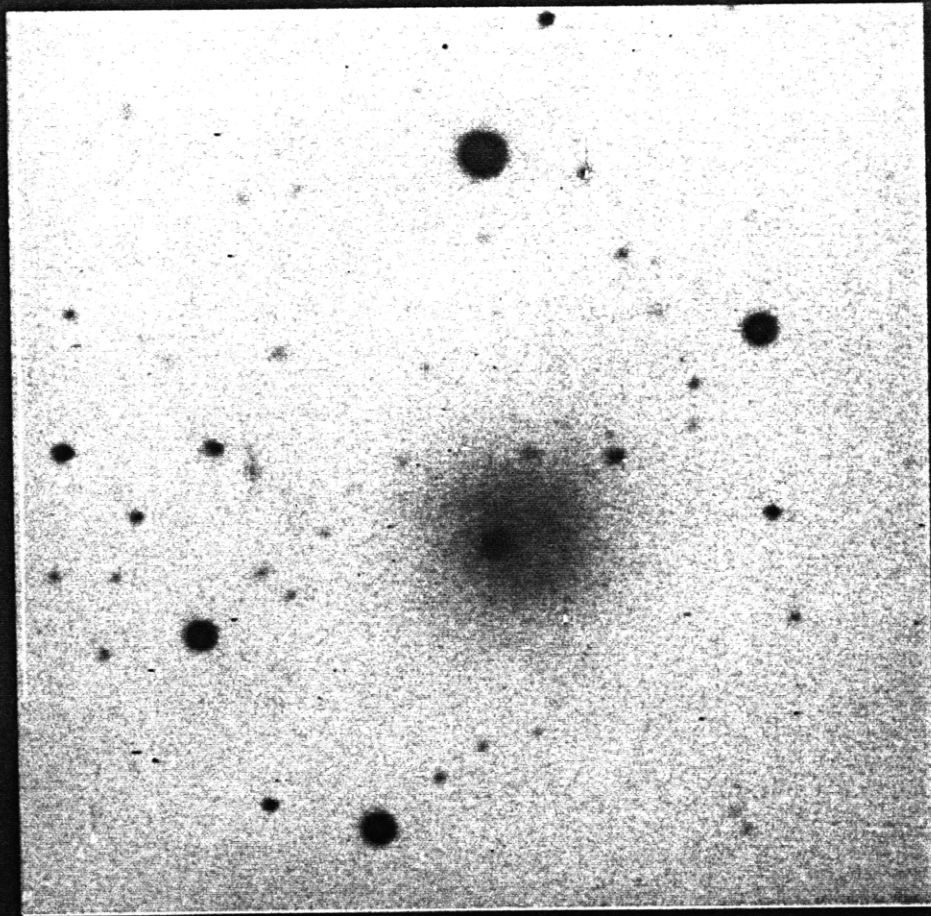


Figure 8-4 (b) Contour plots of same images as shown in Figure 8-4a.

Figure 8-5. Image of P/Halley taken with the CTIO 1.5m telescope on 1987 May 1 when the comet was at $R = 5.65$ AU. (See Table 8-3 for relevant parameters). Note the very asymmetric coma. North is to the right and East is at the bottom in this figure.



Comet P/Halley
(R = 5.65 AU)

R) versus time. A comparison of their lightcurve with Figure 8-3 (when plotted as H versus time) shows an increasing brightness discrepancy between the two curves, reaching roughly 5 magnitudes near perihelion.

There are several reasons for this discrepancy. Firstly, the visual observations are unfiltered, they therefore contain light from both gaseous emission and scattering from the dust. It is therefore difficult to model the visual data because of uncertainties in the dust to gas ratio. Secondly, unlike the lightcurve presented in this chapter, no fixed diaphragm was used for the visual observations. The sublimation model computes the brightness expected within a diaphragm of fixed angular size. If the effective diaphragms used in the observations are unknown or different (depending on the size of the telescope used, the magnification and how much of the coma is used in making the brightness estimate) the data cannot be meaningfully compared to the model. Thirdly, the human eye is a subjective non-linear detector, unlike the CCD detectors and infrared photometers used for the lightcurve presented in Figure 8-3. Again, corrections for this non-linearity are difficult. Observations by different visual observers often show scatter of many magnitudes. For these reasons, and because the quantity, H , is a non-physical parameter, visual lightcurves are not useful for quantitative comparison with the type of models presented here and in Chapter 2.

8.4 Conclusions

1. A lightcurve for P/Halley covering a range in brightness of 20 magnitudes is presented. The main features of the lightcurve are an initial portion ($R > 6$ AU) in which the comet obeys the inverse square law, a rapid brightening due to water sublimation at smaller R , and a pronounced pre-post perihelion photometric asymmetry.
2. Results from the simple H₂O sublimation model developed in Chapter 2 compare favorably with the results from the recent spacecraft rendezvous. In particular, the nucleus size, shape, albedo, composition and crude rotation period were well constrained from remote observations made at large R .
3. Revision of the model input parameters post-perihelion shows that the model is able to match the general photometric behavior of the comet from recovery through perihelion. Detailed brightness variations and the post-perihelion brightness asymmetry (possibly due to seasonal effects) are not well described by the model. This type of simple modelling is therefore a very powerful tool for learning about several basic properties of the comet nucleus but is clearly inadequate for studying detailed properties of the lightcurve.
4. Lightcurves obtained visually (without electronic detectors) are different from CCD lightcurves and are not useful for this type of quantitative analysis.

Table 8-3
Photographic Figure Information

Figure	Comet	Telescope	Date	UT [§]	Filter	Exp [sec]	R [AU]	Δ [AU]	α [deg]	Scale [arcsec]
8-2a	P/Halley	*Palomar 5m	1982 Oct 16	11:50	g	240	11.04	10.93	5.2	60
		*Palomar 5m	1984 Jan 08	06:25	g	300	8.16	7.23	1.7	60
		MHO 1.3m	1984 Oct 24	08:41	R	900	5.89	5.48	9.1	60
		MHO 1.3m	1985 Aug 27	11:16	R	360	2.78	3.11	18.7	60
		KPNO 4m	1985 Sept 23	12:04	cont [‡]	600	2.44	2.28	24.2	120
		KPNO Schmidt	1985 Nov 6	---	--	420	1.85	0.93	17.0	2400
8-2b	P/Halley	KPNO Schmidt [◇]	1986 Mar 22	12:02	--	600	1.03	0.75	65.9	9000 [†]
		CTIO Schmidt [◇]	1986 Apr 30	00:23	--	900	1.62	0.77	28.4	9000 [†]
8-2c	P/Halley	KPNO 2.1m	1986 Mar 08	12:25	cont	20	0.82	1.10	60.3	150
		KPNO 2.1m	1986 Oct 31	12:36	cont	300	3.90	4.62	9.3	100
		KPNO 2.1m	1987 Apr 02	05:25	R	240	5.39	4.59	6.9	140
		CTIO 1.5m	1987 May 01	02:49	R	200	5.65	5.21	9.6	215
8-4a	P/Halley	KPNO 2.1m	1986 Mar 05	12:45	cont	5	0.78	1.17	57.2	150
		KPNO 2.1m	1986 Mar 06	12:42	cont	10	0.80	1.14	58.3	150
		KPNO 2.1m	1986 Mar 07	12:46	cont	10	0.81	1.12	59.3	150
		KPNO 2.1m	1986 Mar 08	12:25	cont	20	0.82	1.10	60.3	150
8-5	P/Halley	CTIO 1.5m	1987 May 01	02:49	R	200	5.65	5.21	9.6	215

[§] UT midtime of exposure.

* Observations provided by D. Jewitt, private communication.

[‡] Continuum filter $\lambda_{\text{cent}} \approx 7007\text{\AA}$, $\Delta\lambda \approx 79\text{\AA}$ FWHM.

[◇] The plates were digitized using the Kitt Peak PDS microdensitometer.

[†] Long dimension, approximate only.

References

- Allen, C. W. (1976), *Astrophysical Quantities*, 3rd edition, University of London, The Athlone Press, P. 162.
- Combes, M., V. I. Moroz, J. F. Crifo, J. M. Lamarre, J. Charra, N. F. Sanko, A. Soufflot, J. P. Bibring, S. Cazes, N. Coron, J. Crovisier, C. Emerich, T. Encrenaz, R. Gispert, A. V. Grigoryev, G. Guyot, V. A. Krasnopolsky, Yu. V. Nikolsky and F. Rocard (1986), "Infrared Sounding of Comet Halley from Vega 1", *Nature* **321**, 266-268.
- Delsemme, A. H. (1985), "The Sublimation Temperature of the Cometary Nucleus: Observational Evidence for H₂O Snows", in *Ices in the Solar System*, eds. J. Klinger, D. Benest, A. Dollfus & R. Smoluchowski, NATO Advanced Science Institutes Series C Vol. **156**, D. Reidel Pub. Co., Dordrecht, p. 367-387.
- Green, D. W. E. and C.S. Morris (1986), "The Visual Brightness and Behaviour of P/Halley During 1981-1986", in *Proceedings of the 20th ESLAB Symposium on the Exploration of Halley's Comet*, ESA Pub. Div., The Netherlands, Vol. I., p. 613-618.
- Hanner, M. S. (1987), "A Preliminary Look at the Dust in Comet Halley", *Adv. Space Research* (in press).
- Hanner, M. S., A. T. Tokunaga, W. F. Golisch, D. M. Griep and C. D. Kaminski (1987), "Infrared Emission From Halley's Dust Coma During March 1986", *Astron. Astrophys.* (submitted).
- Jewitt, D. and G. E. Danielson (1984), "Charge-Coupled Device Photometry of Comet P/Halley", *Icarus* **60**, 435-444.
- Jewitt, D. and K. J. Meech (1986), "Cometary Grain Scattering Versus Wavelength, or 'What Color is Comet Dust' ", *Astrophys. J.* **310**, 937-952.
- Keller, H. U., W. A. Delamere, W. F. Huebner, H. Reitsemä, H. U. Schmidt, W. K. H. Schmidt, F. L. Whipple and K. Wilhelm (1986), "Dust Activity of Comet Halley's Nucleus", in *Proceedings of the 20th ESLAB Symposium on the Exploration of Halley's Comet*, ESA Pub. Div., The Netherlands, Vol. II., p. 359-362.
- Krankowsky, D., P. Lämmerzahl, I. Herrwerth, J. Woweries, P. Eberhardt, U. Dolder, U. Herrmann, W. Schulte, J. J. Berthelier, J. M. Illiano, R. R. Hodges and J. H. Hoffman (1986), " *In Situ* Gas and Ion Measurements at Comet Halley", *Nature* **321**, 326-329.
- Larson, S., Z. Sekanina, D. Levy, S. Tapia and M. Senay (1986), "Comet Halley Near-Nucleus Phenomena in 1986", in *Proceedings of the 20th ESLAB Symposium on the Exploration of Halley's Comet*, ESA Pub. Div., The Netherlands, Vol. II., p. 145-150.
- Levasseur-Regourd, A. C., J. L. Bertaux, R. Dumont, M. Festou, R. H. Giese, F. Giovane, P. Lamy, J. M. Le Blanc, A. Llebaria and J. L. Weinberg (1986), "Optical Probing of Comet Halley from the Giotto Spacecraft", *Nature* **321**, 341-344.

References, contd.

- McDonnell, J. A. M., W. M. Alexander, W. M. Burton., E. Bussoletti, D. H. Clark, R. J. L. Grard, E. Grün, M. S. Hanner, D. W. Hughes, E. Igenbergs, H. Kuczera, B. A. Lindblad, J. -C. Mandeville, A. Minafra, G. H. Schwehm, Z. Sekanina, M. K. Wallis, J. C. Zarnecki, S. C. Chakaveh, G. C. Evans, S. T. Evans, J. G. Firth, A. N. Littler, L. Massonne, R. E. Olearczyk, G. S. Pankiewicz, T. J. Stevenson and R. F. Turner (1986a), "Dust Density and Mass Distribution Near Comet Halley From Giotto Observations", *Nature* **321**, 338-341.
- McDonnell, J. A. M., J. Kissel, E. Grün, R. J. L. Grard, Y. Langevin, R. E. Olearczyk, C. H. Perry and J. C. Zarnecki (1986b), "Giotto's Dust Impact Detection System DIDSY and Particulate Impact Analyser PIA: Interim Assessment of the Dust Distribution and Properties Within the Coma", in *Proceedings of the 20th ESLAB Symposium on the Exploration of Halley's Comet*, ESA Pub. Div., The Netherlands, Vol. II., p. 25-38.
- Meech, K. J. and D. C. Jewitt (1987), "Observations of Comet P/Halley at Minimum Phase Angle", *Astron. Astrophys.* (in press).
- Meech, K. J., D. Jewitt and G. R. Ricker (1986), "Early Photometry of Comet P/Halley: Development of the Coma", *Icarus* **66**, 561-574.
- Meisel, D. D. and C. S. Morris (1982), "Comet Head Photometry: Past, Present, and Future", in *Comets*, ed. L. L. Wilkening, Univ. of AZ Press, Tucson, AZ, p. 413-432.
- Mumma, M. J. , H. A. Weaver, H. P. Larson, D. S. Davis and M. Williams (1986), "Detection of Water Vapor in Halley's Comet", *Science* **232**, 1523-1528.
- Newburn, R. L. and H. Spinrad (1985), "Spectrophotometry of Seventeen Comets. II. The Continuum", *Astron. J.* **90**, 2591-2608.
- Reitsema, H. J., W. A. Delamere, W. F. Huebner, H. U. Keller, W. K. H. Schmidt, K. Wilhelm, H. U. Schmidt and F. L. Whipple (1986), "Nucleus Morphology of Comet Halley", in *Proceedings of the 20th ESLAB Symposium on the Exploration of Halley's Comet*, ESA Pub. Div., The Netherlands, Vol. II., p. 351-354.
- Sagdeev, R. Z., G. A. Avanesov, Ya. L. Ziman, V. I. Moroz, V. I. Tarnopolsky, B. S. Zhukov, V. A. Shamis, B. Smith and I. Toth (1986), "TV Experiment of the Vega Mission: Photometry of the Nucleus and the Inner Coma", in *Proceedings of the 20th ESLAB Symposium on the Exploration of Halley's Comet*, ESA Pub. Div., The Netherlands, Vol. II., p. 317-326.
- Spinrad, H. (1986). "Comets and Their Composition", preprint.
- Tokunaga, A. T. (1986a), "Periodic Comet Halley (1982i)", *IAU Circ. No. 4226*.
- Tokunaga, A. T. (1986b), "Periodic Comet Halley (1982i)", *IAU Circ. No. 4236*.
- Tokunaga, A. T. (1986c), "Periodic Comet Halley (1982i)", *IAU Circ. No. 4274*.

References, contd.

- Tokunaga, A. T., W. F. Golisch, D. M. Griep, C. D. Kaminski and M. S. Hanner (1986), "The NASA Infrared Telescope Facility Comet Halley Monitoring Program. I. Preperihelion Results", *Astron. J.* **92**, 1183-1190.
- Weissman, P. R. (1986), "Post Perihelion Brightening of Halley's Comet: A Case of Nuclear Summer", in *Proceedings of the 20th ESLAB Symposium on the Exploration of Halley's Comet*, ESA Pub. Div., The Netherlands, Vol. III., p. 517-522.
- Whipple, F. L. (1978), "Cometary Brightness Variation and Nucleus Structure", *Moon & Planets* **18**, 343-359.
- Whipple, F. L. (1986), "The Cometary Nucleus - Current Concepts", in *Proceedings of the 20th ESLAB Symposium on the Exploration of Halley's Comet*, ESA Pub. Div., The Netherlands, Vol. II., p. 281-288.
- Whipple, F. L. and Z. Sekanina (1979), "Comet Encke: Precession of the Spin Axis, Nongravitational Motion, and Sublimation", *Astron. J.* **84**, 1894-1909.
- Wilhelm, K., C. B. Cosmovici, W. A. Delamere, W. F. Huebner, H. U. Keller, H. Reitsema, H. U. Schmidt and F. L. Whipple (1986), "A Three-Dimensional Model of the Nucleus of Comet Halley", in *Proceedings of the 20th ESLAB Symposium on the Exploration of Halley's Comet*, ESA Pub. Div., The Netherlands, Vol. II., p. 367-369.
- Woods, T. N., P. D. Feldman, K. F. Dymond and D. J. Sahnou (1986), "Rocket Ultraviolet Spectroscopy of Comet Halley and Abundance of Carbon Monoxide and Carbon", *Nature* **324**, 436-438.

Chapter 9 - Dynamically New Comets

9.1 Introduction

The main goal of the research up to this point has been to develop a simple water-ice sublimation model for comet P/Halley based on ground-based observations made when the comet was at large heliocentric distances, $R \geq 5$ AU. It is when comets are at large R , beyond the distance where H_2O sublimation is significant, that they are potentially the most interesting because it is only then that we may hope to observe the nucleus. The model was able to successfully show that for P/Halley, the sublimation from a water-ice nucleus explained the onset of activity which produced a sustained coma near $R = 5.9$ AU. Furthermore, the model was used to place constraints on several physical characteristics of the nucleus. It is the aim of this chapter to compare the Halley model to a less well studied group of comets which are active at distances where water-ice sublimation is negligible ($R > 6$ AU). It is hoped that such comparison will provide some insight into the nature of the activity in these distant comets.

Oort's (1950) deduction of the existence of a large reservoir of comets with aphelia between 50,000 and 150,000 AU was based upon a small sample of comets ($N = 19$) for which "original" orbits were well determined (with an average mean error in the reciprocal of the semimajor axis, $1/a$, of $\pm 30 \times 10^{-6}$ AU $^{-1}$). The term "original" orbit refers to the orbit of the comet prior to the effects of planetary perturbations as it approaches perihelion. For comets with very large a , only an extremely small fraction of the orbit is ever observed; therefore, the effect of planetary perturbations can be accurately calculated only for the passage through the inner Solar System at the time of discovery. According to Oort's theory, comets are scattered into the inner Solar System as a result of gravitational perturbations associated with the passage of nearby stars. In order to reconcile the observed distribution of $1/a$ with the scattering theory, Oort (1950) and Oort and Schmidt (1951) made the assumption

that the dynamically new comets (those just perturbed into the inner Solar System) subsequently fade after their first passage and are no longer observable, presumably due to a loss of highly volatile ices. If real, this fading would imply a basic difference between short period comets such as P/Halley, and the dynamically new comets. On the basis of this assumption it would therefore be expected that dynamically new comets would be exceptionally bright and active at large R , perhaps due to sublimation of ices more volatile than water, and that there would be a significant pre- to post-perihelion brightness asymmetry for the dynamically new comets.

In order to embark upon any systematic study of the photometric behavior of the dynamically new comets as a class, it is necessary to summarize what is known about them. In this regard, two important questions must be addressed. First, what evidence is there that the dynamically new (hereafter referred to simply as "new") are different from old, more evolved comets? Second, what are the morphological and physical characteristics of comets active at large distances from the sun?

9.1.1 Differences Between New and Old Comets

There is conflicting evidence with regard to the fading of the new comets, or the differences in brightness of new versus old comets. As was mentioned in Chapter 1, one of the pieces of evidence suggesting that water ice is a main constituent in most comets is the fact that the non-gravitational accelerations caused by irregular outgassing from the nucleus vary as a function of R in a manner which is consistent with water ice sublimation. Such perturbations on the orbit are random and tend to destroy the ability to compute an accurate orbital history, hence original orbit for a comet. Marsden and Sekanina (1973) have since re-examined the distribution of original semimajor axes, selecting only those comets with perihelia, q , beyond 3 AU since the nongravitational forces are negligible beyond this distance

(Marsden *et al.* 1973). They found that the clustering of $1/a$ corresponds to an aphelion distance of 50,000 AU, at the low end of the range suggested by Oort. The consequence of decreasing the size of the Oort cloud of comets is that the change in the cometary orbital velocity caused by the passage of a star is much smaller than previously thought; probably insufficient to bring a comet directly from the Oort cloud into the region of the Solar System in which the orbit may be affected by planetary perturbations. As summarized by Weissman (1986), comets which come into the observable region may already have perihelia near the region of the outer planets. Consequently, new comets may lose their highly volatile constituents prior to ever reaching a region of observability. There would therefore be no reason to expect a brightness difference between the new and old comets.

In a subsequent paper, Marsden *et al.* (1978) computed new osculating orbits (depending only on the gravitational attraction of the sun, and referred to the date of perihelion passage) for 110 comets and used these with additional orbital determinations to compute the original and future orbits for 200 comets. The sample of comets included those for small q ; the modifications due to the nongravitational forces were considered. They divided the computation into two accuracy classes depending upon (1) the mean error of $1/a$, (2) the time span of the observations determining the orbit and (3) the number of planets whose perturbations were taken into account. They found a significant difference in the relative numbers of new and old comets between the two classes. In the class where the orbits were the most accurately known, class I, as many as 55% of the comets were new, whereas in class II the fraction of new comets fell to about 21%. The definition of a new comet was somewhat arbitrarily given as those comets for which $(1/a)_{orig} < 100$ (in units of 10^{-6} AU). The larger proportion of old comets in class II, where the orbits were less accurate, was interpreted as evidence for fading by Marsden *et al.* (1978). If a comet fades substantially after its first passage through the inner Solar System it will be observed over a smaller portion of its orbit on successive passages, hence a greater probability of inclusion in class II.

Delsemme (1985), on the other hand, suggested on the basis of the lightcurves of 11 comets, that the new, quasi-new and short period comets are not substantially different from each other in the sense that their sublimation is all controlled by water. He asserted that this is evidence that the new comets are not fresh from the Oort cloud but have spent several revolutions slowly diffusing into the inner Solar System. Delsemme evaluated the nature of the sublimation by determining r_o for each comet, the characteristic heliocentric distance which separates the sublimation steady state from the radiative steady state. The quantity r_o is defined to be that distance at which the solar energy spent in re-radiation is approximately 40 times that spent in sublimation (Marsden *et al.*, 1973). That is, for distances beyond r_o , energy spent in sublimation is less than 2.5% the energy spent in re-radiation and the sublimation drops rapidly. Delsemme determined the value of r_o by comparing the lightcurves to the best fit water ice vaporization curves and finding the distance at which the comet was 4 magnitudes fainter than an extrapolation to the inverse square law behavior for sublimation at small heliocentric distances.

There are several problems with the interpretation made by Delsemme. The comets that he selected were chosen because the observations in each case were made by a single observer (Beyer or Bobrovnikoff). This avoided difficulties with systematic errors, however, most of the comets were observed over a very limited range of heliocentric distances. In fact, in over 60% of the cases, r_o was determined by extrapolation. Furthermore, even with data from a single observer, there was sufficient scatter in the data that a few points could substantially influence the fits for r_o . Finally, Delsemme did not include any comets in his sample which were known to be active at distances where water ice sublimation would *not* be significant. With the exception of comets P/Halley, Kohoutek (1973 XII) and Delavan (1914 V) which were observed near 4 AU, all of the other comets were not observed beyond about $R = 2.5$ AU. It seems, therefore, that his results are not conclusive.

Interestingly, Whipple (1978) analyzed a set of observations made by Beyer and

Bobrovnikoff which included the same sample as the data used by Delsemme (1985), and concluded that the brightness variations as a function of R were *different* for the new and old classes of comets (precisely the opposite of the conclusion reached by Delsemme!). Unfortunately, the rate of brightening was measured using a parameter, n , as determined from

$$H_o = H + 5 \log (\Delta) + 2.5 n \log (R) \quad (9.1)$$

where H_o is the observed magnitude, and H is the absolute magnitude at unit R and unit Δ , the geocentric distance. The value of n was determined from a least squares solution for H and n from Eq. (9.1) over whatever range of R and Δ the observations were made. Eq. 9.1 is a non-physical representation of the brightness variations of a comet as a function of distance from the sun. The value of n is a function of the range of R over which the observations are made. At the distances at which radiative steady state dominates, the comet obeys approximately an inverse square law, hence $n = 2$. When sublimation becomes significant the dependence of brightness with R becomes much steeper. The point at which the transition between the two regimes occurs depends on many parameters such as albedo, rotation rate, nucleus size, etc. (see Chapter 2 for a complete discussion for the particular case of comet P/Halley). Since no attempt was made to determine n over the same range of R for each comet, it is impossible to interpret the results as showing a systematic difference in the behavior of new versus old comets.

Kresák (1977), like Delsemme (1985) submitted that there is no difference between the new and the old comets with regard to absolute brightness, change in brightness as a function of R , asymmetric light curves, spectral characteristics (dust to gas ratio) or morphology of the dust tails. Kresák maintained that in previous analyses where differences between the two groups of comets were noted, selection effects biased the results. Also, Roemer (1962) stated that "comets moving in nearly parabolic orbits do not differ in any fundamental way

from those of the Jupiter family that move in ellipses of short period . . . objects that brighten slowly with decreasing heliocentric distance and objects that brighten more rapidly may be found among either short-period or parabolic comets". Finally, with respect to the ratio of the dust to gas production in new versus old comets as determined spectroscopically, Donn (1977) concluded from the analysis of 85 comets that there is no evidence for a systematic difference between the new and the old comets.

It would appear from the above discussion that there is no conclusive evidence either for or against a claim that there is a systematic difference between the new and the old classes of comets. Part of the difficulty lies in the fact that all of the cometary observations comprise a very heterogeneous set of data which is plagued by observational selection effects which are extremely difficult to take into account. Some of the effects which can bias the data include:

- ◇ Absolute brightness of comet
- ◇ Cometary orbital characteristics
- ◇ Variations in the method of brightness measurement (nuclear magnitude as opposed to total integrated magnitude which depends on the aperture size used, etc.) - brightness estimates for a particular comet can vary by over a factor of 100 depending on the observer and type of measurement made.
- ◇ Different telescope/detector/filter combinations
- ◇ Improvement in instrumentation/techniques as a function of time
- ◇ Uneven geographical distribution of observers (affecting comet discovery and range of R over which the comet is observed) - particularly noteworthy is the preponderance of observers in the northern hemisphere
- ◇ Weather
- ◇ Social Factors (popular interest in a particular comet, events which interrupt observations).

With the present increase in computational ability and the existence of a fairly sizeable set of accurately determined original orbits, it is useful to re-examine the question regarding differences between the new and old comets. It is possible to reduce the severity of one of the

major selection effects, namely the variation in the method of brightness measurement. This can be done by examining the farthest distance at which a comet was last detected. This transforms an uncertain magnitude determination into a simple yes/no value which is a much less sensitive function of the observer.

Figure 9-1a shows the result of plotting the farthest heliocentric distance at which comets on *nearly parabolic orbits* were observed versus time. The orbital data are from Marsden *et al.* (1978) and Everhart and Marsden (1983, 1987) who present original and future orbits for 251 comets, 137 of which fall into the class I accuracy category. The figure shows only class I comets with perihelion passage dates after 1900. The approximate heliocentric distances corresponding to the dates of observation for each comet (found in the extensive compilation by Kronk (1984)), were computed from a 2-body ephemeris program utilizing the orbital elements from Marsden's (1986) *Catalog of Cometary Orbits*. The vertical bars on the data in Figure 9-1a do not represent errors in the distances; rather the length of the bar is 0.1 times the perihelion distance in AU. The effect of the bars is to add a third dimension to the figure. The data for the new comets [$(1/a)_{orig} < 100$] is presented in the top panel of Figure 9-1a and the data for the old comets [$(1/a)_{orig} > 100$] is presented in the bottom panel. Because the division between the new and the old comets is somewhat arbitrary, Figure 9-1b illustrates the effect of assuming that the new comets have orbits where $(1/a)_{orig} < 500$. There is no substantial difference between the two figures, except that many of the large q comets in the [$(1/a)_{orig} > 100$] group of Figure 9-1a are now found in the [$(1/a)_{orig} < 500$] group of Figure 9-1b.

Figure 9-1 quite clearly shows a difference between the dynamically old and new populations. The scatter in both populations of comets is due in part to intrinsic brightness differences among the comets and also to selection effects. The effect of improved instrumentation and techniques is seen in the top panel where there is a general increase with time in the distance at which the last observations of a comet are made. It is significant that

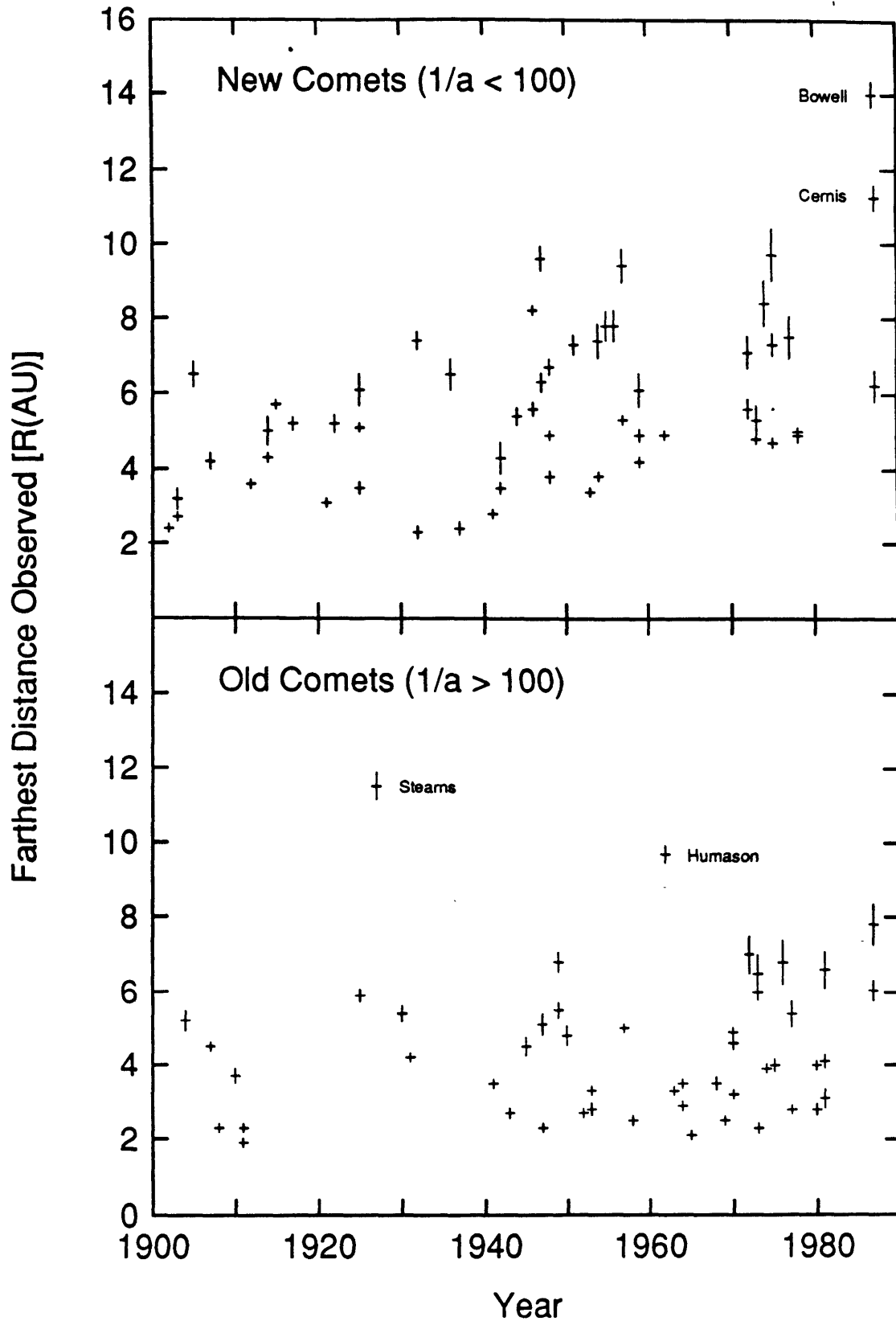


Figure 9-1a. Farthest heliocentric distance at which the comet was observed versus date (years) for 107 comets with nearly parabolic orbits. The upper panel plots the dynamically new comets for which $(1/a)_{orig} < 100$; the lower panel shows the old comets for which $(1/a)_{orig} > 100$. The quantity $(1/a)$ is in units of 10^{-6} AU. See text for discussion.

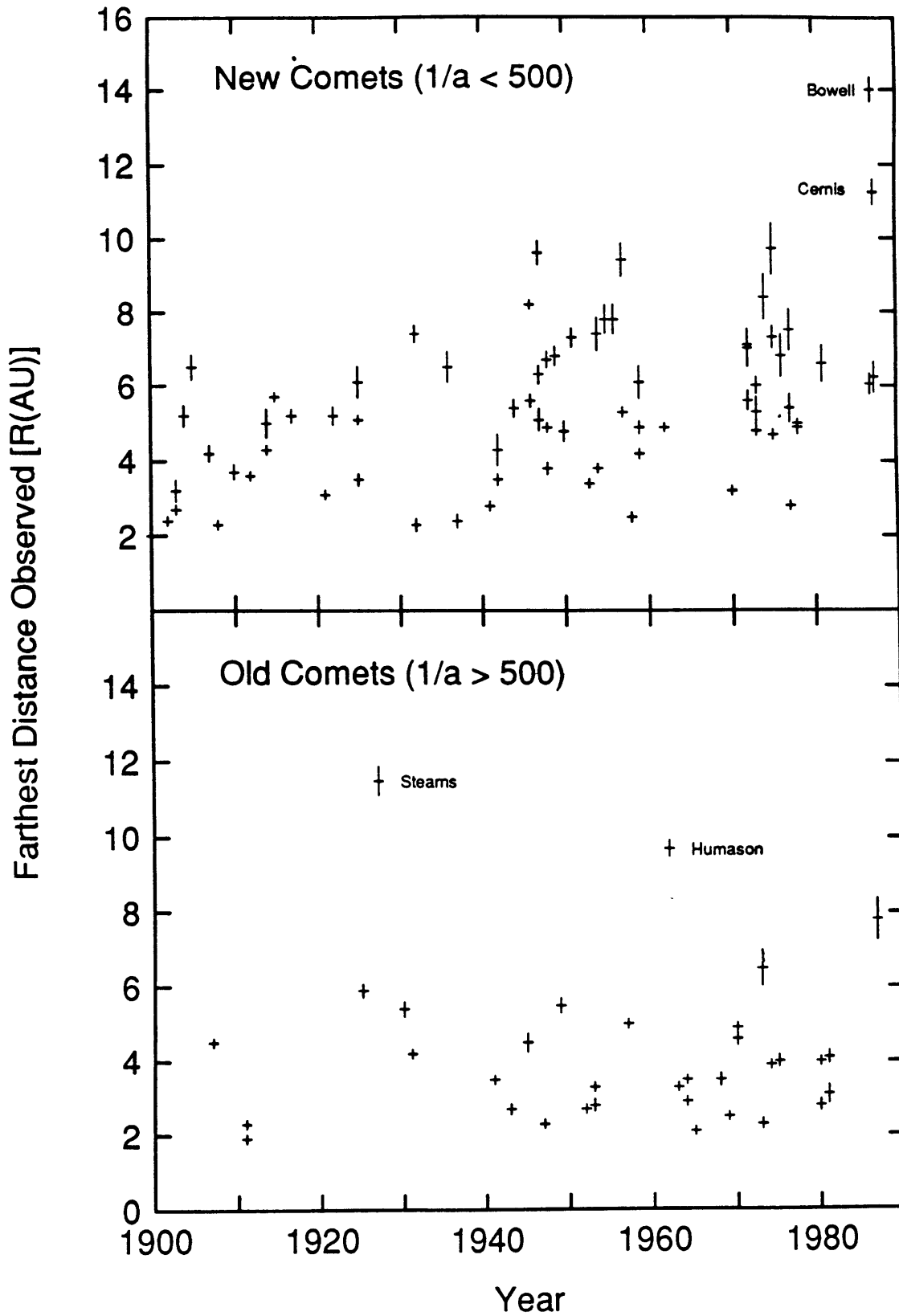


Figure 9-1b. Same as Figure 9-1a, except the division between the new and the old comets is at $(1/a) = 500$ in units of 10^{-6} AU.

this trend is less conspicuous in the bottom panel. The fact that there are a number of old comets (between 1960 and 1980) which were observed out to distances of only 2 - 4 AU and the absence of such a group in the new comets, suggests that the old comets tend to be intrinsically fainter. In general, all of the comets with large q are observed to larger distances than those of small q . Because comets at large q are never at small R , in order to observe them at all, they must be exceptionally bright. Approximately 34% of the new comets shown in Figure 9-1a have $q > 3$, whereas the same number for the old comets is near 14%. When considering the comets in Figure 9-1b, these numbers become 33% and 9%, respectively. Apparently there are many more exceptionally bright new comets than old comets, in agreement with the conclusion of Marsden *et al.* (1978). It is worth noting that it is near 3 AU that a rapid increase in water ice sublimation is expected (although as was seen in Chapter 2, H₂O sublimation can begin at $R \approx 6$ AU). The mean farthest distance seen for the new comets in Figure 9-1a is $R = 5.5$ AU and for the old comets $R = 4.3$ AU ($R = 4.1$ AU if the unusual cases of comet Stearns 1927IV and comet Humason 1962VIII are not included). More than 1/3 of the new comets are observed beyond 6 AU whereas only about 1/10 of the old comets are. Apparently many more new than old comets are observed beyond the distances where H₂O ice sublimation is expected to cause activity, suggesting that there is a different mechanism for activity in these comets.

9.1.2 Characteristics of Comets Active at Large Heliocentric Distances

Now that the possible existence of a brightness difference between the new and the old comets as a class has been suggested, it is reasonable to address the question of whether or not there are particular physical or morphological characteristics which can be used to discriminate between the two classes. Furthermore, is there a difference between the old comets which are active at large distances (say $R > 6$ AU) and the dynamically new comets

active at large distances? The answer to this question will address the fundamental problem of whether the nature of the activity seen in comets at large distances (beyond the H₂O sublimation zone) is the same for the two groups of comets. Ultimately, the goal is to determine whether or not the comets first entering the inner Solar System from the Oort cloud are compositionally different from the periodic comets. Table 9-1 presents a summary of the characteristics of comets in nearly parabolic orbits which are active beyond about 6 AU. The comets in the table comprise a subset of the class I comets used in Figures 9-1a and 9-1b, and include both the new and old comets. The name and the designation is given for each comet in column 1, in addition to the years during which the comet was observed. The approximate date of perihelion passage, $T(\text{yr})$, and the perihelion distance, q (in AU), as obtained from Marsden (1986) are listed in columns 2 and 3. The values of $(1/a)_{orig}$ from Marsden *et al.* (1978) and Everhart and Marsden (1983, 1987) are listed in column 4. In column 5 an estimate of the distance of the formation of the tail is given based on the dynamical analysis of Sekanina (1975) and the descriptions found in Kronk (1984). The values from Sekanina are enclosed in parentheses because they are computed as opposed to observed quantities. Finally, in the last column are additional comments which relate to the activity. Although the table includes both new and old comets, nearly 80% of the comets listed have $(1/a)_{orig} < 500$.

The most obvious characteristic common to all of the comets in Table 9-1 is that they possess comae and in many cases tails out to very large distances. Roemer (1962), Belton (1965) and Sekanina (1975), among others, have all commented upon the fact that the dust tails of distant comets exhibit a peculiar appearance. The tails are nearly parallel sided and very narrow, the width of the tail being determined by the width of the coma. The coma in these specific cases tends to be sharply bounded at the head of the comet; the transition to the low surface brightness tail is quite abrupt. Figure 9-2a shows three of the dynamically new comets (Stearns 1927VI, Baade 1955VI and Wirtanen 1957VI) from Table 9-1 which possessed tails of this type.

Table 9-1
Characteristics of Comets Active at Large Distances

Comet	T [years]	q [AU]	$(1/a)_{orig}$ $\times 10^6$ AU	Tail	Other observations
Kohoutek (1973 XII) (1973-1974)	1973.99	0.142	20	< 4.2 AU	Found \approx 5.1 AU, mag 16 with coma. Last obs. @ 4.8 AU, near mag 22
Morehouse (1908 III) (1908-1909)	1908.98	0.945	174	> 2.1 AU	CO ⁺ dominated spectrum
Mellish (1915 II) (1915-1916)	1915.54	1.005	75	> 2.6 AU	mag \approx 16 @ 5.7 AU nucleus split in 1916 fan shaped tail
Jones (1946 VI) (1946-1948)	1946.82	1.136	44	\approx 7.7 AU	last obs at 8.2 AU
Wilson (1983I) (1986-present)	1987.30	1.200	30		Discovered at R=3.6AU with bright coma.
Ikeya-Seki (1968 I) (1967-1969)	1968.15	1.697	842	> 2.1 AU	last obs \approx 6.7 AU w/coma
Pajdusakova-Mrkos (1948-1950) (1948 V)	1948.37	2.107	34	> 5.6 AU	last obs \approx 6.7 AU w/coma
Humason (1962 VIII) (1961-1965)	1962.94	2.133	4935	> 5.6 AU	CO ⁺ dominated spectrum ion tail at 3.1 AU outbursts near 6 AU last obs \approx 9.7AU w/coma
Baade (1922 II) (1922-1924)	1922.82	2.259	21	> 5.2 AU	
Geddes (1932 VI) (1931-1934)	1932.72	2.314	45	(5.5 AU)	last obs \approx 7.4 AU w/coma
Wirtanen (1949 I) (1948-1951)	1949.33	2.517	498	> 3.9 AU	last obs at 6.8 AU
Minkowski (1951 I) (1950-1953)	1951.04	2.572	37	(2.6-5.5AU)	last obs \approx 7.3 AU w/coma 20 arcsec across

Table 9-1, contd.
Characteristics of Comets Active at Large Distances

Comet	T [years]	q [AU]	$(1/a)_{orig}$ x 10 ⁶ AU	Tail	Other observations
Shoemaker [†] (1985 XII) (1984-present)	1985.68	2.696	487	> 6 AU	extensive coma and tail at 4.9, 6 AU
Lovas (1975 VIII) (1974-1977)	1975.64	3.011	36	> 4.8 AU	last obs ≈ 7.3 AU tail faint & broad
Wirtanen (1947 VIII) (1948-1950)	1947.67	3.261	34	> 4.9 AU	Last obs @ 9.6 AU
Gehrels (1971 I) (1972-1973)	1971.02	3.277	1582	≈ 7.4 AU	never brighter than 16
Thomas (1969 I) (1968-1971)	1969.03	3.316	1502	(3.3 AU)	last obs ≈ 8 AU, diffuse
Cernis (1983 XII) (1983-present)	1983.55	3.318	78		coma at 9 AU, 11.25 AU (R = 11.6 July 1987)
Kopff (1905 IV) (1904-1907)	1905.79	3.340	28	> 3.6 AU	last obs = 6.4 AU diffuse, at mag near 16 nucleus split in 12/1905
Bowell (1982 I) (1980-present)	1982.19	3.364	30	(12 AU)	a ≈ 300-400 μm, low vel narrow tail, obs ≈ 14 AU
Stearns (1927 IV) (1927-1931)	1927.22	3.684	623	6 AU (3.9-5.6AU) narrow	coma to >11 AU, last obs at 11.5 AU. C ₂ obs near 4 AU (van Bies., 1927b)
Baade (1955 VI) (1954-1957)	1955.61	3.870	42	> 5 AU (4-12 AU) (12-30? AU)	a > 100 μm, low velocity last obs ≈ 7.8 AU, diffuse narrow tail
Hartley (1985 XVI) (1984-present)	1985.74	4.000	35		obs. @ 6 AU, diffuse
Van Biesbroeck (1936 I) (1935-1938)	1936.36	4.043	19	(≈ 4 AU)	last obs ≈ 6.5 AU, diffuse

Table 9-1, contd.
Characteristics of Comets Active at Large Distances

Comet	T [years]	q [AU]	$(1/a)_{orig}$ x 10 ⁶ AU	Tail	Other observations
Haro-Chavira (1956 I) (1954-1958)	1956.07	4.077	39	> 5 AU (6-15? AU)	a > 100 μ m, low velocity narrow tail, 7AU diffuse
Shajn-Comas-Solá (1925-1927) (1925 VI)	1925.68	4.181	35	none	Last obs. @ 6AU-diffuse total mag near 16
Humason (1959 X) (1960-1961)	1959.94	4.267	40	> 4.6 AU	Last obs \approx 6.1 AU, diffuse narrow tail
Sandage (1972 IX) (1972-1974)	1972.87	4.276	69	> 4.5 AU (4-8 AU)	last obs. \approx 7.1 AU, diffuse
Wirtanen (1957 VI) (1956-1960)	1957.67	4.447	17.	> 6 AU (>7 AU)	Last obs. @ 9.4 AU mag near 10 @ 4.5 AU Nucleus split at 4.9 AU
Abell (1954 V) (1955-1956)	1954.23	4.496	82	> 7.4 AU (5-7.3 AU)	Last obs \approx 7.4 AU, diffuse
Elias (1981 XV) (1981-1983?)	1981.63	4.743	142	> 5 AU	narrow parallel tail last obs \approx 5-6 AU
Sandage (1973 X) (1973-1975)	1973.85	4.812	536	> 4.8 AU	last obs \approx 6.5 AU diffuse
Araya (1972 XII) (1972-1975?)	1972.97	4.861	476	> 4.9 AU	obs @ 7 AU mag \approx 16
Shoemaker [†] (1984 XV) (1984-present)	1984.68	5.489	1624	> 7.8 AU	at R=7.8 AU coma (R = 9.0 July 1987)
West (1977 IX) (1976-1979)	1977.55	5.606	33	> 7.5 AU	fan-shaped tail last obs \approx 7.5 AU, tail
Lovas (1976 XII) (1977-1978)	1976.83	5.715	142	> 6.8 AU	last obs \approx 6.8 AU with possible fanned tail
van den Bergh (1974-1976) (1974 XIII)	1974.60	6.019	11	> 6.8 AU	last obs \approx 8.4 AU, diffuse

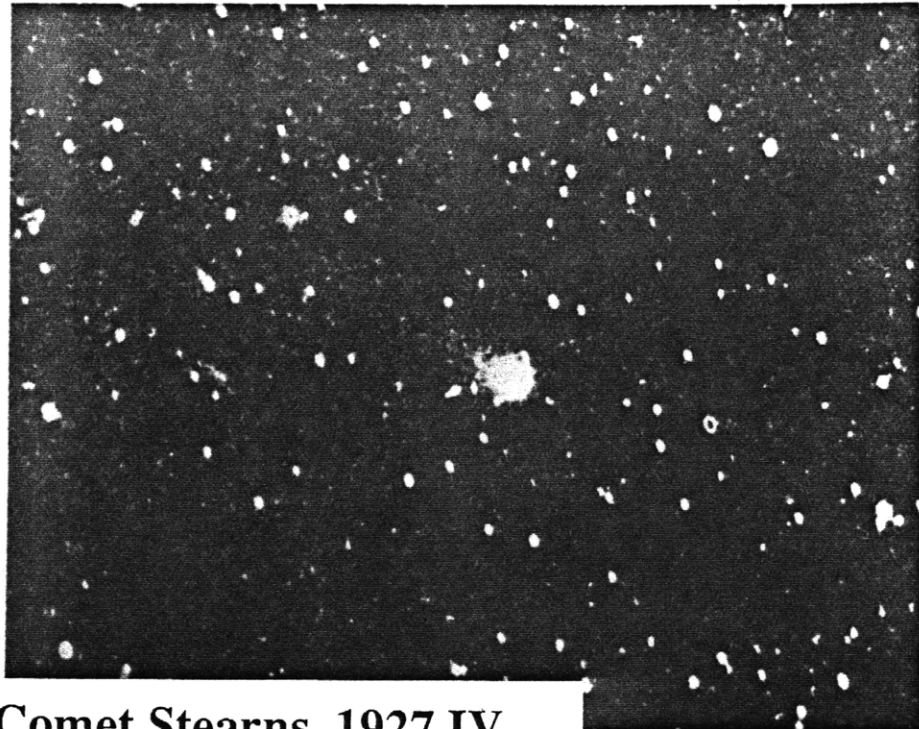
Table 9-1, contd.
Characteristics of Comets Active at Large Distances

Comet	T [years]	q [AU]	$(1/a)_{orig}$ x 10 ⁶ AU	Tail	Other observations
Schuster (1975 II) (1976-1978)	1975.04	6.881	51	> 9.7 AU	last obs ≈ 9.7 AU, tail narrow and faint
† Class 2 comets.					

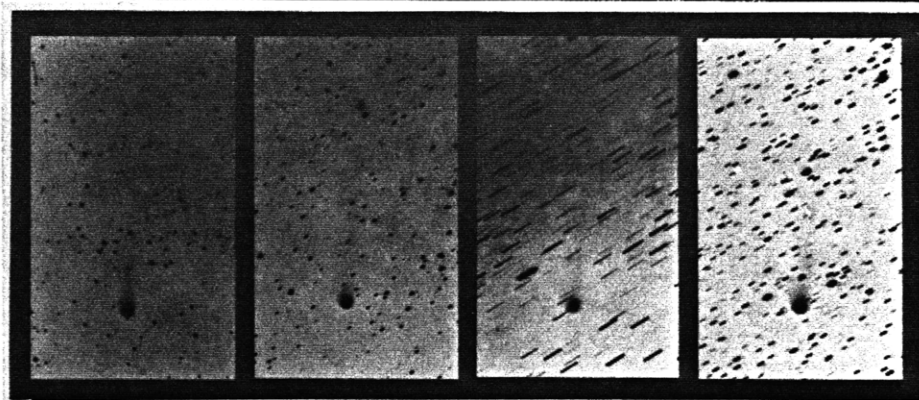
Although the tail of comet Stearns is difficult to see in the photograph, descriptions indicate that it was nearly identical in appearance to the tails of comets Baade and Wirtanen. Four more recently observed comets are shown in Figure 9-2b. All except comet Torres, which does not yet have a well-determined orbit, are dynamically new. Comets Elias and Bowell have particularly striking examples of the tail type discussed above. The tails are narrow and parallel sided, and the comae are sharply bounded - almost spherical. Comet Torres is very similar in appearance to comets Bowell and Elias; based on this and its brightness at $R = 3.6$ AU, it will not be surprising if this comet is active out to large distances. The coma and tail of comet Wilson is somewhat similar to those of the other three comets, but the coma is not as sharply bounded. It should be noted that this comet is at a smaller R , and has a much smaller perihelion distance ($q = 1.2$ AU) than do the other comets in this figure.

Sekanina (1975) has analyzed comets with this type of tail using the "Bessel-Bredikhin" mechanical theory to account for solar radiation pressure. Sekanina models the tails as a distribution of particles emitted at particular times (as opposed to a single particle size emitted continuously). He has shown for the well-observed comets Baade 1955 VI and Haro-Chavira

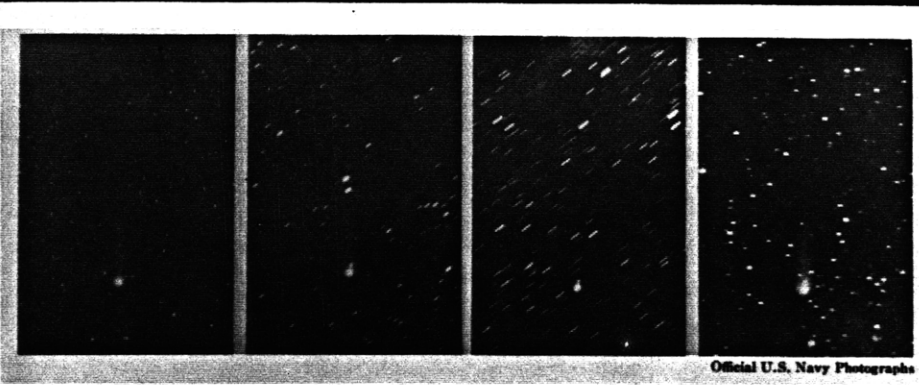
Figure 9-2a. Comparison of three "Oort comets" with tails at large R . The figure shows the form of the dust tails which are characteristic of comets active at large R . Table 9-8 lists specific information about the photographs. The comet Stearns (1927IV) photograph is reproduced from Van Biesbroeck (1927a) and comets Baade (1955 VI = 1954h) and Wirtanen (1957 VI = 1956c) from Roemer (1962).



Comet Stearns, 1927 IV

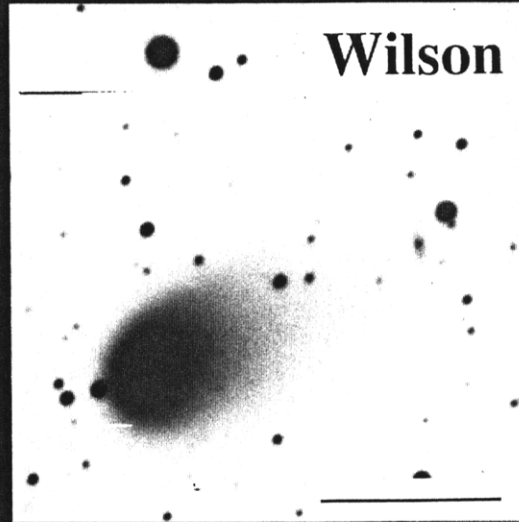


Comet Baade, 1955 VI

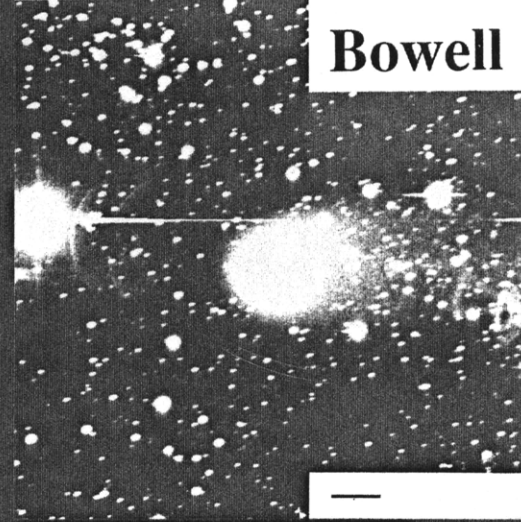


Comet Wirtanen, 1957 VI

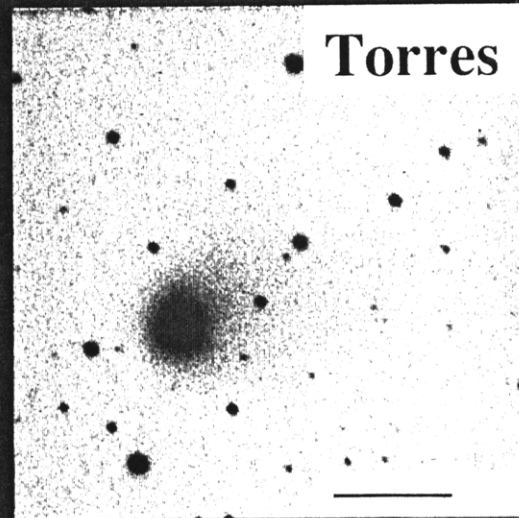
Figure 9-2b. Comparison of four more recent "Oort comets". The appearance of the coma is similar for all four comets (photo details in Table 9-8). Comet Torres does not yet have a well determined orbit, so it is not yet known to be dynamically new, although its brightness and morphology suggest that it may be new.



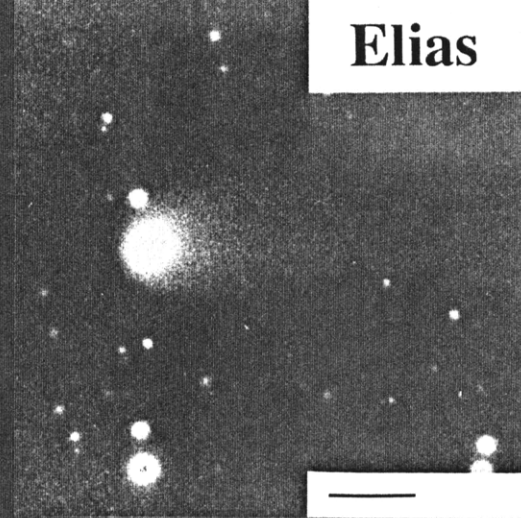
$R = 2.71 \text{ AU}$



$R = 3.37 \text{ AU}$



$R = 3.64 \text{ AU}$



$R = 5.06 \text{ AU}$

1956 I that the particles were subject to very little radiation pressure acceleration, less than 1% of the solar gravity. The ratio of the radiation pressure to the solar gravity is related to the particle size by :

$$\frac{F_{rp}}{F_g} \equiv \beta = 5.73 \times 10^{-4} \frac{Q}{a_g \rho} \quad (9.2)$$

where ρ [kg m^{-3}] is the particle density, Q is the radiation pressure efficiency and a_g [m] is the particle radius (for a derivation of Eq. 9.2 see the discussion in Appendix 5). Given typical icy grain densities (and assuming $Q \approx 1$), Sekanina concluded that the tail grains were large ($a_g \approx 100 \mu\text{m}$). His dynamical analysis of the particle trajectories indicated that for many comets the tails were formed at very large distances (see Table 9-1). Furthermore, because the tails did not widen appreciably as a function of distance from the nucleus, Sekanina estimated that the grain ejection velocities, and therefore the particle velocity dispersions were very small.

To summarize Sekanina's conclusions, particles with a narrow size distribution (\approx few hundred μm) ejected within a limited range of times at low velocity, give rise to the characteristic appearance of the narrow, parallel-sided tails. Sekanina infers that the grains are dragged into the coma by sublimation of ices more volatile than water. Although the list of comets in Table 9-1 which have the parallel-sided tail is incomplete, there are trends which *suggest* that this type of tail is a characteristic of the distant comets, in particular those with large q . The comets with the characteristic tails are shown in Table 9-2, in addition to the comets whose tails were definitely *not* parallel-sided.

Sekanina (1975) maintained that "the occurrence of the characteristic tail in an incoming comet depends on the availability of highly volatile materials at the surface of the comet's nucleus, and therefore on the circumstances at the formation of the comet and during its past

evolution, but definitely not on the distance the comet will reach at perihelion". However, there appears to have been no case of a small q comet observed at large R which had this type of tail (see for example comet Wilson in Figure 9-2b). Based on the particular example of comet Kohoutek 1973 XII, Sekanina attributes the lack of a tail to the fact that for a small q comet the tail is projected along the solar radius vector and therefore in the line of sight as seen from Earth. It is not clear that this is always the case for small q comets. All of the comets in Table 9-2 have $(1/a)_{orig} < 500$ with the exception of comet Stearns which has $(1/a)_{orig} = 623$. Although the list is probably incomplete, it is noteworthy that so many of the comets are new.

The connection between the narrow tails and comets active at large R must be approached cautiously, because although it appears that it may be an indicative property of comets which are active at large R , there is at least one example of such a tail on a short period comet. A narrow dust tail associated with P/Tempel 2 was discovered in the infra-red by the

Table 9-2
Comet Tail Types

Comet	q AU	$(1/a)_{orig}$ $\times 10^6$ AU	Comet	q AU	$(1/a)_{orig}$ $\times 10^6$ AU
Parallel-Sided Tail			Other Tail Type		
Bowell (1982 I)	3.364	30	Mellish (1915 II)	1.005	75
Stearns (1927 IV)	3.684	623	Lovas (1975 VIII)	3.011	36
Baade (1955 VI)	3.870	42	West (1977 IX)	5.606	33
Haro Chavira (1956 I)	4.077	39	Lovas (1976 XII)	5.715	142
Humason (1959 X)	4.267	40			
Wirtanen (1957 VI)	4.447	17			
Elias (1981 XV)	4.743	142			
Schuster (1975 II)	6.881	51			

IRAS satellite (Davies *et al.* 1984). A dynamical analysis of the tail by Eaton *et al.* (1984) indicated that the tail was comprised of sub-millimeter sized particles ejected at low velocity at least 1500 days prior to the IRAS observations (1983 July 12-18). This gives the ejection date as earlier than 1979 June. The tail may be associated with the 1978 December 22 outburst reported by Johnson *et al.* (1981).

All of the evidence thus far presented in the introduction provides a tantalizing suggestion that (i) the dynamically new comets are intrinsically brighter than the old comets, (ii) that the low ejection velocity narrow tails found on many large q comets *may* (but not necessarily) be indicative of sublimation from ices more volatile than water and (iii) that these tails are mostly associated with the new comets (with large q). A quote from Roemer (1962) strengthens these conclusions: "when a long-exposure photograph a few days after the discovery of Comet Humason, 1960e, revealed a tail of the characteristic appearance, I even went so far as to predict (correctly) that this comet was far from the sun and moving in an orbit with large perihelion distance". It would therefore seem from an observational point of view, that the comets which have these morphological characteristics at discovery should be carefully monitored as a function of R in order to ascertain the nature of the activity.

Prior to the recent apparition of comet P/Halley, very few comets were observed over a large range of R , and even fewer of these observations were made in a consistent manner by a single observer. It is therefore difficult to analyse historical observations of most of the distant comets. It is only recently that linear two dimensional detectors have become available which when combined with an increased interest in comet observations should enable some of these comets to be observed over large ranges in R . Of all of the comets on nearly parabolic orbits which have been discovered within the last decade, comet Bowell 1982I stands out. This comet is unusual because of the large number of observations which were obtained from discovery through perihelion in the UV, optical and near IR wavelength regions. Because of the large amount of observational data for this comet, it provides the best test for sublimation

models of ices more volatile than water. The remainder of this chapter will concentrate on the results of this type of modelling for comet Bowell.

9.2 Comet Bowell - Observations at 13.6 AU

Comet Bowell 1982I, discovered in 1980 at heliocentric distance $R = 7.3$ AU (Bowell, 1980), has the most hyperbolic orbit known (eccentricity, $\epsilon = 1.057$). This comet is dynamically new, with a value of $(1/a)_{orig} = 30$, and is probably making its first passage through the inner Solar System from the Oort cloud (Everhart and Marsden; 1983, 1987). The large eccentricity is due to an extremely close encounter with Jupiter. The major characteristics of 1982I as determined from observations around perihelion (1980-1984) are summarized in Table 9-3. The comet is known to exhibit substantial activity at distances beyond which H_2O sublimation is expected to be significant ($R \geq 6$ AU, see Chapter 2). Its lightcurve is quite different from that of P/Halley, in which the activity is controlled largely by H_2O sublimation (Meech *et al.*, 1986). There has been one reported detection of H_2O ice in the near infra-red spectrum of this comet (Campins *et al.*, 1983); however, the identification is controversial (A'Hearn *et al.*, 1984a). Other near infra-red spectra of this comet show no evidence for H_2O ice (Jewitt *et al.*, 1982; A'Hearn *et al.*, 1984a), and water-ice sublimation models are unable to reproduce the lightcurve (Jewitt, 1984). More volatile ices, typified by N_2 , provide a better (but not perfect) match to the near - perihelion photometry (Jewitt, 1984). The best match to the photometry is provided by an inert coma, however, the solid grain coma was found to expand at the very low velocity $v \approx 0.9 \pm 0.2$ m s⁻¹ (Jewitt, 1984; Sekanina, 1982). Sekanina (1982) uses dynamical analysis to estimate the ratio of the radiation pressure acceleration to the gravitational acceleration of particles in the tail; this indicates that comet Bowell has an unusual particle size distribution, with a deficiency of particles with radii $a_g \leq 300\text{-}400$ μm . Given the unusual properties of the comet and the likelihood that H_2O

**Table 9-3 - Comet Bowell Observations
Discovery through Perihelion**

Property	Value	Method	Reference
Grain Size	300-400 μm > 10 μm > 100 μm	Radiation Pressure IR obs / Mie calc. IR obs	Sekanina (1982) Jewitt <i>et al.</i> (1982) Hanner & Campins (1986)
Grain velocity	0.78 m s^{-1} 0.9 m s^{-1}	Tail width; length Coma expansion	Sekanina (1982) Jewitt (1984)
"Turn on"	R = 11-12 AU R \approx 10 AU	Tail length Coma expansion	Sekanina (1982) Jewitt (1984)
Composition	continuum R>5 AU	spectra (vis)	Cochran & McCall (1980) Jewitt <i>et al.</i> (1982) Johnson <i>et al.</i> (1984)
	no ice signature	near IR, CVF	Jewitt <i>et al.</i> (1982) A'Hearn <i>et al.</i> (1981) A'Hearn <i>et al.</i> (1984a) Campins <i>et al.</i> (1982)
	2.2 μm feature	CVF	Jewitt <i>et al.</i> (1982)
	OH R > 5 AU	photometry	A'Hearn <i>et al.</i> (1982) A'Hearn <i>et al.</i> (1984b)
	3.45 μm feature	near IR	Campins <i>et al.</i> (1983)
	CN etc. normal at q	spectra	A'Hearn <i>et al.</i> (1984b)
Grain albedo	0.06 - 0.14	near IR	Jewitt <i>et al.</i> (1982) Hanner <i>et al.</i> (1981)
Grain Temp.	140-155K (R=4-5AU) 174K (R=3.5 AU)	IR IR	Jewitt <i>et al.</i> (1982) Hanner & Campins (1986)
Nucleus Size	$p_v R_n^2 \leq 6 \times 10^6$	CCD photom.	Jewitt (1984)

sublimation was not responsible for its activity at $R \geq 6$ AU, an attempt was made to observe this comet at extremely large R in order to obtain information about the physical processes controlling the activity on the nucleus.

9.2.1 Observations

The present observations were obtained on UT 1986 November 3 with the Kitt Peak 2.1m telescope and an 800x800 Texas Instruments charge coupled device (CCD) at the $f/7.5$ focus. The chip was used in a 2 by 2 pixel averaging mode, giving a plate scale of 0.38 arcsec per 30 μm effective pixel and a field of view of about 2.5 arcmin. The ephemeris for comet Bowell was provided by Marsden (private communication, 1986). An extremely faint, low surface brightness object was identified as the comet by observing its motion with respect

Table 9-4
Observational Parameters

JD -2440000	UT (mid)	Exp [sec]	Tel [m]	Filter	χ Airmass	$\alpha(1950)$	$\delta(1950)$	R(AU) [§]	$\Delta(\text{AU})$ [§]	Phase [deg]
6737.6373	3:17:41	900	2.1	R	1.32	00:17:57.0 [†]	00:06:07	13.562	12.745	2.41
6737.6734	4:09:42	900	2.1	R	1.23	00:17:56.0	00:06:07	"	"	"
6737.7373	5:41:41	900	2.1	R	1.20	00:17:56.4	00:05:58	"	"	"
6737.7726	6:32:35	900	2.1	R	1.26	00:17:55.5	00:05:55	"	"	"
6329.9444	10:40:00	900	4	R	1.84	00:01:32.6 ^{††}	-01:38:46	11.006	10.003	0.20

[†] Positions as measured at the telescope offsetting from nearby SAO stars. The positions are accurate to approximately $\pm 5''$.

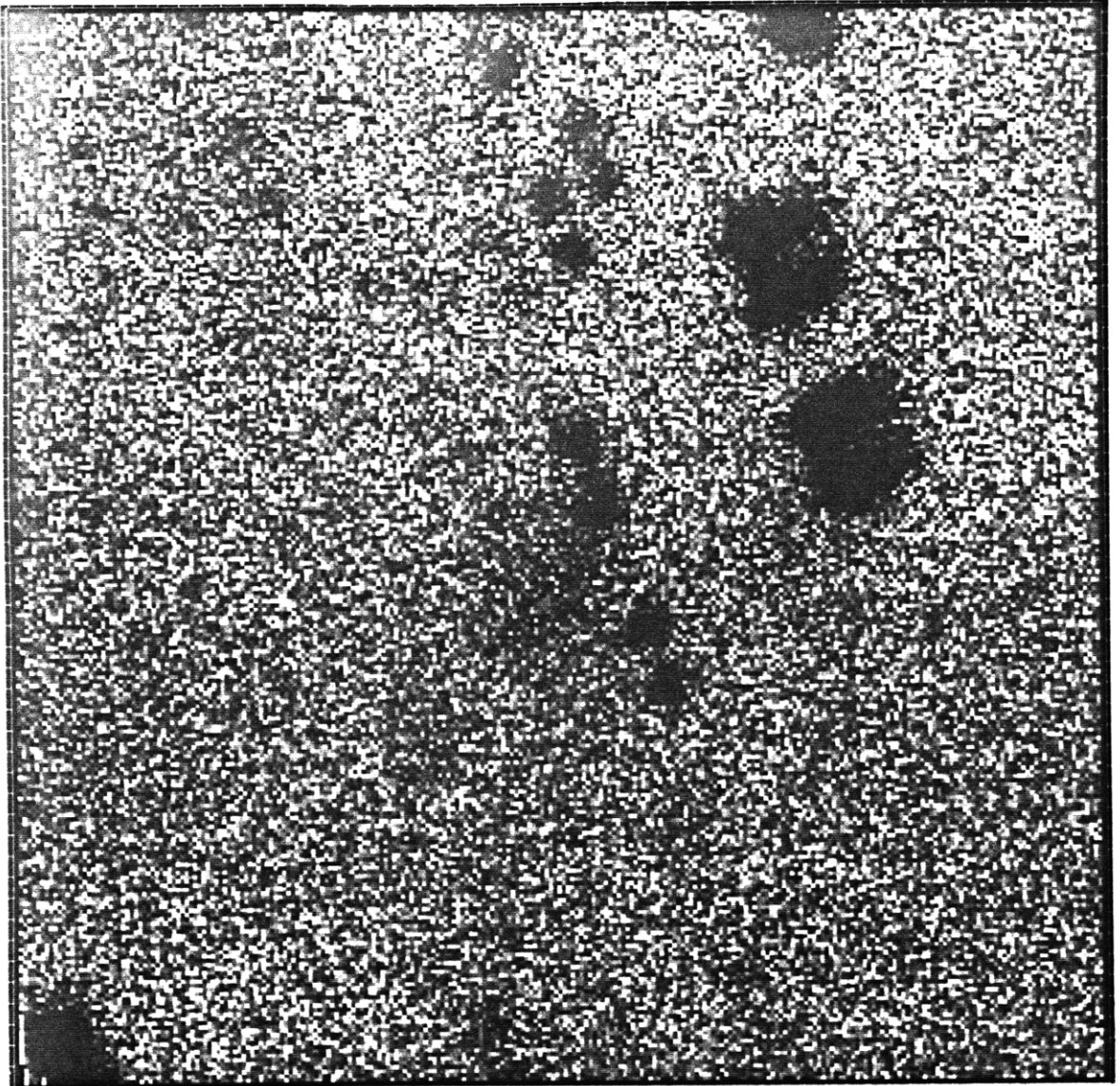
^{††} Positions accurate to approximately $\pm 30''$.

[§] As obtained from the ephemeris provided by Marsden.

to the field stars between exposures. Four images of 900 s each were taken through a Mould R filter, (an interference filter which avoids the red leaks associated with the broadband filters) with the telescope tracked at sidereal rate (see Table 9-4 for observational parameters). The seeing was estimated to be approximately 2.4 arcsec FWHM as measured from the radial profiles of stars. Extinction due to less than ideal photometric conditions was estimated to be no more than $\approx 10\%$. A background subtracted summed image of comet Bowell, made by shifting the individual images according to the ephemeris motion (giving an effective exposure of 1 hour), is shown in Figure 9-3a. Slight deviations in the flatness of the background in the image can make accurate magnitude estimates of an extremely low surface brightness object such as comet Bowell very difficult. For this reason a polynomial fit to the background has been subtracted from the image in Figure 9-3a. A line diagram of the same image showing the location of the comet with respect to trailed stars is given in Figure 9-3b. Unmarked diffuse features in Figure 9-3a are faint field galaxies. An additional observation of this comet was made on UT 1985 September 21 ($R = 11.0$ AU) using the Kitt Peak 4m telescope (see Table 9-3) during photometric conditions. The same CCD (TI#2) was used at the $f/2.6$ prime focus, yielding an effective plate scale of 0.29 arcsec per $15 \mu\text{m}$ pixel and a field of view of 3.9 arcmin on a side. The seeing during the observation was estimated at 1.2 arcsec FWHM. Comet Bowell appeared as a centrally condensed object with an extended diffuse coma. Unfortunately because only one image of the comet (through the Mould R filter) was obtained during the observing run, confirmation of the observation by observing the motion was impossible until 1986 October 30 when the field was re-imaged. The diffuse object seen at the 4m was not visible, confirming its identification with 1982I.

The brightness profile of the comet at $R = 13.6$ AU is shown in Figure 9-4. The brightness was measured as a function of projected distance from the nucleus along a line drawn perpendicular to the projected orbit. The orbit of comet Bowell lies nearly in the ecliptic (inclination $\approx 1.7^\circ$), therefore a profile measured perpendicular to the orbit plane will

Figure 9-3. (a) CCD image of comet Bowell at $R = 13.6$ AU, taken UT 1986 Nov. 3. Four 900 s images were shifted according to the motion of the comet, and a cubic spline was fit to the sky background near the comet and subtracted to produce this 1 hour effective exposure. North is to the left and East to the top. The comet appears diffuse, with a total integrated magnitude within a diaphragm of 15 arcsec radius of $m_R = 20.5 \pm 1.0$. The field of view of the image is approximately 100×100 arcsec. (See Table 9-8).



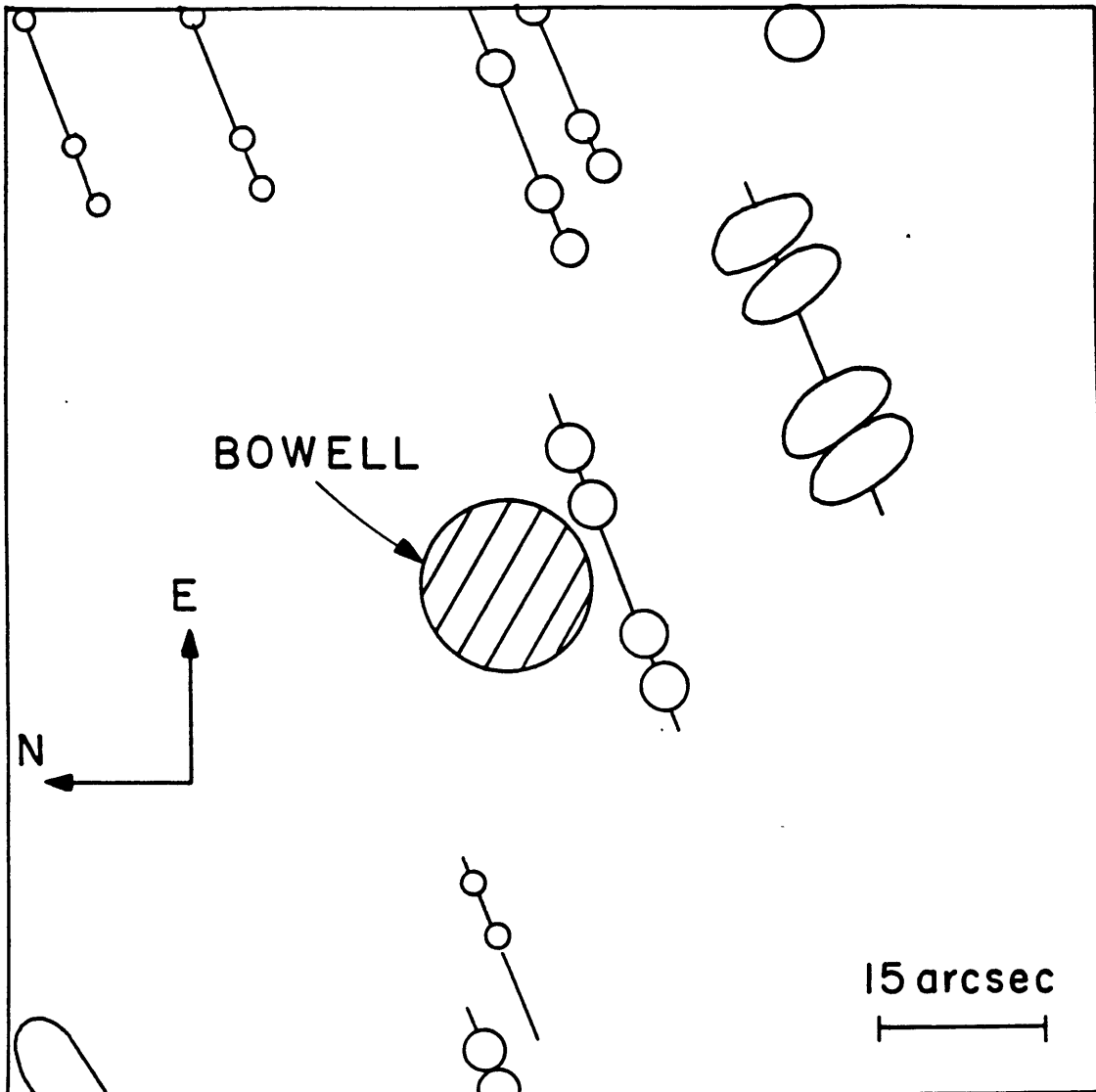


Figure 9-3. (b) Line diagram of Fig. 9-3a showing the location of the brighter field stars and galaxies with respect to the comet. The circle indicates the position but not the size of comet Bowell. A scale bar is shown for reference.

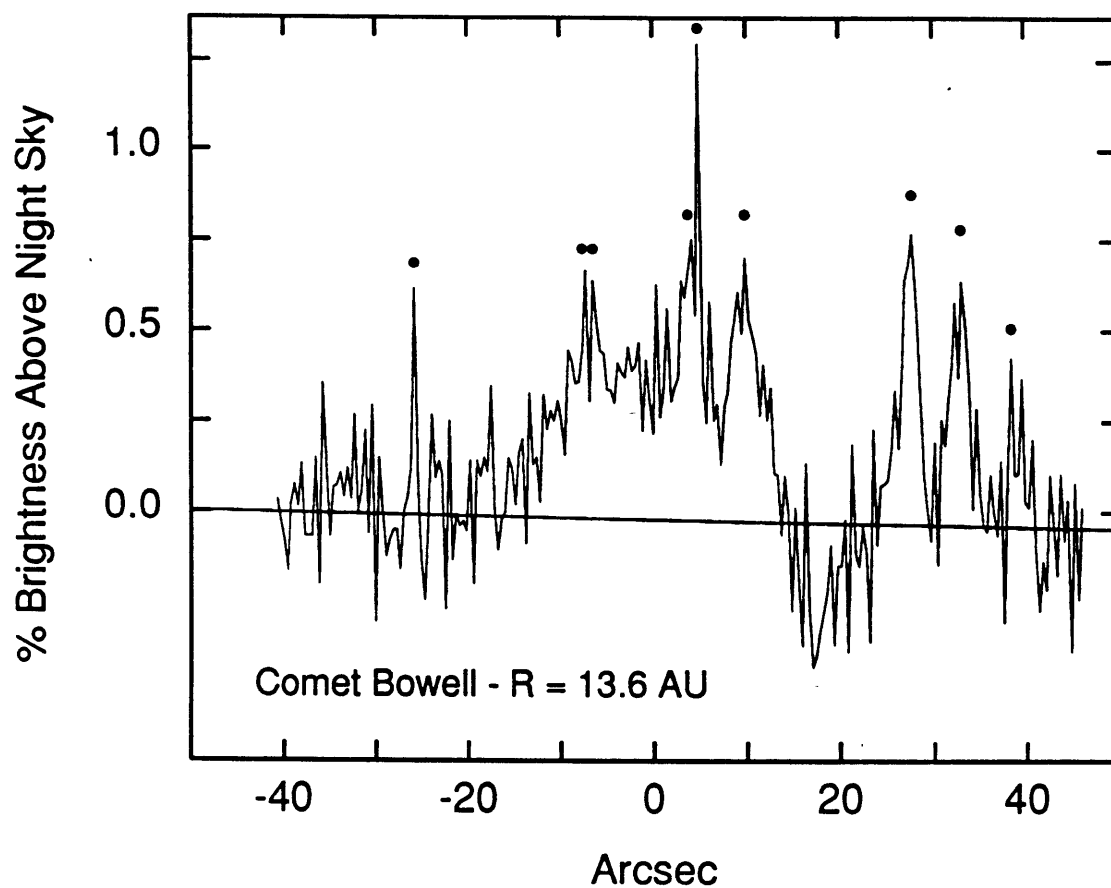


Figure 9-4. Surface brightness profile E-W through comet Bowell at $R = 13.6$ AU. The profile is the mean surface brightness within a band of width 7.6 arcsec centered on the comet. The level of the sky background is shown by a straight line. Several stars contaminate the profile; these are indicated by dots.

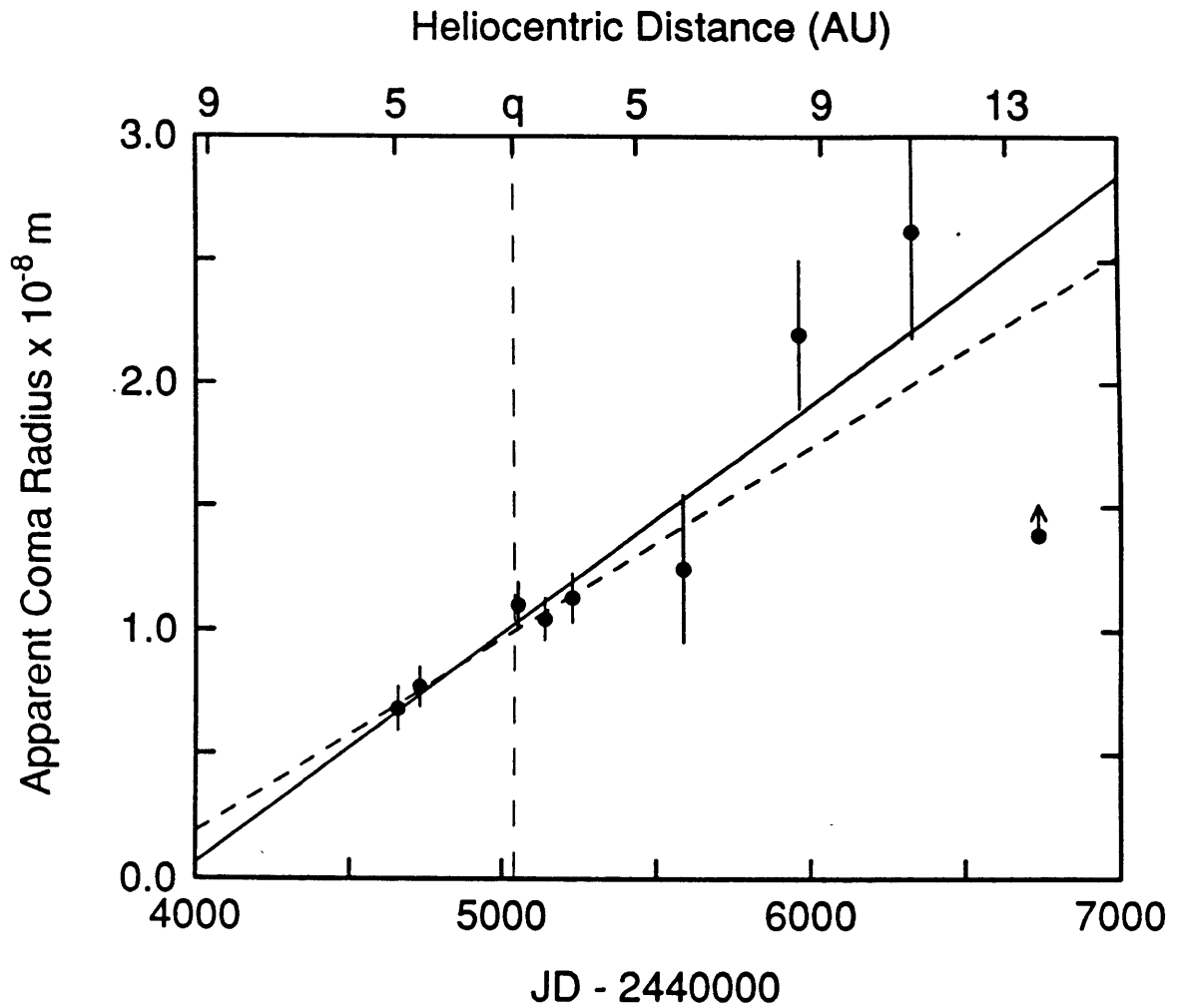


Figure 9-5. Plot of the coma radius versus JD and heliocentric distance. Perihelion ($q=3.364$ AU) is marked with a vertical line. The least squares fit to the radius prior to 1984 is shown as the dashed line, the fit including the new data is shown as the solid line. The velocity of expansion is $v = 1.1 \pm 0.2 \text{ m s}^{-1}$. The data point at $\text{JD} = 2446737.6$ represents a lower limit and is not included in the fit.

not be affected by radiation pressure since it will only accelerate dust along the line of sight. From Figure 9-4 an estimate of the lower limit of the radius of the coma is $P_{13.6AU} = 15 \pm 2$ arcsec. A similar measurement from the 4m image yields $P_{11.0AU} = 36 \pm 3$ arcsec. These and earlier radius measurements (Jewitt, 1984; Baum *et al.*, 1986) are plotted against the Julian Day Number (JD) in Figure 9-5. The large error bars assigned to measurements from Baum *et al.* (1986) reflect the fact that the radii were obtained from profiles which were computed in circular annuli centered on the nucleus instead of from cuts perpendicular to the orbital plane, and hence may contain the effects of radiation pressure. It is clear from Figure 9-5 that the coma size is not symmetric with respect to perihelion (represented by a vertical dashed line) as would be expected for a normal coma (Mendis & Ip, 1976). A least squares fit to the data in Figure 9-5 (excluding the lower limit at JD = 2446737.6) gives the coma expansion velocity $v = 1.1 \pm 0.2 \text{ m s}^{-1}$. The fit is shown as the solid line in Figure 9-5. There is good agreement with the previous best fit by Jewitt (1984) of $v = 0.9 \pm 0.2 \text{ m s}^{-1}$, shown as a dashed line in the figure. The inferred time of coma formation (the time at which the coma radius was zero) is $JD_0 = 2443934 \pm 900$ days ($R \approx 10$ AU), is also in agreement with previous determinations by Jewitt (1984) and Sekanina (1982).

The surface brightness of the coma of comet Bowell is < 1% of the surface brightness of the night sky in the R filter (see Figure 9-4), making accurate photometry extremely difficult. The best estimate of the magnitude within an aperture of radius 5 arcsec is $m_R(5'') = 21.7 \pm 1.0$ mag at $R = 13.6$ AU, where the large uncertainty is due to sky subtraction error and to variable extinction. At $R = 11.0$ AU the magnitude within an aperture of radius 5.0 arcsec is $m_R(5'') = 20.0 \pm 0.2$. As a matter of interest, a crude estimate of the *total* brightness of the coma can be computed. At $R = 11.0$ AU the brightness is $m_R \approx 17.9$ and at $R = 13.6$ AU $m_R \approx 20.5$; even at 13.6 AU the comet is not particularly faint, but its diffuseness makes it hard to detect. In previous observations, the grain cross section within a diaphragm of 5 arcsec radius remained constant (Jewitt, 1984) at $C = (1.6 \pm 0.3) \times 10^9 \text{ m}^2$ [where $C = 2.24 \times 10^{22}$

$R^2 \Delta \pi 10^{0.4(m_R(\text{sun})-m_R(5''))} / p$; and $p \approx 0.06$ (Hanner *et al.*, 1981) is the geometric albedo of the grains]. The new photometry shows that the total cross section has decreased by about an order of magnitude to $C = (1.8 \pm 0.3) \times 10^8 \text{ m}^2$ at $R = 11.0 \text{ AU}$ and $C = 7 \times 10^7 \text{ m}^2$ (within a factor of 2) at $R = 13.6 \text{ AU}$. The quoted errors reflect not only the statistical uncertainty, but also the uncertainty in assuming a brightness profile which falls off as the inverse of the projected distance from the nucleus. Thus, the photometry suggests that the coma production is declining, and that the decline began at about the same critical heliocentric distance at which the activity began ($R \approx 10 \text{ AU}$).

9.2.2 Nature of the Activity - CO_2 Sublimation

9.2.2.1 Possible Mechanisms

Numerous hypotheses have been put forth to explain the existence of a coma at large R , including (i) sublimation from small amounts of "super-volatiles" such as CO_2 or C_2H_4 at large R (Mukai, 1986; Houppis & Mendis, 1981) (ii) gravitational perturbations by the sun on a *dormant* coma which is a remnant of the comet's formation (Sekanina, 1982), (iii) electrostatic snap-off (Jewitt, 1984), or (iv) chemical instabilities (Donn & Urey, 1956) and phase transitions in the ice at low temperatures (Smoluchowski, 1981; Hanner & Campins, 1986). Of all these processes, the one which provides the most natural explanation for the appearance of a coma near $R = 10\text{-}11 \text{ AU}$ is the sublimation of material more volatile than H_2O . In particular, it is intriguing that near $R = 10 \text{ AU}$, the momentum carried by sublimating CO_2 would just be sufficient to drag sub-mm particles into the coma from a nucleus of a few km radius. The equation relating the largest particle radius, a_{crit} which may be lifted from a nucleus of radius R_n and density ρ_n to the gas mass loss rate ($\mu m_H Q$) where Q is the molecular production rate is given by:

$$a_{\text{crit}} = \frac{9 f \mu m_h Q v_{\text{th}}}{64 \pi^2 \rho_g \rho_n R_n^3 G} \quad (9.3)$$

This relation is derived in Appendix 6. The quantities f and v_{th} are the drag coefficient (which depends on the momentum transfer during collisions) and the gas thermal velocity, respectively, and G is the gravitational constant. It is assumed that the grain density $\rho_g \approx \rho_n$. The mass loss rate is a model dependent parameter. Figure 9-6 shows the critical grain radius as a function of R for a CO_2 nucleus. The mass loss rate is obtained from a CO_2 sublimation model as discussed below in section 9.2.2.2.

The existence of CO_2 has been inferred in other comets. Comet Schwassmann-Wachmann 1 orbits the sun between 5-7 AU and has dramatic outbursts in which CO^+ has been detected (Cochran *et al.* 1980). It has been suggested that the sublimation of CO_2 or CO which is suddenly exposed to the surface is directly related to the comet's activity (Cowan and A'Hearn, 1982). In addition, CO_2^+ is frequently observed in cometary plasma tails. Recent observations of sudden increases in the column density of CO_2^+ ions in the tail of comet P/Halley suggest that CO_2 probably plays a role in the outbursts (Feldman *et al.*, 1986). The birth and probable death of the coma of 1982I near $R = 10$ AU, the existence of sub-mm grains in the coma and the ability of CO_2 sublimation to drag large grains from the coma at this distance all motivate a closer look at the CO_2 sublimation hypothesis.

9.2.2.2 CO_2 Sublimation Model

In order to evaluate the feasibility of CO_2 sublimation for comet Bowell, a comparison is made of the available broadband photometry corrected to a 5 arcsec radius diaphragm (the present photometry, that summarized by Jewitt, 1984 and photometry from Hanner & Veeder,

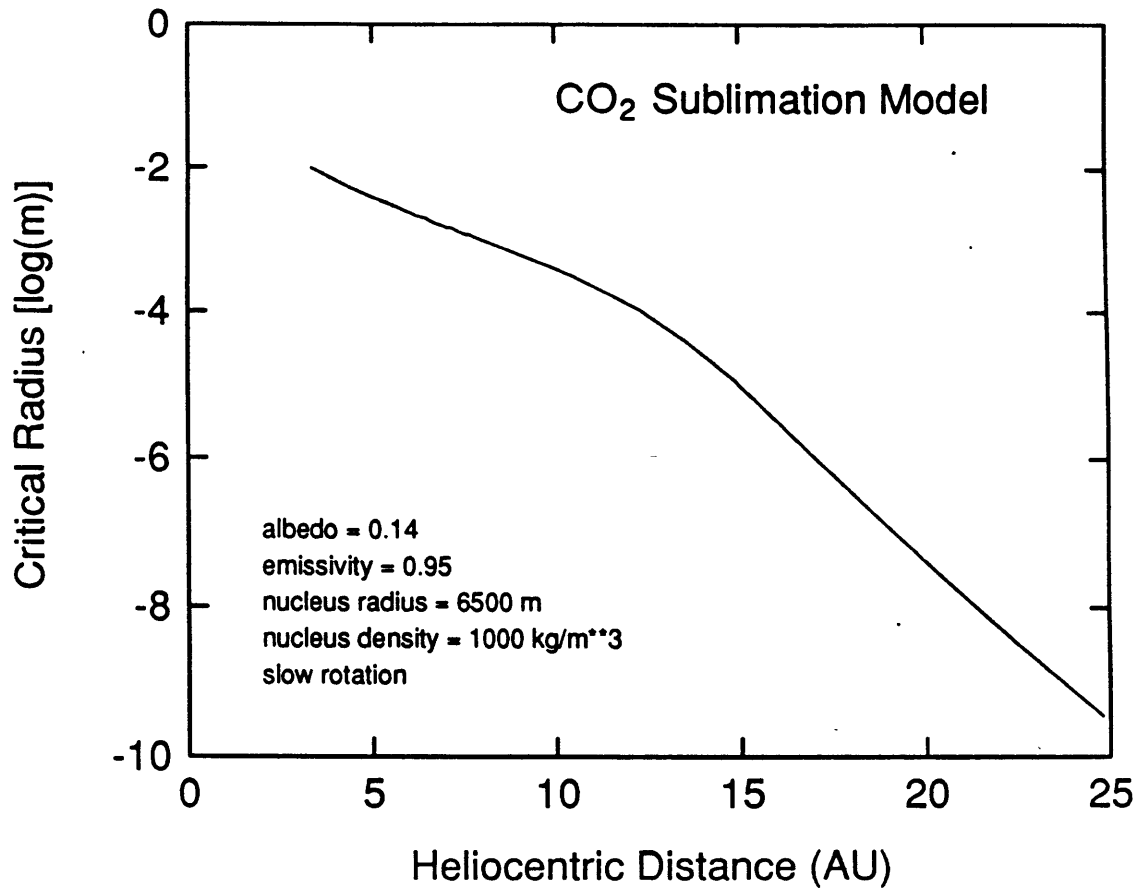


Figure 9-6. Log of the critical radius (in m) for the maximum spherical particle to be removed from the gravitational field of the nucleus for a given CO₂ sublimation model as a function of heliocentric distance. The model is described in the text and the parameters are listed on the figure.

1984) to a simple CO₂ sublimation model. The CCD R magnitudes (this paper) have been converted to the J bandpass (used by Jewitt, 1984) assuming $(R-J)_{\text{sun}} = 0.57$ (Johnson, 1966). The model assumes equilibrium sublimation from a nucleus of negligible conductivity, and is analogous to the model successfully applied to comet P/Halley (see Chapter 2 for a complete description). Unfortunately, in the case of comet Bowell, relatively few of the input parameters are well known. What *is* known is an upper limit to the product of the 0.65 μm geometric albedo and cross section of the nucleus (Jewitt, 1984; see also Table 9-3), $C_n \leq 6 \times 10^6 \text{ m}^2$; in addition, the analysis of the tail morphology provides a good estimate of the mean particle size (Sekanina, 1982). Observations (Jewitt, 1984; Hanner *et al.*, 1981) also indicate that the albedo of the grains is low (a value of $p \approx 0.06$ is adopted). Figure 9-7 presents a comparison of the CO₂ model with the J magnitude within a 5" radius diaphragm. It is interesting that the sublimating CO₂ model is able to fit the broadband photometry quite well. Also shown in Figure 9-7 is a "constant cross section" model which shows the brightness variation that an extended source would have within a fixed diaphragm as the geometrical factors change (dashed line). This model fits the photometry well near perihelion, but is inadequate at larger distances.

A strict analogy with P/Halley would suggest that CO and not CO₂ should be the dominant volatile since the abundance of CO relative to H₂O is near 20% in P/Halley (Woods *et al.*, 1986), whereas the abundance of CO₂ relative to H₂O is only about 3.5% (Krankowsky *et al.*, 1986). Models for the much more volatile CO are compatible with the comet Bowell data only for very high grain/nucleus albedos; however, high grain albedos are inconsistent with measured values (Jewitt, 1984; Hanner *et al.*, 1981).

The velocity as a function of the distance, r , from the nucleus may be computed from:

$$1 - \frac{R_n}{r} = \frac{a}{bc} \left\{ (v_t - b) \ln \left[\frac{v_{th} - b - v_o}{v_{th} - b - v_t} \right] + (v_{th} - b) \ln \left[\frac{v_{th} + b - v_t}{v_{th} + b - v_o} \right] \right\} \quad (9.4)$$

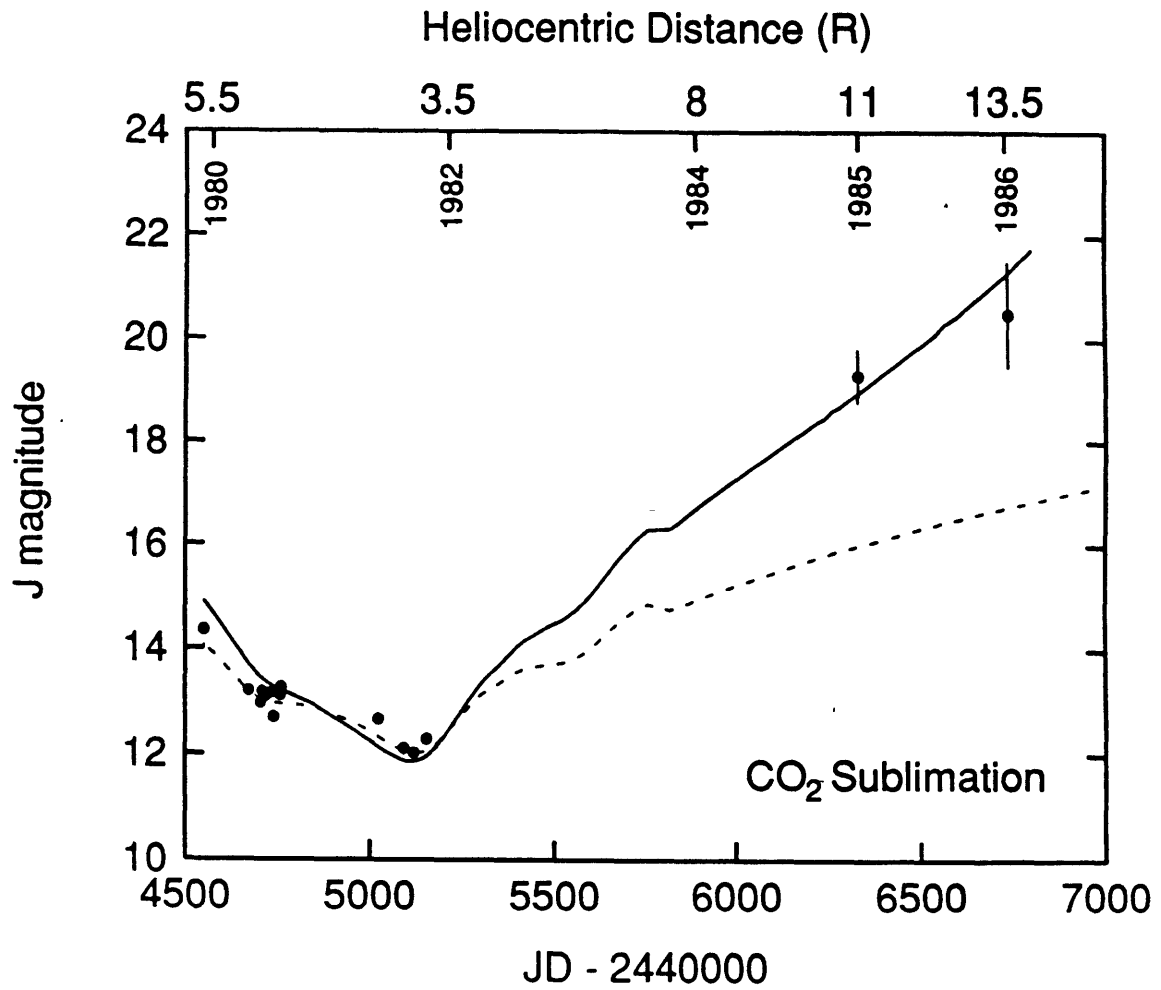


Figure 9-7. J magnitudes within a 5 arcsec radius diaphragm are plotted versus JD. The heliocentric distances and dates are marked at the top of the graph. The CO_2 sublimation model described in the text is shown as the solid line, the dashed curve represents the brightness variation that comet Bowell would have as the distances R , Δ and the phase angle changed if the intrinsic coma brightness remained unchanged.

where b and c are constants which depend on the nucleus and dust properties, v_0 is the initial grain velocity and v_t is the grain velocity at r . The terminal velocity is reached as $r \rightarrow \infty$. Equation 9.4 is derived and discussed in Appendix 6. Both constants, b and c are a function of the mass loss rate from the nucleus. The CO_2 sublimation model discussed above was used to predict the terminal velocity of the $300 \mu\text{m}$ grains of comet Bowell. The results are shown in Figure 9-8 which plots $v_t(\infty)$ as a function of heliocentric distance. The upper curve neglects the effects of the gravity of the nucleus. From the figure, it is apparent that $v_t(\infty)$ for the grains should be on the order of 20 m s^{-1} at perihelion ($R = 3.36 \text{ AU}$), decreasing as R increases. However, the observed grain velocities are only $v \approx 1 \text{ m s}^{-1}$, near the expected escape speed from the nucleus. It is difficult to reconcile the slow coma expansion with the expected 20 m s^{-1} terminal speed for the grains. One possible solution to this dilemma could be offered if the mass of dust ejected into the coma at high speed near perihelion were negligible compared to the total mass of dust present in the coma. The mass of dust in the observing diaphragm is equal to the integral of the mass loss rate over the time it takes the grains to cross the diaphragm. Therefore, if the comet experiences high ejection velocities and high mass loss for a relatively short time, it is possible that the total amount of material ejected at high velocity would represent only a small fraction of the total mass of dust in the coma and would hence be undetected. Unfortunately, calculations indicate that the high terminal velocity is sustained for a period of time long enough that the high velocity dust grains should have been readily detectable. Although the CO_2 model has difficulty explaining the observed low velocity of the grains, the initiation of the coma near $R = 10\text{-}11 \text{ AU}$ and the apparent *turn off* at the same distance most strongly suggest sublimation of a volatile, most likely CO_2 .

For grains moving at 1 m s^{-1} , the diaphragm crossing time is on the order of 1 year. The comet has now been observed for more than 6 years, significantly longer than the diaphragm crossing time. The long diaphragm crossing time effectively provides a long time constant for photometric changes. The nearly constant coma cross section at $R \leq 10 \text{ AU}$ suggests that the

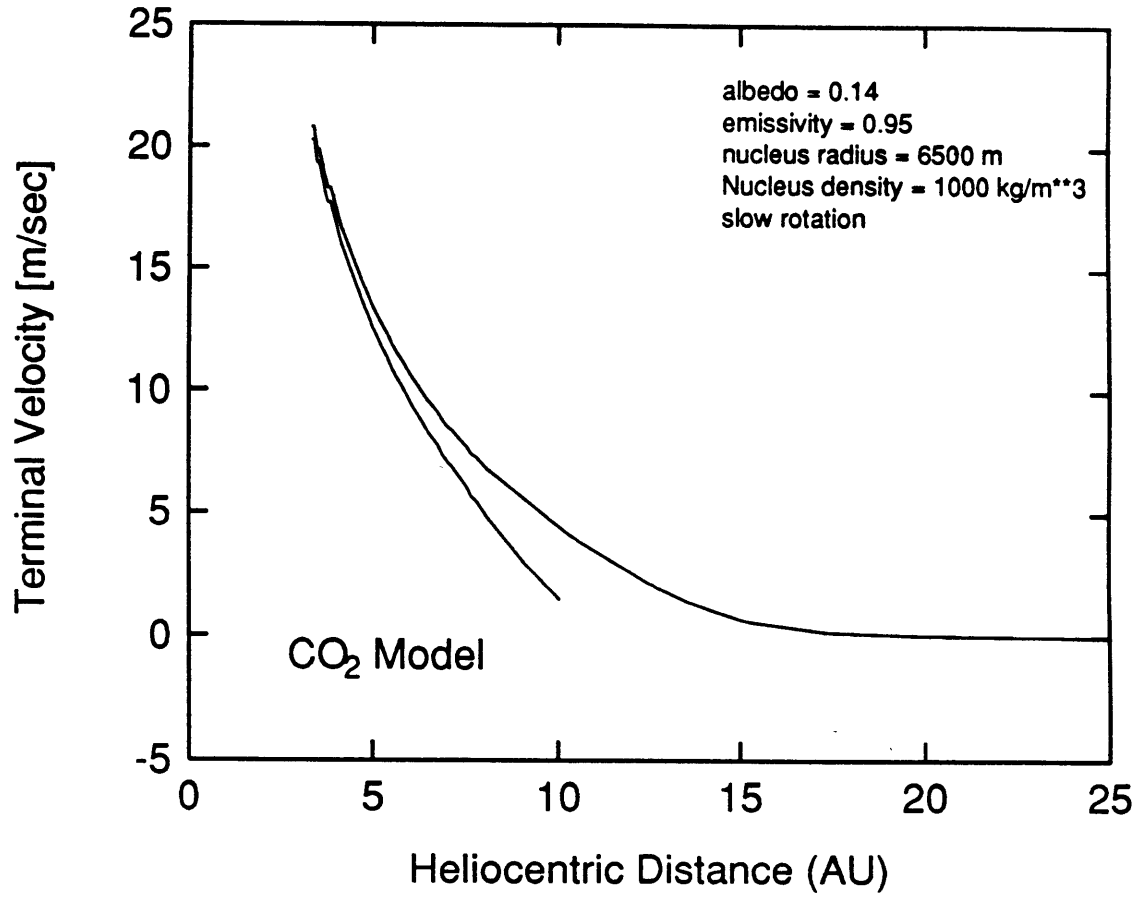


Figure 9-8. Terminal grain velocity in a gas flow (m s^{-1}) as a function of heliocentric distance. The model for sublimation from a CO_2 nucleus is described in the text.

mechanism producing the coma has been continuous and was not a single impulsive ejection at large R . The suggestion of an ice phase transition (Hanner and Campins, 1986) thus seems unlikely on the basis that the coma was active both before and after perihelion whereas a phase transition would occur on the inbound journey as the comet first began to heat and would not naturally produce continued activity at the same distance post-perihelion.

9.3 Comet Cernis

There are currently several dynamically new comets which are at small enough R that if they possessed active comae similar to that of comet Bowell, they should still be visible. One comet in particular seemed like a good candidate; comet Cernis (1983I \equiv 1983 XII). Comet Cernis was discovered near perihelion ($q = 3.32$ AU) with a photographic brightness near 9th mag (MPC 8089, Marsden, 1983). Positions for this comet were reported in the *Minor Planet Circulars* during 1983-1985. The fact that the comet had many astrometric positions measured over two years of its orbit (suggesting that the orbit was well known) and the fact that it was dynamically new, $1/a_{orig} = 78$ (see Table 9-1), suggested that it might still be observable in 1986.

Observations of comet Cernis were made using the CTIO Curtis Schmidt and IIIaJ unfiltered plates during photometric conditions. The plate scale of the Schmidt is 96.6 arcsec mm^{-1} , giving a field of view of $\approx 5^\circ \times 5^\circ$. The comet was identified on two consecutive nights by noting its motion relative to the field stars. The comet appeared extended and diffuse at $R = 8.99$ AU ($\Delta = 8.50$ AU, $\alpha = 5.8^\circ$), and was not far from its predicted position. Positions obtained from plate solutions were sent to Brian Marsden (MPC 10891, Marsden 1986b) who used them to update the orbital elements. No attempt was made to obtain magnitude estimates from the plates since the comet images were trailed and in very dense star fields.

Additional observations of comet Cernis were obtained on 1987 May 1 using the CTIO 1.5m telescope with an 800 x 800 Texas Instruments CCD at the $f/7.5$ Cassegrain focus. The CCD was used in 2 x 2 pixel binning mode, giving an effective plate scale of 0.544 arcsec per 30 μm pixel and a field of view of ≈ 215 arcsec on a side. The chip was preflashed to a level of $\approx 200e^-$ above bias to remove any potential nonlinearity. The 4m prime focus CCD Grinnell system and data acquisition software were used remotely from the 1.5m in order to make use of the Grinnell's ability to blink pairs of images. The telescope was guided at sidereal rate and Cernis was identified by its motion with respect to field stars. Exposure times were limited (180 s) so that Cernis would trail by less than ≈ 1 pixel during an integration.

Table 9-5
Comet Cernis Photometry

Date	JD [-2440000]	Tel	R [AU]	Δ [AU]	α [deg]	Aper [‡] [arcsec]	λ [μm]	mag	R_c [†]	Ref. [§]
1987 05 01	6916.6963	CTIO 1.5m	11.25	10.66	4.3	8.7	0.65	19.42±0.10	19.27	1
	6916.7184					8.7	0.65	19.03±0.10	18.88	1
	6916.7404					8.7	0.55	19.62±0.10	---	1
	6916.7935					8.7	0.65	19.18±0.10	19.03	1
						10.9	0.65	18.91±0.10	19.00	1
					13.1	0.65	18.74±0.10	19.03	1	
1983 08 09	5555.5	IRTF 3m	3.33	3.07	17.6	7.4	1.25	12.36±0.05	12.58	2
						7.4	1.65	12.03±0.05		2
						7.4	2.25	11.94±0.05		2
1983 08 10	5556.5					9.5	1.25	12.22±0.05	12.76	2
						9.5	1.65	11.85±0.05		2
						9.5	2.25	11.72±0.05		2
1983 08 11	5557.5					9.5	1.25	12.24±0.06	12.78	2

[‡] Aperture diameter in arcsec

[†] Mould R magnitude, assuming solar colors; corrected to 10 arcsec diameter diaphragm (see text).

[§] 1 = present work; 2 = Hanner, 1984.

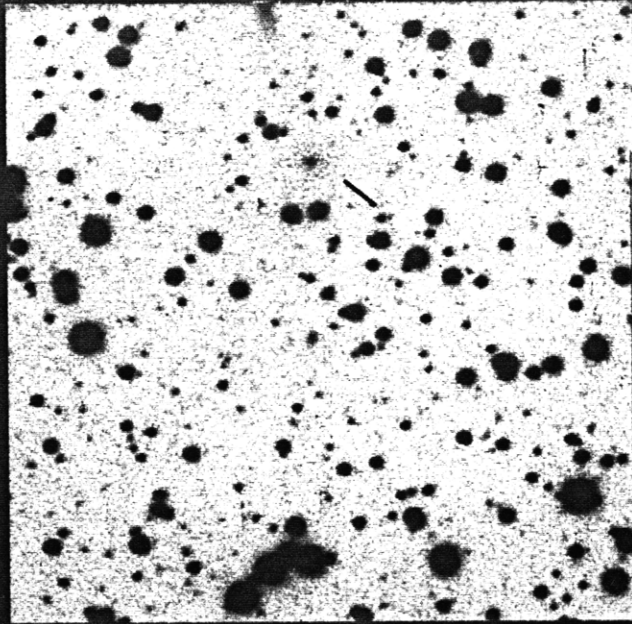
Images were taken through Mould V ($\lambda_{cent} = 0.546 \mu\text{m}$, $\Delta\lambda = 0.11 \mu\text{m}$) and R ($\lambda_{cent} \approx 0.65 \mu\text{m}$, $\Delta\lambda = 0.1 \mu\text{m}$) filters. Sensitivity variations were removed by dividing the images by dome flat field exposures. Extinction corrections were made assuming the CTIO mean extinction (Gutiérrez-Moreno *et al.*, 1982) and absolute calibration was achieved from measurements of the standards SA 107-106, SA 108-478, SA 109-381 and SA 112-223 (Landolt, 1983). Photometry of fieldstars in the Cernis frames indicated that the sky was photometric to within 1-2%. Two images of Cernis are shown in Figure 9-9. The motion of the comet is clearly visible. The comet appears diffuse, with a coma extending at least 10^8 m at the comet. The reduced data are presented in Table 9-5. In addition to the photometry obtained at CTIO, there is some near infrared photometry reported in the literature for Cernis (Hanner, 1984). This is also included in the Table. Feldman and A'Hearn (1985) have observed comet Cernis in the UV, but these observations will not be included in this discussion. The R magnitudes listed in column 10 of Table 9-5 have been corrected to a standard diaphragm size (10 arcsec diameter), assuming a $1/p$ surface brightness profile. The (J-R) solar color of 0.55 was used to correct the J magnitude measurements of Hanner (1984) to the R bandpass.

It is not possible to compute a sublimation model for comet Cernis as was done for P/Halley and comet Bowell because there exist accurate magnitudes at only two distances. However, the Cernis photometry may be compared with the general shape of the lightcurves for the other two comets. In Figure 9-10 the data for comets P/Halley and Bowell are plotted. The R magnitude (assuming $(R-J) = 0.55$ for Bowell) is plotted versus the heliocentric distance. For P/Halley only the preperihelion lightcurve is plotted, whereas both pre- and post-perihelion data are plotted for Bowell. The comet Cernis R magnitude measurements from Table 9-5 are also plotted in the figure as filled circles. The comet Cernis data seem to match the comet Bowell data amazingly well, even though the data were not shifted to match

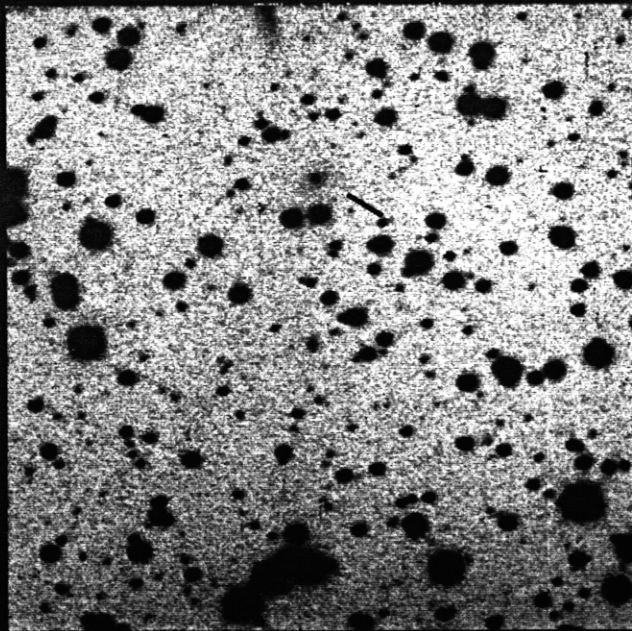
Figure 9-9. Two images of comet Cernis taken on 1987 May 1 with the 1.5m telescope at CTIO. The UT start time of each exposure is indicated in the figure, other observational parameters may be found in Table 9-8. The motion of the comet between the 2 frames is easily visible. The length of the bar marking the position of the comet corresponds to approximately 10^8 m at the comet in the plane of the sky. North is to the left and East to the top.

Cernis

R = 11.25 AU



6:37:52 UT



6:55:19 UT

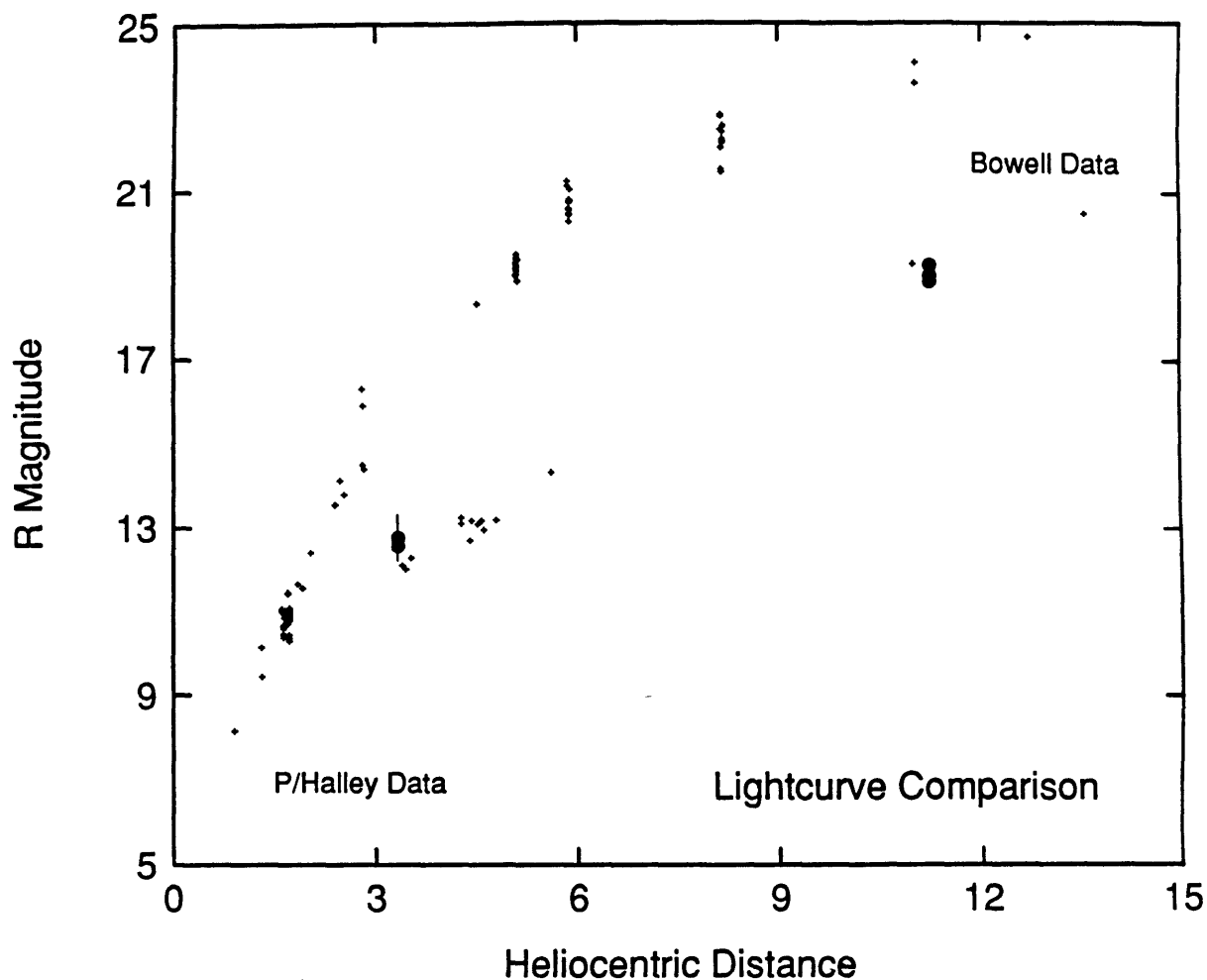


Figure 9-10. Comparison of the sublimation model lightcurves of comets P/Halley (H_2O) and Bowell (CO_2). The R magnitude within a 10 arcsec diameter diaphragm is plotted versus heliocentric distance. The CO_2 sublimation curve does not show the rapid brightening that the H_2O curve does between $3 < R \text{ [AU]} < 6$. The comet Cernis observations listed in Table 9-5 are plotted for comparison. The limited Cernis data suggests that this comet may be very similar to comet Bowell with respect to the sublimation of volatiles.

the Bowell observations! Both comets Bowell and Cernis have a very different behavior compared to P/Halley as a function of distance from the sun. The rapid onset of sublimation apparent for P/Halley is not present for either Bowell or Cernis. It appears, from the limited data on Cernis, that its lightcurve may be very similar to that of comet Bowell. It is expected that Cernis will be visible at least as far out as Bowell ($R > 14$ AU); further observations are planned.

9.4 Other Dynamically New Comets and Comets Active at Large R

Very few CCD observations exist of the other dynamically new comets and comet active at large R which may be currently observable. During the course of this research, observations have been obtained for the comets listed in Table 9-6.

Other Active Comets Currently Observed				
Comet	q [AU]	$1/a_{\text{orig}}$ [$\times 10^{-6}$ AU]	R_{current}^{\S} [AU]	R_{obs}^{\dagger} [AU]
Wilson (1986l)	1.200	30	1.6	2.71,1.21
Torres (1987j)	3.624	?	3.7	3.65
Shoemaker (1985 XII)	2.696	487	6.7	4.92,6.05
Hartley (1985 XVI)	4.000	35	6.6	6.22
Shoemaker (1984 XV)	5.489	1624	9.00	7.81
P/Schwassman-Wachmann 1	5.772	----	5.90	5.92 . . .
[Shoemaker (1987o)]	5.464	?	5.7	-----]

\S As of 1987 July

\dagger Distances at which observations have been obtained.

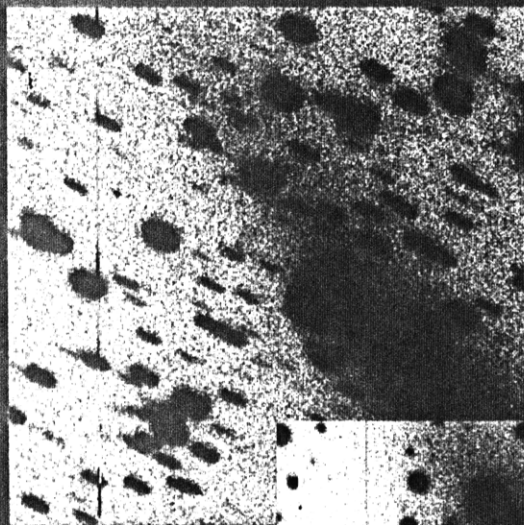
Insufficient data exist for the computation of sublimation models for these comets; however continuing observations are planned for all. The discovery of comet Wilson at $R = 3.6$ AU pre-perihelion was especially fortunate as this will enable extensive observations to be made over a large range of R for the purpose of modelling the brightness. Comet Wilson was especially active at $R = 2.7$ AU when it possessed a dust tail of length $> 4 \times 10^8$ m at the comet. Comet Shoemaker 1985 XII had an even longer tail ($> 8 \times 10^8$ m) at nearly $R = 5$ AU! Both comet tails are shown in Figure 9-11. The existence of such extensive activity at these distance suggests that both comets will probably be observable far beyond the region of significant H_2O sublimation.

Comets Torres and Shoemaker (1987o), recently discovered, do not yet have sufficiently well-determined orbits to compute values of $1/a_{orig}$. There are reasons to suggest that both comets may be of interest with regard to activity at large R . An image of comet Torres is shown in Figure 9-2b, where its appearance is similar to three new comets. Comet 1987o is especially interesting because of its exceptionally large perihelion distance. At discovery at $R = 5.57$ AU (Shoemaker, 1987), its brightness was approximately 16th mag with a 30 arcsec coma. For comparison at a similar distance P/Halley was near mag 20 pre-perihelion and had very little coma. There have been very few comets with such large q which have not been very active at large R .

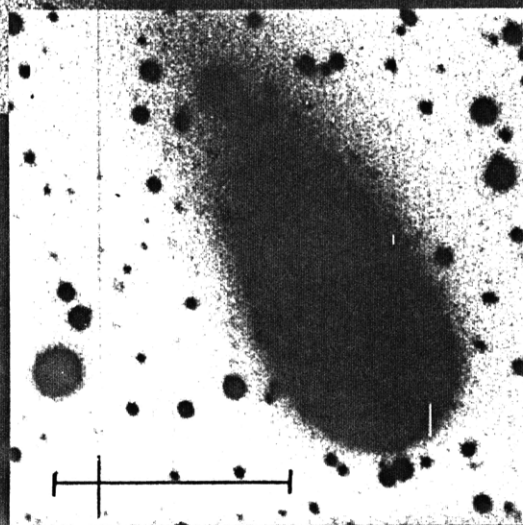
In Figure 9-12 a comparison is made of nine dynamically new and active comets at distances $2.7 < R$ [AU] < 13.6 . Information concerning each image is listed in Table 9-8. The scale bars indicate lengths of 10^8 m at the distances of the comets. The most striking aspect of this figure is the extensive comae which most of the comets have at distances beyond the zone of H_2O activity. Many of these comets should continue to be observable for several years; hopefully sufficient data will be obtained so that sublimation models can be used to understand the nature of their activity.

Figure 9-11. Long dust tails of comets Wilson and Shoemaker (1984f = 1985XII) at large R (see Table 9-8 for details of photographs). The tail of comet Wilson extends $> 4 \times 10^8$ km at the comet in the plane of the sky, and that of comet Shoemaker extends $> 8 \times 10^8$ km.

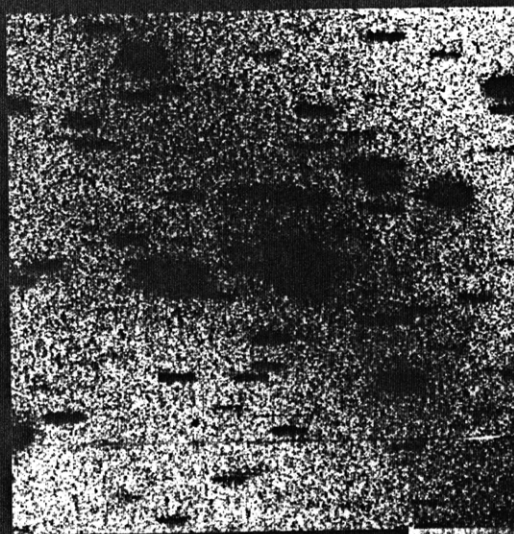
Wilson



R = 2.71 AU



R = 4.92 AU



Shoemaker (1985 XII)

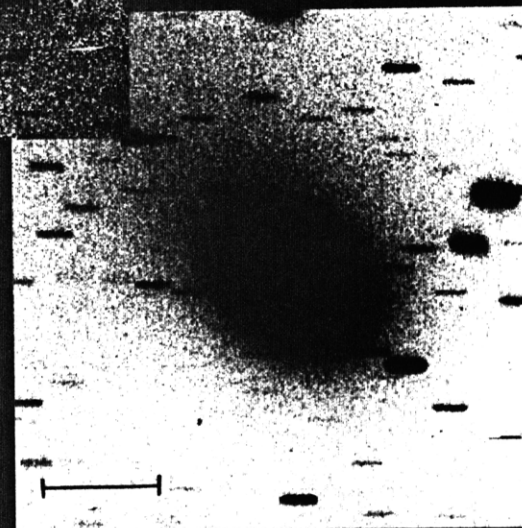
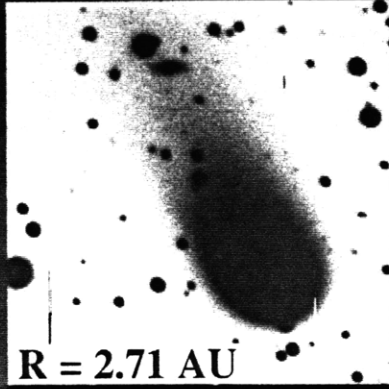
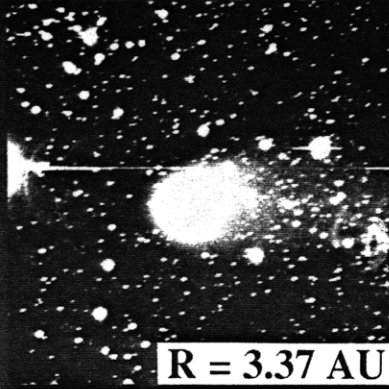


Figure 9-12. Comparison of "Oort comets" and comets which are active at large R . The comets are arranged in order of increasing R . Detailed information concerning the observational circumstances of each comet is listed in Table 9-8. The scale bars correspond to approximately 10^8 m at the comet in the plane of the sky. North is left and East to the top in these images. Two images of comet P/Schwassmann-Wachmann 1 at $R = 5.92$ AU are presented, one to show the inner structure of the coma, and the second to show the extent of the coma. The image of Cernis at $R = 8.99$ AU was taken with the CTIO Schmidt telescope and digitized with the PDS at Kitt Peak headquarters.



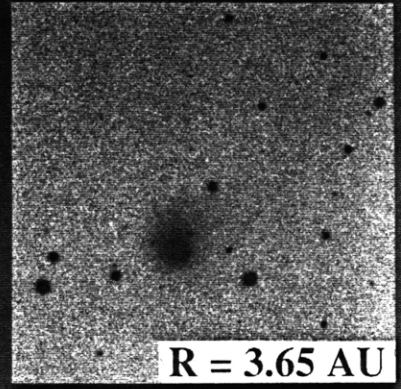
R = 2.71 AU

Wilson



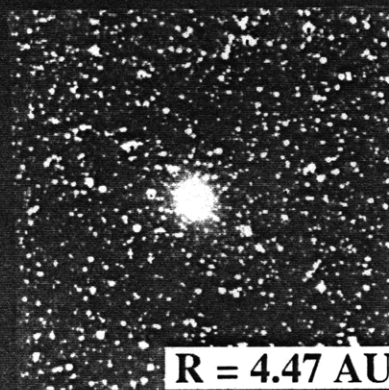
R = 3.37 AU

Bowell



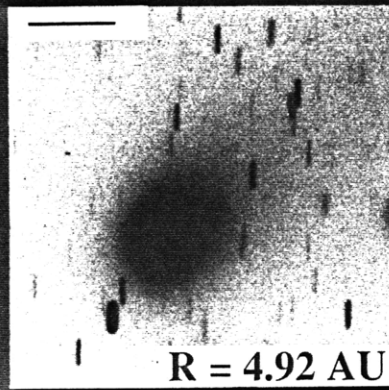
R = 3.65 AU

Torres



R = 4.47 AU

Bowell



R = 4.92 AU

Shoemaker 1985 XII



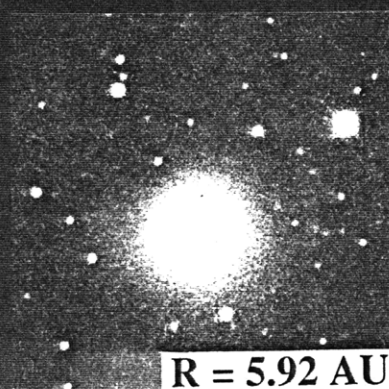
R = 5.06 AU

Elias



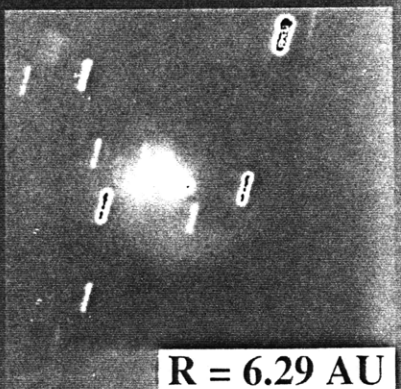
R = 5.92 AU

SW 1



R = 5.92 AU

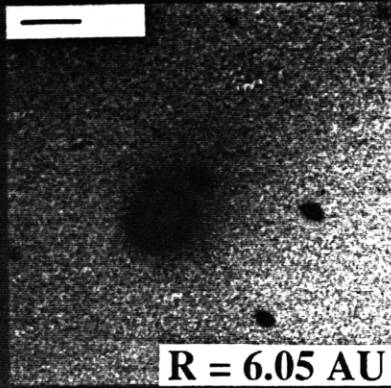
SW 1



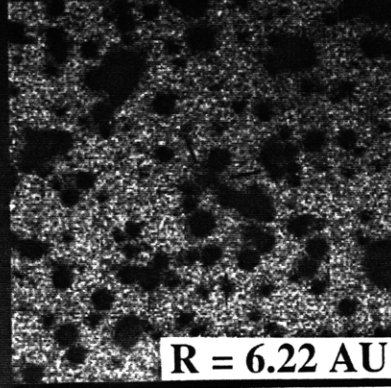
R = 6.29 AU

SW 1

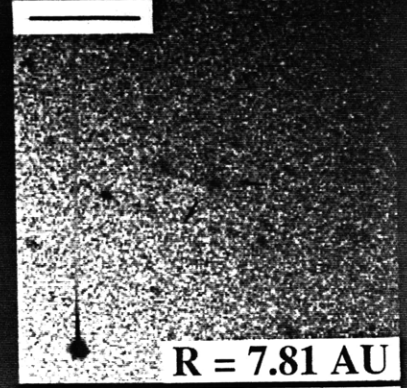
Figure 9-12. Continued.



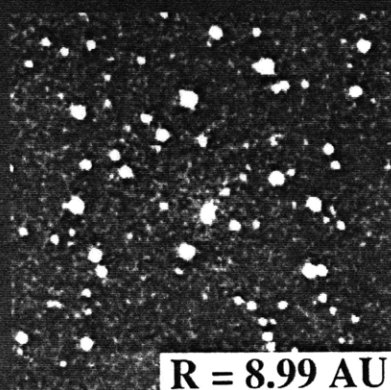
R = 6.05 AU
Shoemaker 1985 XII



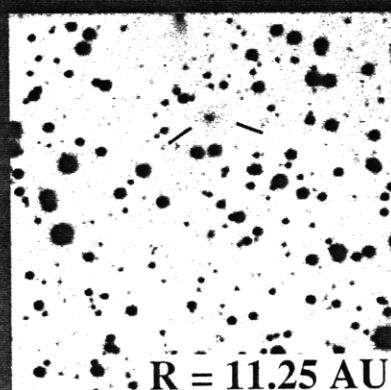
R = 6.22 AU
Hartley



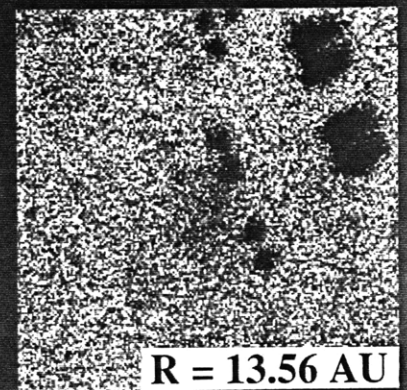
R = 7.81 AU
Shoemaker 1984 XV



R = 8.99 AU
Cernis



R = 11.25 AU
Cernis



R = 13.56 AU
Bowell

9.5 Comet Stearns (1927IV)

Historical observations of active comets have not been used in this research because of the difficulty in analyzing and interpreting non-linear photographic data from many different sources. The one exception is for comet Stearns (1927 IV) for which an extensive set of observations exists, primarily made by one observer. This comet is of special interest since prior to comet Bowell, it held the record for being observed at the largest distance, $R = 11.5$ AU (Van Biesbroeck, 1932). This comet, like Bowell, was active at very large distances from the sun, and in many ways the two comets are similar. Both comets displayed extensive comae to $R > 10$ -11 AU and both showed the peculiar narrow tails characteristic of many comets active at large R . The only known published photograph of Stearns appears in Figure 9-2a, which may be compared with images of more recently observed comets active at large R in Figure 9-2b. Comet Stearns possessed a tail similar to those of comets Bowell and Elias, however, it is difficult to see the tail in Figure 9-2a.

Relatively little observational data exist from which independent determinations of the physical characteristics of the comet may be made. However, it is of interest to see if the photographic lightcurve is compatible with sublimation from H_2O or any more volatile ices. Photographic observations from 1927 - 1932 (Van Biesbroeck, 1930 & 1932; Burton, 1927) are listed in Table 9-7. The photographic magnitude is plotted as a function of date in Figure 9-13. Several sublimation models were computed for both H_2O and CO_2 in an attempt to match the observations. Admittedly, there are very few constraints on the model, however, selecting a range of parameters which encompassed those which were appropriate for P/Halley and Bowell, water sublimation was able to reproduce the data fairly well, especially the apparent brightening near perihelion. This was only possible, however, by introducing a shift in the absolute brightness of approximately 10 magnitudes! An arbitrary shift is allowable because the effective observing "diaphragm" of the observations is unknown; it is

Table 9-7
Summary of Comet Stearns (1927IV) Observations

Date (UT) (1927-1931)	JD -2420000	R [AU]	Δ [AU]	α [deg]	mag (photographic)
<i>1927</i>					
03 13	4952.5	3.69	3.04	13	8.5
03 15.305	4954.805	3.68	3.01	13	9.5
03 16.404	4955.904	3.68	3.00	12	11.0
03 26.275	4965.775	3.68	2.88	10	12.0
03 31.241	4970.741	3.69	2.84	9	9.5
04 22	4992.5	3.70	2.75	6	10.5
04 22.224	4992.724	3.70	2.75	6	9.5
04 28.208	5998.708	3.70	2.77	7	9.5
05 06.266	5006.766	3.71	2.80	8	9.5
05 07	5007.5	3.71	2.81	8	10.0
05 20	5020.5	3.72	2.92	11	9.0
05 25.293	5025.793	3.73	2.98	12	10.0
06 22.218	5053.718	3.78	3.38	15	12.0
06 25	5056.5	3.78	3.43	15	11.5
07 02.214	5063.714	3.80	3.55	15	12.0
07 20.220	5081.720	3.84	3.84	15	12.5
07 26	5087.5	3.85	3.94	15	12.3
08 02.191	5094.691	3.87	4.05	14	12.5
08 30.081	5122.581	3.96	4.43	12	12.8
09 21.061	5144.561	4.03	4.66	10	13.5
10 28.010	5181.510	4.17	4.86	9	13.5
12 01	5215.5	4.32	4.87	10	14.0
<i>1928</i>					
01 25.348	5270.848	4.58	4.71	12	12.5
02 16.303	5292.803	4.69	4.68	12	13.5
02 26	5303.5	4.75	4.67	12	13.0
03 15.301	5320.801	4.84	4.69	12	13.0
03 24.307	5329.807	4.89	4.72	12	13.0
04 13.264	5349.764	5.00	4.81	12	13.8
04 18.213	5354.713	5.03	4.84	11	14.0
04 22.284	5358.784	5.05	4.87	11	14.5
09 08.202	5497.702	5.87	5.97	10	14.5
09 19.142	5508.642	5.94	6.04	10	14.5
10 06.178	5525.678	6.04	6.13	9	15.0
11 04.020	5554.520	6.22	6.30	9	15.5

Table 9-7
Summary of Comet Stearns (1927IV) Observations

Date (UT) (1927-1931)	JD -2420000	R [AU]	Δ [AU]	α [deg]	mag (photographic)
<i>1929</i>					
04 14	5715.5	7.23	7.48	8	15.5
06 15.317	5777.817	7.63	7.82	7	16.0
07 05.226	5797.726	7.75	7.87	7	15.5
07 28.193	5820.693	7.90	7.92	7	16.0
07 31.244	5823.744	7.92	7.93	7	16.0
09 03.141	5857.641	8.13	7.99	7	16.0
09 28.059	5882.559	8.29	8.07	7	16.5
10 01.207	5885.707	8.31	8.08	7	16.5
10 02.154	5886.654	8.31	8.08	7	16.0
10 04.194	5888.694	8.33	8.09	7	16.0
11 22	5937.5	8.63	8.40	6	16.5
<i>1930</i>					
04 22.345	6088.845	9.57	10.03	5	16.5
04 23.36	6089.86	9.58	10.04	5	16.5
07 01.295	6158.795	10.00	10.21	6	16.5
09 17.22	6236.72	10.48	10.13	5	16.5
09 18.131	6237.631	10.48	10.13	5	16.5
10 22.112	6271.612	10.69	10.23	5	17.0
11 18.107	6298.607	10.84	10.43	5	17.5
12 22.039	6332.539	11.05	10.83	5	17.0
<i>1931</i>					
02 14.09	6386.59	11.37	11.63	5	17.5
03 12.077	6412.577	11.53	11.97	4	barely vis.

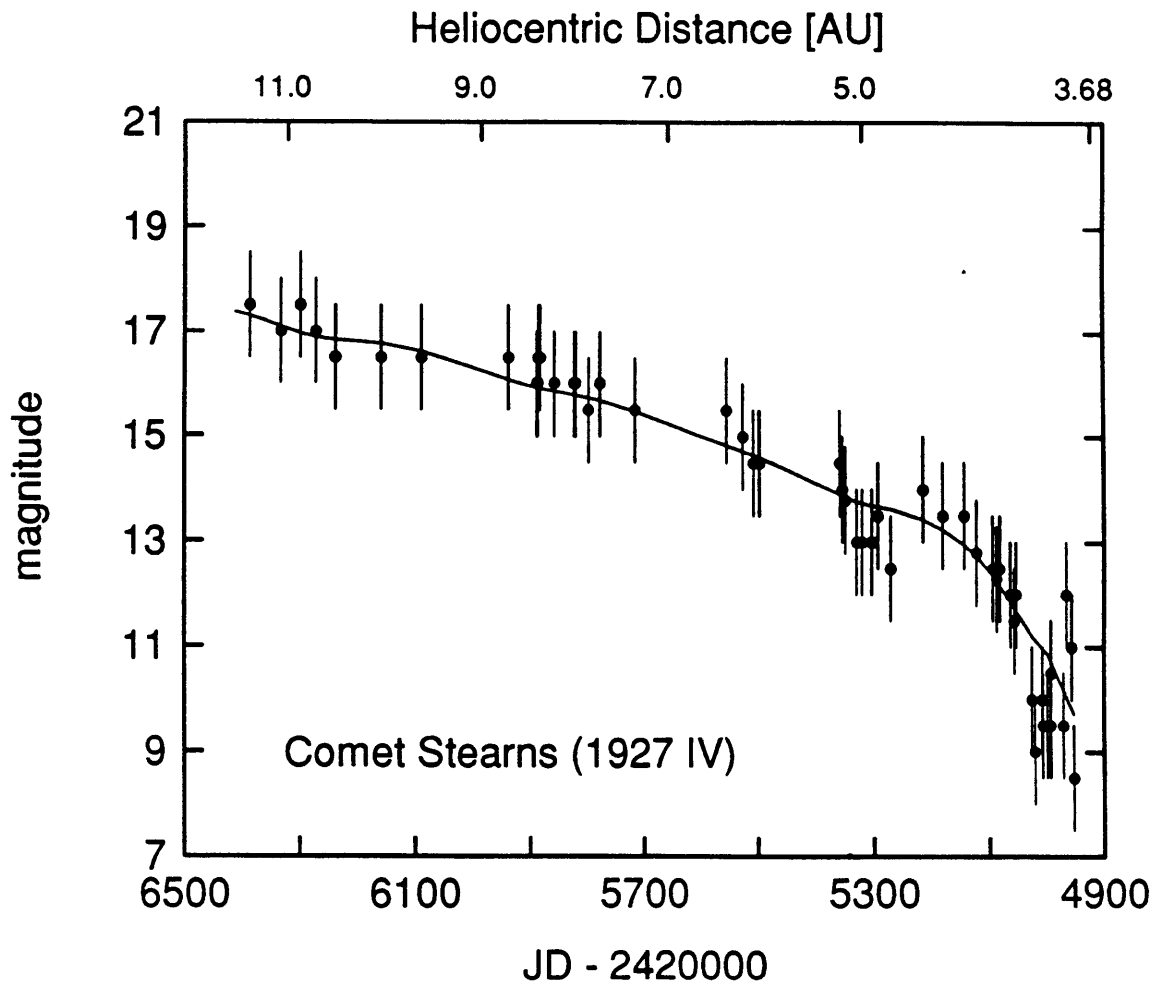


Figure 9-13. Photographic magnitude versus Julian Day Number (JD) for comet Stearns (1927 IV). Data are from Table 9-7. The solid line represents the H₂O model as described in the text. The heliocentric distances are indicated at the top of the figure.

likely to be very large. The error bars in the figure (± 1 mag) have been arbitrarily assigned to the data to reflect this uncertainty. Additionally, a systematic shift of a few magnitudes may be expected because of the unknown photometric system used. However, a brightness discrepancy of 10 magnitudes is very unlikely to occur from systematic errors alone.

The sublimation model assumed a nucleus of the size of P/Halley, however, if the nucleus were 100 times larger than P/Halley, the greater brightness of Stearns could be accounted for. The size implied would be on the scale of the largest asteroids, and is very unlikely for a comet. Not only was the comet bright out to large R , but the comet had an observable coma out to $R = 11$ AU. This suggests that the large sublimating area may have come from a coma of icy grains. It is possible that some process, perhaps sublimation of a super-volatile at large R , produced the coma and that when the comet neared perihelion (3.7 AU) H_2O sublimation began from the coma grains causing the observed brightening. Comet Bowell is believed to have also had detectable sublimation from icy grains. A'Hearn *et al.* (1982) observed that OH emission first appeared near 4 AU and then gradually decreased as the comet approached perihelion. They interpreted the appearance and disappearance of OH as due to vaporization of ice from the grains.

9.6 Conclusions

1. Comet Bowell has been observed at $R = 11.0$ and at the record distance $R = 13.6$ AU. The comet is still active at this great distance; it has an extended low surface brightness dust coma with a radius greater than 15 arcsec ($> 1.38 \times 10^8$ m at the comet). The surface brightness of the coma is less than about 0.5% of the brightness of the night sky. The total integrated red magnitude of the comet is $m_R \approx 20.5$.
2. The mean expansion rate of the coma has been constant at $v = 1.1 \pm 0.2$ m s⁻¹ over the 6 years since discovery, with coma initiation occurring near $R = 10$ -11 AU pre-perihelion.
3. Although all previous observations were compatible with a coma of constant cross section, the recent photometry ($R = 11.0$ and 13.6 AU) shows that the coma is at last fading. The demise of the coma starting near $R \approx 10$ AU post-perihelion mirrors the inferred appearance of the coma at $R \approx 10$ AU pre-perihelion. This critical distance strongly implies that sublimation of a volatile ice is the cause of the activity. CO₂ is a plausible candidate volatile in view of its known presence in other comets, and also in view of the fact that the momentum condition for dragging large (300-400 μm) grains from the nucleus is first satisfied near $R = 10$ AU. The major difficulty with the CO₂ driven coma model is that it does not easily explain the observed constant slow expansion speed.
4. Comet Cernis has been observed at $R = 8.99$ and $R = 11.25$ AU. The comet is still active; a $\approx 10^8$ m coma is visible.

5. A comparison of the sublimation models for comets P/Halley and Bowell with the Cernis photometry at $R = 11.25$ AU and $R = 3.33$ AU (Hanner, 1984) shows that Cernis is probably very much like Bowell with regard to its activity. Neither Bowell nor Cernis show the rapid onset of sublimation present in the P/Halley H₂O sublimation model. Comet Cernis will probably be visible at least to the distance at which Bowell was last observed.

6. Continuing observations of several other comets at large R (Shoemaker 1985 XII, Hartley 1985 XVI, Shoemaker 1984 XV, P/Schwassmann-Wachmann 1) indicate that many comets are active beyond the zone where H₂O sublimation is significant. Observations of these comets over a large range of heliocentric distances are needed.

Table 9-8
Photographic Figure Information

Figure	Comet	Telescope	Date	UT [†]	Filter	Exp [sec]	R [AU]	Δ [AU]	α [deg]	Scale [§] [arcsec]
9-2a	Stearns [*]	Yerkes 24"	1927 Mar 12	---	---	1440	3.69	3.04	13	\diamond
	Baade [‡]	USNO	1955 Autumn	---	---	---	3.9	≈ 3.7	≈ 10	---
	Baade [‡]	USNO	1955 Autumn	---	---	---	3.9	≈ 3.7	≈ 10	---
	Baade [‡]	USNO	1955 Autumn	---	---	---	3.9	≈ 3.7	≈ 10	---
	Wirtanen [‡]	Flagstaff 40"	1957 Jul 21	---	103aO/GG13	1800	4.46	4.04	12	---
	Wirtanen [‡]	Flagstaff 40"	1958 Apr 27	---	103aD/GG11	7200	4.85	4.44	11	---
	Wirtanen [‡]	Flagstaff 40"	1958 May 23	---	103aO	3660	4.93	4.24	9	---
9-2b	Wilson	KPNO 2.1m	1986 Oct 31	3:22	R	100	2.71	2.61	21.4	150
	Bowell ^{**}	Palomar 1.5m	1982 Mar 23	---	r ^{††}	---	3.37	3.16	17	480
	Torres	CTIO 1.5m	1987 May 02	2:22	R	60	3.65	2.76	8.7	215
	Elias ^{**}	Palomar 5m	1982 Mar 31	8:19	R	200	5.06	4.13	4.6	215
9-3a	Bowell	KPNO 2.1m	1986 Nov 03	5:04	R	3600	13.56	12.75	2.4	100
9-9	Cernis	CTIO 1.5m	1987 May 01	6:39	R	180	11.25	10.66	4.3	215
	Cernis	CTIO 1.5m	1987 May 01	6:57	R	180	11.25	10.66	4.3	215
9-11	Wilson	KPNO 2.1m	1986 Oct 31	3:22	R	100	2.71	2.61	21.4	150
	Tail	KPNO 2.1m	1986 Oct 31	3:59	R	500	2.71	2.61	21.4	150
	1985 XII	KPNO 2.1m	1986 Oct 30	8:56	R	900	4.92	4.30	9.7	150
	Tail	KPNO 2.1m	1986 Oct 30	9:30	R	900	4.92	4.30	9.7	150
9-12	Wilson	KPNO 2.1m	1986 Oct 31	3:22	R	100	2.71	2.61	21.4	140
	Bowell ^{**}	Palomar 1.5m	1982 Mar 23	---	r	---	3.37	3.16	17	480
	Torres	CTIO 1.5m	1987 May 02	2:22	cont [□]	400	3.65	2.76	8.7	200
	Bowell ^{**}	KPNO 2.1m	1981 May 04	4:23	R	300	4.47	3.66	8.6	---
	1985 XII	KPNO 2.1m	1986 Oct 30	8:56	R	900	4.92	4.30	9.7	140
	Elias ^{**}	Palomar 5m	1982 Mar 31	8:19	R	200	5.06	4.13	4.6	200

Table 9-8, contd.

Photographic Figure Information

Figure	Comet	Telescope	Date	UT [†]	Filter	Exp [sec]	R [AU]	Δ [AU]	α [deg]	Scale [§] [arcsec]
	S W 1	CTIO 1.5m	1987 May 1	9:22	V	60	5.92	5.78	9.8	200
	S W 1	CTIO 1.5m	1987 May 1	9:22	V	60	5.92	5.78	9.8	200
	S W 1 ^{**}	Palomar 1.5m	1981 Feb	---	r	---	6.29	5.30	1.9	160
	1985 XII	KPNO 2.1m	1987 Apr 01	3:08	R	470	6.05	6.65	7.2	140
	1985 XVI	CTIO 1.5m	1987 May 01	8:48	R	80	6.22	5.51	7.0	100
	1984 XV	KPNO 2.1m	1986 Oct 30	4:32	R	300	7.81	7.18	5.8	70
	Cernis	CTIO Schmidt	1986 May 7	6:30	IIIaJ	2400	9.00	8.50	5.7	280
	Cernis	CTIO 1.5m	1987 May 01	6:39	R	180	11.25	10.66	4.28	200
	Bowell	KPNO 2.1m	1986 Nov 03	5:04	R	3600	13.56	12.75	2.41	75

[†] UT midtime of exposure

[§] Size of image field in arcsec.

^{*} Photo from Van Biesbroeck (1927a) - Figure 2.

[◇] Tail is described by Van Biesbroeck as extending approximately 10 arcmin in length at position angle 215°.

[‡] Photos from Roemer (1962) - Plates II and III.

^{**} Images provided by D. Jewitt, private communication.

^{††} Thuan-Gunn (1976) magnitude system, $\lambda_{cent} = 0.65 \mu\text{m}$, $\Delta\lambda \approx 0.1 \mu\text{m}$.

[□] CTIO continuum filter, $\lambda_{cent} = 0.58 \mu\text{m}$, $\Delta\lambda \approx 0.01 \mu\text{m}$.

1985 XII = Shoemaker (1984f)

1985 XVI = Hartley (1984v)

1984 XV = Shoemaker (1984r)

References

- A'Hearn, M. F., E. Dwek, P. D. Feldman, R. L. Millis, D. G. Schleicher, D. T. Thompson and A. T. Tokunaga (1982), "The Grains and Gas in Comet Bowell (1980b)", *ICCE Proceedings*, Budapest, Hungary.
- A'Hearn, M. F., E. Dwek and A. T. Tokunaga (1981), "Where is the Ice in Comets?", *Astrophys. J.* **248**, L147-L151.
- A'Hearn, M. F., E. Dwek and A. T. Tokunaga (1984a), "Infrared Photometry of Comet Bowell and Other Comets", *Astrophys. J.* **282**, 803-806.
- A'Hearn, M. F., D. G. Schleicher, P. D. Feldman, R. L. Millis and D. T. Thompson (1984b), "Comet Bowell 1980b", *Astron. J.* **89**, 579-591.
- Baum, W. A., T. J. Kreidl and D. G. Schleicher (1986), "Ices in Cometary Grains", *Bull. Amer. Astron. Soc.* **18**, 794.
- Belton, M. J. S. (1965), "Some Characteristics of Type II Comets Tails and the Problem of the Distant Comets", *Astron. J.* **70**, 451-465.
- Bowell, E. (1980), "Comet Bowell (1980b)", *IAU Circ. No.* 3465.
- Burton, H. E. (1927), "Observations of Comets", *Astron. J.* **38**, 35-36.
- Campins, H., G. H. Rieke, M. J. Lebofsky and L. A. Lebofsky (1982), "A Search for Frosts in Comet Bowell (1980b)", *Astron. J.* **87**, 1867-1873.
- Campins, H., G. H. Rieke and M. J. Lebofsky (1983), "Ice in Comet Bowell", *Nature* **301**, 405-406.
- Cochran, A. L., E. S. Barker and W. D. Cochran (1980), "Spectrophotometric Observations of P/Schwassmann-Wachmann 1 During Outburst", *Astron. J.* **85**, 474-477.
- Cochran, A. L. and M. L. McCall (1980), "Spectrophotometric Observations of Comet Bowell (1980b)", *Pub. Astron. Soc. Pac.* **92**, 854-857.
- Cowan, J. J., and M. F. A'Hearn (1982), "Vaporization in Comets; Outbursts from Comet Schwassmann-Wachmann 1", *Icarus* **50**, 53-62.
- Davies, J. K., S. F. Green, B. C. Stewart, A. J. Meadows, and H. H. Aumann (1984), "The IRAS Fast-Moving Object Search", *Nature* **309**, 315-319.
- Delsemme, A. H. (1985), "The Sublimation Temperature of the Cometary Nucleus: Observational Evidence for H₂O Snows", in *Ices in the Solar System*, eds. J. Klinger, D. Benest, A. Dollfus and R. Smoluchowski, NATO Advanced Science Institutes Series C Vol. 156, D. Reidel Pub. Co. Dordrecht, p. 367-387.
- Donn, B (1977), "A Comparison of the Composition of New and Evolved Comets", in *Comets Asteroids Meteorites Interrelations, Evolution and Origins*, ed. A. H. Delsemme, Univ. of Toledo, p. 93-97.

References, contd.

- Donn, B. and H. C. Urey (1956), "On the Mechanism of Comet Outbursts and the Chemical Composition of Comets", *Astrophys. J.* **123**, 339-342.
- Eaton, N., J. K. Davies and S. F. Green (1981), "The Anomalous Dust Tail of Comet P/Tempel 2", *Mon. Not. Roy. Astron. Soc.* **211**, 15P-19P.
- Everhart, E. and B. G. Marsden. (1983), "New Original and Future Cometary Orbits", *Astron. J.* **88**, 135-137.
- Everhart, E. and B. G. Marsden (1987), "Original and Future Cometary Orbits. III", *Astron. J.* **93**, 753-754.
- Feldman, P. D. and M. F. A'Hearn (1985), "Ultraviolet Albedo of Cometary Grains", in *Ices in the Solar System*, eds. J. Klinger, D. Benest, A. Dollfus and R. Smoluchowski, NATO Advanced Science Institutes Series C Vol. **156**, D. Reidel Pub. Co., Dordrecht, p. 453-461.
- Feldman, P. D., M. F. A'Hearn, M. C. Festou, L. A. McFadden, H. A. Weaver and T. N. Woods (1986), "Is CO₂ Responsible for the Outbursts of Comet Halley?", *Nature* **324**, 433-436.
- Gutiérrez-Moreno, A., H. Moreno and G. Cortes (1982), "A Study of Atmospheric Extinction at Cerro Tololo Inter-American Observatory", *Pub. Astron. Soc. Pac.* **94**, 722-728.
- Hanner, M. S. (1984), "Comet Cernis: Icy Grains at Last?", *Astrophys. J.* **277**, L75-L78.
- Hanner, M. S. and H. Campins (1986), "Thermal Emission from the Dust Coma of Comet Bowell and a Model for the Grains", *Icarus* **67**, 51-62.
- Hanner, M. S. and G. Veeder (1984), "JHK Photometry of Comet Bowell (1982I)", *Icarus* **60**, 445-448.
- Hanner, M. S., G. J. Veeder and D. L. Matson (1981), "Infrared Thermal Emission of Comet Bowell", *Bull. Amer. Astron. Soc.* **3**, 705-706.
- Houppis, H. L. F. and D. A. Mendis (1981), "Dust Emission from Comets at Large Heliocentric Distances 1. The Case of Comet Bowell (1980b)", *Moon & Planets* **25**, 397-412.
- Jewitt, D. C., B. T. Soifer, G. Neugebauer, K. Matthews and G. E. Danielson (1982), "Visual and Infrared Observations of the Distant Comets P/Stephan-Oterma (1980g), Panther (1980u), and Bowell (1980b)", *Astron. J.* **87**, 1854-1866.
- Jewitt, D. (1984), "Coma Expansion and Photometry of Comet Bowell (1980b)", *Icarus* **60**, 373-385.
- Johnson, H. L. (1966), "Astronomical Measurements in the Infrared", in *Ann. Rev. Astron. Astrophys.* Vol. 4, eds. Goldberg, L., Layzer, D. & Phillips, J. G., Annual Reviews Inc., CA, p. 193-205.

References, contd.

- Johnson, J. R., U. Fink and S. M. Larson (1984), "Charge Coupled Device (CCD) Spectroscopy of Comets: Tuttle, Stephan-Oterma, Brooks 2, and Bowell", *Icarus* **60**, 351-372.
- Johnson, P. E., D. W. Smith and R. W. Shorthill (1981), "An Outburst of Comet Tempel-2 Observed Spectrophotometrically", *Nature* **289**, 155-156.
- Krankowsky, D., P. Lämmerzahl, I. Herrwerth, J. Woweries, P. Eberhardt, U. Dolder, U. Herrmann, W. Schulte, J. J. Berthelier, J. M. Illiano, R. R. Hodges and J. H. Hoffman (1986), "In Situ Gas and Ion Measurements at Comet Halley", *Nature* **321**, 326-329.
- Kresák, L. (1977), "An Alternate Interpretation of the Oort Cloud Origin of Comets?", in *Comets Asteroids Meteorites Interrelations, Evolution and Origins*, Ed. A. H. Delsemme, Univ. of Toledo, p. 93-97.
- Kronk, G. W. (1984), *Comets, A Descriptive Catalog*, Enslow Pub., Inc. Hillside, N.J..
- Landolt, A. U. (1983), "UBVRI Photometric Standard Stars Around the Celestial Equator", *Astron. J.* **88**, 439-460.
- Marsden, B. G. (1983-1986), *Minor Planet Circulars*, IAU, Cambridge, MA.
- Marsden, B. G. (1986a), *Catalog of Cometary Orbits*, IAU Central Bureau for Astronomical Telegrams, SAO, Cambridge, MA.
- Marsden, B. G. (1986b), *Minor Planet Circulars*, IAU, Cambridge, MA.
- Marsden, B. G. and Z. Sekanina (1973), "On the Distribution of 'Original' Orbits of Comets of Large Perihelion Distance", *Astron. J.* **78**, 1118-1124.
- Marsden, B. G., Z. Sekanina and D. K. Yeomans (1973), "Comets and Nongravitational Forces. V.", *Astron. J.* **78**, 211-225.
- Marsden, B. G., Z. Sekanina and E. Everhart (1978), "New Osculating Orbits for 110 Comets and Analysis of Original Orbits for 200 Comets", *Astron. J.* **83**, 64-71.
- Meech, K. J., D. Jewitt and G. R. Ricker (1986), "Early Photometry of Comet P/Halley: Development of the Coma", *Icarus* **66**, 561-574.
- Mendis, D. A. and W. -H. Ip (1976), "The Neutral Atmospheres of Comets" *Astrophys. Space Sci.* **39**, 335-385.
- Mukai, T. (1986), "Analysis of a Dirty Water-Ice Model for Cometary Dust", *Astron. Astrophys.* **164**, 397-407.
- Oort, J. H. (1950), "The Structure of the Cloud of Comets Surrounding the Solar System, and a Hypothesis Concerning its Origin", *Bull. Astron. Inst. Neth.* Vol. **11**, No. 408, 91-110.

References, contd.

- Oort, J. H. and M. Schmidt (1951), "Differences Between New and Old Comets", *Bull. Astron. Inst. Neth.* Vol. 11, No. 419, 259-269.
- Roemer, E. (1962), "Activity in Comets at Large Heliocentric Distance", *Pub. Astron. Soc. Pac.* 74, 351-365.
- Sekanina, Z. (1982), "Comet Bowell (1980b): An Active-Looking Dormant Object?", *Astron. J.* 87, 161-169.
- Sekanina, Z. (1975), "A Study of the Icy Tails of the Distant Comets", *Icarus* 25, 218-238.
- Shoemaker, C. S. and E. M. Shoemaker (1987), "Comet Shoemaker (1987o)", *IAU Circ.* No. 4384.
- Smoluchowski, R. (1981), "Amorphous Ice and the Behavior of Cometary Nuclei", *Astrophys. J.* 244, L31-L34.
- Thuan, T. X. and J. E. Gunn (1976), "A New Four Color Intermediate Photometric System", *Pub. Astron. Soc. Pac.* 88, 543-547.
- Van Biesbroeck, G. (1927a), "Comet Notes", *Popular Astronomy* 35, 225-229.
- Van Biesbroeck, G. (1927b), "Comet Notes", *Popular Astronomy* 35, 350-352.
- Van Biesbroeck, G. (1930), "Observations of Comets at the Yerkes Observatory", *Astron. J.* 40, 51-60.
- Van Biesbroeck, G. (1932), "Observations of Comets at the Yerkes Observatory", *Astron. J.* 42, 25-32.
- Weissman, P. R. (1986), "The Oort Cloud and the Galaxy: Dynamical Interactions", in *The Galaxy and the Solar System*, eds. R. Smoluchowski, J. N. Bahcall and M. S. Matthews, Univ. of AZ Press, Tucson, p. 204-237.
- Whipple, F. L. (1978), "Cometary Brightness Variation and Nucleus Structure", *Moon and Planets*, 18, 343-359.
- Woods, T. N., P. D. Feldman, K. F. Dymond and D. J. Sahnou (1986), "Rocket Ultraviolet Spectroscopy of Comet Halley and Abundance of Carbon Monoxide and Carbon", *Nature* 324, 436-438.

Chapter 10 - Summary / Future Work

It has been shown that by comparing simple H₂O ice sublimation models with observations as a function of R , information concerning several physical characteristics of a comet nucleus may be obtained. In particular, as was shown in Chapter 2, the H₂O sublimation model for P/Halley indicated that the albedo of the nucleus was low, the comet rotated slowly, and most importantly that the activity seen at $R \approx 6$ AU was due to H₂O ice sublimation. Subsequent refinements of the physical properties of both the nucleus and dust grains in the coma (Chapters 3-7) and information obtained from the spacecraft encounter all upheld the early conclusions. The simple sublimation model was able to reproduce the general brightening (but not the short-term brightness changes) from recovery through perihelion quite well (Chapter 8).

The success of the model to correctly yield information about important basic physical properties of a well-observed comet, lead to its application with less well-observed comets. The long-standing problem of whether or not a compositional difference exists between the periodic comets and new comets from the Oort cloud was addressed (in Chapter 9) by the application of the sublimation model to the dynamically new comet Bowell. Comet Bowell is the best observed comet of its class; it was recovered at $R = 7.3$ AU and observed fairly frequently through perihelion, after which the observations nearly stopped. The observations at $R = 11.0$ and 13.56 AU presented in this thesis show that the comet is still active. The observations are consistent with activity caused by sublimation from CO₂ ice.

Statements concerning a comparison between the compositions of new and old comets cannot yet be made based on this one comet. There are several dynamically new comets which are presently known to be active beyond the region of H₂O sublimation ($R > 6$ AU). Very few observations are being made of these comets, probably because of the incorrect belief that comets *cannot* be observed to large distances. Some of my future research will be

to observe these comets a few times per year until they become unobservable. (The timescale for these observations is several years). The data collected over a large range of distances can then be compared to sublimation models. It is hoped that observations of these comets will yield a consistent picture about the behavior of comets at large distances, and in particular, address the question regarding the compositional differences between new and old comets. At present, little observational work is being done in this area, so in effect, observations of the very distant comets are opening up a new branch of cometary investigations.

BIOGRAPHICAL NOTE

Karen Jean Meech

Department of Earth, Atmospheric and Planetary Sciences
 M.I.T. 54-416
 Cambridge, MA 02139
 (617) 253-5415

Date & place of birth: July 9, 1959 - Denver, Colorado

Education

B.A. (Physics) Rice University (Houston, TX) 1981, cum laude

Honors

1977-1981	President's Honor Roll (6 semesters)
1980	Board of Governor's Scholarship
	Sigma Pi Sigma (honor society of the Society of Physics Students)
1981	Heaps Prize in Physics for Senior Research Project on M33
	One of 5 nominees for national Apker Award (<i>Phys. Today</i> 12/81, p.67)
1986-1987	NASA Graduate Student Researchers Fellowship

Professional Experience

1/86 - 8/87	Graduate research assistant
9/82 - 1/86	Graduate research and teaching assistant
9/81 - 9/82	Assistant at the American Association of Variable Star Observers
9/81 - 9/82	Research Specialist at MIT
9/80 - 5/81	Quantum Physics course grader at Rice University
	Lab Assistant, Molecular Physics lab at Rice University
8/80	EARTHWATCH Scholarship - participated in Archeoastronomical expedition to Cusco, Peru under Drs. Anthony Aveni & R. T. Zuidema
6/79 - 8/79	Assistant at the American Association of Variable Star Observers
6/78 - 8/78	EARTHWATCH scholarship - research assistant at the Maria Mitchell Observatory (Nantucket, MA)

Publications**1987**

Meech, K. J. and D. C. Jewitt (1987). "Plasma Tail Dynamics of Comet P/Halley. I. The Observations", to be submitted to *Astrophys. J. Suppl.*

Meech, K. J. and D. C. Jewitt (1987), "Observations of Comet Bowell at Record Heliocentric Distance", *Nature* (in press).

Meech, K. J. and D. C. Jewitt (1987), "Observations of Comet P/Halley at Minimum Phase Angle", *Astron. Astrophys.* (in press).

Meech, K. J. and D. C. Jewitt (1987), "Periodic Comet d'Arrest", *IAU Circ.* No. 4365.

French, R. G., J. L. Elliot, L. M. French, J. A. Kangas, K. J. Meech, M. Ressler, M. W. Buie, J. A. Frogel, J. B. Holberg, J. J. Fuensalida and M. Joy (1987), "Normal Modes and Resonances in the Uranian Rings: Results from Earth-Based and Voyager Occultation Observations", *Icarus* (submitted).

Jewitt, D. C. and K. J. Meech (1987). "Continuum Surface Brightness Profiles of Ten Active Comets. I.", *Astrophys. J.* **317**, 992-1001.

Jewitt, D. C. and K. J. Meech (1987), "CCD Photometry of Comet P/Encke", *Astron. J.* **93**, 1542-1548.

Millis, R. L., L. H. Wasserman, O. G. Franz, W. Hubbard, L. Lebofsky, R. Goff, R. Marcialis, M. Sykes, J. Frecker, D. Hunten, B. Zellner, H. Reitsema, G. Schneider, E. Dunham, J. Klavetter, K. Meech, T. Oswalt, J. Rafert, E. Strother, J. Smith, H. Povenmire, B. Jones, D. Kornbluh, L. Reed, K. Izon, M. F. A'Hearn, W. Osborn, D. Parker, W. T. Douglas, J. D. Beish, A. Klemola, M. Rios, A. Sanchez, J. Piironen, M. Mooney, R. S. Ireland and D. Laibow (1987), "Results of the 1984 November Occultation by Ceres", *Icarus* (submitted).

1986

Meech, K. J. (1986), "The Recovery and the Development of the Coma and Tail of Halley's Comet", *Pittsburgh Conference & Exposition on Analytical Chemistry and Applied Spectroscopy*, 389b.

Meech, K. J. and D. C. Jewitt (1986), "Observations of Comet P/Halley at Minimum Phase Angle", in *Proceedings of the 20th ESLAB Symposium on the Exploration of Halley's Comet* (held in Heidelberg Germany 27-31 October 1986), eds. B. Battrick, E. J. Rolfe and R. Reinhard, ESA SP-250, ESLAB Pub. Division, Netherlands, Vol. I, 553-556.

Meech, K. J., D. Jewitt, and G. R. Ricker (1986), "Early Photometry of Comet p/Halley: Development of the Coma", *Icarus* **66**, 561-574.

Publications, contd.

Jewitt, D. and K. Meech (1986), "Cometary Grain Scattering versus Wavelength or "What Color is Comet Dust?" ", *Astrophys. J.* **310**, 937-952.

Jewitt, D. C. and K. J. Meech (1986), "Scattering Properties of Cometary Grains - Comet P/Halley", in *Proceedings of the 20th ESLAB Symposium on the Exploration of Halley's Comet* (held in Heidelberg Germany 27-31 October 1986), eds. B. Battrick, E. J. Rolfe and R. Reinhard, ESA SP-250, ESLAB Pub. Division, Netherlands, Vol. II., 47-51.

1985

Elliot, J. L., R. L. Baron, E. W. Dunham, R. G. French, K. J. Meech, D. J. Mink, D. A. Allen, M. C. B. Ashley, K. C. Freeman, E. F. Erickson, J. Goguen, H. B. Hammel (1985), "The 1983 June 15 Occultation by Neptune. I. Limits on a Possible Ring System", *Astron. J.* **90**, 2615-2623.

French, Richard G., Pamela A. Melroy, Richard L. Baron, Edward W. Dunham, Karen J. Meech, Douglas J. Mink, J. L. Elliot, David A. Allen, Michael C. B. Ashley, Kenneth C. Freeman, Edwin F. Erickson, Jay Goguen, H. B. Hammel (1985), "The 1983 June 15 Occultation by Neptune. II. The Oblateness of Neptune", *Astron. J.* **90**, 2624-2638.

French, R. G., R. L. Baron, J. L. Elliot, L. M. French, J. A. Kangas, K. J. Meech, M. Ressler, J. Frogel, J. Jimenez, M. Joy, E. F. Erickson, K. Matthews, B. T. Soifer, G. Neugebauer, P. Nicholson (1985), "The 4 May and 24 May 1985 Occultations by the Uranian Rings", *Bull. Amer. Astron. Soc.* **17**, No. 3, 718.

Jewitt, D. and K. J. Meech (1985), "Rotation of the Nucleus of Comet p/Arend- Rigaux", *Icarus* **64**, 329-335.

Meech, K. and D. Jewitt (1985). Periodic Comet Halley. *IAU Circular No. 4148*.

1984

Elliot, J. L., R. G. French, K. J. Meech and J. H. Elias (1984), "Structure of the Uranian Rings. I. Square-Well Model and Particle Size Constraints", *Astron. J.* **89**, 1587-1603.

1983

Meech, K. J. (1983), "Photoelectric Sequences For EX Hydrae, V2051 Ophiuchi and VV Puppis", *Pub. Astron. Soc. Pacific.* **95**, 662-665.

Publications, contd.

Meech, K. J. and J. L. Elliot (1983), "The Angular Diameter of MKE 30 Occulted by Neptune on 15 June 1983", *Bull. Amer. Astron. Assoc.* **15**, 817.

Elliot, J. L., J. H. Elias, R. G. French, J. A. Frogel, W. Liller, K. Matthews, K. J. Meech, D. J. Mink, P. D. Nicholson and B. Sicardy (1983), "The Rings of Uranus: Occultation Profiles From Three Observatories", *Icarus* **56**, 202-208.

1978

Meech, K. J. (1978), "S4082 in Cygnus, an SR Star", *Inf. Bull. Var. Stars, Commission #27, No. 1464*.

Meech, K. J. (1978), "S4831 a Probable RV Tauri Type", *Inf. Bull. Var. Stars, Commission #27, No. 1465*.

Meech, K. J. (1978), "Verification of S4846 in Cygnus", *Inf. Bull. Var. Stars, Commission #27, No. 1466*.

Oral Presentations

"The Angular Diameter of MKE 30, Occulted by Neptune on 15 June 1983", *Bull. Amer. Astron. Soc.* **15**, 817. Division of Planetary Sciences Meeting, Ithaca NY - October 1983.

"Development of the Coma of Comet P/Halley", *Bull. Amer. Astron. Soc.* **17**, 685. Division of Planetary Sciences Meeting, Baltimore, MD - October 1985.

Dana Hall School Science Club, Wellesley MA - November 1985.

Physics Colloquium University of Connecticut, Storrs CT - February 1986.

"Development of the Coma and Tail of Comet P/Halley", *Pittsburgh Conference & Exposition on Analytical Chemistry and Applied Spectroscopy*, Pittsburg Analytical Chemistry Conference (invited speaker), Atlantic City NJ - March 1986.

Astrophysics Colloquium Yale University, New Haven CT - April 1986.

Kitt Peak Colloquium, Tucson, AZ - October 1986.

"Continuum Radial Surface Brightness Profiles of Ten Comets", *Bull. Amer. Astron. Soc.* **18**, 826. Division of Planetary Sciences Meeting, Paris, France - November, 1986.

Astrophysics Colloquium, University of Hawaii, Honolulu HI - January 1987.

Planetary Science Colloquium, Center for Astrophysics, Cambridge MA - February 1987.

Cerro Tololo Interamerican Observatory Colloquium - May 1987.

Appendix 1 - Calculation of Ephemerides

A1.1 Geocentric Two Body Orbit

The motion of a particle (comet) of mass m in a central force field, where the force is Newton's law of Gravitation is given by:

$$m \ddot{\mathbf{r}} = - \frac{G M m}{r^2} \frac{\mathbf{r}}{r} \quad (\text{A1.1})$$

where M is the mass of the central body (in this case the sun, $M = 1.989 \times 10^{30}$ kg), and $G = 6.673 \times 10^{-11}$ Nt m² kg⁻² is the Gravitational constant. The product GM is often written as μ ; so that Eq. A1.1 becomes:

$$\ddot{\mathbf{r}} = - \mu \mathbf{r}^{-3} \mathbf{r} \quad (\text{A1.2})$$

According to Kepler's first law, the comet moves in a plane which contains the sun. The path of the comet is described by a conic section of eccentricity, e , with the sun at one focus. The path is given by (Pollard, 1976):

$$r = \frac{h^2 / \mu}{1 + e \cos(\nu)} \quad (\text{A1.3})$$

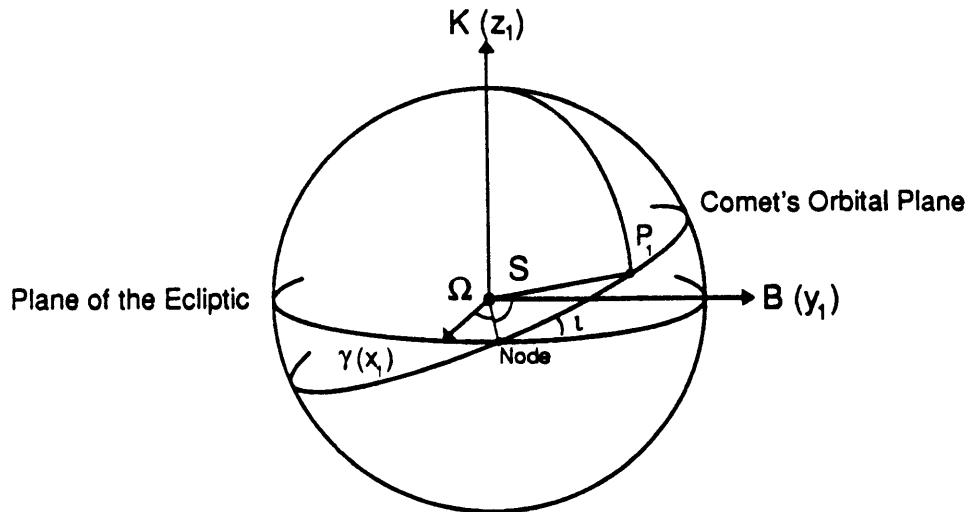
where mh is the angular momentum of the comet, and the angle, ν , is called the true anomaly. It is the angle measured from the point of closest approach to the sun, perihelion to the position, r , on the orbit. The *shape* of the orbit is determined by the values of the semi-major

axis, a , and the eccentricity. The *orientation* of the orbit is determined by the parameters i , Ω and ω , which are the inclination of the comet's orbital plane to the Earth's orbital plane (ecliptic), the longitude of the ascending node, and the argument of the perihelion, respectively. These values are defined in Figure A1-1. The final parameter which is required to compute the position of a comet is ν , which describes the position on the orbit as a function of time.

The basic procedure for computing the position of a comet at a particular time (or a series of positions as a function of time - an ephemeris) is as follows. The comet orbital elements refer to the position of the sun and the plane of the ecliptic. Using a coordinate system centered on the sun and defined by the plane of the ecliptic, spherical trigonometry is used to convert the angular orbital elements into heliocentric ecliptic rectangular coordinates. The coordinate system is rotated to refer to the celestial equator, an extension of the Earth's equator. Since the coordinates of interest are those positions which are referred to the Earth, the geocentric equatorial rectangular coordinates are computed by translating the coordinate axes. Finally, the geocentric rectangular coordinates are converted to the standard coordinates on the celestial sphere (used for observing): the right ascension (α) and declination (δ). The notation used throughout the computation follows that of Smart (1971).

A1.1.1 Heliocentric Ecliptic Coordinates

Referring to Figure A1-1 the coordinate axes are defined such that the x-axis lies in the plane of the ecliptic and is defined to be in the direction of the vernal equinox, γ . The y-axis is also in the plane of the ecliptic. The sun, S , is at the origin. The point P_1 indicates the intersection of the comet's position vector, $r(t)$ with the celestial sphere:

Figure A1-1

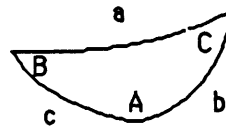
The symbols used in the Figure are defined as follows:

Ecliptic	- mean plane of the Earth's orbit
Node	- point at which the comet's orbit crosses the ecliptic
P_1	- point of intersection of the projection of the comet's radius vector with the celestial sphere
γ Vernal Equinox	- the ascending node of the ecliptic on the celestial equator (the projection of the Earth's equator)
Ω Longitude of ascending node	- angular measure from the direction of the vernal equinox to the ascending node in the plane of the ecliptic
i inclination	- angle between the plane of the comet's orbit and the ecliptic
ω argument of perihelion	- angular measure from the ascending node (in the orbital plane of the comet) to the direction of perihelion.
v true anomaly	- angular measure from the point of closest approach to the sun, perihelion to the position, r , on the orbit

$$\begin{aligned}
 x_1 &= r \cos (P_1 S \gamma) \\
 y_1 &= r \cos (P_1 S B) \\
 z_1 &= r \cos (P_1 S K).
 \end{aligned}
 \tag{A1.4}$$

Using the law of cosines, $\cos (a) = \cos (b) \cos (c) + \sin (b) \sin (c) \cos (A)$, where the variables are as in the figure below,

Figure A1-2



the cosines of the angles in Eqs. A1.4 can be written as follows:

$$\begin{aligned}
 \cos (P_1 S \gamma) &= \cos (\Omega) \cos (\omega + \nu) + \sin (\Omega) \sin (\omega + \nu) \cos (180 - \iota) \\
 \cos (P_1 S B) &= \cos (\omega + \nu) \cos (90 - \Omega) + \sin (\omega + \nu) \sin (90 - \Omega) \cos (\iota) \\
 \cos (P_1 S K) &= \cos (90) \cos (\omega + \nu) + \sin (90) \sin (\omega + \nu) \cos (90 - \iota).
 \end{aligned}
 \tag{A1.5}$$

Substituting Eq. A1.5 into Eqs. A1.4 gives:

$$\begin{aligned}
 x_1 &= r [\cos (\Omega) \cos (\omega + \nu) - \sin (\Omega) \sin (\omega + \nu) \cos (\iota)] \\
 y_1 &= r [\cos (\omega + \nu) \sin (\Omega) + \sin (\omega + \nu) \cos (\Omega) \cos (\iota)] \\
 z_1 &= r [\sin (\omega + \nu) \sin (\iota)]
 \end{aligned}
 \tag{A1.6}$$

where r , the heliocentric distance, is defined as follows:

$$r = [x_1^2 + y_1^2 + z_1^2]^{1/2}$$

Eqs. A1.6 are the heliocentric ecliptic rectangular coordinates of the comet.

A1.1.2 Heliocentric Equatorial Coordinates

The ecliptic plane is inclined by an angle ϵ , known as the obliquity of the ecliptic, to the plane of the celestial equator. Converting from heliocentric ecliptic coordinates involves a rotation about Sy by the angle ϵ . The heliocentric equatorial rectangular coordinates are then given by:

$$\begin{aligned} x &= x_1 \\ y &= y_1 \cos(\epsilon) - z_1 \sin(\epsilon) \\ z &= y_1 \sin(\epsilon) + z_1 \cos(\epsilon) \end{aligned} \tag{A1.7}$$

A1.1.3 Comet's Geocentric Right Ascension and Declination

The first step in the computation of the geocentric spherical coordinates of the comet requires a translation of the origin from the sun to the Earth (E). In the translated coordinate system, where the Earth is at the origin (see Figure A1-3), let (X, Y, Z) be the coordinates of the Sun with respect to the Earth (or conversely, the heliocentric rectangular coordinates of the Earth with respect to the sun are given by $(-x', -y', -z')$, where the primes refer to the Earth). Let the comet be at point P , and the coordinates of the comet with respect to the Earth be (ξ, η, ζ) . Therefore,

$$\begin{aligned} \xi &= x + X \\ \eta &= y + Y \end{aligned} \tag{A1.8}$$

$$\zeta = z + Z$$

$$\Delta = [\xi^2 + \eta^2 + \zeta^2]^{1/2}$$

where Δ is defined to be the geocentric distance, or the distance between the Earth and comet. The coordinates of the Sun with respect to the Earth may be computed in the same manner in which the heliocentric ecliptic coordinates for the comet were obtained, taking $t = 0$ for the Earth. Instead of an exact computation, the position of the sun may be interpolated from tabulated values at intervals of a few days. Alternatively, positions of the sun at any time, t , may be computed from approximate formulas provided in the *Almanac for Computers*. Although only approximations, the positions are sufficiently accurate for the computation of cometary ephemerides.

Figure A1-3

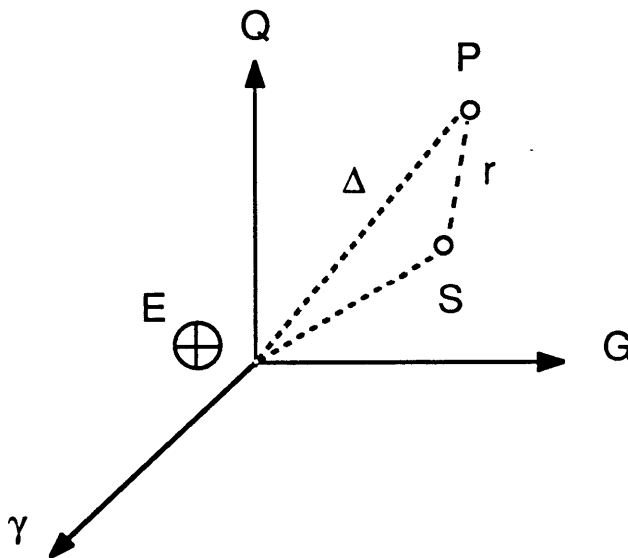
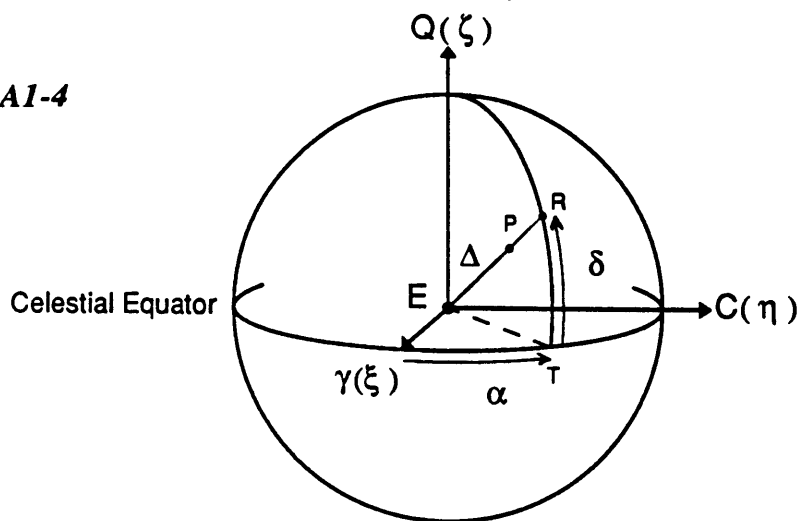


Figure A1-4 depicts the celestial sphere centered on the Earth. As in Figure A1-1, one of the coordinate axes (ξ) is defined by the direction of the vernal equinox. However, unlike Figure A1-1, the celestial equator defines the ξ - η plane. As before, the position of the comet is denoted by P . The intersection of the projection of the line EP cuts the celestial sphere at R . The right ascension (α) is the angle measured eastward from the vernal equinox along the celestial equator to the point where the great circle passing through Q and R cuts the celestial equator (T). The declination (δ) is the angle TR . The right ascension and declination can

Figure A1-4



be obtained from the coordinates (ξ, η, ζ) by using the law of cosines. This gives:

$$\begin{aligned} \xi &= \Delta \cos (RE\gamma) \\ \eta &= \Delta \cos (REC) \\ \zeta &= \Delta \cos (REQ) \end{aligned} \tag{A1.9}$$

where:

$$\begin{aligned} \cos (RE\gamma) &= \cos (\alpha) \cos (\delta) + \sin (\alpha) \sin (\delta) \cos (90) \\ \cos (REC) &= \cos (\delta) \cos (90 - \alpha) + \sin (\delta) \sin (90 - \alpha) \cos (90) \\ \cos (REQ) &= \cos (90 - \delta) \end{aligned} \tag{A1.10}$$

Substitution of Eqs. A1.10 into Eqs. A1.9 results in the following expressions relating the geocentric rectangular coordinates to the spherical coordinates of the comet:

$$\begin{aligned}\xi &= \Delta \cos (\alpha) \cos (\delta) \\ \eta &= \Delta \sin (\alpha) \cos (\delta) \\ \zeta &= \Delta \sin (\delta),\end{aligned}\tag{A1.11}$$

or after rearranging:

$$\tan (\alpha) = \frac{\eta}{\xi} \quad \frac{\tan (\delta)}{\sin (\alpha)} = \frac{\zeta}{\eta} \quad \Delta = \frac{\zeta}{\cos (\alpha) \cos (\delta)}\tag{A1.12}$$

A1.1.4 Position on the Orbit as a Function of Time

From the previous discussion it appears that the computation of the α and δ of the comet is fairly straightforward. However, there is one parameter, namely the true anomaly, which has not yet been discussed. Kepler's second law states that the time rate of change of the area swept out by the sun-planet (or comet) radius is constant. Physically, this says that angular momentum is conserved. Mathematically, this is expressed as

$$\frac{1}{2} r^2 \frac{d\nu}{dt} = \frac{dA}{dt} = \text{constant}\tag{A1.13}$$

where the constant is just $h/2$. Combining Eq. A1.13 with Eq. A1.3 yields a differential equation for ν as a function of t . Taking $p = h^2 / \mu$, the differential equation is

$$\frac{dv}{[1 + e \cos(v)]} = \sqrt{\frac{\mu}{p^3}} dt \quad (\text{A1.14})$$

For a parabolic orbit $e = 1$ (the energy per unit mass, $-\mu / 2a$, is zero) and Eq. A1.14 is directly integrable.

$$\frac{1}{3} \tan^3\left(\frac{v}{2}\right) + \tan\left(\frac{v}{2}\right) = \frac{2\sqrt{\mu}}{\sqrt{p^3}} (t - \tau) \quad (\text{A1.15})$$

The constant of integration in Eq. A1.15, τ , is the time of perihelion passage. An iterative solution to equation A1.15 produces the desired $v(t)$ for a parabolic orbit.

In the case of elliptical motion ($e < 1$; energy < 0) Eq. A1.14 is not directly integrable, so another method of solution must be found. A change of variables:

$$\tan\left(\frac{v}{2}\right) = \left(\frac{1+e}{1-e}\right)^{1/2} \tan\left(\frac{E}{2}\right) \quad (\text{A1.16})$$

is introduced so that Eq. A1.3 becomes:

$$r \equiv a [1 - e \cos(E)] \quad (\text{A1.17})$$

where for elliptic motion $p = h^2 / \mu = a(1 - e^2)$. The angle E is called the eccentric anomaly.

With the change of variables, Eq. A1.14 becomes:

$$[1 - e \cos(E)] dE = \sqrt{\frac{\mu}{a^3}} dt \quad (\text{A1.18})$$

Equation A1.17 is easily integrated, with the solution

$$E - e \sin(E) = \eta (t - \tau) \equiv M \quad (\text{A1.19})$$

Equation A1.18 is known as Kepler's equation, and it can be easily solved numerically. The quantity $\eta \equiv [\mu / a^3] = 2 \pi / T$ is the mean motion, where T is the period of the comet.

A similar parameterization may be used for hyperbolic motion, however, in practice there are very few comets on orbits which are sufficiently hyperbolic that a separate solution is needed. The parabolic solution is sufficient for both parabolic orbits and nearly parabolic orbits.

A1.2 Refinements of the Two-Body Ephemeris

A1.2.1 Perturbations

In general, a comet will not follow an unperturbed orbit where the only gravitational interaction is with the sun. This orbit is called the osculating orbit. The orbit is perturbed by close approaches to the planets. After accounting for the influence of the planets, most comets still exhibit non-gravitational motion. It was this type of motion which lead Whipple (1950,1951) to infer that the nucleus of a comet is a solid body. The perturbations arise from anisotropic ejection of material from the nucleus, which creates jet forces. It is especially important to account for both the effects due to anisotropic ejection of material and planetary perturbations if one is attempting to recover or re-observe a periodic comet as it approaches the sun from aphelion. However, for comets close to the sun which are being observed, the orbital elements are frequently updated to include these effects. In most cases the simple two-body ephemeris is sufficiently accurate to find comets for observation.

A1.2.2 Aberration, Light Travel and Topocentric position

Strictly speaking, the effects of aberration, the finite light travel time (comets are observed at their positions for time $t = t_{present} - \Delta / c$, where c is the speed of light), and the fact that the observer is on the surface of a sphere, not at the center of the Earth, must be accounted for. However, in most cases the deviations from a two-body orbit are small compared to other errors; therefore the corrections are omitted. Without going into a detailed discussion about the magnitudes of these effects, it should suffice to say that the simple two-body program was sufficiently accurate to find over 80% of the objects attempted. Failures may have been due in part to (1) mis-estimated brightness, (2) poor elements (orbits for newly discovered comets) and (3) using elements far from epoch of osculation.

References

- ____ (1984-7), *The Almanac for Computers 198_*, Nautical almanac Office, United States Naval Observatory, Washington.
- ____ (1984-7), *The Astronomical Almanac*, US Government Printing Office, Washington.
- Pollard, H. (1976), *Celestial Mechanics*, (Carus Mathematical Monographs #18), The Mathematical Association of America, USA
- Smart, W. M. (1971), *Text-Book on Spherical Astronomy*, Cambridge University Press, Cambridge.
- Tattersfield, D. (1984), *Orbits for Amateurs With a Microcomputer*, Halsted Press, New York.
- Whipple, F. L. (1950), "A Comet Model. I. the Acceleration of Comet Encke", *Astrophys. J.* **111**, 375-394.
- Whipple, F. L. (1951), "A Comet Model. II. Physical Relations for Comets and Meteors", *Astrophys. J.* **113**, 464-474.

Appendix 2

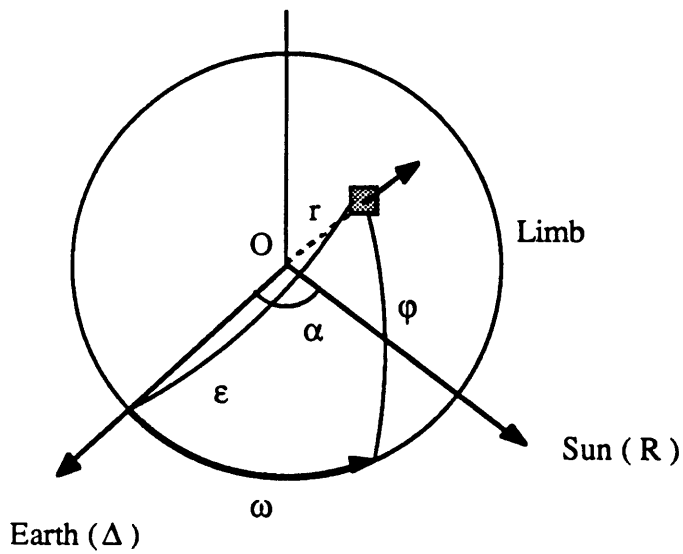
Relationship Between Albedo, Size and Brightness of the Nucleus

There is a simple relationship between the apparent brightness, the geometrical cross section and the geometric albedo of the surface of a comet nucleus. The comet nucleus scatters solar radiation incident upon its surface. The relationship between the brightness of the sun and the brightness of the nucleus is:

$$m_{\text{O}} - m = -2.5 \log \left[\frac{F_{\text{O}}}{F_{\text{c}}} \right] \quad (\text{A2.1})$$

where m_{O} is the apparent magnitude of the sun, m is the apparent magnitude of the comet nucleus (a measured quantity), F_{O} is the solar flux ($1360.74 \text{ J s}^{-1} \text{ m}^{-2}$) incident at the Earth and F_{c} is the flux incident at the Earth which has been scattered from the comet. All quantities in Eq. A2.1 refer to a specific wavelength or bandpass. Both the magnitudes and the flux densities are typically specified for a particular wavelength region, or bandpass. The solar flux at the Earth is just $F_{\text{O}} = L / (4 \pi R_{\text{e}}^2)$ where $L_{\text{O}} = 3.8268 \times 10^{26} \text{ J s}^{-1}$ is the solar luminosity and $R_{\text{e}} = 1.495 \times 10^{11} \text{ m}$ is the mean Earth-sun distance ($R_{\text{e}} = 1$ Astronomical Unit [AU]).

The amount of light scattered from the comet is a function of the angular separation, α , between the Earth and the sun as seen from the comet. Figure A2-1 defines the coordinate system and variables used in this discussion (after Russell, 1916). The computation of F_{c} requires the integration of the scattered light from each surface element on the nucleus. The amount of energy, dE (at a particular wavelength, λ) scattered per unit time, dt , per wavelength interval, $d\lambda$, into a solid angle $d\Omega$, from an element of surface area $d\sigma$ is related to the specific intensity via:

Figure A2-1

O Object center

α phase angle - the angle between the sun and the Earth as seen from the object

ω longitude of surface element, $d\sigma$, on the object

ϕ latitude of surface element on body, measured from the photometric equator as defined by the intersection of the Earth-object line with the surface of the body

ϵ angle between the object-Earth line and the normal to a surface element on the body

Δ Earth-object distance

R Sun-object distance

r radius of the body

$$I = \frac{dE}{dt d\Omega d\lambda d\sigma \cos(\epsilon)} \quad (\text{A2.2})$$

where ϵ is the angle between the object-Earth line and the normal to the surface element. The flux, by definition, is the total energy flowing through the surface per unit time per unit area in a particular $\Delta\lambda$; hence from Eq. A2.2

$$F_c = \int I \cos(\epsilon) d\Omega \quad (\text{A2.3})$$

where $d\Omega = dA / \Delta^2$ and the element of area, $dA = r^2 \cos(\varphi) d\varphi d\omega$. From spherical trigonometry,

$$\cos(\epsilon) = \cos(\omega) \cos(\varphi) + \sin(\omega) \sin(\varphi) \cos(\pi/2) = \cos(\omega) \cos(\varphi) \quad (\text{A2.4})$$

Therefore, Eq. A2.3 becomes:

$$F_c(\alpha) = \left(\frac{r}{\Delta^2}\right) \int_{\varphi=-\frac{\pi}{2}}^{\varphi=\frac{\pi}{2}} \int_{\omega=-\frac{\pi}{2}+\alpha}^{\omega=\frac{\pi}{2}} I(\omega, \varphi) \cos^2(\varphi) \cos(\omega) d\varphi d\omega \equiv \left(\frac{r}{\Delta}\right)^2 j(\alpha) \quad (\text{A2.5})$$

where by definition the limb of the object is at longitude $\omega = \pi/2$. Eq. A2.5 represents the scattered flux at any phase angle, α , from the cometary nucleus.

The scattered flux and the geometric albedo of the body are related through the Bond albedo. By definition, the Bond albedo is the ratio of the total amount of scattered radiation to the incident radiation. Assuming that the solar specific intensity is isotropic (independent of

angle), the incident flux at the comet is (πI) , and the energy absorbed per second at the comet is $P_{in} = (\pi r^2) (\pi I)$. The power out is computed by integrating $F_c(\alpha)$ over the surface of a sphere of radius Δ centered on the object:

$$\begin{aligned} P_{out} &= \int_0^{\pi} F(\alpha) [2 \pi \Delta \sin(\alpha)] [\Delta d\alpha] \\ &= 2 \pi \Delta^2 \int_0^{\pi} F(\alpha) \sin(\alpha) d\alpha \end{aligned} \quad (\text{A2.6})$$

Therefore, the Bond albedo, A , is given by:

$$A \equiv \frac{2 \pi \Delta^2 \int_0^{\pi} F(\alpha) \sin(\alpha) d\alpha}{[\pi r^2] [\pi I]} \quad (\text{A2.7})$$

which can be simplified using Eq. A2.5, yielding

$$A = \frac{2}{\pi I} \int_0^{\pi} j(\alpha) \sin(\alpha) d\alpha. \quad (\text{A2.8})$$

Let $\phi(\alpha) = j(\alpha) / j(0)$, where $j(0)$ is the amount of light scattered at zero phase angle. Eq. A2.8 then becomes:

$$A = \left[\frac{j(0)}{\pi I} \right] 2 \int_0^{\pi} \phi(\alpha) \sin(\alpha) d\alpha. \quad (\text{A2.9})$$

The term $[j(0) / \pi I] \equiv p$ is known as the geometric albedo and is defined as the "ratio of the flux received from a planet to that expected from a perfectly reflecting Lambert (perfectly diffusing surface, where the intensity varies as the cosine of the angle of emission from measured from the normal to the surface) disk of the same size at the same distance at zero phase angle" (in *Asteroids*, 1982 p. 1161). The second term in Eq. A2.9, is known as the phase integral: $q \equiv 2 \int \phi(\alpha) \sin(\alpha) d\alpha$. The phase integral specifies the pattern into which the surface scatters light.

The final expression relating the geometric albedo, the nucleus cross section and the apparent brightness at $\alpha=0^\circ$ is obtained by substituting the value for $F_c(\alpha=0)$ (Eq. A2.5) into Eq. A2.1. The solar flux, F_O at the Earth can be expressed in terms of the solar flux incident at the comet, $F_i = \pi I = L_O / [4 \pi R^2] = F_O [R_e / R]^2$. The substitutions yield:

$$m_O - m(0) = -2.5 \log \left[\frac{(\pi I) (R / R_e)^2}{(r / \Delta)^2 j(0)} \right] \quad (\text{A2.10})$$

or using the definition of geometric albedo and rearranging,

$$p r^2 = \frac{R^2 \Delta^2}{R_e^2} 10^{0.4[m_O - m(0)]} \quad (\text{A2.11})$$

The term $m(0)$ denotes that the brightness was measured at $\alpha = 0$ deg. If the distances R and Δ are expressed in AU, the equation becomes:

$$p r^2 = 2.235 \times 10^{22} R^2 \Delta^2 10^{0.4[m_0 - m(0)]} \quad (\text{A2.12})$$

which is identical to Eqs. 2.3 and 3.1. The albedo, p , is a function of the wavelength as are m_0 and $m(0)$.

Often the nucleus brightness measurements are not made at zero phase angle. In order to use Eq. A2.12 the magnitude must be reduced to zero phase angle. The variation of brightness with phase, $m(\alpha)$, can be expressed as

$$m(\alpha) \equiv m = m(0) + \beta \alpha + \text{nonlinear term} \quad (\text{A2.13})$$

where β is the linear phase coefficient [mag deg^{-1}], and the nonlinear term is due to an opposition surge seen in asteroids (see Chapter 4 for a more complete discussion). Representing the phase terms in Eq. A2.13 as a function $\Phi(\alpha)$, Eq. A2.12 may also be expressed as:

$$p r^2 = \frac{2.235 \times 10^{22} R^2 \Delta^2 10^{0.4[m_0 - m]}}{f(\alpha)} \quad (\text{A2.14})$$

where

$$f(\alpha) = 10^{-0.4\Phi(\alpha)}.$$

References

Gehrels, T., editor (1982). *Asteroids*, Univ. of AZ Press, Tucson, AZ.

Russell, H. N. (1916), "On the Albedo of the Planets and Their Satellites", *Astrophys. J.* **43**, 173-195.

*Appendix 3**Latent Heats of Sublimation and Vapor Pressures*

The formulae for the latent heats and vapor pressures used in this paper are as follows.
All latent heats, $L(T)$, are in J kg^{-1} and pressures in N m^{-2} .

$$L_{\text{H}_2\text{O}}(T) = 2.863 \times 10^6 - 1.106 \times 10^3 * T \quad (\text{after Cowan and A'Hearn, 1982})$$

$$\begin{aligned} \log(P_{\text{H}_2\text{O}}/760) = & -2445.5646/T + 8.2312 * \log(T) - 0.01677006 * T \\ & + 1.20514 \times 10^{-5} * T^2 - 1.757169 \quad (\text{Washburn, 1928}) \end{aligned}$$

$$L_{\text{CO}_2}(T) = 5.724 \times 10^5 \quad (\text{Smith, 1929})$$

$$\log(P_{\text{CO}_2}/760) = -1367.3/T + 14.9082 \quad T > 138\text{K}$$

$$\log(P_{\text{CO}_2}/760) = -1275.6/T + 0.00683 * T + 13.307 \quad T < 138\text{K}$$

(Eggerton and Edmondson, 1928)

References

- Cowan, J. J. and M. F. A'Hearn (1982). "Vaporization in Comets; Outbursts From Comet Schwassmann-Wachmann 1", *Icarus* **50**, 53-62.
- Eggerton, A. C. and W. Edmondson (1928), "Vapor Pressure of Chemical Compounds in the Crystalline State", In *International Critical Tables, Vol. III*. McGraw Hill, NY, 207.
- Smith, A. W. (1929), "Latent Heat of Vaporization", in *International Critical Tables, Vol. V.*, McGraw-Hill, NY, p. 138.
- Washburn, E. W. (1928), "The Vapor Pressures of Ice and Water up to 100°C", In *International Critical Tables, Vol. III.*, McGraw Hill, NY, 210-212.

Appendix 4
Cometary Comae

A4.1 Surface Brightness Profile

Many cometary observations require the knowledge of how the coma surface brightness varies as a function of the projected distance, p [m], from the nucleus in the plane of the sky. The surface brightness, $B(p)$, for an optically thin coma is proportional to the number of particles, n , within the observing diaphragm. That is, $B(p) \propto n$ where

$$n = \int N(r) \sigma dl \quad (\text{A4.1})$$

The integrand is the product of the number density of particles, N [m^{-3}], as a function of distance, r [m], from the nucleus and the projected diaphragm size, σ [m^2], at the distance of the nucleus integrated along the line of sight through the coma, dl (see Figure A4-1).

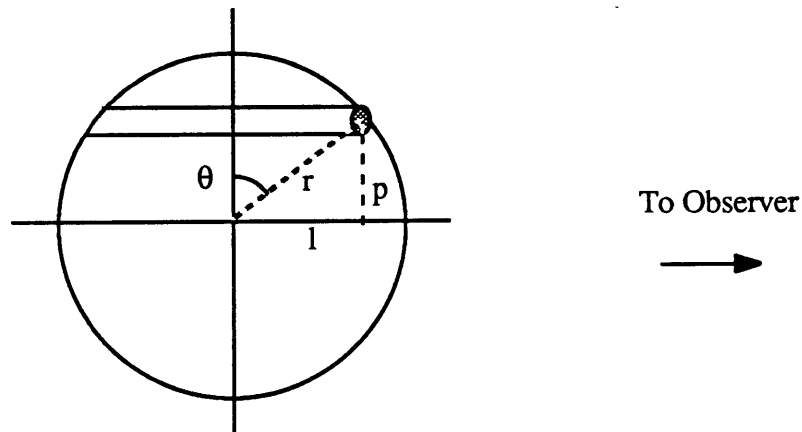


Figure A4-1

From the equation of continuity, the particles leaving the surface of the nucleus of radius r_n must also pass through a sphere of radius $r_n + \Delta r$. Mathematically, this is expressed as:

$$Q = \frac{4 \pi (r_n + \Delta r)^2 \Delta r N(r_n)}{\Delta t} \quad (\text{A4.2})$$

where Q is the dust production rate in grains s^{-1} . Assuming that $r_n \gg \Delta r$, and that $\Delta r / \Delta t$ is the velocity, v , in m s^{-1} (assumed to be \approx constant with r) the expression for the number density as a function of r is:

$$N(r) = \frac{Q}{4 \pi v r^2} = \frac{Q}{4 \pi v r_n^2} \left(\frac{r_n}{r} \right)^2 \quad (\text{A4.3})$$

Therefore, the number of grains along the line of sight into the coma is given by:

$$n = \frac{Q \sigma}{4 \pi v} \int_{-\infty}^{\infty} \frac{dl}{l^2 + p^2} \quad (\text{A4.4})$$

Equation A4.4 is easily integrated using the substitution $l = p \tan(\theta)$, $dl = p \sec^2(\theta)$. Letting the projected circular diaphragm, σ , have an angular radius ϕ [arcsec] at a distance Δ [AU] from the earth, the number of grains is:

$$n = \frac{Q \pi \phi^2 \Delta}{4 d v p} \quad (\text{A4.5})$$

The quantity $d = 206265 / 1.495 \times 10^{11}$ is the scale factor when both ϕ and p' are measured in arcsec ($p' = pd/\Delta$). The surface brightness is then

$$B(p') = \frac{Q \pi \phi^2 \Delta}{4 v d p'} \left(\frac{F_O}{R^2} \right) \pi a^2 Q_s \quad (\text{A4.6})$$

where F_O / R^2 is the solar flux [$\text{J s}^{-1} \text{m}^{-2}$] at the distance (R) of the comet, πa^2 is the geometric cross section of the grains and $Q_s = Q_s(\lambda)$ is the scattering efficiency.

The expression for the surface brightness in Eq. A4.6 is not valid for a diaphragm centered on the nucleus because here $p = 0$. At any distance p [m] from the center, the number of grains is given by Eq. A4.5. The number of grains in a column per unit area [m^{-2}] is then

$$n'(p) = \frac{n(p)}{dA} = \frac{Q}{4 v p} \quad (\text{A4.7})$$

Integrating in circular annuli about the center to get the total number in a column centered on the nucleus

$$n' = \int_{p=0}^{\phi\Delta/d} (2 \pi p) n(p) dp = \frac{Q \pi}{2 v} \int_{p=0}^{\phi\Delta/d} dp = \frac{Q \pi \phi \Delta}{2 v d} \quad (\text{A4.8})$$

The ratio between the brightness at a distance p [arcsec] and the brightness at the center is just

$$n(p) / n(p=0) = \frac{\phi}{2 p} \quad (\text{A4.9})$$

Eq. A4.9 is useful for estimating the amount of coma contamination in a sky measurement. In the case of IR observations, the sky measurements are often made by chopping into the coma. (Note: This method assumes that the aperture size is small compared to the extent of the coma so that surface brightness variations across the aperture are negligible).

A4.2 Optical Depth in the Coma

One of the assumptions implicit in the computation of the surface brightness profile is that the coma is optically thin. The optical depth is defined as the integral

$$\tau \equiv \int_{l_1}^{l_2} k_{\lambda} \rho \, dl \quad (\text{A4.10})$$

where k_{λ} [$\text{m}^2 \text{kg}^{-1}$] is the mass extinction coefficient, ρ [kg m^{-3}] is the particle density, and dl is the path length. For computing the optical depth, the integrand is more conveniently expressed in terms of the extinction cross section of the particles and the number density

$$k_{\lambda} \rho = \sigma_E [\text{m}^2] N(r) [\text{m}^{-3}] \quad (\text{A4.11})$$

Substituting the expression for $N(r)$ from Eq. A4.3 and integrating yields:

$$\tau = \int_{-\infty}^{\infty} (\pi a^2 Q_s) \left[\frac{Q}{4 \pi v r^2} \right] dl = \frac{a^2 Q_s Q}{4 v} \int_{-\infty}^{\infty} \frac{dl}{l^2 + p^2} = \frac{Q \pi a^2 Q_s}{4 v p} \quad (\text{A4.12})$$

The condition for an optically thin coma is $\tau \ll 1$. At $R = 1$ AU a typical molecular production rate for a water ice comet is $Q_{gas} \approx 10^{30}$ molecules sec^{-1} . Assuming a maximum dust to gas mass ratio of 1 (this is an upper limit) and dust grain sizes near $a \approx 1 \mu\text{m}$, and $\rho \approx 10^3 \text{ kg m}^{-3}$, the dust particle production rate is of the order $Q \leq 7.2 \times 10^{18}$ grains sec^{-1} . Using the Bobrovnikoff velocity relation (Delsemme, 1982) of $v \approx 600 R^{-0.5} \text{ m sec}^{-1}$, the distance from the nucleus at which $\tau \approx 1$ is

$$p = \frac{(7.2 \times 10^{18}) (\pi) (10^{-6})^2}{(4) (600)} < 10^{+4} \text{ m} \quad (\text{A4.13})$$

At $R = 1$ AU, this subtends an angle of ≤ 0.01 arcsec, which is comparable to the nucleus radius, and is therefore unresolvable. For comparison, at $\phi = 1$ arcsec $\tau \approx 10^{-2}$. Therefore, for all practical purposes, the coma is optically thin.

A4.3 Coma Brightness as a Function of Δ

As the geocentric distance, Δ , from an object increases, the brightness varies as Δ^{-2} . For an extended coma which has a surface brightness profile which varies as $1/p$ and which is not contained within the observing diaphragm, the brightness will vary as Δ^{-1} since the area of the scatterer depends on Δ (see Eq. A4.8).

References

- Delsemme, A. H. (1982), "Chemical Composition of Cometary Nuclei", in *Comets*, ed. L. L. Wilkening, Univ. of AZ Press, Tucson, AZ, p. 85-130.

Appendix 5 - Radiation Pressure

Radiation pressure plays an important role in cometary studies because of its interaction with the dust grains in the coma. The shapes of the comae and the formation of tails are in large part determined by the effects of radiation pressure (see Chapter 7). Radiation pressure analysis of measurements of the shapes and orientations of dust tails has lead to estimates of the grain sizes within the tails. A very simple discussion of the radiation forces is presented below.

The force felt by a particle of cross section $Q_{pr} \pi a^2$ where Q_{pr} is the radiation pressure efficiency, depends on the solar luminosity, $L_{\odot} = 3.827 \times 10^{26} \text{ [J s}^{-1} \text{ m}^{-2}]$, and its distance from the sun, R . The force is just the time rate of change of momentum, where the momentum is, $p = E / c$, and $c = 2.998 \times 10^8 \text{ [m s}^{-1}]$ is the speed of light. Therefore, since the energy absorbed by the particle at a distance R from the sun per unit time is:

$$\dot{E} = \frac{L_{\odot}}{4 \pi R^2} [Q_{pr} \pi a^2] \quad (\text{A5.1})$$

the radiation force, F_{rp} , exerted is just $dp/dt = \dot{E} / c$:

$$F_{rp} = \frac{Q_{pr} a^2 L_{\odot}}{4 c R^2} . \quad (\text{A5.2})$$

The gravitational force is just:

$$F_g = \frac{G M m}{R^2} \quad (\text{A5.3})$$

where $G = 6.673 \times 10^{-11}$ [N m² kg⁻²] is the gravitational constant, $M = 1.989 \times 10^{30}$ [kg] is the solar mass, and $m = 4 \pi a^3 \rho / 3$ is the mass of the particles with density ρ . Taking the ratio F_{rp} / F_g and evaluating the constants yields:

$$\beta \equiv \frac{F_{rp}}{F_g} = 5.7398 \times 10^{-4} \frac{Q_{pr}}{\rho a} \quad (\text{A5.4})$$

In general, the radiation pressure coefficient, $Q_{pr} = Q_{pr}(\lambda)$ is obtained from Mie theory calculations. It is a function of the parameter $X \equiv 2 \pi a / \lambda$ and the optical properties of the grain. As seen in Figure 7a and 7b from Burns *et al.* (1979) which are the results of Mie scattering calculations, β is strongly peaked near $a \approx 10^{-7}$ m (assuming a solar spectrum). The interaction of the solar radiation with the particles is strongest when $a \approx \lambda / 2 \pi$. If the particles are much smaller than the wavelength of radiation, they do not effectively interact with the radiation and the scattering efficiency is very low. For very large particles, the gravitational force is much stronger than the radiation pressure force. Materials which are strongly back scattering feel a greater change in momentum and typically have higher values of β than do dielectrics which are forward scattering.

Since cometary dust grains are known to have sizes ranging from sub-micron (McDonnell *et al.*, 1986) to a few microns (Jewitt & Meech, 1986; and Chapter 6), it is expected and observed that radiation pressure effects are important in cometary comae. A particularly interesting illustration of the effects of radiation pressure is seen in the dust coma of P/Halley. Observations were obtained by D. Jewitt with the IIDS (Image Intensified Dissector-Scanner) spectrograph at the Cassegrain focus of the Kitt Peak 2.1 m telescope on 1986 May 2 during photometric conditions. The observational technique and initial data reductions (to obtain reflectivity gradients) were nearly identical to those described in Chapter 6. The only observational difference in this case was that spectra were obtained at many coma

positions offset from the nucleus.

As discussed in Chapter 6, the reflectivity gradient, $S'(\lambda_1, \lambda_2)$, is a convenient measure of the color of the continuum. The reflectivity gradient is among other things, a function of the grain scattering efficiency, the grain size and the wavelength of light. The reflectivity gradient in $\% / 10^3 \text{ \AA}$ (measured between $3750 \leq \lambda [\text{\AA}] \leq 6850$) is plotted as a function of distance from the nucleus (measured in arcsec) in the top portion of Figure A5-1. The figure shows that the grain color is a weak function of position in the coma; redder (hence larger) particles on the sunward side and bluer (hence smaller) particles on the tailward side. The color gradient may be interpreted as the result of radiation pressure particle size sorting. For an assumed density, β is inversely proportional to a (Eq. A5.4). Therefore, the smallest particles experience the greatest radiation pressure acceleration and are pushed back into the tail before they travel far from the nucleus on the sunward side.

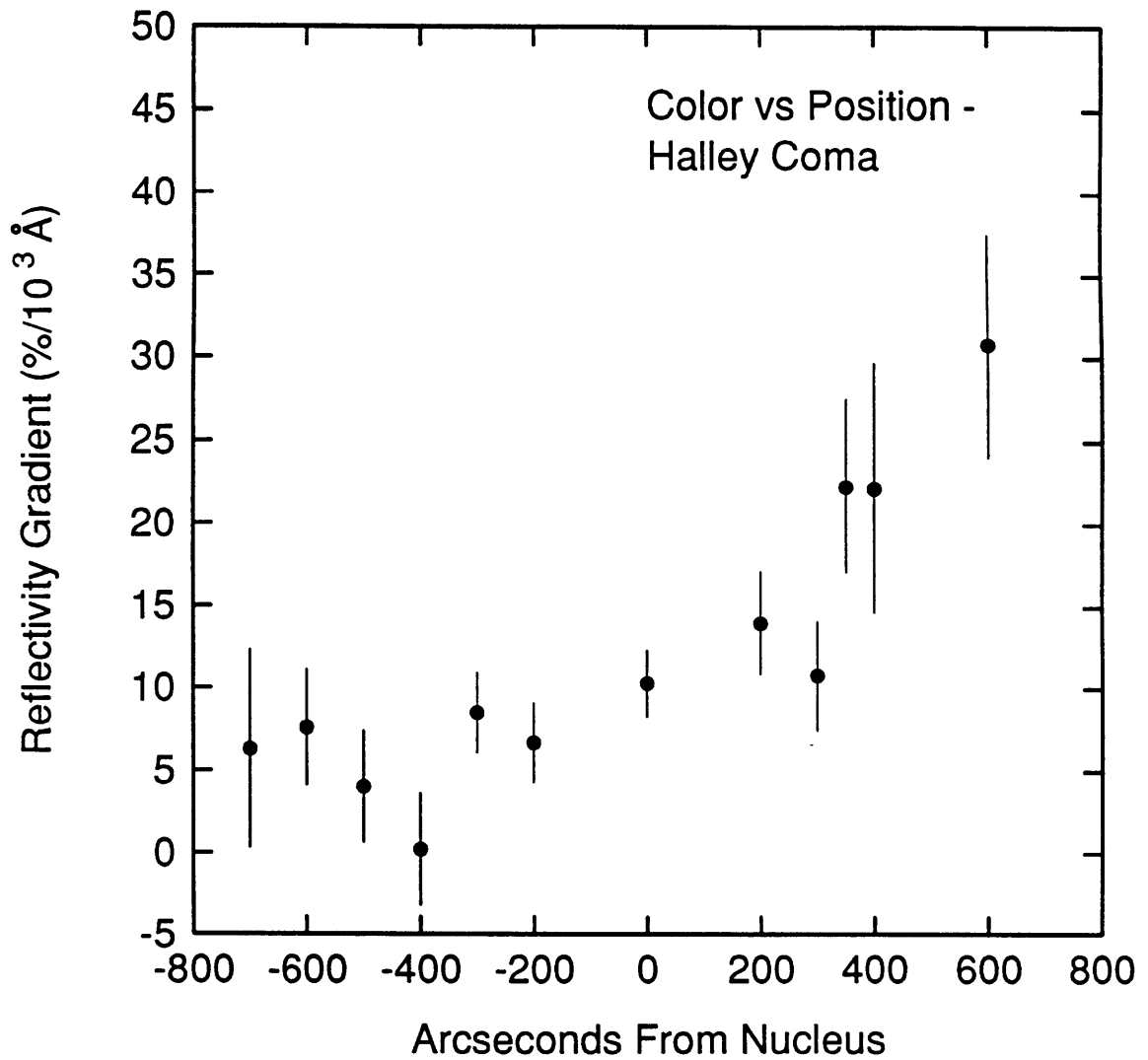


Figure A5-1. The reflectivity gradient in the grain coma of comet P/Halley versus distance along the projected sun-comet line, measured in arcseconds from the nucleus. Positive units on the x-axis indicate displacement towards the sun. The graph shows that the reflectivity gradient is a weak function of position on the coma. The approximate gradient is $dS'/dx \approx 0.01\%$ per 10^3 \AA per linear arcsecond. The observations were obtained on UT 1986 May 3, when the comet was at $R = 1.6 \text{ AU}$, $\Delta = 0.7 \text{ AU}$.

References

Burns, J. A., P. L. Lamy and S. Soter (1979), "Radiation Forces on Small Particles in the Solar System", *Icarus* **40**, 1-48.

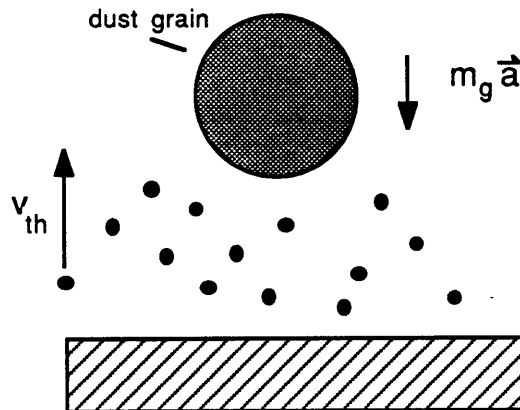
Jewitt, D. and K. J. Meech (1986), "Cometary Grain Scattering Versus Wavelength, or 'What Color is Comet Dust'?", *Astrophys. J.* **310**, 937-952.

McDonnell, J. A. M. *et al.* (1986), "Dust Density and Mass Distribution Near Comet Halley From Giotto Observations", *Nature* **321**, 338-340.

Appendix 6 - Grain Terminal Velocity

Although the dynamics of dust in a gas flow near the nucleus is very complicated, especially considering the highly anisotropic mass loss known to occur from comets (typified by the jet activity in P/Halley as seen by the Vega and Giotto spacecraft, (see Sagdeev *et al.*, 1986; Keller *et al.*, 1986), a simple solution to the problem is possible in the case of radially symmetric outflow. An approximate solution to the problem is especially appropriate in the case of the dynamically new comets such as comet Bowell where relatively little is known about the nature of the activity.

Figure A6-1



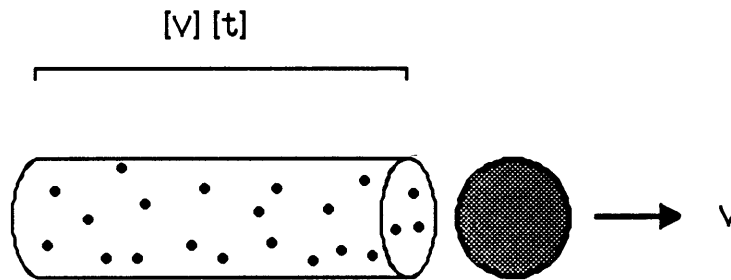
The equation of motion for a dust grain is given by (see Figure A6-1)

$$m_g \frac{d^2 r}{dt^2} = \frac{-G M m_g}{r^2} + F_{drag} \quad (A6.1)$$

where m_g [kg] is the mass of the dust grain, M [kg] is the mass of the nucleus, $G = 6.673 \times$

10^{-11} [Nt m² kg⁻²] is the gravitational constant and r [m] is the distance from the center of the nucleus. In the following calculation it is assumed that the dust grains and the nucleus are spherical with radii a [m] and R_n [m], respectively. The total drag force, F_{drag} , is the product of the momentum per molecule, $(\mu m_h)(v_I)$ with the number of collisions per second. The quantity (μm_h) is the mean molecular weight of the gas. The volume swept out by a dust grain of radius a , in time, t , is $(\pi a^2 v_I t)$. When multiplied by the gas number density, $N(r)$ [molecules m⁻³] this gives the number of collisions in time t (see Figure A6-2).

Figure A6-2



The velocity, $v_I = v_{th} - v_g$, is the relative velocity between the grain (v_g) and the molecules. For simplicity, the value of v_{th} is taken to be equal to the mean thermal speed of the gas in a direction perpendicular to the surface, $(2 k T / \pi \mu m_h)^{1/2} / 2$ where $k = 1.38 \times 10^{-23}$ J deg⁻¹ is the Boltzman constant. The number density is related to the total production rate of molecules from the nucleus, Q [molecules s⁻¹], via $N(r) = Q / (4 \pi R_n^2 v_{th}) [R_n / r]^2 = N(R_n) [R_n / r]^2$. The drag force is therefore given by

$$F_{drag} = f \mu m_h \pi a^2 N(R_n) R_n^2 [v_{th} - v_g]^2 r^{-2} \quad (\text{A6.2})$$

where f is the drag coefficient. Taking $4 \pi a^3 \rho_g / 3$ as the mass of a grain and $4 \pi R_n^3 \rho_n / 3$ as the mass of the nucleus, where ρ_g and ρ_n are the densities of grain and nucleus, respectively, and substituting Eq. (A6.2) into Eq. (A6.1) we obtain:

$$\frac{d^2 r}{dt^2} = \frac{c}{2a} [(v_{th} - v)^2 - b^2] \left(\frac{R_n}{r^2} \right) \quad (\text{A6.3})$$

where

$$c = \frac{3 f \mu m_h Q}{8 \pi R_n v_{th} \rho_g} \quad \text{and} \quad b = v_{th} \sqrt{a / a_{crit}}$$

(and where $v_g = v$). The largest grain that can be lifted off the nucleus with a given mass loss rate is a_{crit} . The size of a_{crit} can be obtained by equating the drag force (Eq. A6.2) with the gravitational force exerted on the grain by the nucleus, $G M m_g / R_n^3$. This yields:

$$a_{crit} = \frac{9 f (\mu m_h Q) v_{th}}{64 \pi^2 \rho_g \rho_n R_n^3 G} \quad (\text{A6.4})$$

With the substitution $v = (dr / dt)$ and $(d^2 r / dt^2) = v (dv / dr)$, Eq. (A6.3) is separable:

$$\int_{v_o}^{v_t} \frac{v dv}{[(v_{th} - v)^2 - b^2]} = \frac{c R_n}{2 a} \int_{R_n}^r \frac{dr}{r^2} \quad (\text{A6.5})$$

where v_o is the initial grain velocity (usually taken to be zero) and v_t is the grain velocity in the gas flow at any distance, r , from the nucleus. Letting $x = (v_{th} - v)$, the LHS of Eq. A6.5

becomes (with $v_{th} = u$):

$$\int \frac{(x - u) dx}{(x^2 - b^2)} = \int \frac{x dx}{(x^2 - b^2)} - u \int \frac{dx}{(x^2 - b^2)}$$

and upon integration,

$$\begin{aligned} &= \frac{1}{2} \ln [b^2 - (v_{th} - v)^2] \Big|_{v=v_o}^{v=v_t} - \frac{u}{2b} \ln \left[\frac{v_{th} - v - b}{v_{th} - v + b} \right] \Big|_{v=v_o}^{v=v_t} \\ &= \frac{1}{2b} \left\{ b \ln \left[\frac{b^2 - v_{th}^2 + 2v_{th}v_t - v_t^2}{b^2 - v_{th}^2 + 2v_{th}v_o - v_o^2} \right] + u \ln \left[\frac{(v_{th} - v_t + b)(v_{th} - v_o - b)}{(v_{th} - v_t - b)(v_{th} - v_o + b)} \right] \right\} \\ &= \frac{1}{2b} \left\{ b \ln \left[\frac{(b - v_{th} + v_t)(v + v_{th} - v_t)}{(b - v_{th} + v_o)(v + v_{th} - v_o)} \right] + u \ln \left[\frac{(v_{th} + b - v_t)(v_{th} - b - v_o)}{(v_{th} - b - v_t)(v_{th} + b - v_o)} \right] \right\} \\ &= \frac{1}{2b} \left\{ (v_{th} - b) \ln \left[\frac{v_{th} - b - v_o}{v_{th} - b - v_t} \right] + (v_{th} + b) \ln \left[\frac{v_{th} + b - v_t}{v_{th} + b - v_o} \right] \right\} \quad (A6.6) \end{aligned}$$

Integrating the RHS of Eq. A6.5 and combining with the Eq. A6.6 we obtain:

$$1 - \frac{R_n}{r} = \frac{a}{cb} \left\{ (v_{th} - b) \ln \left[\frac{v_{th} - b - v_o}{v_{th} - b - v_t} \right] + (v_{th} + b) \ln \left[\frac{v_{th} + b - v_t}{v_{th} + b - v_o} \right] \right\} \quad (A6.7)$$

Although the equation appears formidable, it can be solved numerically by assuming $v_o = 0$ and re-writing Eq. (A6.7) in the form:

$$F(v) = c_3 + c_1 \ln \left[\frac{c_1}{c_1 - v} \right] + c_2 \ln \left[\frac{c_2 - v}{c_2} \right] \quad (\text{A6.8})$$

$$\frac{dF(v)}{dv} = \frac{c_1}{c_1 - v} - \frac{c_2}{c_2 - v}$$

where:

$$c_1 = v_{th} - b \quad \text{and} \quad c_2 = v_{th} + b \quad \text{and} \quad c_3 = \frac{bc}{a} \left[\frac{R_n}{r} - 1 \right]$$

for $v = v_{th}$ and $v_o = 0$. Newton's method can be used to obtain a solution with few iterations. The method is as follows. An initial guess to the velocity, v , is used to compute the value of the function $F(v)$, and the slope [$F'(v) = dF(v)/dv$] at that point. A line with this slope is extended until it intersects the $F(v) = 0$ axis. The point of intersection is the new estimate of v given by $v_{new} = v - F(v) / F'(v)$. To obtain the terminal grain velocity, v_t , let the distance from the nucleus, $r = \infty$. Figure A6-3 illustrates the form of the function $F(v)$ for the particular case of comet Bowell discussed in Chapter 9. In practice, the grain reaches its terminal velocity at $r \ll \infty$. Again, for the particular case of the comet Bowell CO_2 model, the distance at which the grains reach v_t is at $r \approx 5R_n$ (see Figure A6-4).

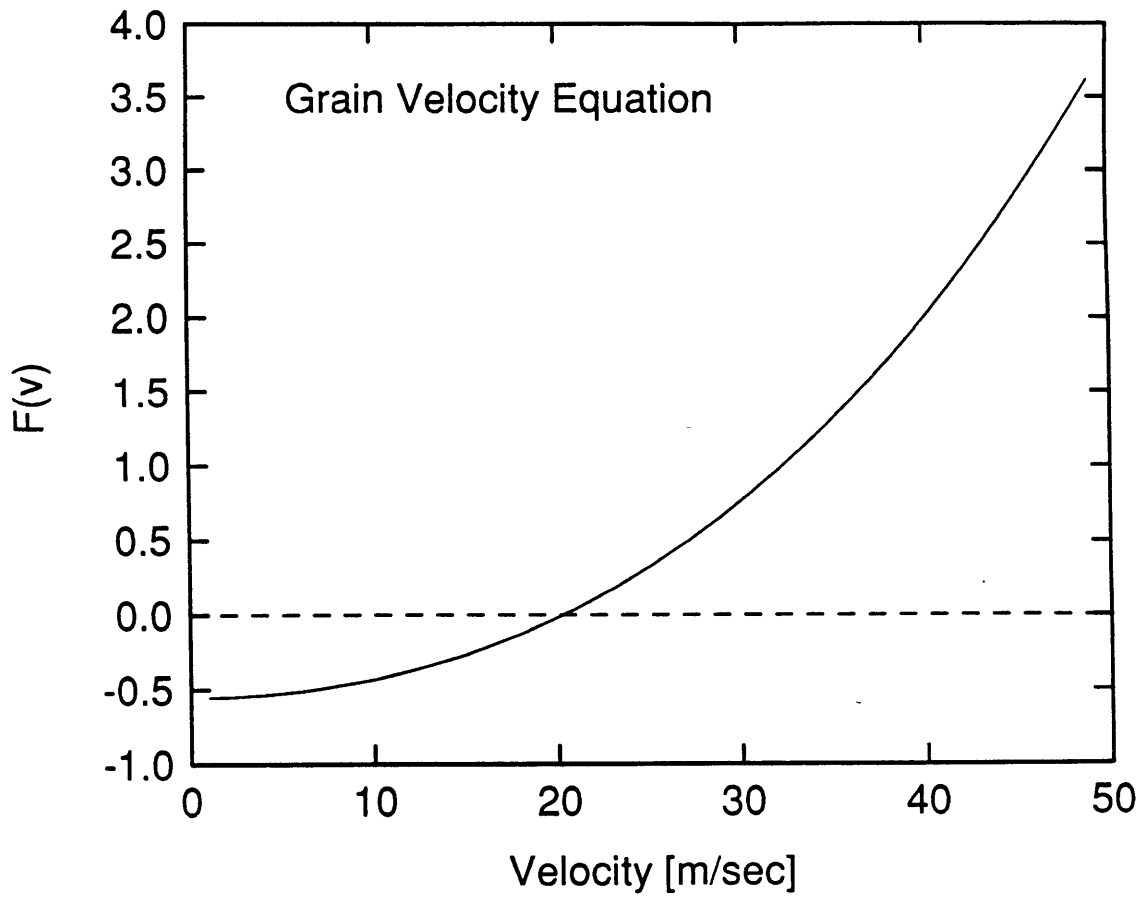


Figure A6-3. Form of the equation of grain velocity in a gas flow. The constants used in evaluating the equation are relevant to comet Bowell (see Chapter 9).

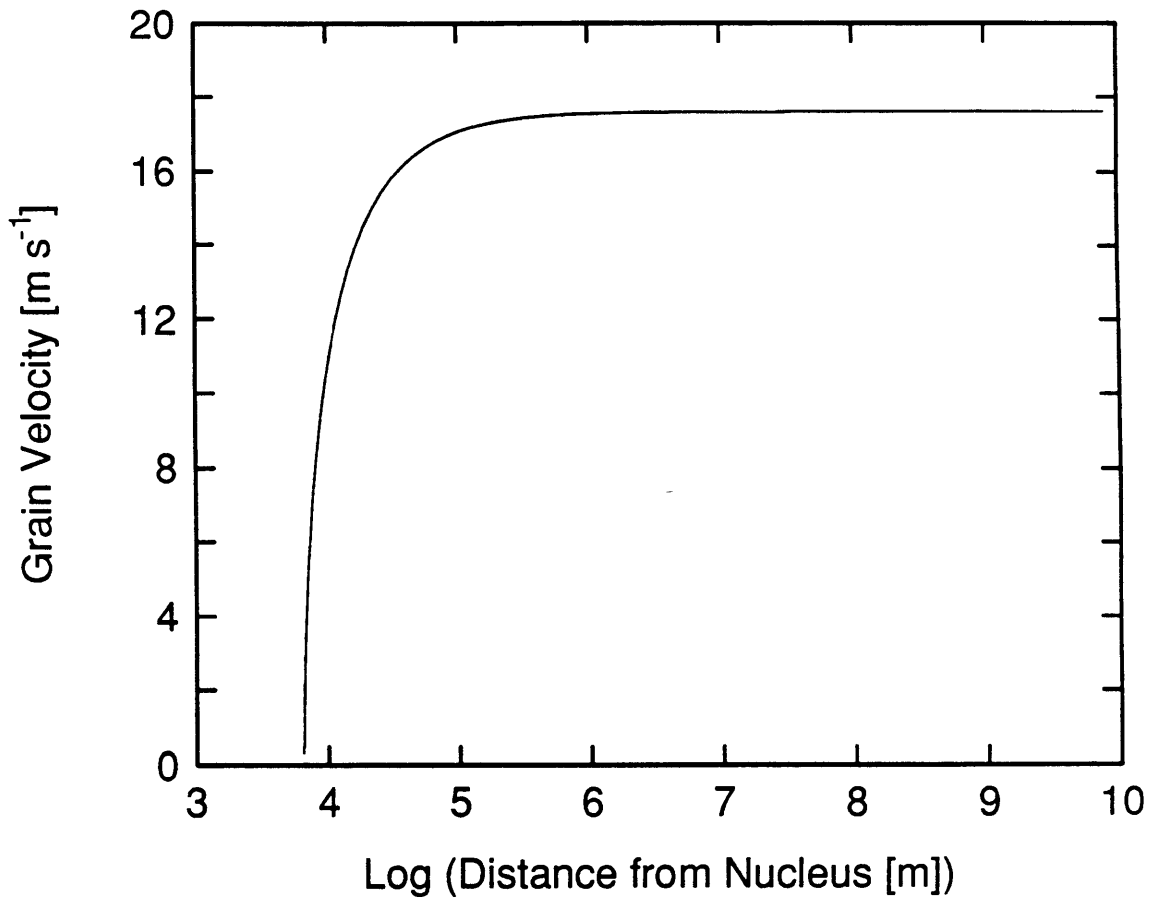


Figure A6-4. Grain velocity as a function of distance from the nucleus. Model input for mass loss from nucleus assumes the parameters relevant to comet Bowell (Chapter 9). The terminal velocity is reached very close to the nucleus.

The derivation of the grain velocity in a gas flow described above is only an approximation to the complicated interaction between the gas and dust near the nucleus in comets. Specifically, the model does not take account of

- ◇ v_{gas} leaving the nucleus $\neq v_{th}$ because the gas must overcome surface force fields, in general, $1/2 v_{th} < v < 2/3 v_{th}$ (Delsemme & Miller, 1971)
- ◇ a particle size distribution of grains
- ◇ icy grains which may sublime as they leave the nucleus (although not appreciably in the small region in which the grains come to their terminal velocity)
- ◇ the adiabatic expansion of the gas which causes it to speed up
- ◇ the effects of collisions among the gas molecules.

It is unlikely that the radial outflow of gas would be collisionless, even in the case of comet Bowell at large distances. The mean free path between molecules is $mfp = [N(r) \sigma]^{-1}$, where $\sigma \approx 10 \text{ \AA}^2$ is a typical molecular cross section for collision. In the case of comet Bowell at 10 AU, the total mass loss from CO_2 sublimation from a nucleus of $R_n = 6500 \text{ m}$ is $dM/dt \approx 8 \times 10^2 \text{ kg s}^{-1}$. The nucleus temperature at this distance would be 92 K, hence the thermal velocity would be $v_{th} \approx 10^2 \text{ m s}^{-1}$. (Note: all of the numbers relating to mass loss from the nucleus are based on the CO_2 sublimation model as described in Chapter 9). This gives a $mfp \approx 50 \text{ m}$ at the nucleus, increasing as the square of the distance from the nucleus. This suggests that collisions will be important. For gas free paths less than $0.1R_n$, gas-dynamical methods must be used to compute the gas speed (Wallis, 1982). However, given that the nature of the modelling presented in this thesis is to use *simple* models using ground-based measurements of the brightness of the comet as a function of distance, it is not justified to use the more complex solutions. Furthermore, Wallis found that when the gas-dynamic models were used, the effect was to decrease the initial gas ejection velocity to a

small fraction ($\approx 10\%$) of its original v_{th} . This is due, in part, to the fact that molecular collisions remove some of the energy from the gas flow. Therefore, given the nature of the sublimation models described in this thesis, it is valid to use the thermal velocity (or $0.1v_{th}$). In the case of comet Halley, it may be more appropriate to use the Bobrovnikoff relationship for velocity as a function of R (see Delsemme, 1982), since these coma expansion velocities were based upon observation.

References

- Delsemme, A. H. (1982), "Chemical Composition of Cometary Nuclei", in *Comets*, ed. L. L. Wilkening, Univ. of Arizona Press, AZ, p. 85-130.
- Delsemme, A. H. and D. C. Miller (1971), "Physico-Chemical Phenomena in Comets. III. The Continuum of Comet Burnham (1960II)", *Plan. Space Sci.* **19**, 1229-1257.
- Keller, *et al.* (1986), "First Halley Multicolor Camera Imaging Results From Giotto", *Nature* **321**, 320-326.
- Sagdeev, *et al.* (1986), "Television Observations of Comet Halley From Vega Spacecraft", *Nature* **321**, 262-266.
- Wallis, M. K. (1982), "Dusty Gas-Dynamics in Real Comets", in *Comets*, ed. L. L. Wilkening, Univ. of Arizona Press, AZ, p. 357-369.